Université de Montréal

NOUVELLES CONSTRUCTIONS DE MÉTHODES DE VOLUMES/ÉLÉMENTS FINIS POUR LES ÉCOULEMENTS TRANSSONIQUES/SUPERSONIQUES COMPRESSIBLES

par

Aziz Madrane

Département de mathématiques et de statistique
Faculté des arts et sciences

Thèse présentée à la Faculté des études supérieures
en vue de l'obtention du grade de PhilosophiæDoctor (Ph.D.)
en mathématiques

novembre 1998

Université de Montréal

Faculté des études supérieures

Cette thèse intitulée

NOUVELLES CONSTRUCTIONS DE MÉTHODES DE VOLUMES/ÉLÉMENTS FINIS POUR LES ÉCOULEMENTS TRANSSONIQUES/SUPERSONIQUES COMPRESSIBLES

présentée par

Aziz Madrane

a été évaluée par un jury composé des personnes suivantes :

Michel Delfour
(président-rapporteur)

Paul Arminjon
(directeur de recherche)

Serge Dubuc
(membre du jury)

Bram van Leer
(examinateur externe)

Thèse acceptée le :
25. 11. 1998

sommaire

Nous présentons dans cette thèse la conception de nouveaux schémas de type volumes finis, pour les équations ou systèmes d'équations hyperboliques, et l'analyse théorique et numérique de problèmes hyperboliques non linéaires pour la prédiction des écoulements compressibles, stationnaires ou instationnaires en utilisant des maillages adaptatifs.
Cette construction est une méthode de volumes finis, d'abord proposée par Arminjon, puis par Arminjon et Viallon, qui s'inspire de l'utilisation faite par le schéma de Nessyahu-Tadmor en une dimension spatiale, du schéma décalé de Lax-Friedrichs, du type Godunov pour les lois de conservation hyperboliques en une dimension spatiale, dans lequel la résolution des problèmes de Riemann aux interfaces des cellules est évitée grâce à l'utilisation de la forme décalée du schéma de Lax-Friedrichs. L'interpolation linéaire par morceaux des données initiales (MUSCL) et des limiteurs de pentes conduisent à une approximation non oscillatoire du second ordre.
Finalement pour résoudre le système des équations de Navier-Stokes bidimensionnelles, nous présentons une formulation mixte éléments/volumes finis sur des maillages triangulaires non structurés. Cette formulation consiste à traiter séparement les termes de convection et les termes de diffusion. C'est-à-dire que le terme convectif sera calculé par la méthode des volumes finis et le terme diffusif par la méthode des éléments finis (élément P1-Lagrange) sur des maillages triangulaires non structurés.

remerciements

Les travaux qui ont abouti à cette thèse ont été effectués au Centre de Recherches Mathématiques (CRM) et à l'Institut National de Recherche en Informatique et Automatique Rocquencourt (Paris) dont je remercie les directions. Je tiens à exprimer toute ma gratitude à Monsieur le professeur Paul Arminjon pour m'avoir proposé cet intéressant sujet, qui m'a permis d'avoir plusieurs articles. Pour cela je le remercie très chaleureusement.

Je remercie aussi tout particulièrement Monsieur Jérôme Jaffré qui m'a accueilli au sein de son projet de recherche ESTIME à l'Institut National de Recherche en Informatique et Automatique (INRIA), ainsi que Monsieur Hassan Kaddouri Université du Littoral avec qui j'ai eu des échanges très fructueux.

Je suis très reconnaissant envers Monsieur Alain Dervieux, responsable du projet SINUS à l'INRIA de Sophia Antipolis, pour m'avoir donné de judicieux conseils.

Je suis très honoré que Monsieur Bram van Leer ait accepté d'être examinateur externe. Je remercie également Messieurs Michel Delfour et Serge Dubuc d'être membres du jury.

Je tiens à remercier Madame Marie-Claude Viallon, de l'Université de Saint-Etienne, pour les discussions enrichissantes que nous avons eues, pour sa serviabilité et sa gentillesse.

Je n'oublie pas Monsieur le professeur Jacques Fortin (Université Laval) qui m'a soutenu moralement et scientifiquement pendant mon séjour au Canada.

Je tiens à remercier encore Monsieur le professeur Bram van Leer pour son invitation au département d'aérospatiale à l'Université du Michigan, où j'aurai l'occasion de faire une extension tridimensionnelle de notre travail.

Je remercie également l'équipe de THOMSON, Tubes Electronique, France, pour la confiance qu'ils nous ont accordée en nous confiant un projet industriel.

Je voudrais encore remercier les membres de ma famille pour leur patience et leur soutien tout au long de ce travail.

Pour terminer j'exprime ma reconnaissance envers les gouvernements du Maroc, de la France et du Canada pour les bourses et le soutien financier qu'ils m'ont accordés tout au long de mes études universitaires.

Table des matières

Liste des figures

INTRODUCTION

Un peu d'histoire ...

Des problèmes d'origines diverses peuvent être modélisés à l'aide de lois de conservation hyperboliques non linéaires, citons notamment le problème de la dynamique des gaz [1], [2]; le modèle de l'élasticité non linéaire (dynamique des câbles) [3],[4]; le système de Saint-Venant régissant un écoulement d'eau peu profonde ([5],[6]); la simulation des réservoirs de pétrole ([7],[8]); les pipe-lines ([10]); problèmes d'électrostatique et électrodynamique ([9]); certains problèmes issus de la biologie ([11]) ... etc.

L'étude mathématique des lois de conservation hyperboliques a connu ces vingt dernières années un progrès considérable tant sur le plan théorique que numérique, en effet sur le plan théorique l'introduction de la compacité par compensation ([12],[11],[13]) a été d'un grand intérêt dans la démonstration de résultats d'existence de solutions entropiques pour les systèmes hyperboliques non linéaires, à partir des solutions visqueuses ([12]), sans passer par le schéma de Glimm [14].

Sur le plan de la résolution numérique des lois de conservation scalaires, de nouveaux types de schémas aux différences tels que les schémas TVD (Variation Totale Décroissante) quasi d'ordre deux ([15],[6],[57]) ont été développés.

Ces schémas ont l'avantage de ne pas osciller aux voisinages des chocs contrairement au schéma d'ordre deux de Lax-Wendroff, mais ils sont précis seulement à l'ordre un au voisinage des extremas de la solution. Pour tenter de remédier à cet inconvénient, on a développé récemment les schémas type ENO[1] ([16]). En raison de la non-linéarité des équations, des discontinuités peuvent apparaître dans les solutions après un temps fini. A cause de la viscosité numérique qu'ils développent, les schémas du premier

[1]Essentiellement Non Oscillant

ordre simulent mal les chocs (discontinuités) en les étalant trop. D'où l'importance des schémas d'ordre deux pour le calcul des chocs.

Des schémas du type Godunov reposant sur l'utilisation d'un solveur approché du problème de Riemann ont été élaborés pour la résolution numérique des systèmes de lois de conservation hyperboliques ([17], [18]).

D'autres travaux sur différents problèmes liés aux lois de conservation hyperboliques ont été réalisés récemment, on peut citer par exemple les travaux [19], [4] et [6], sur le problème des conditions aux limites; les travaux [20] sur le problème de Riemann généralisé. Le traitement numérique des problèmes ayant un terme source a fait l'objet des travaux [21], [22] et [23]. Des problèmes hyperboliques sous forme non conservative ont été étudiés dans [24].

Malgré les progrès enregistrés ces dernières années, la théorie des problèmes hyperboliques non linéaires est encore relativement pauvre et beaucoup de questions restent ouvertes notamment en ce qui concerne :

- L'unicité de la solution entropique dans le cas des systèmes hyperboliques non linéaires.
- La convergence des schémas multidimensionnels du second ordre.
- La convergence des schémas unidimensionnels d'ordre un pour les systèmes.
- La résolution du problème de Riemann multidimensionnel.

Plan général de la thèse:

Ce travail est décomposé comme suit :

• Dans le premier chapitre, nous posons le problème à résoudre et nous rappelons brièvement quelques propriétés des équations d'Euler pour les fluides compressibles en insistant sur leur caractère hyperbolique.

• Dans le second chapitre, nous commençons par illustrer la méthode de volumes finis sur l'équation de Poisson. Par suite, nous montrons un lien entre la méthode des volumes finis et l'élément de Raviart-Thomas. Cet élément fini est basé sur une formulation mixte du problème de Dirichlet

$$\begin{cases} -\Delta u &= f & \text{dans} \quad \Omega \\ u &= 0 & \text{sur} \quad \Gamma \end{cases}$$

en introduisant la variable $p = \text{grad}\, u$.

Après avoir intégré le terme de masse par la formule du trapèze, nous montrons que la discrétisation de ce dernier problème, dans le cas où Ω est un domaine rectangulaire et où la triangulation de $\bar{\Omega}$ en rectangles est uniforme, est exactement la même que celle provenant de la méthode des volumes finis.

Nous terminons ce chapitre en montrant l'équivalence entre les formulations volumes finis et éléments finis pour l'équation de convection-diffusion sur des maillages non structurés.

• Nous présentons aux chapitres trois et quatre, la conception de nouveaux schémas de type volumes finis, pour les équations ou systèmes d'équations hyperboliques, et l'analyse théorique et numérique de problèmes hyperboliques non linéaires pour la prédiction des écoulements compressibles, stationnaires ou instationnaires en utilisant des maillages adaptatifs.

Cette construction est une méthode de volumes finis qui s'inspire de l'utilisation faite par le schéma de Nessyahu-Tadmor en une dimension spatiale, du schéma décalé de Lax-Friedrichs, du type Godunov pour les lois de conservation hyperboliques en une dimension spatiale, dans lequel la résolution des problèmes de Riemann aux interfaces des cellules est évitée grâce à l'utilisation de la forme décalée du schéma de Lax-Friedrichs. L'interpolation linéaire par morceaux des données initiales (MUSCL) et des limiteurs de pentes conduisent à une approximation non oscillatoire du second ordre.

Les applications numériques qui nous servent de test et au traitement des conditions aux limites de type fluide/fluide et fluide/paroi, sont des problème stationnaires, un problème de réflexion, le problème de la Double ellipse modélisant l'avant de la navette Hermes et le problème de l'écoulement autour d'une aile d'avion NACA-0012. Ces expériences numériques utilisent un schéma explicite en temps.

• Le chapitre quatre est consacré à la validation de nos résultats; pour ce faire, on a comparé nos résultats avec ceux obtenus, pour les mêmes problèmes et dans les mêmes conditions, avec une méthode d'éléments finis discontinus proposée par Jaffré et al. [72]. Cette méthode s'applique aussi bien sur des maillages structurés que non structurés. Les équations d'Euler sont écrites en formulation conservative et en coordonnées eulériennes. Les variables conservatives sont approchées par des fonctions linéaires par morceaux. La méthode comporte deux étapes de calcul. La première étape est une

étape éléments finis, incluant l'utilisation du solveur de Riemann monodimensionnel de Roe avec correction entropique de Dubois-Melhman. La deuxième étape est une étape de limitation de pente multidimensionnelle effectuée sur les variables physiques.
On utilise un schéma explicite en temps respectant une condition CFL[2]. Enfin une technique de maillages adaptatifs a été utilisée par la méthode des éléments finis discontinus et par notre méthode (volumes finis). Elle apporte des gains en temps de calcul importants.

• Enfin le dernier chapitre a pour objet la résolution numérique du système des équations de Navier-Stokes bidimensionnelles.
Nous présentons une formulation mixte éléments/volumes finis sur des maillages triangulaires non-structurés. Cette formulation consiste à traiter séparement les termes de convection et les termes de diffusion. C'est à dire que le terme convectif sera calculé par la méthode des volumes finis et le terme diffusif par la méthode des éléments finis (élément P1-Lagrange) sur des maillages triangulaires non structurés. Nous présentons à la fin de ce chapitre une série de résultats numériques, écoulement supersonique autour de la double ellipse, autour d'un profil d'aile à faible incidence, pour mettre en évidence le décollement de la couche limite et le capture de l'onde de choc.

Les travaux qui sont présentés dans cette thèse ont fait l'objet des publications suivantes:

• **Paul Arminjon, Aziz Madrane** , " A staggered Lax-Friedrichs-type mixed finite volume/finite element method for the simulation of viscous compressible flows on unstructured triangular grids", submitted (July 7, 1998) to Journal of Comp. Physics.

• **Paul Arminjon, Aziz Madrane** , " A mixed finite volume/finite element method for viscous compressible flows on staggered unstructured grids" , in Progress in Numerical Solutions of Partial Differential Equations, A Conference to honour P.Roe on the occasion of his 60^{th} birthday, Arcachon, France, July 11-13, 1998.

• **Paul Arminjon, Aziz Madrane** , " A staggered Lax-Friedrichs-type finite volume/finite element method for the two-dimensional Navier-Stokes equations", Proc. 6^{th}. Conf. of the Computational Fluid Dynamics Society of Canada, Québec, June 7-9, 1998, E. Fournier and M. Fortin, Editors, pp. VIII 103-108.

---

[2]Courant-Friedrichs-Lewy

• **Paul Arminjon, Aziz Madrane** , " A mixed finite volume/finite element method for 2-dimensional compressible Navier-Stokes equations on unstructured grids", 7^{th} Int.Conf. on Hyperbolic Problems, Zürich, February 9-13, 1998, Book of abstracts + Proceedings (accepted, June 29, 1998), M.Fey and R.Jeltsch, editors.

• **Paul Arminjon, Aziz Madrane and Marie Claude Viallon,** " Comparison of a finite volume version of the Lax-Friedrichs and Nessyahu-Tadmor schemes and discontinuous finite element method for compressible flows on unstructured grids ", Proceedings of Symposium Honoring S.K.Godunov, May 1-2, 1997, The University of Michigan, Ann Arbor (Mi.), to appear as a special volume in J.Comp.Physics, B.van Leer, editor, 134(1) : 199, 1997.

• **Paul Arminjon, Marie Claude Viallon, Aziz Madrane and Lahcen Kaddouri,** " Discontinuous finite elements and 2-Dimensional Finite Volume Versions of the Lax-Friedrichs and Nessyahu-Tadmor difference schemes for Compressible Flows on Unstructured Grids ", CFD Review, John Wiley, pp.241-261, 1997, M.Hafez and K.Oshima, Editors.

• **Paul Arminjon, Marie Claude Viallon and Aziz Madrane (1997),** " A Finite Volume Extension of the Lax-Friedrichs and Nessyahu-Tadmor Schemes for Conservation Laws on Unstructured Grids ", Int. J. Comp. Fluid Dynamics, Vol.9, No.1, 1-22, (1997).

• **Paul Arminjon, Marie Claude Viallon and Aziz Madrane** , " From Lax-Friedrichs to a Multidimensional Finite Volume Extension of the Nessyahu-Tadmor Scheme for Compressible Flows ", Proc. Int. Conf. on Numerical Meth. for the Euler and Navier-Stokes Equations. Centre de Rech. Math. Univ. de Montréal, P.Arminjon and A.Dervieux, editors, september 1995, to appear in the Am.Math.Soc-CRM series.

Chapitre 1

Modèle mathématique

1. Le modèle mathématique

On considère les équations d'Euler de la dynamique des gaz modélisant l'écoulement de fluides compressibles parfaits et non conducteurs de chaleur.

Soit Ω un ouvert de $\mathbb{R}^2$, de frontière Γ; les équations d'Euler s'écrivent en formulation **conservative** et en coordonnées eulériennes

$$\frac{\partial}{\partial t}U(x,y;t) + \frac{\partial}{\partial x}F(U(x,y;t)) + \frac{\partial}{\partial y}G(U(x,y;t)) = 0 \quad \text{pour } (x,y;t) \in \Omega \times \mathbf{R}_+ \tag{1.1}$$

Celles-ci doivent être accompagnées de conditions initiales et de conditions aux limites sur $\Gamma \times \mathbf{R}_+$.

Dans toute la suite, on notera U pour $U(x,y;t)$ quand aucune ambigüité n'est à craindre.

Les variables U sont des fonctions de $\Omega \times \mathbb{R}_+$ dans $\mathbf{R}^4$ et F et G sont des fonctions de $\mathbf{R}^4$ dans $\mathbf{R}^4$:

$$U = \begin{pmatrix} \rho \\ \rho u \\ \rho v \\ \rho E \end{pmatrix} \; ; \quad F(U) = \begin{pmatrix} \rho u \\ \rho u^2 + p \\ \rho uv \\ (\rho E + p)u \end{pmatrix} \; ; \quad G(U) = \begin{pmatrix} \rho v \\ \rho uv \\ \rho v^2 + p \\ (\rho E + p)v \end{pmatrix}$$

où ρ est la densité du fluide, u et v les deux composantes de la vitesse de l'écoulement, $E = \frac{1}{2}q^2 + \epsilon = \frac{1}{2}(u^2 + v^2) + \epsilon$ l'energie totale spécifique (par unité de masse), ϵ énergie interne spécifique, p la pression.

Le système (1.1) est complété par la loi d'état des gaz parfaits:

$$p = (\gamma - 1)(\rho E - \frac{1}{2}\rho(u^2 + v^2)) \text{ où } \epsilon = \frac{1}{\gamma - 1}\frac{p}{\rho}$$

où γ est le rapport des coefficients de chaleur ($\gamma = 1.4$ pour un gaz parfait). Deux autres quantités physiques importantes sont la vitesse du son c et le nombre de Mach M :

$$c = \sqrt{\frac{\gamma p}{\rho}}\ ,\ M = \frac{\sqrt{u^2 + v^2}}{c}\ .$$

A ces équations on ajoute des conditions aux limites variables suivant le type de problème considéré. On distingue pour cela les frontières de type fluide/fluide (Γ_∞) et celles de type fluide/paroi (Γ_B).

Par exemple pour un écoulement externe autour de la double ellipse, le domaine Ω et ses frontières Γ_∞ (entrée dans le domaine de calcul) , Γ_B et Γ_S (sortie) sont schématisés sur la figure suivante:

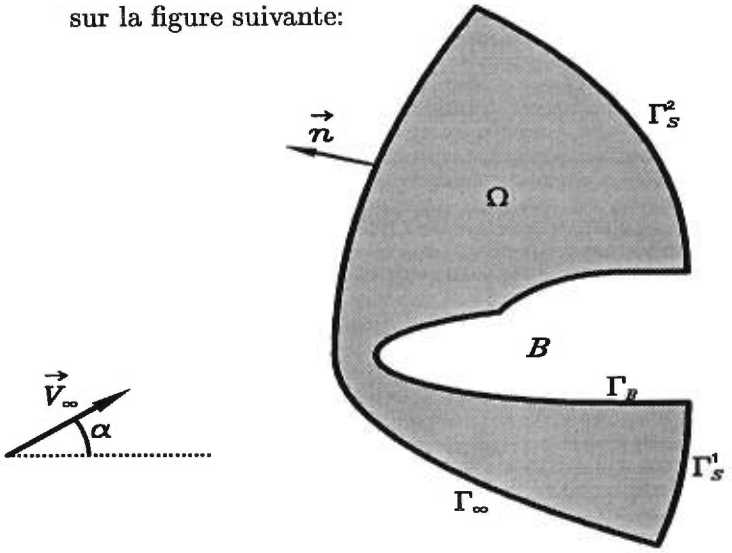

FIGURE 1.1. Domaine de calcul pour l'écoulement hypersonique autour de la double ellipse

$\star$ Sur Γ_B, on impose la condition de glissement $V.n = 0$, avec V la vitesse du fluide $\left(V = \begin{pmatrix} u \\ v \end{pmatrix}\right)$ et $n \in R^2$ vecteur normal à Γ_B et sortant du domaine de calcul (normale extérieure).

$\star$ Sur Γ_∞, on supposera que l'écoulement est uniforme (champ entrant, de vitesse V_∞ normalisée à l'unité).

$$\rho_\infty = 1, \quad V_\infty = \begin{pmatrix} cos\alpha \\ sin\alpha \end{pmatrix}, \quad p_\infty = \frac{1}{\gamma M_\infty^2}$$

où α est l'angle d'incidence de l'obstacle par rapport au fluide et M_∞ désigne le nombre de Mach à l'infini.

$\star$ Sur Γ_S, l'écoulement est libre.

Pour les problèmes instationnaires, il est aussi nécessaire de définir la condition initiale:

$$U(x,y;0) = U_0(x,y) \quad \forall\,(x,y) \in \Omega.$$

2. Propriétés et définitions

On rappelle ici quelques définitions essentielles, et on introduit les notations indispensables liées aux principales propriétés du système des équations d'Euler (1.1).

2.1. Propriétés du système des équations d'Euler.

- Fonctions homogènes

On vérifie facilement que les fonctions de flux F et G sont des fonctions homogènes en U de degré un, c'est-à-dire:

$$\begin{cases} F(\lambda U) = \lambda F(U) \\ \qquad\qquad\qquad\qquad \forall\,\lambda \in \mathbf{R},\ \forall\, U \in \mathbf{R}^4 \\ G(\lambda U) = \lambda G(U) \end{cases}$$

ce qui implique la relation suivante:

$$\begin{cases} F(U) = F'(U).U \\ \qquad\qquad\qquad\qquad \forall\, U \in \mathbf{R}^4 \\ G(U) = G'(U).U \end{cases}$$

où $F'(U)$ et $G'(U)$ sont les matrices jacobiennes (4×4) des dérivées de F et G par rapport aux composantes du vecteur U.

Le système d'équations (1.1) se met dons aussi sous la forme:

$$U_t + F'(U).U_x + G'(U).U_y = 0 \tag{2.1}$$

avec les notations suivantes:

$$U_t = \frac{\partial U}{\partial t}, \quad U_x = \frac{\partial U}{\partial x}, \quad U_y = \frac{\partial U}{\partial y}.$$

(2.1) est une écriture des équations d'Euler sous forme non conservative.

- Loi hyperbolique

Considérons la forme générale non conservative d'un système d'équations aux dérivées partielles:

$$U_t + A \cdot U_x + B \cdot U_y = 0 \tag{2.2}$$

où A (respectivement B) est la matrice jacobienne de F (respectivement G).

L'expression des matrices A et B est donnée en annexe 1.

Le système (2.2) de 4 équations du premier ordre peut être classé différemment par rapport à la variable temps t, selon les propriétés de la matrice caractéristique A_n:

$$\begin{cases} A_n = A_n(\boldsymbol{n}; U) = n_1 A + n_2 B\,, \\ \boldsymbol{n} = \begin{pmatrix} n_1 \\ n_2 \end{pmatrix} \in \mathbf{R}^2 \text{ et } U \in \mathbf{R}^4\,. \end{cases} \tag{2.3}$$

Le système (2.2) par rapport à la variable t est dit:

- parabolique si toutes les valeurs propres de A_n sont réelles et si les vecteurs propres correspondants ne sont pas linéairement indépendants pour tout (n_1, n_2) (c'est le cas de l'équation de la chaleur).
- elliptique si toutes les valeurs propres de A_n sont complexes (équation des ondes ou de Navier-Stokes stationnaires).
- hyperbolique si toutes les valeurs propres de A_n sont réelles et si les vecteurs propres correspondants sont linéairement indépendants pour tout (n_1, n_2).
- hybride si aucune des classifications précédentes n'est possible.

PROPOSITION 1.1.

Le système des équations d'Euler (1.1) est hyperbolique pour la direction t dans le domaine Ω. De plus la matrice A_n est diagonalisable et il existe une matrice inversible $P_n(U) = P_n(\boldsymbol{n}; U)$ et une matrice diagonale $\Lambda_n(U) = \Lambda_n(\boldsymbol{n}; U)$ contenant les valeurs

propres de A_n, telles que:

$$A_n = P_n \Lambda_n P_n^{-1} \tag{2.4}$$

L'expression des matrices $P_n(U)$ et $P_n^{-1}(U)$ est donnée en annexe.

Les valeurs propres de A_n sont :

$$\lambda_1(\boldsymbol{n}) = V.\boldsymbol{n} - c,\ \lambda_2(\boldsymbol{n}) = \lambda_3(\boldsymbol{n}) = V.\boldsymbol{n},\ \lambda_4(\boldsymbol{n}) = V.\boldsymbol{n} + c$$

où c est la vitesse du son.

On voit qu'il faut se donner autant de conditions de Dirichlet en chaque point x de Γ qu'il y a de valeurs propres négatives pour que le problème soit localement bien posé.

On distingue habituellement les 4 cas suivants :

1.Entrée supersonique : $V.\boldsymbol{n} < 0$ et $|V.\boldsymbol{n}| > c$

On a alors :

$$\lambda_1(\boldsymbol{n}) < \lambda_2(\boldsymbol{n}) = \lambda_3(\boldsymbol{n}) < \lambda_4(\boldsymbol{n}) \leq 0$$

donc quatre conditions à imposer, par exemple $\rho, \rho u, \rho v, p$

2.Sortie supersonique : $V.\boldsymbol{n} > 0$ et $|V.\boldsymbol{n}| > c$

On a alors :

$$0 \leq \lambda_1(\boldsymbol{n}) < \lambda_2(\boldsymbol{n}) = \lambda_3(\boldsymbol{n}) < \lambda_4(\boldsymbol{n})$$

donc aucune condition à imposer (sortie libre)

3.Entrée subsonique : $V.\boldsymbol{n} < 0$ et $|V.\boldsymbol{n}| < c$

On a alors :

$$\lambda_1(\boldsymbol{n}) < \lambda_2(\boldsymbol{n}) = \lambda_3(\boldsymbol{n}) \leq 0 \leq \lambda_4(\boldsymbol{n})$$

donc trois conditions à imposer.

4.Sortie subsonique : $V.\boldsymbol{n} > 0$ et $|V.\boldsymbol{n}| < c$

On a alors

$$\lambda_1(\boldsymbol{n}) \leq 0 \leq \lambda_2(\boldsymbol{n}) = \lambda_3(\boldsymbol{n}) < \lambda_4(\boldsymbol{n})$$

donc une seule condition à imposer (en général la pression)

Et finalement le cas de l'écoulement glissant sur une paroi : $(V.\boldsymbol{n} = 0)$: 1 condition, $V.\boldsymbol{n} = 0$

2.2. Solution faible et solution entropique.

Rappelons qu'un problème hyperbolique non linéaire n'a pas toujours de solution classique définie pour tout $t > 0$ même si la condition initiale est très régulière. En effet le caractère hyperbolique des équations conduit à des solutions discontinues. P.D. Lax [49] a introduit la notion de solution faible, qui vérifie:

$$\int\int_{\Omega\times]0,+\infty[} \left(\Phi_t U + \vec{\nabla}\Phi.\vec{\mathbb{F}}(U)\right)(x,y;t)\,dS\,dt \;+\; \int_{\Omega} \Phi(x,y;0)\,U_0(x,y)\,dS \;=0 \quad (2.5)$$

où $dS = dxdy$, $\vec{\mathbb{F}}(U) \overset{\text{noté}}{=} \begin{pmatrix} F(U) \\ G(U) \end{pmatrix}$ et Φ est une fonction définie dans $\mathbf{R}^4$, continûment différentiable et à support compact dans $\mathbf{R}^2\times]0,+\infty[$.

Dans le cas scalaire, un théorème d'unicité de la solution faible au sens défini ci-dessus vérifiant une condition d'entropie a été démontré S. N. Kruzhkov [31]; l'existence de cette solution est obtenue par des méthodes de viscosité s'appuyant essentiellement sur la vérification du principe du maximum et sur une estimation de la variation totale. Mais dans le cas général des systèmes (équations d'Euler par exemple) le problème reste ouvert, bien qu'il existe néanmoins des résultats en dimension un. Dans le cas discret, des études analogues ont été menées pour définir et déterminer si un schéma numérique est entropique, c'est-à-dire s'il y a convergence vers une solution vérifiant une condition d'entropie. On citera par exemple les travaux de Leroux [34] sur les schémas de type Godunov et ceux d'Osher sur les E-schémas [53].

DÉFINITION 1. *(Relations de Rankine et Hugoniot)*

Soit U une solution de (1.1) discontinue suivant une trajectoire régulière, définie pour tout $(x,y;t)$ et de normale $(-\nu,\boldsymbol{n})$; on note U_1 et U_2 deux états situés respectivement à gauche et à droite de la discontinuité, la relation de Rankine et Hugoniot s'écrit alors:

$$[\vec{\mathbb{F}}(U_1) - \vec{\mathbb{F}}(U_2)].\boldsymbol{n} = \nu[U_1 - U_2].$$

On peut interpréter $\boldsymbol{n}$ et ν respectivement comme la direction et la vitesse de propagation de la discontinuité.

On montre qu'il peut exister plusieurs solutions de (2.5) dont certaines n'ont aucun sens physique.

DÉFINITION 2. *(Solution entropique, [50])*

Une fonction convexe η est appelée une entropie pour le système (1.1) s'il existe deux fonctions (q_1, q_2) appelées flux d'entropie telles que:

$$\frac{d\eta(U)}{dU} \cdot \frac{dq_1(U)}{dU} = \frac{dF(U)}{dU},$$
$$\frac{d\eta(U)}{dU} \cdot \frac{dq_2(U)}{dU} = \frac{dG(U)}{dU}.$$

Une solution faible U de (1.1) est appelée une solution entropique si pour toute entropie η de flux q_1, q_2 du système (1.1), U vérifie:

$$\frac{\partial \eta(U)}{\partial t} + \frac{\partial q_1(U)}{\partial x} + \frac{\partial q_2(U)}{\partial y} \leq 0$$

au sens des distributions.

Soit $\boldsymbol{n}$ un vecteur de $\mathbb{R}^2$. On s'intéresse au problème de Riemann dans la direction $\boldsymbol{n}$, à l'instant t:

$$\begin{cases} U_t + \vec{\nabla}.\vec{\mathbb{F}}(U).\boldsymbol{n} = 0 \\ \\ U(x,y;0) = \begin{cases} U_g & \text{si } \boldsymbol{X}.\boldsymbol{n} < 0 \\ \\ U_d & \text{si } \boldsymbol{X}.\boldsymbol{n} > 0 \end{cases} \quad \text{avec} \quad \boldsymbol{X} = \begin{pmatrix} x \\ y \end{pmatrix} \end{cases} \tag{2.6}$$

On s'est ramené ainsi au cas monodimensionnel [70].

On décompose la vitesse suivant ses composantes normales V_n et tangentielles V_t. Soient $A_n(U)$ le jacobien du flux $\vec{\mathbb{F}}(U).\boldsymbol{n}$, $\Lambda_n(U)$ la matrice diagonale réelle et $P_n(U)$ la matrice de passage définies par les relations (2.3) et (2.4).
Dans le cas où le vecteur $\boldsymbol{n}$ est de norme (euclidienne) égale à un, les valeurs propres de la matrice $A_n(U)$ sont (voir annexe 1):

$V_n - c$: valeur propre simple.

V_n : valeur propre double.

$V_n + c$: valeur propre simple.

On note $\lambda_n^k(U)$ les valeurs propres et $r_n^k(U)$ les vecteurs propres à droite associés, pour $k = 1, \ldots, 4$.

DÉFINITION 3.

On dit que le $k^{ème}$ champ caractéristique est linéairement dégénéré si:

$$\frac{d\lambda_n^k(U)}{dU}.r_n^k(U) = 0$$

On dit que le $k^{ème}$ champ est vraiment non linéaire si :

$$\frac{d\lambda_n^k(U)}{dU}.r_n^k(U) \neq 0$$

dans ce cas le vecteur $r_n^k(U)$ est normalisé de sorte que

$$\frac{d\lambda_n^k(U)}{dU}.r_n^k(U) = 1$$

PROPOSITION 1.2.

Pour le système des équations d'Euler (1.1) les champs caractéristiques associés aux valeurs propres $V_n - c$ et $V_n + c$ sont vraiment non linéaires.
Les champs caractéristiques associés à la valeur propre double V_n sont linéairement dégénérés.

On rappelle que si le $k^{\text{ème}}$ champ caractéristique est vraiment non linéaire, il se crée un k-choc ou une k-détente alors qu'une discontinuité de contact est associée au champ linéairement dégénéré.
Les relations de Rankine et Hugoniot et la conservation de la quantité de mouvement impliquent la continuité des composantes tangentielles de la vitesse au passage d'un k-choc. Sur la discontinuité de contact, il peut y avoir glissement et les composantes tangentielles de la vitesse peuvent présenter une discontinuité [70].
Les chocs physiquement admissibles (entropiques) satisfont la condition suivante:

PROPOSITION 1.3. *(Conditions de choc de Lax)*

Un k-choc entre deux états U_1 et U_2 est admissible si sa vitesse ν_k vérifie:

$$\lambda^k_{\nu_k}(U_2) < \nu_k < \lambda^k_{\nu_k}(U_1)$$

$$\lambda^k_{\nu_k}(U_2) < \nu_k < \lambda^{k+1}_{\nu_k}(U_2)$$

$$et \quad \lambda^{k-1}_{\nu_k}(U_1) < \nu_k < \lambda^{k+1}_{\nu_k}(U_2)$$

Dans le cadre des équations d'Euler on a aussi le critère suivant:

PROPOSITION 1.4.

Un choc entre deux états U_1 et U_2 est admissible si l'une des trois relations suivantes est vérifiée:

(i) $p_2 > p_1$

(ii) $\rho_2 > \rho_1$

(iii) $(V_n)_1 > (V_n)_2$

DÉFINITION 4. *(Invariants de Riemann)*

On appelle k-invariant de Riemann une fonction Ψ_n telle que:

$$\frac{d\Psi_n(U)}{dU}.r^k_n = 0$$

3. Décomposition de flux

3.1. Schémas décentrés.

On considère les équations (1.1) dans le cas monodimensionnel ($p = 1$). On note $F(U)$ la fonction flux définie dans $\mathbb{R}^4$ et $A(U)$ son jacobien. Le schéma explicite conservatif à trois points du premier ordre en temps et en espace s'écrit

$$U_i^{n+1} = U_i^n - \frac{\triangle t}{\triangle x}(\Phi^n_{i+\frac{1}{2}} - \Phi^n_{i-\frac{1}{2}}) \tag{3.1}$$

où $x_i = i\triangle x$, $t^n = n\triangle t$ et $U_i^n \approx U(x_i, t^n)$.

Le schéma (3.1) est dit "à trois points" si la fonction de flux numérique Φ vérifie

$$\Phi^n_{i+\frac{1}{2}} = \Phi(U_i^n, U_{i+1}^n) \tag{3.2}$$

il est dit *compatible* avec le flux F si Φ satisfait

$$\Phi(U, U) = F(U) \qquad \text{pour tout } U$$

Définition du décentrage : Nous rappelons la définition proposée par A.Harten, P.D.Lax et B. van Leer dans [48]:

DÉFINITION 5.

Un schéma de la forme (3.1) est dite décentré s'il vérifie

(i) pour tout état $U^\star$ voisin de U et V ("état de référence")

$$\Phi(U,V) = F(U^\star) + A^+(U^\star)(U-U^\star) + A^-(U^\star)(V-U^\star) + o(|U-U^\star| + |V-U^\star|)$$

où

$$A^+ = \frac{1}{2}(A + |A|), \quad A^- = \frac{1}{2}(A - |A|), \quad |A| = T|D|T^{-1}$$

avec $D = diag.(\lambda_k)$, matrice des valeurs propres λ_k de A, et T matrice de transformation inversible. On a donc

$$D^+ = diag.(max(\lambda_k, 0)), \quad D^- = D - D^+.$$

(ii) quand les vitesses caractéristiques associées à Φ sont toutes positives, alors on a $\Phi(U,V) = F(U)$,

(iii) quand les vitesses caractéristiques associées à Φ sont toutes négatives, alors on a $\Phi(U,V) = F(V)$.

Un choix simple et possible pour $U^\star$ est de prendre $U^\star = \frac{U+V}{2}$, ainsi on obtient

$$\begin{aligned} \Phi(U,V) &= \frac{1}{2}(F(U)+F(V)) - \frac{1}{2}\left|A\left(\frac{U+V}{2}\right)\right|(V-U) + o(|V-U|) \\ &= \frac{1}{2}(F(U)+F(V)) - \frac{1}{2}d(U,V), \end{aligned} \tag{3.3}$$

où $d(U,V)$ contient les termes de viscosité et donc précise le schéma utilisé

$$d(U,V) = \left|A\left(\frac{U+V}{2}\right)\right|(V-U) + o(|V-U|); \tag{3.4}$$

la condition de compatibilité devient $d(U,U) = 0$.

3.2. Quelques exemples de décentrage.

Les différents types de décentrage sont fondés sur le principe de la partition du flux, ou sur la résolution approchée du problème de Riemann (schémas de type Godunov), les derniers cités sont construits directement à partir de cette idée.

Solveurs de Riemann

- **Le Q-schéma de van Leer** Ce schéma se construit naturellement à partir de la forme (3.4) en négligeant les termes en $o(|V-U|)$

$$d(U,V) = \left|A\left(\frac{U+V}{2}\right)\right|(V-U). \tag{3.5}$$

On remarque que pour ce schéma, lorsqu'une des valeurs propres est nulle on a une absence totale de viscosité ($d(U,V)=0$) pour le champ associée à cette valeur propre; la conséquence est que ce schéma permet de capturer exactement certains chocs stationnaires mais qu'il ne peut pas vérifier la condition d'entropie.

- **Le flux de Roe** [56] Ce schéma se construit naturellement comme un solveur de Riemann approché en calculant la solution du problème de Riemann suivant

$$U_t + \tilde{A}U_x = 0, \qquad U(x,0) = \begin{cases} U_G, & si \quad x<0 \\ U_D, & si \quad x>0 \end{cases} \tag{3.6}$$

Le terme visqueux se met alors sous la forme

$$d(U,V) = \left|\tilde{A}(U,V)\right|(V-U) \tag{3.7}$$

où $\tilde{A}$ est une matrice appellée jacobien moyen de Roe (voir [48] pour l'existence d'une telle matrice pour tout système entropique) telle que

$$\tilde{A}(U,V) = A(m(U,V)),$$

où m est une moyenne particulière de U et V [56].

- **Q-schémas** Ils sont de la forme

$$d(U,V) = Q(U,V)(V-U), \tag{3.8}$$

les schémas cités précédemment sont des Q-schémas.

- **Le flux d'Osher** [53] Il est formellement défini comme suit

$$d(U,V) = \int_U^V |A(W)|dW \tag{3.9}$$

Décomposition de flux (flux-vector splitting)

D'autres flux sont construits en généralisant à des systèmes non linéaires la décompo-

sition de flux naturelle pour une équation scalaire linéaire ($F(U) = aU$),

$$\Phi(U,V) = \begin{cases} aU & , \quad si \quad a > 0, \\ aV & , \quad sinon. \end{cases}$$

Les flux numériques s'écrivent dans le cas des systèmes non linéaires

$$\Phi(U,V) = F^+(U) + F^-(V), \tag{3.10}$$

où les flux F^+, F^- vérifient la relation de compatibilité

$$F^+(U) + F^-(U) = F(U).$$

- **Le flux de Steger-Warming** [42] La construction de ce flux utilise la propriété d'homogénéité des flux d'Euler i.e. $F(W) = A(W)W$. Ainsi, Steger et Warming posent $F^{\pm}(W) = A^{\pm}(W)W$. On relie cette décomposition au décentrage en obtenant le terme de viscosité sous la forme

$$d(U,V) = \frac{1}{2}(|A(U)| + |A(V)|)(V - U) + \frac{1}{2}(|A(U)| - |A(V)|)(V + U). \tag{3.11}$$

- **Le flux de van Leer** [51] De la même manière que pour le flux Steger-Warming, on construit le flux de van Leer en donnant sa décomposition

$$F^{\pm}(W) = F^{\pm}_{vl}(W)$$

Les flux sont homogènes et différentiables, ainsi on a

$$F^{\pm}(W) = A^{\pm}_{vl}(W)W$$

où $A^{\pm}_{vl}$ désignent les matrices jacobiennes du flux de van Leer, différentes de $A^{\pm}$. On obtient alors un décentrage de la forme (3.11).

REMARQUE 1.1.

Dans le cas linéaire à coefficients constants c'est à dire quand la matrice A est constante en espace et en particulier indépendante des états U et V, tous les flux numériques décentrés sont identiques

$$\Phi(U,V) = A^+U + A^-V$$

L'étude de stabilité linéaire ne nous permettra pas de les distinguer et de les différencier, seules les applications dans le cas non linéaire (équations d'Euler par exemple) nous permettront de le faire (stabilité non linéaire).

L'analyse de la précision d'un tel décentrage par rapport à un autre ne nous permet pas à l'heure actuelle de sélectionner le meilleur flux. Par contre, en fonction du type d'application, nous sommes capables de dire si un flux numérique donne des solutions attendues ou pas, ou bien s'il est stable. Par exemple pour les équations d'Euler, le choix du décentrage dépend en grande partie du régime de Mach de l'écoulement: lorsque le nombre de Mach est petit (10^{-3} parfois) le schéma de Roe peut être utilisé pour des raisons de précision et d'économie, quand le régime de Mach est plus grand que 3 (voire jusqu'à 25) on utilise, par exemple , la décomposition de van Leer ou bien le flux de Osher. Pour des régimes de Mach intermédiaires à ceux donnés, tous les décentrages sont stables , on choisira ceux qui sont les plus simples à mettre en oeuvre.

4. Un modèle d'équation non-linéaire: l'équation de Burgers

L'équation de Burgers s'écrit comme suit :

$$\frac{\partial u}{\partial t} + \frac{\partial}{\partial x}\left(\frac{u^2}{2}\right) = \mu u_{xx} \quad , \quad \mu > 0 \tag{4.1}$$

Cette équation est du type parabolique et peut être considérée comme une équation de la chaleur avec un terme de convection ou comme une équation d'advection non-linéaire complétée par un terme dissipatif linéaire. Dans le cas $\mu = 0$, elle est de nature hyperbolique et le caractère non linéaire du terme de convection peut conduire à l'obtention de solutions discontinues comme le montre l'exemple qui suit.
Considérons le problème de Riemann pour l'équation de Burgers non visqueuse défini par :

$$\begin{cases} \frac{\partial u}{\partial t} + \frac{\partial}{\partial x}\left(\frac{u^2}{2}\right) = 0 \\ u(x,0) = u_o(x) = \begin{cases} u_g & si \quad x < 0 \\ u_d & si \quad x > 0 \end{cases} \end{cases} \tag{4.2}$$

La solution du problème (4.2) est :

a) une détente si $u_g \leq u_d$:

$$\begin{cases} u_g & si \quad \dfrac{x}{t} \leq u_g \\ \dfrac{x}{t} & si \quad u_g < \dfrac{x}{t} < u_d \\ u_d & si \quad \dfrac{x}{t} \geq u_d \end{cases}$$

et la solution est continue;

b) un choc si $u_g > u_d$:

$$\begin{cases} u_g & si \quad \dfrac{x}{t} < \dfrac{1}{2}(u_g + u_d) \\ u_d & si \quad \dfrac{x}{t} > \dfrac{1}{2}(u_g + u_d) \end{cases}$$

et la solution est discontinue.

Exemples :

Si $u_g = -u_d$ on doit avoir $u_g > 0$ et $u_d < 0$; le choc est alors dit stationnaire (figure 1.2). Si $u_g > \frac{1}{2}(u_g + u_d) > 0 > u_d$ on a un choc transsonique (figure 1.3). Si $u_g > u_d > 0$ on a un choc supersonique (figure 1.4). Dans le cas général ($\mu \neq 0$), la solution de l'équation

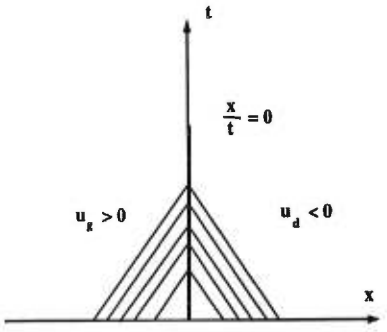

FIGURE 1.2. Choc stationnaire

de Burgers peut s'obtenir à l'aide d'un changement de variable ([69]), $u = 2\mu\frac{v_x}{v}$, (4.1) se ramène à $v_t = \mu v_{xx}$. D'autre part la présence d'un terme de diffusion ne permet pas d'obtenir de solution discontinue; toutefois, pour des valeurs faibles du coefficients de viscosité μ, les solutions peuvent présenter des profils raides (couche limite, choc visqueux).

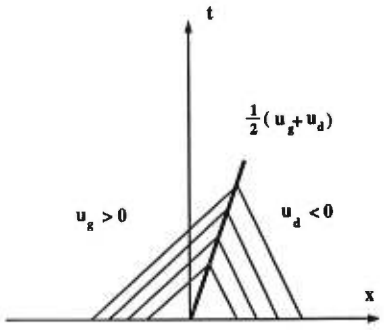

FIGURE 1.3. Choc transsonique

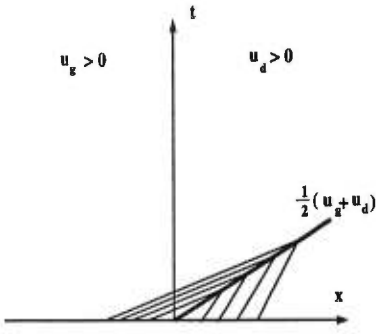

FIGURE 1.4. Choc supersonique

Chapitre 2

Méthode des volumes finis

1. Introduction

Notre propos dans ce paragraphe est de mettre en évidence les bases de la méthode des volumes finis. Pour une étude plus approfondie de cette méthode nous renvoyons le lecteur à [60].

Pour illustrer la méthode des volumes finis, nous allons considérer l'équation de Poisson

$$-\Delta u = f \tag{1.1}$$

posée dans un domaine D rectangulaire. On commence par mailler le domaine D en rectangles et on considère les points de la grille où on veut calculer la valeur de u . Une portion d'une telle grille est montrée sur la Fig 2.5. la partie hachurée est le volume fini V de faces e,w,n et s. L'équation (4.1) peut être réécrite sous la forme

$$-divJ = f \tag{1.2}$$

où

$$J = gradu \tag{1.3}$$

Le théorème de Gauss est utilisé pour intégrer (1.2) à travers le volume fini V. Ce qui nous donne

$$\int_{\partial V} J.nds + \int_V f dxdy = 0 \tag{1.4}$$

où ∂V dénote la frontière de V et n la normale à ∂V

Afin d'aboutir à l'équation discrétisée, on fait essentiellement deux hypothèses:

(i) la valeur de $J \cdot n$ sur chacune des faces du volume fini est la même, notée par J_{face} (voir Fig 2.6)

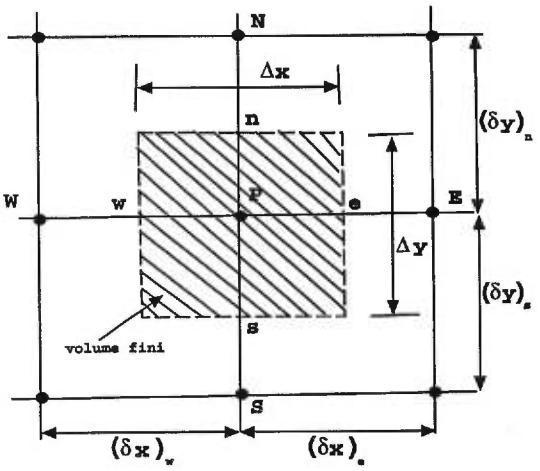

FIGURE 2.5. Volume fini

(ii) la restriction de u à un segment de la grille est un polynôme du premier degré de la variable concernée.

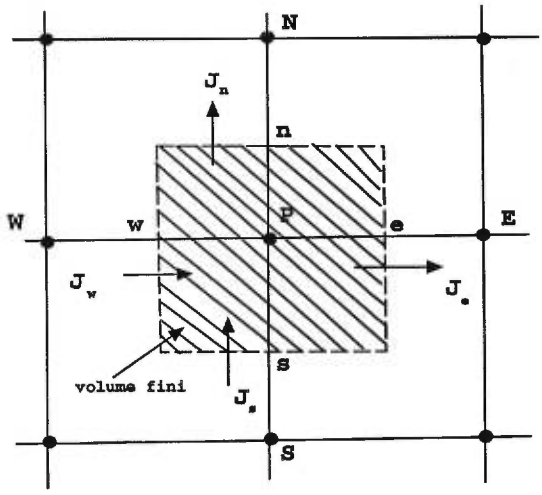

FIGURE 2.6. Calcul du flux

Avec ces deux hypothèses, l'équation discrétisée de (1.2) peut être exprimée de la manière suivante:

$$a_p u_P = a_E u_E + a_W u_W + a_N u_N + a_S u_S + b \tag{1.5}$$

où

$$\begin{cases} a_E = \frac{\Delta y}{(\delta x)_e} \\ a_W = \frac{\Delta y}{(\delta x)_w} \\ a_N = \frac{\Delta x}{(\delta y)_n} \\ a_S = \frac{\Delta x}{(\delta y)_s} \\ a_P = a_E + a_W + a_N + a_S \end{cases} \tag{1.6}$$

et b provient de la discrétisation du terme de source.

REMARQUE 2.1. *La propriété la plus attractive de la méthode des volumes finis est que la conservation de quantités telles que la masse, la quantité de mouvement et l'énergie est exactement satisfaite sur chaque groupe de volumes finis, et bien sûr sur le domaine tout entier.*

REMARQUE 2.2. *La méthode dévelopée ici n'est pas limitée à des grilles en coordonnées cartésiennes mais peut être utilisée avec une grille dans n'importe quel système de coordonnées orthogonales.*
Pour des domaines dont la géométrie est plus complexe, on peut utiliser des coordonnées curvilignes, cf. [61], *aussi* [62].
Il existe aussi des méthodes des volumes finis basées sur les éléments finis, cf. [58] .

REMARQUE 2.3. *Des schémas variés, basés sur la méthode des volumes finis, ont été développés pour le traitement des problèmes de convection-diffusion. Voir par exemple* [60] *et* [59].

2. Un lien entre la méthode des volumes finis et l'élément fini de Raviart-Thomas

Soit Ω un polygone convexe de frontière Γ et soit $f \in L^2(\Omega)$. Considérons le problème de Dirichlet suivant: trouver $u \in H^2(\Omega)/$

$$\begin{cases} -\Delta u = f \quad \text{dans} \quad L^2(\Omega) \\ \quad u = g \quad sur \quad \Gamma \end{cases} \tag{2.1}$$

où $g \in H^2(\Omega)$. (On désigne par $\Gamma = \partial\Omega$ la frontière de Ω).

2.1. Existence, unicité et régularité de la solution.

2.1.1. Dans un premier temps, $g = 0$.

On cherche

$$u \in H^2(\Omega) \cap H_0^1(\Omega) \ / \ -\Delta u = f \tag{2.2}$$

Alors

$$\forall v \in V = H_0^1(\Omega) \ , \ -\int_\Omega v\Delta u \, dx = \int_\Omega fv \, dx.$$

Appliquant la formule de Green

$$\int_\Omega \left(v\frac{\partial}{\partial x_k}\frac{\partial u}{\partial x_k} + \frac{\partial v}{\partial x_k}\frac{\partial u}{\partial x_k} \right) dx = \int_\Gamma v\frac{\partial u}{\partial n_k} d\Gamma = 0.$$

Il vient (puisque $v_{/\Gamma} = 0$)

$$-\int_\Omega v\Delta u \, dx = \sum_{k=1}^{n} \int_\Omega \frac{\partial v}{\partial x_k}\frac{\partial u}{\partial x_k} \, dx = \int_\Omega \vec{\nabla} v \cdot \vec{\nabla} u \, dx.$$

Alors u solution de (2.2) vérifie

$$\begin{cases} u \in V = H_0^1(\Omega)/ \\ \int_\Omega \vec{\nabla} u \cdot \vec{\nabla} v \, dx = \int_\Omega fv \, dx, \quad \forall v \in V. \end{cases} \tag{2.3}$$

Réciproquement, si u vérifie (2.3) alors $\forall \phi \in \mathcal{C}_0^\infty(\Omega) \subset V$ on a au sens des distributions

$$\int_\Omega \vec{\nabla} u \cdot \vec{\nabla} \phi \, dx = -\langle \Delta u, \phi \rangle = \langle f, \phi \rangle$$

donc $-\Delta u = f$ dans $\mathcal{D}'(\Omega)$, mais puisque $f \in L^2(\Omega)$, cette égalité est vraie dans $L^2(\Omega)$. Comme $u \in V, u_{/\Gamma} = 0$ (au sens du théorème de trace sur Γ). D'autre part $u \in H_0^1(\Omega)$ et $\Delta u \in L^2(\Omega)$ alors $u \in H^2(\Omega)$ d'après le théorème de Lions.

On a donc prouvé l'équivalence des problèmes (2.2) et (2.3), on va montrer l'existence et l'unicité de la solution du problème (2.3). On cherche $u \in V \ / \ a(u,v) = L(v) \quad \forall u \in V$, où

$$a(u,v) = \int_\Omega \vec{\nabla} u \cdot \vec{\nabla} v \, dx$$

est (d'après l'inégalité de Poincaré) un produit scalaire sur l'espace de Hilbert $V = H_0^1(\Omega)$, donc a est une forme bilinéaire continue (par Cauchy-Schwarz) et coercive sur V (puisque $a(u,u) = \|u\|^2$), et $L(v) = \int_\Omega fv \, dx$ est clairement une forme linéaire continue sur V.

$$(|L(v)| \leq \|f\|_{L^2} \cdot \|v\|_{L^2} \leq \|f\|_{L^2} \cdot \|v\|_V).$$

Alors, d'après le théorème de Lax-Milgram, il y a existence et unicité de u vérifiant (2.2).

2.1.2. Existence et unicité de la solution de (2.1).

$$u \in H^2(\Omega)/ \begin{cases} -\Delta u = f \text{ dans } L^2(\Omega) \\ u_{/\Gamma} = g_{/\Gamma} \text{ où } g \in H^2(\Omega). \end{cases} \tag{2.4}$$

Posons $\tilde{u} = u - g$. $\tilde{u} \in H^2(\Omega) \cap H_0^1(\Omega)$ et vérifie $-\Delta\tilde{u} = f + \Delta g$. Alors il y a existence et unicité de $\tilde{u}$ d'après (2.1.1) et donc de $u = \tilde{u} + g$.

2.1.3. Régularité.

Dans le cas qui nous intéresse $n = 2$, comme $u \in H^2(\Omega)$, alors u est continue sur $\bar{\Omega}$

$$\left(H^m(\Omega) \subset \mathcal{C}(\bar{\Omega}) \text{ si } m > \frac{n}{2}\right).$$

3. Formulation mixte du problème continu (2.1)

Une formulation mixte du problème (2.1) avec $g = 0$ est basée sur l'introduction de la variable $p = grad\ u$. Alors l'équation $-\Delta u = f$ devient $div\ p = -f$. D'où la formulation variationnelle mixte du problème (2.1):

$$\begin{cases} \text{trouver} \quad (p,u) \in H(div;\Omega) \times L^2(\Omega) \quad \text{tel que} \\ \int_\Omega p \cdot q dx + \int_\Omega u\ div\ q dx = 0 \qquad \forall q \in H(div;\Omega) \\ \int_\Omega v\ div\ p dx = -\int_\Omega f v dx \qquad \forall v \in L^2(\Omega). \end{cases} \tag{3.1}$$

3.1. Les espaces $H(div;\Omega)$.

Nous supposons dans ce paragraphe que Ω est un ouvert borné de $\mathbb{R}^N$ de frontière Γ lipschitzienne.

Pour toute fonction vectorielle $v = (v_1, \ldots, v_N)$, la divergence de v est le scalaire défini par

$$divv = \sum_{i=1}^{N} \frac{\partial v_i}{\partial x_i}$$

Nous introduisons les espaces suivants:

$$H(div;\Omega) = \{v \in (L^2(\Omega))^N \quad ; \quad divv \in L^2(\Omega)\}$$

qui est un espace de Hilbert pour la norme :

$$\| v \|_{H(div;\Omega)} = \left\{ \| v \|^2_{0,\Omega} + \| divv \|^2_{0,\Omega} \right\}^{\frac{1}{2}}$$

THÉORÈME 2.1. *Le problème (3.1) admet une solution unique* $(p,u) \in H(div;\Omega) \times L^2(\Omega)$. *De plus, u est solution de (2.4) et* $p = grad\ u$

Démonstration cf. [63].

Par la suite, on s'intéresse à l'approximation du problème (3.1) par la méthode des éléments finis.

Soient Q_h et V_h deux espaces de dimension finie tels que $Q_h \subset H(div;\Omega)$ et $V_h \subset L^2(\Omega)$. Alors le problème approché du problème (3.1) est de

$$\begin{cases} \text{trouver} \quad (p_h, u_h) \in Q_h \times V_h \quad \text{tel que} \\ \int_\Omega p_h \cdot q_h dx + \int_\Omega u_h \ div\ q_h dx = 0 \qquad \forall q_h \in Q_h \\ \int_\Omega v_h \ div\ p_h dx = -\int_\Omega f v_h dx \qquad \forall v_h \in V_h. \end{cases} \tag{3.2}$$

REMARQUE 2.4. *Les espaces* Q_h *et* V_h *doivent être construits de telle manière que la condition inf-sup (connue sous le nom de la condition de Babuska-Brezzi) et la coercivité sur le noyau soient vérifiées,(cf.*[64],[65]*).*

Avant la construction des espaces Q_h et V_h, commençons tout d'abord par préciser quelques notations qu'on peut trouver dans [66].

On considère une décomposition T_h de $\bar{\Omega}$ en quadrilatères convexes

$$\bar{\Omega} = \bigcup_{K \in T_h} \bar{K}$$

Soit $\hat{K}$ le carré unité $[0,1]^2$ et soit K un quadrilatère convexe quelconque. Il existe une transformation F_K qui transforme $\hat{K}$ en K.

On définit $Q_k(\hat{K})$ $(k \geq 0)$ comme étant l'espace des polynômes de degré inférieur ou égal à k en chacune des variables $\hat{x}_1$ et $\hat{x}_2$.

On note par

$$h_K = \text{ longueur du plus grand côté de } K \tag{3.3}$$

$$h = \max_{K \in T_h} h_K. \tag{3.4}$$

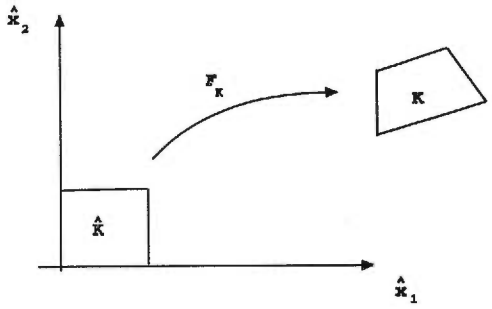

FIGURE 2.7. Transformation

Pour définir l'espace Q_h, on commence par définir

$$\hat{D} = \{(a_0 + a_1\hat{x}_1, b_0 + b_1\hat{x}_2), a_i, b_i \in \mathbb{R}, i = 0, 1\} \tag{3.5}$$

et l'ensemble $\hat{\Sigma}$ des degrés de liberté suivants:

$$\int_{\hat{e}} \hat{q} \cdot \hat{n} d\hat{s} \qquad \forall \hat{e} \in \partial\hat{K}, \quad \text{pour} \quad \hat{q} \in \hat{D} \tag{3.6}$$

où $\hat{e}$ est un côté de la frontière $\partial\hat{K}$ de $\hat{K}$ et $\hat{n}$ est la normale extérieure à $\partial\hat{K}$.
Il est facile de montrer que $(\hat{K}, \hat{D}, \hat{\Sigma})$ est un élément fini.
Maintenant, pour passer de l'élément de référence $\hat{K}$ à l'élément courant K , on utilise la transformation de Piola:

$$q = F_K\hat{q} \quad \Longleftrightarrow q \circ F_K = \frac{1}{J} DF_k\hat{q} \tag{3.7}$$

où DF_k est la matrice jacobienne associée à F_k et J est le jacobien de la transformation F_k (qui n'est autre que le déterminant de DF_K). L'espace Q_h est alors défini par

$$Q_h = \{q \in H(div; \Omega); \quad q|_K = F_K\hat{q}, \quad \hat{q} \in \hat{D}, \quad \forall K \in T_h\} \tag{3.8}$$

tandis que l'espace V_h est défini par

$$V_h = \{v \in L^2(\Omega); v|_K \circ F_K = \hat{v} \in Q_0(\hat{K}), \quad K \in T_h\} \tag{3.9}$$

THÉORÈME 2.2. *Le problème (3.2) (Q_h et V_h étant définis par (3.8) et (3.9)) possède une solution unique, De plus, si $u \in H^2(\Omega)$ et $\Delta u \in H^1(\Omega)$ alors*

$$\| p - p_h \|_{H(div;\Omega)} + \| u - u_h \|_{0,\Omega} \leq Ch\{|u|_{1,\Omega} + |u|_{2,\Omega} + |\Delta u|_{1,\Omega}\}. \tag{3.10}$$

Démonstration cf. [63] et [67] .

Maintenant, revenons aux degrés de liberté de l'élément fini de RAVIART-THOMAS On voit facilement l'analogie avec la méthode des volumes finis (voir Fig.2.6).

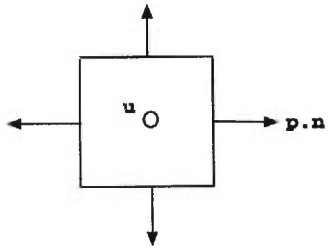

FIGURE 2.8. L'élément Q_o

Nous pouvons montrer qu'en utilisant une formule de quadrature adéquate pour le terme $\int_K p \cdot q \, dx$, on aboutit à la même équation discrétisée (1.5). En effet; considérons un domaine rectangulaire Ω et une triangulation uniforme T_h de $\bar{\Omega}$ en rectangles K. Notons par e_1, e_2, e_3 et e_4 les côtés d'un élément courant K de la triangulation T_h (voir Fig.2.9)

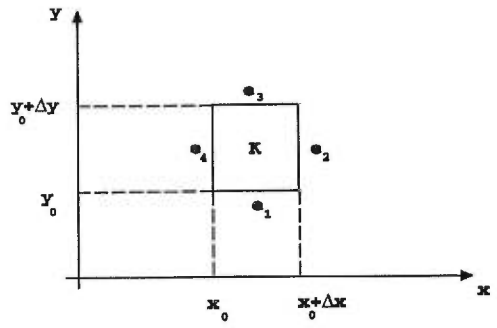

FIGURE 2.9. Les faces d'un élément K

Les fonctions de bases de l'espace Q_h (défini par (3.8)) dont les restrictions à K ne sont pas identiquement nulles sont données par les expressions suivantes:

$$\begin{cases} p_1 = (0, \dfrac{1}{\Delta x \Delta y}(y - y_0 - \Delta y)), \\ p_2 = (\dfrac{1}{\Delta x \Delta y}(x - x_0), 0), \\ p_3 = (0, \dfrac{1}{\Delta x \Delta y}(y - y_0)), \\ p_4 = (\dfrac{1}{\Delta x \Delta y}(x - x_0 - \Delta x), 0). \end{cases} \tag{3.11}$$

Les expressions (3.11) viennent du fait que les p_i, $1 \leq i \leq 4$, sont définies par

$$p_i = (a_i + b_i x, c_i + d_i y)$$

telles que

$$\int_{e_j} p_i \cdot n ds = \delta_{ij} \quad , \quad 1 \leq i, j \leq 4$$

où n est la normale unitaire extérieure à K et $\delta_{ij} = \begin{cases} 1 & \text{si} \quad i = j \\ 0 & \text{si} \quad i \neq j \end{cases}$

La matrice élémentaire qui provient du calcul de $\int_K p \cdot q \, dx$ par la formule du trapèze est donnée par

$$\begin{pmatrix} \frac{1}{2}\frac{\Delta y}{\Delta x} & 0 & 0 & 0 \\ 0 & \frac{1}{2}\frac{\Delta x}{\Delta y} & 0 & 0 \\ 0 & 0 & \frac{1}{2}\frac{\Delta y}{\Delta x} & 0 \\ 0 & 0 & 0 & \frac{1}{2}\frac{\Delta x}{\Delta y} \end{pmatrix}$$

Maintenant, les éléments de la triangulation T_h voisins de K qui interviennent dans le calcul du système (3.2) sont montrés sur la Fig.2.10. Tout calcul fait,on obtient

$$\begin{cases} \frac{\Delta y}{\Delta x}\alpha_1 + u_P - u_S = 0 \\ \frac{\Delta x}{\Delta y}\alpha_2 + u_P - u_E = 0 \\ \frac{\Delta y}{\Delta x}\alpha_3 + u_P - u_N = 0 \\ \frac{\Delta x}{\Delta y}\alpha_4 + u_P - u_W = 0 \\ \alpha_1 + \alpha_2 + \alpha_3 + \alpha_4 + b = 0 \end{cases} \tag{3.12}$$

où α_i , $1 \leq i \leq 4$, est le degré de liberté correspondant à la composante normale de p sur le côté e_i et b provient de l'intégration du second membre f. Finalement, en

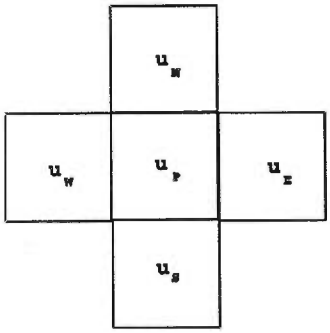

FIGURE 2.10. Les éléments voisins de K

exprimant les α_i , $1 \leq i \leq 4$, à partir des quatre premières équations de (3.12) et en les reportant dans la dernière équation de (3.12) on obtient

$$a_P u_P = a_E u_E + a_W u_W + a_N u_N + a_S u_S + b \tag{3.13}$$

où

$$\begin{cases} a_E = a_w = \frac{\Delta y}{\Delta x} \\ a_N = a_S = \frac{\Delta x}{\Delta y} \\ a_P = a_E + a_W + a_N + a_S \end{cases} \tag{3.14}$$

L'équation (3.13) et les relations (3.14) ne sont autres que (1.5) et (1.6) dans le cas où le maillage est uniforme.

REMARQUE 2.5. *L'élément fini que nous avons présenté dans ce paragraphe est l'élément de RAVIART-THOMAS de plus bas degré. Pour des degrés plus élevés et pour une décomposition de $\bar{\Omega}$ en triangles, nous renvoyons le lecteur à* [63] *et* [68].

4. Equivalence entre les formulations volumes finis et éléments finis pour l'équation de convection-diffusion

Soit Ω un ouvert de $\mathbb{R}^2$, de frontière Γ. Soit $\overrightarrow{V}$ un champ de vecteur donné, $f \in L^2(\Omega)$ et μ constante positive.

Considèrons le problème de convection-diffusion suivant:

$$\begin{cases} -\mu \Delta u + div(\overrightarrow{V} u) = f \quad \text{dans} \quad \Omega \\ u = 0 \quad \text{sur} \quad \Gamma \end{cases} \tag{4.1}$$

Soit $\mathcal{T}_h$ une triangulation donnée, on définit le maillage dual $\mathcal{C}_h$ de $\mathcal{T}_h$. On note $C_i, i = 1, \cdots, ns$ les éléments de $\mathcal{C}_h$. Pour la construction de $\mathcal{C}_h$, on a les propriétés suivantes:

(i) $\bigcup_{i=1}^{ns} C_i = \Omega$

(ii) $C_i \cap C_j = \emptyset \quad \forall i \neq j$

(iii) C_i est fermé et connexe

(iv) $a_i \in C_i \quad i = 1, \cdots, ns.$

Dans notre cas, chaque élément C_i sera un domaine polygonal construit par les milieux de triangles voisins à a_i (voir figure (2.11)). Dans ce cas spécial C_i est appelée région barycentrique. On doit maintenant présenter le schéma volumes finis de Galerkin pour

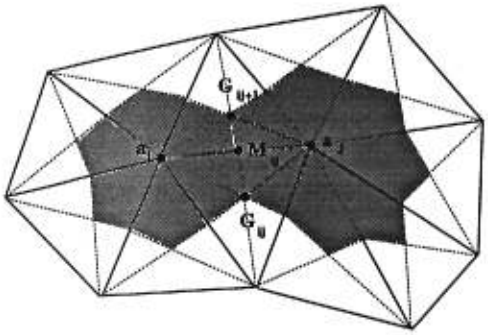

FIGURE 2.11. Cellules barycentriques autour des sommets $\mathbf{a_i}$, $\mathbf{a_j}$

l'équation de convection-diffusion. Après multiplication de l'équation 4.1 par la fonction caractéristique χ_i de la cellule C_i, nous l'intégrons sur le domaine Ω et nous utilisons la formule de Green pour obtenir l'intégrale sur le bord de C_i

$$\int_\Omega \left(div(\overrightarrow{V}u) - \mu\Delta u \right) \chi_i dxdy = \int_\Omega f\chi_i dxdy \tag{4.2}$$

$$\int_{\partial C_i} \left(u\overrightarrow{V}\cdot\overrightarrow{n} - \mu\overrightarrow{\nabla}\cdot\overrightarrow{n} \right) d\sigma = \int_{C_i} f dxdy \tag{4.3}$$

Dans la méthode de volumes finis, la fonction u_h est approchée par une fonction constante sur chaque cellule C_i. Pour calculer le gradient de u_h sur le bord de la cellule, nous lissons la fonction inconnue au voisinage du contour ∂C_i, en choisissant u_h comme fonction linéaire par morceau de la forme

$$u_h = \sum_{i=1}^{ns} u_i \phi_i$$

où ϕ_i est la fonction linéaire par morceau associée au sommet a_i (voir figure 2.12). On rappelle que les fonctions de bases associées au triangle T de sommets $a_i a_j a_k$ (voir figure 2.13) sont données par

$$\phi_i^T = 1 - ((y_k - y_i)(x - x_i) + (x_j - x_k)(y - y_i))/V^T$$

$$\phi_j^T = ((y_k - y_i)(x - x_i) + (x_i - x_k)(y - y_i))/V^T$$

$$\phi_k^T = ((y_i - y_j)(x - x_i) + (x_j - x_i)(y - y_i))/V^T$$

où $V^T = (x_j - x_i)(y_k - y_i) - (x_k - x_i)(y_j - y_i) = 2mes(T)$. Nous pouvons définir le gradient $\overrightarrow{\nabla}u$ de u par

$$\overrightarrow{\nabla u} = \sum_{i=1}^{ns} u_i \overrightarrow{\nabla}\phi_i(x,y) = \sum_{i=1}^{ns} u_i \left(\sum_{m\in k_T(i)} \overrightarrow{\nabla}\phi_i^m(x,y) \right)$$

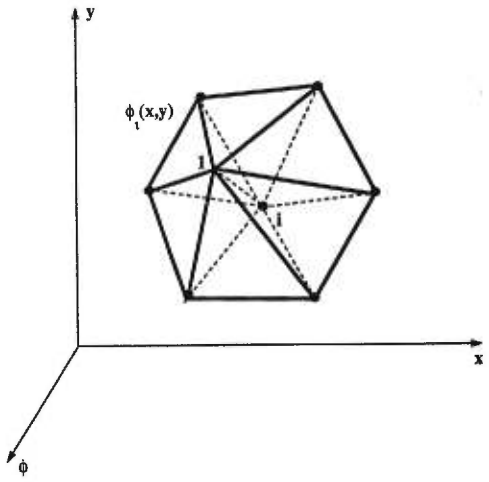

FIGURE 2.12. Fonction de base

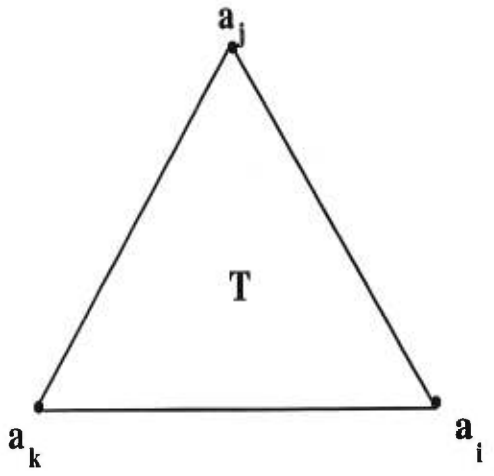

FIGURE 2.13. Triangle T de sommets $a_i a_j a_k$

où

$$\overrightarrow{\nabla}\phi_i^T = \left(-\frac{(y_k - y_j)}{V^T}, -\frac{(x_j - x_k)}{V^T}\right)$$
$$\overrightarrow{\nabla}\phi_j^T = \left(\frac{(y_k - y_i)}{V^T}, \frac{(x_i - x_k)}{V^T}\right)$$
$$\overrightarrow{\nabla}\phi_k^T = \left(\frac{(y_i - y_j)}{V^T}, -\frac{(x_j - x_i)}{V^T}\right)$$

et $k_T(i)$ est l'ensemble des triangles voisins du sommet i.

Pour obtenir l'équation suivante, prenons la valeur moyenne de la quantité $\overrightarrow{V}u$ pour chaque $\partial C_i \cap \partial C_j$:

$$\sum_{j\in K(i)} \left(\overrightarrow{V}u\right)_I \int_{\partial C_i \cap \partial C_j} \overrightarrow{n}\, d\sigma - \mu \sum_{j\in K(i)\cup\{i\}} u_j \int_{\partial C_i} \overrightarrow{\nabla}\phi_j \cdot \overrightarrow{n}\, d\sigma = \int_{C_i} f dxdy \quad (4.4)$$

où I est le milieu de l'arête $a_i a_j$. Pour compléter le schéma, nous utilisons les approximations suivantes:

$$\begin{cases} \left(\overrightarrow{V}u\right)_I \simeq \frac{1}{2}\left(\overrightarrow{V}_i u_i + \overrightarrow{V}_j u_j\right) \\ \int_{C_i} f dxdy \simeq f_i \text{mes}(C_i) \end{cases} \quad (4.5)$$

Nous rappellons la formulation pour le schéma de Lagrange-Galerkin pour l'équation de convection-diffusion

$$\sum_{T\in\mathcal{T}_h} \left(-\int_T u_h \overrightarrow{V}\cdot\overrightarrow{\nabla}\phi_i dxdy + \mu \int_T \overrightarrow{\nabla}u_h \overrightarrow{\nabla}\phi_h dxdy\right) = \sum_{T\in\mathcal{T}_h} \int_T f\phi_i dxdy \quad (4.6)$$

Nous considérons la formule de quadrature, pour approcher les intégrales ci-dessus:

$$\int_T \phi(x,y)dxdy \simeq \frac{mes(T)}{3}\sum_{i=1}^{3}\phi(a_i^T) \quad (4.7)$$

LEMME 4.1. *Les schémas (4.4-4.5) et (4.6-4.7) sont identiques*

Preuve

Pour le terme source nous avons :

$$\sum_{T\in\mathcal{T}_h} \int_T f\phi_i dxdy = \sum_{T\in\mathcal{T}_h} \frac{mes(T)}{3}\sum_{l=1}^{3}(f\phi_i)(a_i^T) = f_i \text{mes}(C_i) \simeq \int_{C_i} f dxdy$$

Pour le terme de diffusion nous avons:

La normale sortante à la cellule est intégrée sur chaque triangle (voir figure 2.14) :

$$\int_{C_i\cap T} \overrightarrow{n_i}\, d\sigma = (\overrightarrow{I_{ij}G_T}^{\perp} + \overrightarrow{G_T I_{ik}}^{\perp})$$

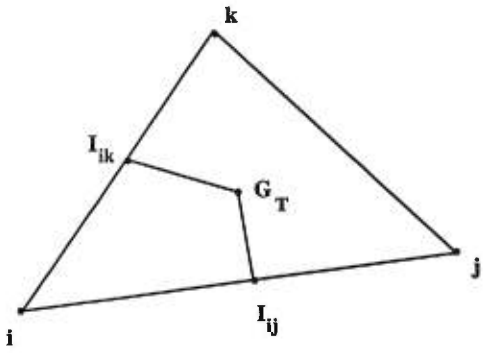

FIGURE 2.14. Détails d'un triangle

Notons que $\overrightarrow{\phi_i^T}$ s'écrit aussi (voir figure 2.14)

$$\overrightarrow{\phi_i^T} = \frac{-1}{mes(T)}(\overrightarrow{I_{ij}G_T}^{\perp} + \overrightarrow{G_T I_{ik}}^{\perp}) = \frac{-1}{mes(T)} \int_{\partial C_i \cap T} \overrightarrow{n_i} d\sigma$$

donc

$$\int_{\partial C_i \cap T} \overrightarrow{n_i} d\sigma = -mes(T)\overrightarrow{\phi_i^T}$$

Et pour le terme de convection (voir [57]), on utilise le résultat géométrique suivant, dû en particulier au choix du volume de contrôle:

$$\int_{\partial C_i \cap \partial C_j} \overrightarrow{n} d\sigma = -2 \int_{\Omega} \phi_i \overrightarrow{\nabla} \phi_i dx dy$$

et les relations

$$\sum_{j \in k(i)} \int_{\Omega} \phi_i \overrightarrow{\nabla} \phi_j dx = 0, \quad \int_{\Omega} \overrightarrow{\nabla} \phi_i dx = 0, \quad \int_T \phi_j dx = \frac{1}{3} mes(T)$$

Ainsi dans le cas d'une approximation centrée, les termes hyperboliques des deux formulations sont identiques.

Chapitre 3

Généralisation du schéma de Nessyahu-Tadmor

1. Approximation

1.1. Rappel du schéma de Nassyahu-Tadmor.

C'est un schéma de type van Leer construit sur le schéma de Lax-Friedrichs. Pour

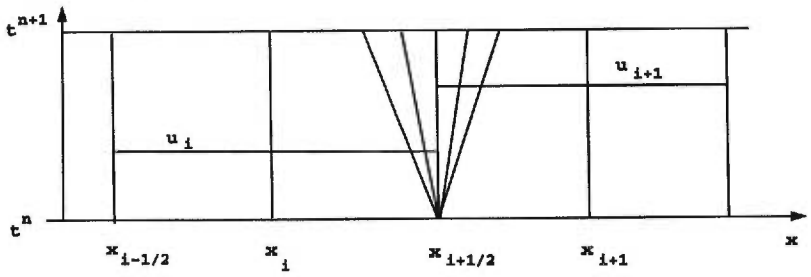

FIGURE 3.15. Problème de Riemann en $x_{i+\frac{1}{2}}$

résoudre la loi de conservation scalaire

$$u_t + (f(u))_x = 0 \tag{1.1}$$

Le schéma de Lax-Friedrichs consiste à approcher

$$u_t(x_{i+\frac{1}{2}}, t^n)$$

par

$$\frac{(u_{i+\frac{1}{2}}^{n+1} - \frac{u_i^n + u_{i+1}^n}{2})}{\triangle t}$$

et

$$f(u(x_{i+\frac{1}{2}}, t^n))_x$$

par

$$\frac{(f(u_{i+1}^n) - f(u_i^n))}{\triangle t}$$

d'où :

$$u_{i+\frac{1}{2}}^{n+1} = \frac{1}{2}(u_i^n + u_{i+1}^n) - \lambda(f(u_{i+1}^n) - f(u_i^n))$$

Mais il s'interprète aussi comme la résolution d'un problème de Riemann en $x_{i+\frac{1}{2}}$ avec intégration de l'équation (1.1) sur $(x_i, x_{i+1}) \times (t^n, t^{n+1})$.

Le deuxième pas du schéma de Lax-Friedrichs s'écrit de même sur une grille décallée:

$$u_i^{n+2} = \frac{1}{2}(u_{i-\frac{1}{2}}^{n+1} + u_{i+\frac{1}{2}}^{n+1}) - \lambda(f(u_{i+\frac{1}{2}}^{n+1}) - f(u_{i-\frac{1}{2}}^{n+1}))$$

où $\lambda = \frac{\triangle t}{\triangle x}$

Pour le schéma de Nassyahu-Tadmor on considère une approximation linéaire par morceaux de la solution

$$u(x, t^n) \simeq u_i^n + \frac{x - x_i}{\triangle x}\delta_i^n \quad , \quad x \in (x_{i-\frac{1}{2}}, x_{i+\frac{1}{2}})$$

on définit $u_{i+\frac{1}{2}}^{n+1}$ comme la valeur moyenne de la solution du problème de Riemann généralisé sur (x_i, x_{i+1}). On écrit le schéma en intégrant (1.1) sur $(x_i, x_{i+1}) \times (t^n, t^{n+1})$:

$$\int_{t^n}^{t^{n+1}} \int_{x_i}^{x_{i+1}} (u_t + (f(u))_x) dt dx = 0$$

ce qui implique

$$\triangle x u_{i+\frac{1}{2}}^{n+1} - (\int_{x_i}^{x_{i+\frac{1}{2}}} u(x, t^n) dx + \int_{x_{i+\frac{1}{2}}}^{x_{i+1}} u(x, t^n) dx)$$

$$+ \int_{t^n}^{t^{n+1}} f(u(x_{i+1}, t)) dt - \int_{t^n}^{t^{n+1}} f(u(x_i, t)) dt = 0$$

Sur $(x_i, x_{i+\frac{1}{2}})$, $u(x, t^n) = u_i^n + \frac{x - x_i}{\triangle x}\delta_i^n$

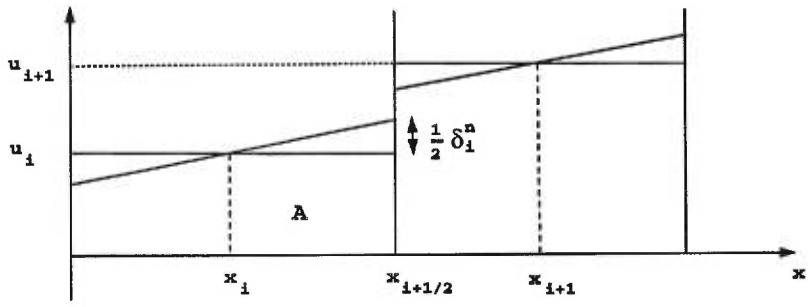

FIGURE 3.16. L'estimation de l'aire A

donc il s'agit pour calculer

$$\int_{x_i}^{x_{i+\frac{1}{2}}} u(x, t^n) dx$$

d'évaluer l'aire A :

$$A = \frac{\triangle x}{2} u_i^n + \frac{\triangle x}{8} \delta_i^n$$

On approche ensuite

$$\frac{1}{\triangle t} \int_{t^n}^{t^{n+1}} f(u(x_i, t))dt \approx f(u(x_i, t^{n+\frac{1}{2}}))$$

puis

$$u(x_i, t^{n+\frac{1}{2}}) \approx u(x_i, t^n) + \frac{\triangle t}{2} u_t(x_i, t^n)$$

d'après (1.1) on a

$$u(x_i, t^{n+\frac{1}{2}}) \approx u_i^n - \frac{\triangle t}{2} f'(u_i^n) \frac{\delta_i^n}{\triangle x}$$

expression que l'on note $u_i^{n+\frac{1}{2}}$.

REMARQUE 3.1.

On peut choisir pour approcher $f(u(x_i, t^n))_x$ par une autre expression que

$$f'(u_i^n) \frac{\delta_i^n}{\triangle x}$$

On déduit de ce qui précède le premier pas du schéma :

$$u_{i+\frac{1}{2}}^{n+1} = \frac{u_i^n + u_{i+1}^n}{2} + \frac{\delta_i^n - \delta_{i+1}^n}{8} - \lambda(f(u_{i+1}^{n+\frac{1}{2}}) - f(u_i^{n+\frac{1}{2}}))$$

et de même manière le second pas :

$$u_i^{n+2} = \frac{u_{i-\frac{1}{2}}^{n+1} + u_{i+\frac{1}{2}}^{n+1}}{2} + \frac{\delta_{i-\frac{1}{2}}^n - \delta_{i+\frac{1}{2}}^n}{8} - \lambda(f(u_{i+\frac{1}{2}}^{n+\frac{3}{2}}) - f(u_{i-\frac{1}{2}}^{n+\frac{3}{2}}))$$

N.B. On peut procéder comme le schéma de van Leer et choisir

$$\delta_i^n = \frac{u_{i+1}^n - u_{i-1}^n}{2}$$

puis corriger les pentes en prenant

$$\delta_i^n = \text{MinMod}\{u_{i+1} - u_i, u_i - u_{i-1}\}$$

où

$$\text{MinMod} = \frac{sign(a) + sign(b)}{2} \min(|a|, |b|)$$

1.2. Généralisation du schéma de L.F en dimension deux.

En dimension un , on utilise deux maillages décalés, l'un centré sur $x_{i+\frac{1}{2}}$, et l'autre centré sur x_i.

On définit, en dimension deux, sur un maillage triangulaire non structuré, les deux maillages de la façon suivante:

Cela consiste à définir une subdivision $\mathcal{T}_h$ de Ω par des triangles

$$\Omega = \bigcup_{i=1}^{N_e} K_i \ ; \ K_i \in \mathcal{T}_h,$$

et

$$K \cap K' = \begin{cases} \phi \\ 1 \text{ sommet} \qquad \text{ceci pour } K, K' \in \mathcal{T}_h \\ 1 \text{ côté} \end{cases}$$

Les noeuds de la triangulation sont les sommets des triangles.

Les degrés de liberté sont les valeurs de l'inconnues u aux noeuds.

On note

$$\begin{cases} u_i^n = u(a_i, t^n) \quad \text{et} \quad u_{ij}^n = u(M_{ij}, t^n) \\ a_i \quad \text{sommet} \end{cases}$$

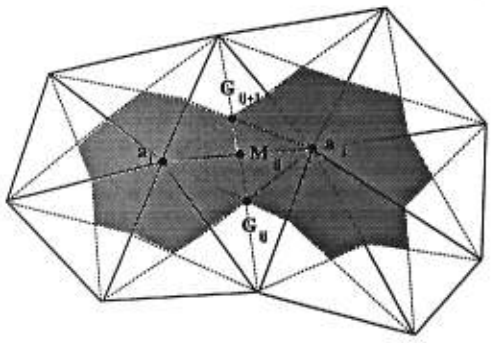

FIGURE 3.17. Cellules barycentriques autour des sommets $\mathbf{a_i}$, $\mathbf{a_j}$

On construit le premier maillage centré sur les sommets a_i avec les cellules barycentriques C_i. Le contour de C_i est défini en joingnant les milieux des côtés adjacents à a_i et les centres de gravité des triangles dont a_i est sommet.

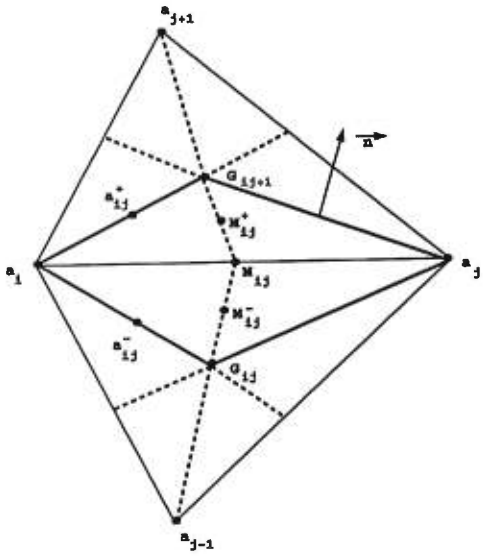

FIGURE 3.18. Cellules L_{ij} $(\mathbf{a_i G_{ij} a_j G_{i,j+1}})$.

On construit le second maillage centré sur les milieu M_{ij} avec des parallélogrammes L_{ij}. Le contour L_{ij} est défini en joingnant les sommets a_i et a_j dont M_{ij} est milieu avec les centres de gravité des triangles dont $a_i a_j$ est un côté.

On aura besoin par la suite des vecteurs normaux (unitaires) à certaines arêtes du maillage.

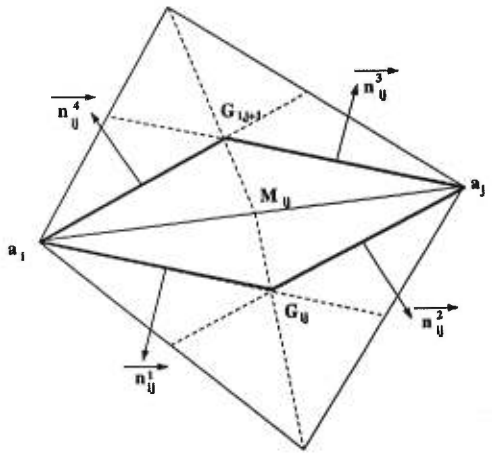

FIGURE 3.19. Le bord de la cellule L_{ij}

$$\vec{\nu}_{ij}^{\,k} = \begin{pmatrix} \nu_{ijx}^k \\ \nu_{ijy}^k \end{pmatrix} \text{ pour } k = 1,2, \quad \vec{n}_{ij}^{\,k} = \begin{pmatrix} n_{ijx}^k \\ n_{ijy}^k \end{pmatrix} \text{ pour } k = 1,\ldots,4$$

et

$$\vec{\eta}_{ij} = \begin{pmatrix} \eta_{ijx} \\ \eta_{ijy} \end{pmatrix}, \quad \vec{\theta}_{ij} = \begin{pmatrix} \theta_{ijx} \\ \theta_{ijy} \end{pmatrix}.$$

$$\begin{cases} \vec{\nu}_{ij}^1 & \text{vecteur normal au segment} \quad G_{ij}M_{ij} \quad \text{orienté vers l'extérieur de} \quad C_i \\ \vec{\nu}_{ij}^2 & \text{vecteur normal au segment} \quad G_{ij+1}M_{ij} \quad \text{orienté vers l'extérieur de} \quad C_i \\ \vec{\eta}_{ij} = G_{ij}M_{ij}\vec{\nu}_{ij}^1 + G_{ij+1}M_{ij}\vec{\nu}_{ij}^2 \end{cases}$$

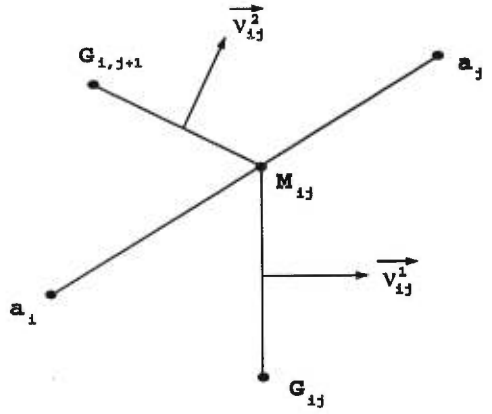

FIGURE 3.20. Partie du bord de la cellule C_i $(\Gamma_{ij} = G_{ij}M_{ij} \cup M_{ij}G_{ij+1})$

$$\begin{cases} \vec{n}_{ij}^1 & \text{vecteur normal au segment} \quad a_iG_{ij} \quad \text{orienté vers l'extérieur de} \quad L_{ij} \\ \vec{n}_{ij}^2 & \text{vecteur normal au segment} \quad G_{ij}a_j \quad \text{orienté vers l'extérieur de} \quad L_{ij} \\ \vec{n}_{ij}^3 & \text{vecteur normal au segment} \quad a_jG_{ij+1} \quad \text{orienté vers l'extérieur de} \quad L_{ij} \\ \vec{n}_{ij}^4 & \text{vecteur normal au segment} \quad G_{ij+1}a_i \quad \text{orienté vers l'extérieur de} \quad L_{ij} \\ \vec{\theta}_{ij} = |\overrightarrow{a_iG_{ij}}|\vec{n}_{ij}^1 + |\overrightarrow{a_iG_{i,j+1}}|\vec{n}_{ij}^4 \\ \vec{\theta}_{ji} = |\overrightarrow{a_jG_{ij}}|\vec{n}_{ij}^2 + |\overrightarrow{a_jG_{i,j+1}}|\vec{n}_{ij}^3. \end{cases}$$

On s'intéresse à la résolution de l'équation scalaire:

$$u_t + (f(u))_x + (g(u))_y = 0 \tag{1.2}$$

1.3. Formulation variationnelle : volumes finis.

Soit S_h l'espace d'approximation des fonctions constantes sur chaque cellule.

$$S_h = \{v \in L^2(\Omega); v_{|_{C_i}} = \text{ constante}; \quad i = 1, ns\}$$

L'ensemble des fonctions $(\chi_i)_{i=1,ns}$ définies par:

$$\chi_i(x,y) = \begin{cases} 1 & (x,y) \in C_i \\ 0 & \text{Sinon} \end{cases}$$

est une base de S_h.

On cherche u solution des équations

$$\int\int_{\Omega} (u_t + (f(u))_x + (g(u))_y)\chi_j dxdy = 0 \quad j = 1, ns$$

Ce qui donne

$$\sum_{i=1}^{ns} \int\int_{C_i} (u_t + (f(u))_x + (g(u))_y)\chi_j dxdy = 0 \quad j = 1, ns$$

C_i étant le support de χ_i on a :

$$\int\int_{C_i} (u_t + (f(u))_x + (g(u))_y)\chi_j dxdy = 0 \quad j = 1, ns$$

On obtient la première étape du schéma en intégrant (1.2) sur L_{ij}

Sur la frontière de L_{ij} , la valeur de $u(x,y,t^n)$ est u_i^n sur C_i et u_j^n sur C_j.

Donc l'intégration de (1.2) sur L_{ij} entre t^n et t^{n+1} conduit à :

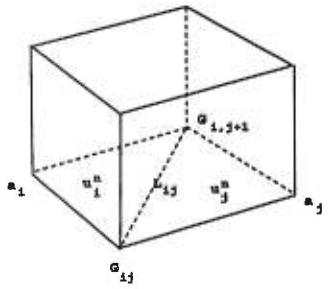

FIGURE 3.21. Intégration sur L_{ij}.

$$\int_n^{n+1} \int_{L_{ij}} (u_t + (f(u))_x + (g(u))_y) = 0$$

D'après le théorème de divergence on obtient $(L_{ij} = (L_{ij} \cap C_i) \cup (L_{ij} \cap C_j))$

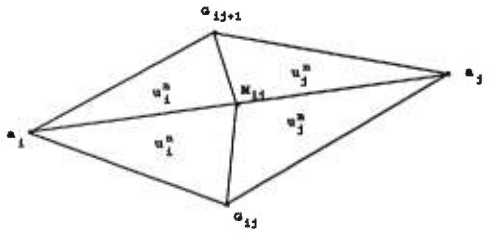

FIGURE 3.22. Intégration sur ∂L_{ij}.

$$\int_{L_{ij}} u(x,y,t^{n+1})dA - \int_{L_{ij}\cap C_i} u(x,y,t^n)dA - \int_{L_{ij}\cap C_j} u(x,y,t^n)dA + \int_{t^n}^{t^{n+1}} \int_{\partial L_{ij}} (f(u)n_x + g(u)n_y)d\sigma\, dt = 0. \quad (1.3)$$

On approche ensuite par :

$$Aire(L_{ij})u_{ij}^{n+1} - Aire(L_{ij}\cap C_i)\cdot u_i^n - Aire(L_{ij}\cap C_j)\cdot u_j^n + \Delta t(f(u_i^n)\theta_{ijx} + g(u_i^n)\theta_{ijy}) + \Delta t(f(u_j^n)\theta_{jix} + g(u_j^n)\theta_{jiy}) = 0. \quad (1.4)$$

Notons que l'approximation de u_t sur L_{ij} est donnée par :

$$u_t \cong \left(u_{ij}^{n+1} - \frac{A(L_{ij}\cap C_i)\cdot u_i^n + A(L_{ij}\cap C_j)\cdot u_j^n}{A(L_{ij})}\right) / \Delta t$$

La deuxième étape s'obtient par intégration sur la cellule barycentrique entre t^{n+1} et t^{n+2}

$$Aire(C_i)u_i^{n+2} - \sum_{j \text{ voisin de } i} Aire(L_{ij}\cap C_i)u_{ij}^{n+1} + \Delta t \sum_{j \text{ voisin de } i} (f(u_{ij}^{n+1})\eta_{ijx} + g(u_{ij}^{n+1})\eta_{ijy}) = 0 \quad (1.5)$$

où sur la frontière de C_i, $\partial C_i = \bigcup_{j \text{ voisin de } i} \Gamma_{ij}$, la valeur de $u(x,y,t^{n+1})$ sur Γ_{ij} est approché par u_{ij}^{n+1}.

On passe ainsi d'une solution constante par morceaux sur C_i à une solution constante par morceaux sur L_{ij}.

1.4. Généralisation du schéma de N.T en dimension deux.

On dispose au départ des valeurs u_i^n aux sommets de la triangulation. On peut par exemple construire un profil linéaire par morceaux sur chaque cellule C_i de la façon suivante:

On construit d'abord un profil linéaire par morceaux sur chaque triangle de départ, profil continu , à l'aide des u_i^n puis on approche les pentes sur C_i en faisant une moyenne des pentes de u dans tous les triangles dont a_i est un sommet.

$$u(x,y,t^n) = u_i^n + (x-x_i)P_i^n + (y-y_i)Q_i^n \qquad (x,y)\in C_i \quad (1.6)$$

Le profil étant linéaire par morceaux, on ne peut plus identifier la valeur moyenne sur C_i avec la valeur au sommet; ou la valeur moyenne sur L_{ij} avec la valeur en M_{ij}. Car

C_i n'est pas un triangle , et il n'y a aucune raison pour que la valeur donnée par (1.6) au sommet a_i soit la moyenne de cette fonction linéaire sur C_i.

Cependant, on est tout de même conduit à faire l'approximation:

$$Aire(L_{ij})u_{ij}^{n+1} \equiv \int_{L_{ij}} u(x,y,t^{n+1})dA \tag{1.7}$$

$$Aire(C_i)u_i^{n+2} \equiv \int_{C_i} u(x,y,t^{n+2})dA. \tag{1.8}$$

Lorsqu'on intègre sur L_{ij} l'équation (1.2) pour écrire la première étape du schéma, et lorsqu'on intrégre sur C_i pour la seconde étape.

On obtient la première étape du schéma en écrivant :

$$\int_{t^n}^{t^{n+1}} \int_{L_{ij}} (u_t + f(u)_x + g(u)_y)dAdt = 0$$

$$\int_{L_{ij}} u(x,y,t^{n+1})dA = \int_{L_{ij}\cap C_i} u(x,y,t^n)dA + \int_{L_{ij}\cap C_j} u(x,y,t^n)dA - \int_{t^n}^{t^{n+1}} \int_{\partial L_{ij}} (f(u)n_x + g(u)n_y)d\sigma dt. \tag{1.9}$$

1.5. Approximation de $\int_{L_{ij}\cap C_i} u(x,y,t^n)dA$.

$u(x,y,t^n)$ est la fonction linéaire sur C_i définie ci-dessus , on doit calculer le volume de deux prismes. On rappelle: le volume de la partie hachurée $= B.\frac{H_1+H_2+H_3}{3}$ on note

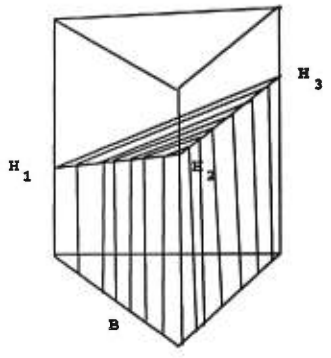

FIGURE 3.23. Le volume d'intégration

$$\begin{cases} L_{ij}^g & \text{le triangle} \quad L_{ij} \quad \text{qui contient} \quad G_{ij} \\ L_{ij}^d & \text{le triangle} \quad L_{ij} \quad \text{qui contient} \quad G_{ij+1} \end{cases}$$

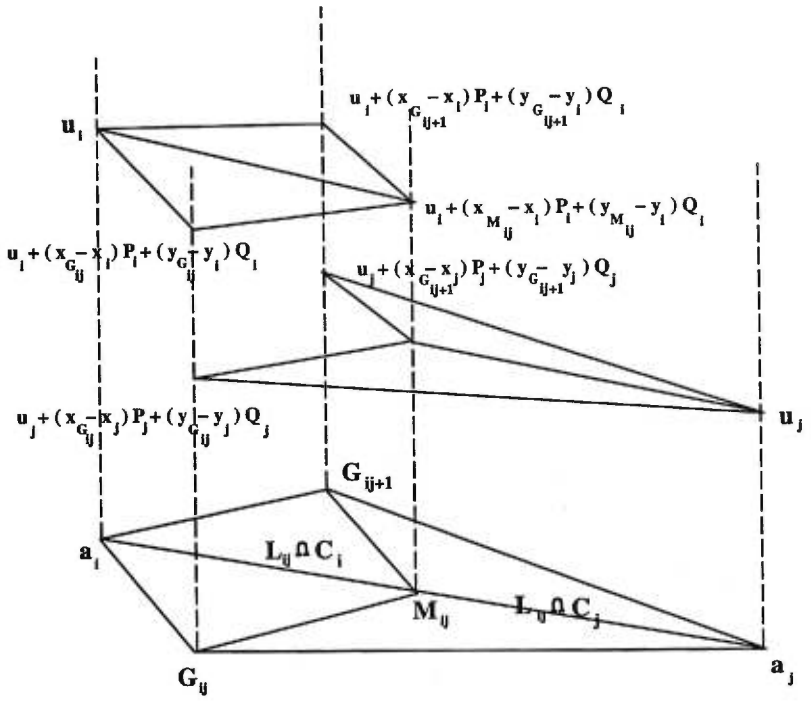

FIGURE 3.24. Les 2 domaines d'intégration $L_{ij} \cap C_i$ et $L_{ij} \cap C_j$

Le volume gauche du prisme porté par $L^g_{ij} \cap C_i$ est égal à

$$Aire(L^g_{ij} \cap C_i)(u_i + \frac{1}{3}(x_{M_{ij}} - x_i + x_{G_{ij}} - x_i)P_i + \frac{1}{3}(y_{M_{ij}} - y_i + y_{G_{ij}} - y_i)Q_i)$$

La surface de $L^g_{ij} \cap C_i$ est égale à :

$$Aire(L^g_{ij} \cap C_i) = \frac{1}{2}((x_{G_{ij}} - x_i)(y_{M_{ij}} - y_i) - (x_{M_{ij}} - x_i)(y_{G_{ij}} - y_i))$$

On calcule de la même manière le volume droit du prisme porté par $L^d_{ij} \cap C_i$; ce qui donne :

$$\begin{aligned}
&\int_{L_{ij} \cap C_i} u_i + (x - x_i)P_i + (y - y_i)Q_i)dA = \\
&\text{Aire}(L_{ij} \cap C_i)\{u^n_i + \frac{1}{3}(x_{M_{ij}} - x_i)P^n_i + \frac{1}{3}(y_{M_{ij}} - y_i)Q^n_i\} \\
&+\frac{1}{3}\text{Aire}(L^d_{ij} \cap C_i)\{(x_{G_{ij}} - x_i)P^n_i + (y_{G_{ij}} - y_i)Q^n_i\} \\
&+\frac{1}{3}\text{Aire}(L^g_{ij} \cap C_i)\{(x_{G_{i,j+1}} - x_i)P^n_i + (y_{G_{i,j+1}} - y_i)Q^n_i\} \qquad (1.10)
\end{aligned}$$

1.6. Approximation de $\int_{L_{ij} \cap C_j} u(x, y, t^n)dA$.

On procède de la même manière ce qui est égal à (on omet l'exposant n)

$$\int_{L_{ij}\cap C_j} u_j + (x-x_j)P_j + (y-y_j)Q_j)dA =$$
$$\text{Aire}(L_{ij}\cap C_j)\{u_j^n + \frac{1}{3}(x_{M_{ij}} - x_j)P_j^n + \frac{1}{3}(y_{M_{ij}} - y_j)Q_j^n\}$$
$$+\frac{1}{3}\text{Aire}(L_{ij}^d \cap C_j)\{(x_{G_{ij}} - x_j)P_j^n + (y_{G_{ij}} - y_j)Q_j^n\}$$
$$+\frac{1}{3}\text{Aire}(L_{ij}^g \cap C_j)\{(x_{G_{i,j+1}} - x_j)P_j^n + (y_{G_{i,j+1}} - y_j)Q_j^n\} \qquad (1.11)$$

où

$$\text{Aire}(L_{ij}^d \cap C_j) = \frac{1}{2}\{(x_{M_{ij}} - x_j)(y_{G_{ij}} - y_j) - (x_{G_{ij}} - x_j)(y_{M_{ij}} - y_j)\}.$$

1.7. Approximation de $\int_{t^n}^{t^{n+1}} \int_{\partial L_{ij}} \{f(u)n_x + g(u)n_y\}d\sigma dt$.

Elle peut être intégrée par la règle du point médian en respectant le temps

$$\int_{t^n}^{t^{n+1}} \int_{\partial L_{ij}} (f(u)n_x + g(u)n_y)d\sigma dt \cong$$

$$\Delta t \int_{\partial L_{ij}} \Big\{f(u(x,y,t^{n+1/2}))n_x + g(u(x,y,t^{n+1/2}))n_y\Big\}d\sigma$$

et on approche ensuite à l'aide d'un développement limité au premier ordre:

$$u(x,y,t^{n+1/2}) \cong u(x,y,t^n) - \frac{\Delta t}{2}\{f'(u(x,y,t^n))u_x(x,y,t^n) + g'(u(x,y,t^n))u_y(x,y,t^n)\}.$$

Sur $L_{ij}\cap C_i$ on sait que $u_x \equiv P_i^n$ et $u_y \equiv Q_i^n$, mais il faut se donner une valeur de $u(x,y,t^n)$ sur a_iG_{ij} et sur a_iG_{ij+1} (et de la même manière pour a_jG_{ij} et a_jG_{ij+1}) on peut prendre par exemple la valeur de $u(x,y,t^n)$ au milieu de l'arête, c'est à dire, on suppose que

$$u(x,y,t^n) \cong u_i^n + \frac{1}{2}(x_{G_{ij}} - x_i)P_i^n + \frac{1}{2}(y_{G_{ij}} - y_i)Q_i^n \equiv u_{a_i,G_{ij}}^n$$

On définit alors

$$u_{a_iG_{ij}}^{n+1/2} = u_{a_i,G_{ij}}^n - \frac{\Delta t}{2}\{f'(u_{a_i,G_{ij}}^n)P_i^n + g'(u_{a_i,G_{ij}}^n)Q_i^n\}$$

On obtient donc l'approximation de

$$\begin{aligned}
&\frac{1}{\Delta t}\int_{t^n}^{t^{n+1}}\int_{\partial L_{ij}}\{f(u)n_x+g(u)n_y\}d\sigma dt \\
&\quad\cong f(u^{n+1/2}_{a_i,G_{ij}})n^1_{ijx}\cdot|a_iG_{ij}|+f(u^{n+1/2}_{a_i,G_{i,j+1}})n^4_{ijx}\cdot|a_iG_{i,j+1}| \\
&\qquad+f(u^{n+1/2}_{a_j,G_{ij}})n^2_{ijx}\cdot|a_jG_{ij}|+f(u^{n+1/2}_{a_j,G_{i,j+1}})n^3_{ijx}\cdot|a_jG_{i,j+1}| \\
&\qquad+g(u^{n+1/2}_{a_i,G_{ij}})n^1_{ijy}\cdot|a_iG_{ij}|+g(u^{n+1/2}_{a_i,G_{i,j+1}})n^4_{ijy}\cdot|a_iG_{i,j+1}| \\
&\qquad+g(u^{n+1/2}_{a_j,G_{ij}})n^2_{ijy}\cdot|a_jG_{ij}|+g(u^{n+1/2}_{a_j,G_{i,j+1}})n^3_{ijy}\cdot|a_jG_{i,j+1}|. \qquad (1.12)
\end{aligned}$$

1.8. Premier pas du schéma de N.T.

$$Aire(L_{ij})u^{n+1}_{ij}-(1.10)-(1.11)+\Delta t(1.12)=0$$

u^{n+1}_{ij} représente la valeur de la solution au point M_{ij}.

On construit alors une approximation linéaire par morceaux sur chaque L_{ij}

$$u(x,y,t^{n+1})\equiv u^{n+1}_{ij}+(x-x_{M_{ij}})P^{n+1}_{ij}+(y-y_{M_{ij}})Q^{n+1}_{ij}$$

et on peut calculer par exemple les valeurs P^{n+1}_{ij} et Q^{n+1}_{ij} en reconstruisant un profil linéaire par triangle, profil continu, à l'aide des valeurs au milieu de chaque côté.

On approche ensuite les pentes en calculant la moyenne des pentes obtenues sur les deux triangles qui ont pour côté commun a_ia_j dont M_{ij} est le milieu.

1.9. Deuxième pas du schéma de N.T..

On obtient ce deuxième pas en intégrant sur la cellule C_i, entre t^{n+1} et t^{n+2}, exactement de la même manière que ci-dessus.

$$\begin{aligned}
&\text{Aire}(C_i)u^{n+2}_i-\sum_{j\text{ voisin de }i}\int_{L_{ij}\cap C_i}u(x,y,t^{n+1})dxdy \\
&=-\Delta t\sum_{j\text{ voisin de }i}\int_{\Gamma_{ij}}\{f(u(x,y,t^{n+3/2}))\nu_x+g(u(x,y,t^{n+3/2}))\nu_y\}d\sigma
\end{aligned}$$

ainsi sur $L_{ij}\cap C_i$ l'expression de $u(x,y,t^{n+1})$ est une fonction linéaire par morceaux . Son intégration sur un parallèlépipède se fait comme (1.10).

Pour obtenir $u(x,y,t^{n+\frac{3}{2}})$ on fait un développement limité d'ordre un en temps et on décompose Γ_{ij} à $G_{ij}M_{ij}\cup M_{ij}G_{i,j+1}$ pour approcher $u(x,y,t)$ sur $G_{ij}M_{ij}$ par la valeur de $u(x,y,t)$ au milieu de l'arête $G_{ij}M_{ij}$ (de même sur $M_{ij}G_{i,j+1}$ par la valeur au milieu de $M_{ij}G_{i,j+1}$).

1.10. Approximation des pentes.

Pour approximer (P_i, Q_i) , on peut utiliser une technique des moindres carrés ([25],[26]). Si $u_i = u(G_i)$ où G_i est le centre de gravité du triangle T, pour estimer

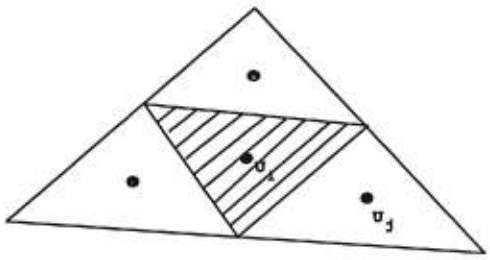

FIGURE 3.25. Estimation des pentes

$\nabla u_i = (P_i, Q_i)$, on peut minimiser la quantité

$$I = \sum_{j=1}^{3} \{u_T^n + \overrightarrow{GG}_j \cdot (\text{grad u})_T^n - u_{T_j}^n\}^2.$$

Le minimum est obtenu lorsque

$$\frac{\partial I}{\partial a_T^n} = \frac{\partial I}{\partial b_T^n} = 0$$

Ce qui donne

$$\tilde{a}_T^n = \frac{1}{D} \sum_{j=1}^{3} (y_{G_j} - y_G)^2 \sum_{j=1}^{3} (u_{T_j}^n - u_T^n)(x_{G_j} - x_G)$$

$$-\frac{1}{D} \sum_{j=1}^{3} (x_{G_j} - x_G)(y_{G_j} - y_G) \sum_{j=1}^{3} (u_{T_j}^n - u_T^n)(y_{G_j} - y_G)$$

$$\tilde{b}_T^n = \frac{1}{D} \sum_{j=1}^{3} (x_{G_j} - x_G)^2 \sum_{j=1}^{3} (u_{T_j}^n - u_T^n)(y_{G_j} - y_G)$$

$$-\frac{1}{D} \sum_{j=1}^{3} (x_{G_j} - x_G)(y_{G_j} - y_G) \sum_{j=1}^{3} (u_{T_j}^n - u_T^n)(x_{G_j} - x_G)$$

Où le dénominateur

$$D = \sum_{j=1}^{3} (x_{G_j} - x_G)^2 \sum_{j=1}^{3} (y_{G_j} - y_G)^2 - \left[\sum_{j=1}^{3} (x_{G_j} - x_G)(y_{G_j} - y_G)\right]^2$$

1.11. Limiteurs bidimensionnels.

On décrit ici une technique de limitation pour les gradients.

La procédure de limitation est réalisée par triangles. Nous posons

$$\nabla u_T = \begin{pmatrix} u_{T,x} \\ u_{T,y} \end{pmatrix}.$$

La notation $u_{T,x}$ signifie que la dérivée en x de u est restreinte au triangle T.

On note par $\mathcal{T}_i$ l'ensemble des triangles $T \in \mathcal{T}_h$ tels que $T \cap C_i \neq \emptyset$.

La procédure de limitation s'écrit

$$u_x^{lim} = \frac{1}{2}\{\min_{T\in\mathcal{T}_i} sign(u_{T,x}) + \max_{T\in\mathcal{T}_i} sign(u_{T,x})\} \min_{T\in\mathcal{T}_i} |u_{T,x}|.$$

Le calcul de u_y^{lim} est identique à u_x^{lim} (le procédé peut aussi se généraliser en $3-D$).

REMARQUE 3.2.

L'introduction des limiteurs peut affecter la précision spatiale de la solution, mais la limitation n'intervient que lorsque apparaissent des oscillations c'est à dire près des chocs et des discontinuités. Pour localiser avec plus de précision les chocs il est suggéré d'augmenter le nombre de points dans ces zones par raffinements locaux.

REMARQUE 3.3.

Enfin cette technique de limitation est très robuste car elle permet le calcul de solutions stationnaires pour un grand nombre d'écoulements. Sous cette forme, elle permet d'obtenir des solutions d'ordre deux à moindre coût, mais la solution est plus dissipative.

1.12. Extension du schéma au systéme (1.1) du chapitre 1.

1.12.1. Equations.

Nous cherchons des solutions stationnaires des équations d'Euler qui s'écrivent dans une formulation conservative en deux dimension d'espace comme (1.1).

Notons

$$\overrightarrow{\mathcal{F}}(U) = \begin{pmatrix} F(U) \\ G(U) \end{pmatrix}$$

où

$$U = (\rho, \rho u, \rho v, \rho E)^T$$

On peut réécrire le système (1.1) sous la forme

$$\frac{\partial U}{\partial t} + \vec{\nabla} \cdot \vec{\mathcal{F}}(U) = 0 \quad \text{dans} \quad \Omega \times \mathbb{R}_+ \tag{1.13}$$

1.12.2. Maillage : Eléments Finis.

On approche Ω par un ouvert polygonal Ω_h que nous subdivisons en triangles. Les noeuds A_i de la triangulation $\mathcal{T}_h$ ainsi obtenue sont les sommets des triangles. Soit ns le nombre de noeuds et na le nombres d'arêtes. Les degrés de liberté sont les valeurs de l'inconnu U aux noeuds, soit $4ns$ inconnues (4 composantes en 2-D, 5 en 3-D). On note

$$U(A_i, t^n) = U_i(t^n) \quad \text{et} \quad U(M_{ij}, t^{n+1}) = U_{ij}(t^{n+1})$$

1.12.3. Formulation variationnelle: Volumes Finis.

Le système (1.1) ne possède pas en général de solutions classiques, même avec une donnée initiale trés régulière. C'est pourquoi, on cherche les solutions faible (au sens des distributions) du problème variationnel associé, qui correspond à une formulation intégrale de (1.1) : c'est elle qui exprime les différentes lois de conservation de la masse, quatité de mouvement de l'énergie pour tout volume inclus dans le domaine de l'écoulement. Pour chaque noeud A_i, on définit la cellule C_i (" volume de controle"); de même pour chaque milieu de l'arête A_iA_j on définit la cellule L_{ij}. On pose

$$\Omega_h = \bigcup_{i=1}^{ns} C_i \ \textit{ns: nombre de sommets de } \mathcal{T}_h, \ \Omega_h = \bigcup_{k=1}^{na} L_k \ \textit{na : nombre d'arêtes de } \mathcal{T}_h$$

On introduit les espaces d'approximation

$$\mathcal{U}_h = \{v | v \in L^2(\Omega), v(x,y) = v(x_i, y_i), \ \forall (x,y) \in C_i, i = 1, \cdots, ns\}$$

$$\mathcal{V}_h = \{v | v \in L^2(\Omega), v(x,y) = v(x_k, y_k), \ \forall (x,y) \in L_k, k = 1, \cdots, na\}$$

où (x_i, y_i) sont les coordonnées du noeud A_i et (x_k, y_k) sont les coordonnées du point milieu m_{ij} du segment A_iA_j.

Au temps t fixé ($t > 0$), on intègre les équations (1.1) sur Ω_h après multiplication par les fonctions de base χ_h de $\mathcal{V}_h$ si le pas du temps est impair et par les fonctions de base ψ_i de $\mathcal{U}_h$ si le pas du temps est pair.

Les fonctions caractéristiques des cellules L_k et C_i sont définis par

$$\psi_i(\overrightarrow{X}) = \begin{cases} 1 & si \quad \overrightarrow{X} \in C_i \\ 0 & \text{sinon} \end{cases} \qquad \chi_k(\overrightarrow{X}) = \begin{cases} 1 & si \quad \overrightarrow{X} \in L_k \\ 0 & \text{sinon} \end{cases}$$

On aboutit au système suivant :

premier pas du temps

$$\int_{L_k} \frac{\partial U_h}{\partial t} dxdy + \int_{L_k} \overrightarrow{\nabla} \cdot \overrightarrow{\mathcal{F}}(U_h) dxdy = 0 \qquad \forall k = 1, \ldots, na \tag{1.14}$$

second pas du temps

$$\int_{C_i} \frac{\partial U_h}{\partial t} dxdy + \int_{C_i} \overrightarrow{\nabla} \cdot \overrightarrow{\mathcal{F}}(U_h) dxdy = 0 \qquad \forall i = 1, \ldots, ns \tag{1.15}$$

On applique la formule de Green, ceci nous donne

premier pas du temps

$$\int_{L_{ij}} \frac{\partial U_h}{\partial t} dxdy + \int_{\partial L_{ij}} \overrightarrow{\mathcal{F}}(U_h) \cdot \overrightarrow{n_{ij}} d\sigma = 0 \tag{1.16}$$

second pas du temps

$$\int_{C_i} \frac{\partial U_h}{\partial t} dxdy + \int_{\partial C_i} \overrightarrow{\mathcal{F}}(U_h) \cdot \overrightarrow{\nu_{ij}} d\sigma = 0 \tag{1.17}$$

Comme $\partial C_i = \bigcup_{j \in k(i)} \partial C_{ij} \cup \partial C_i \cap \Gamma_b \cup \partial C_i \cap \Gamma_\infty$ où $\partial C_{ij} = \partial C_i \cap \partial C_j$

premier pas du temps

$$\int_{L_{ij}} \frac{\partial U_h}{\partial t} dxdy + \int_{\partial L_{ij}} \overrightarrow{\mathcal{F}}(U_h) \cdot \overrightarrow{n_{ij}} d\sigma = 0 \tag{1.18}$$

second pas du temps

$$\int_{C_i} \frac{\partial U_h}{\partial t} dxdy + \sum_{j \in K(i)} \int_{\partial C_{ij}} \overrightarrow{\mathcal{F}}(U_h) \cdot \overrightarrow{\nu_{ij}} d\sigma \tag{1.19}$$

$$+ \int_{\partial C_i \cap \Gamma_b} \overrightarrow{\mathcal{F}}(U_h) \cdot \overrightarrow{n_i} d\sigma \tag{1.20}$$

$$+ \int_{\partial C_i \cap \Gamma_\infty} \overrightarrow{\mathcal{F}}(U_h) \cdot \overrightarrow{n_i} d\sigma = 0 \tag{1.21}$$

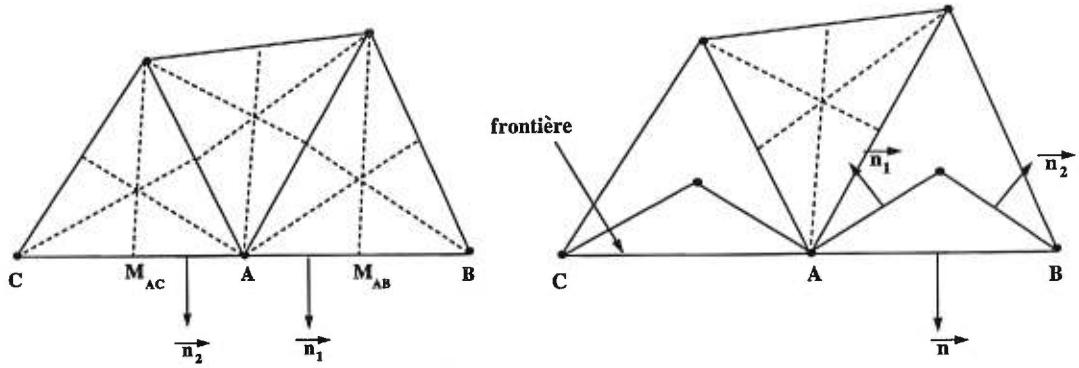

FIGURE 3.26. Définition des cellules frontière

1.12.4. Calcul des termes de bords.

On détaille dans ce paragraphe le calcul de $\int_{\partial C_i \cap \Gamma} \overrightarrow{\mathcal{F}}(U_h) \cdot \overrightarrow{n_i} d\sigma$, (voir figure 3.26)

Bord glissant

Le long du corps (sur Γ_b), on impose une condition de glissement pour un écoulement non visqueux. Le vecteur vitesse $\overrightarrow{V}$ doit être tangent à la paroi. Pour un segment $\Gamma_b \cap \partial C_i$ on a:

$$\overrightarrow{V} \cdot \overrightarrow{n}_i = 0$$

où $\overrightarrow{n}_i$ est le vecteur normal au segment considéré .

Cette condition réduit l'intégrale le long de chaque morceau de surface en une intégrale de pression:

$$\int_{\partial C_i \cap \Gamma_b} \overrightarrow{\mathcal{F}}(U_h) \cdot \overrightarrow{n_i} d\sigma \simeq \left(0, \int_{\partial C_i \cap \Gamma_b} p \cdot \overrightarrow{n_i} d\sigma, 0\right)^T$$

La condition de glissement est ainsi vérifiée de façon faible seulement.

Bord infini Γ_∞

Sur Γ_{in} , entrée de l'écoulement

On approche l'intégrale par une décomposition de flux de Steger-Warming. On a :

$$\int_{\partial C_i \cap \Gamma_{in}} \overrightarrow{\mathcal{F}}(U_h) \cdot \overrightarrow{n_i} d\sigma \simeq \mathcal{A}^+(U_i, \overrightarrow{\eta}_i) U_i + \mathcal{A}^-(U_\infty), \overrightarrow{\eta}_i) U_\infty$$

avec

$$\mathcal{A}^+(U, \overrightarrow{\eta}_i) = (A(U) \cdot \eta_{i,x} + B(U) \cdot \eta_{i,y})^+$$

et

$$\mathcal{A}^-(U, \overrightarrow{\eta}_i) = (A(U) \cdot \eta_{i,x} + B(U) \cdot \eta_{i,y})^-$$

où $\mathcal{A}^+$ et $\mathcal{A}^-$ sont les parties positive et négative de la matrice jacobienne du flux d'Euler.

On remarque que sur Γ_{in} l'écoulement est entrant est supersonique :

$$M \gg 1 \quad et \quad \overrightarrow{V} \cdot \overrightarrow{\eta_i} < 0$$

Les valeurs propres de la matrice jacobienne du flux sont négatives donc la partie positive $\mathcal{A}^+(U_i, \overrightarrow{\eta}_i)$ est nulle. On impose alors simplement des conditions à l'infini entrant.

Sur Γ_{out} sortie de l'écoulement

L'écoulement ici est sortant. De plus, dans les résultats présentés dans cette partie la sortie est supersonique donc :

$$M \gg 1 \quad et \quad \overrightarrow{V} \cdot \overrightarrow{\eta_i} > 0$$

Les valeurs propres de la matrice jacobienne du flux sont positives donc la partie négative $\mathcal{A}^-(U_i, \overrightarrow{\eta}_i)$ est nulle.

On obtient alors :

$$\int_{\partial C_i \cap \Gamma_{out}} \overrightarrow{\mathcal{F}}(U_h) \cdot \overrightarrow{n_i} d\sigma \simeq \mathcal{A}^+(U_i, \overrightarrow{\eta}_i) U_i$$

1.12.5. Approximation d'ordre élevé.

Le schéma M.U.S.C.L. (Monotonic Upwind Scheme for Conservation Law) initialement dévelopé par van Leer [39] a été adapté au cas des éléments finis triangulaires par Fezoui [38].

On notera par la suite $\widetilde{U}$ le vecteur des *variables physiques* et on désignera par S l'opérateur de passage aux variables conservatives, $S(\widetilde{U}) = U$

On suppose que chaque composante de $\widetilde{U}$ varie linéairement sur un volume de contrôle C_i respectivement sur L_k.

$$\begin{cases} \widetilde{U}(x, y, t^n) = \widetilde{U}_i^n + (x - x_i) P_i^n + (y - y_i) Q_i^n \quad \forall (x, y) \in C_i \\ \widetilde{U}(x, y, t^{n+1}) = \widetilde{U}_{ij}^{n+1} + (x - x_{ij}) P_{ij}^{n+1} + (y - y_{ij}) Q_{ij}^{n+1} \quad \forall (x, y) \in L_{ij} \end{cases}$$

Pour approximer (P_i, Q_i) et (P_{ij}, Q_{ij}), on utilise la technique des moindres carrés voir section 1.10 . Et pour la limitation des pentes voir section 1.11.

L'algorithme du schéma explicite d'ordre deux avec limiteur s'écrit :

Premier pas du temps:

1. Prédiction

$$\widetilde{U}^{n+1/2}_{a_iG_{ij}} = \widetilde{U}^{n}_{a_i,G_{ij}} - \frac{\Delta t}{2}\{F'(\widetilde{U}^{n}_{a_i,G_{ij}})P^n_i + G'(\widetilde{U}^{n}_{a_i,G_{ij}})Q^n_i\}$$

où

$$\widetilde{U}(x,y,t^n) \cong \widetilde{U}^n_i + \frac{1}{2}(x_{G_{ij}} - x_i)P^n_i + \frac{1}{2}(y_{G_{ij}} - y_i)Q^n_i \equiv \widetilde{U}^n_{a_i,G_{ij}}$$

2. Correction

$$\text{Aire}(L_{ij})\widetilde{U}^{n+1}_{ij} - (1.10) - (1.11) + \Delta t(1.12) = 0$$

dans (1.10), (1.11) et (1.12) , on remplace u par $\widetilde{U}$

Deuxième pas du temps:

1. Prédiction:

$$\widetilde{U}^{n+3/2}_{G_{ij}M_{ij}} = \widetilde{U}^{n+1}_{G_{ij}M_{ij}} - \frac{\Delta t}{2}\{F'(\widetilde{U}^{n+1}_{G_{ij}M_{ij}})P^{n+1}_{ij} + G'(\widetilde{U}^{n+1}_{G_{ij}M_{ij}})Q^{n+1}_{ij}\}$$

où

$$\widetilde{U}(x,y,t^{n+1}) \cong \widetilde{U}^{n+1}_{M_{ij}} + \frac{1}{2}(x_{G_{ij}} - x_{M_{ij}})P^{n+1}_{ij} + \frac{1}{2}(y_{G_{ij}} - y_{M_{ij}})Q^{n+1}_{ij} \equiv \widetilde{U}^{n+1}_{G_{ij}M_{ij}}$$

2. Correction:

$$\text{Aire}(C_i)\widetilde{U}^{n+2}_i - \sum_{j \text{ voisin de } i}\int_{L_{ij}\cap C_i}\widetilde{U}(x,y,t^{n+1})dxdy$$

$$+\Delta t \sum_{j \text{ voisin de } i}\int_{\Gamma_{ij}}\{F(\widetilde{U}(x,y,t^{n+3/2}))\nu_x + G(\widetilde{U}(x,y,t^{n+3/2}))\nu_y\}d\sigma + \text{T de B} = 0$$

$$U^{n+2}_i = S(\widetilde{U}^{n+2}_i)$$

1.12.6. Analyse de stabilité.

Dans cette partie, on va considérer deux modèles d'advection en dimension deux.

modèle d'advection à vitesse constante

Considérons le problème suivant:

$$u_t + \overrightarrow{V}\cdot\overrightarrow{\nabla}u = 0 \quad \text{,dans } \mathbb{R}^2, \quad \text{avec}\,\overrightarrow{V} \in \mathbb{R}^2 \tag{1.22}$$

La discrétisation décentrée nous donne le schéma suivant :

$$Aire(C_i)(u_i^{n+1} - u_i^n) = -\Delta t \sum_{j \in K(i)} \alpha_{ij}(\theta_{ij} u_i^n + (1 - \theta_{ij}) u_j^n) \tag{1.23}$$

avec

$$\alpha_{ij} = \eta_x^{ij} V^x + \eta_y^{ij} V^y, \quad \eta_x^{ij} = \int_{\partial C_i \cap \partial C_j} \nu_x d\sigma, \quad \eta_y^{ij} = \int_{\partial C_i \cap \partial C_j} \nu_y d\sigma \tag{1.24}$$

$$\theta_{ij} = \frac{1}{2}(sign(\alpha_{ij}) + 1) \tag{1.25}$$

PROPOSITION 1.1. *Le schéma (*1.23,1.24 *et* 1.25*) satisfait le principe du maximum, si pour chaque cellule C_i, on a l'inégalité suivante :*

$$Aire(C_i) - \Delta t \int_{\partial C_i^+} \vec{V} \cdot \vec{n} d\sigma \geq 0 \tag{1.26}$$

où ∂C_i^+ est la partie de ∂C_i où $\int \vec{V} \cdot \vec{n} d\sigma$ est positive.

Preuve :

Soit $K(i)$ l'ensemble des indices j des volumes de contrôle C_j voisins de C_i (i.e. tels que $\partial C_i \cap \partial C_j \neq \emptyset$ ou n'est pas réduit à un point). On note

$$\partial C_{ij} = \partial C_i \cap \partial C_j, \quad j \in K(i)$$

alors

$$\partial C_i = \bigcup_{j \in K(i)} \partial C_{ij}$$

Par suite, la portion de la frontière ∂C_i où $\int \vec{V} \cdot \vec{n} d\sigma > 0$ (resp, $< 0, = 0$) correspond à la réunion des ∂C_{ij} sur lesquels l'intégrale est strictement positive (resp. strictement négative, égale à 0). On peut alors définir une partition de $K(i)$ de la façon suivante

$$K(i) = K^+(i) \cup K^-(i) \cup K^o(i)$$

$$K^+(i) = \{j \in K(i); \int_{\partial C_{ij}} \vec{V} \cdot \vec{n} d\sigma > 0\}$$

$$K^-(i) = \{j \in K(i); \int_{\partial C_{ij}} \vec{V} \cdot \vec{n} d\sigma < 0\}$$

$$K^o(i) = \{j \in K(i); \int_{\partial C_{ij}} \vec{V} \cdot \vec{n} d\sigma = 0\}$$

Ceci permet de définir aussi une partition de ∂C_{ij}

$$\partial C_i = \partial C_i^+ \cup \partial C_i^- \cup \partial C_i^o$$

avec

$$\partial C_i^+ = \bigcup_{j \in K^+(i)} \partial C_{ij}, \quad \partial C_i^- = \bigcup_{j \in K^-(i)} \partial C_{ij}, \quad \partial C_i^o = \bigcup_{j \in K^o(i)} \partial C_{ij}$$

Comme ∂C_i est un contour fermé C^1 par morceau et que $\overrightarrow{V}$ est constant, on a

$$\int_{\partial C_i} \overrightarrow{V} \cdot \overrightarrow{n} d\sigma = \int_{\partial C_i^+} \overrightarrow{V} \cdot \overrightarrow{n} d\sigma + \int_{\partial C_i^-} \overrightarrow{V} \cdot \overrightarrow{n} d\sigma = 0 \tag{1.27}$$

Le schéma (1.23,1.24 et 1.25) s'écrit aussi

$$u_i^{n+1} = u_i^n - \frac{\Delta t}{\text{Aire}(C_i)} \sum_{j \in K(i)} \alpha_{ij} (\theta_{ij} u_i^n + (1 - \theta_{ij}) u_j^n) \tag{1.28}$$

$$\alpha_{ij} = \int_{\partial C_{ij}} \overrightarrow{V} \cdot \overrightarrow{n} d\sigma \tag{1.29}$$

$$\theta_{ij} = \frac{1}{2}(sign(\alpha_{ij}) + 1) \tag{1.30}$$

Par définition, le schéma (1.28,1.29 et 1.30) respecte le principe du maximum, si pour tout noeud i la double inégalité est vérifiée

$$\min_k |u_k^o| \leq |u_i^n| \leq \max_k |u_k^o|, \quad \forall n$$

$u^o = (u_k^o)_k$ est la solution initiale discrète arbitraire vérifiant

$$\max_k |u_k^o| < \infty$$

Le principe du maximum traduit le fait que seules les solutions bornées sont admissibles.

LEMME 1.1. *Une condition suffisante pour que le schéma défini par (*1.28,1.29 *et* 1.30*) vérifie le principe du maximum est*

$$\min_k |u_k^n| \leq |u_i^{n+1}| \leq \max_k |u_k^n|, \quad \forall i, \quad \forall n \tag{1.31}$$

La preuve du lemme (1.1) se fait par induction sur n .

Il nous suffit donc de montrer que le schéma (1.28,1.29 et 1.30) vérifie (1.31). On a

$$\sum_{j \in K(i)} \alpha_{ij} (\theta_{ij} u_i^n + (1 - \theta_{ij}) u_j^n) = \sum_{j \in K^+(i)} \alpha_{ij} u_i^n + \sum_{j \in K^-(i)} \alpha_{ij} u_j^n$$

$$= \left(\int_{\partial C_i^+} \overrightarrow{V} \cdot \overrightarrow{\nu} d\sigma \right) u_i^n + \sum_{j \in K^-(i)} \left(\int_{\partial C_{ij}} \overrightarrow{V} \cdot \overrightarrow{\nu} d\sigma \right) u_j^n$$

Par suit

$$u_i^{n+1} = \sum_{k \in \{i\} \cup K(i)} \beta_k u_k^n \tag{1.32}$$

avec

$$\beta_i = 1 - \frac{\Delta t}{\text{Aire}(C_i)} \int_{\partial C_i^+} \overrightarrow{V} \cdot \overrightarrow{\nu} d\sigma \tag{1.33}$$

$$\beta_k = -\frac{\Delta t}{\text{Aire}(C_i)} \int_{\partial C_{ik}} \overrightarrow{V} \cdot \overrightarrow{\nu} d\sigma \quad \forall k \in K^-(i), \ \beta_k = 0, \ k \in K^+(i) \tag{1.34}$$

LEMME 1.2. *Les coefficients β_k définis par (1.32,1.33 et 1.34) vérifient*

$$(i)\beta_k \in [0,1], \forall k \in \{i\} \cup K^-(i), \qquad (ii) \sum_{k \in \{i\} \cup K^-(i)} \beta_k = 1 \tag{1.35}$$

Si (1.35) est vérifié, alors on a bien (1.31), donnons preuve (1.35)

$\beta_k \geq 0, \quad \forall k \in \{i\} \cup K^-(i)$

D'aprés l'hypothèse de la proposition (1.1) (1.26), on a bien $\beta_i \geq 0$. Pour $k \in K^-(i)$ on a, par définition de $K^-(i)$

$$\int_{\partial C_{ik}} \overrightarrow{V} \cdot \overrightarrow{\nu} d\sigma < 0$$

et donc $\beta_k \geq 0, \forall k \in K^-(i)$.

Les coefficients β_k vérifient (ii)

on a

$$\sum_k \beta_k = 1 - \frac{\Delta t}{\text{Aire}C_i} \left(\int_{\partial C_i^+} \overrightarrow{V} \cdot \overrightarrow{\nu} d\sigma + \int_{\partial C_i^-} \overrightarrow{V} \cdot \overrightarrow{\nu} d\sigma \right) = 1, \quad \text{d'après(1.27)}$$

On déduit aussi que $\beta_k \leq 1$ pour tout k appartenant à $\{i\} \cup K^-(i)$, ce qui achève la démonstration.

Modèle d'advection à vitesse non constante:

Ce cas sera étudié sous forme conservative

$$u_t + div(\overrightarrow{V} u) = 0 \tag{1.36}$$

où $\overrightarrow{V}$ est donné mais non constant, $\overrightarrow{V} = \overrightarrow{V}(x,y)$.

Il est raisonable de considèrer un schéma numérique qui approxime cette loi conservative stable si elle préserve la positivité des variables indépendantes.

Le schéma conservatif s'écrit :

$$\text{Aire}(C_i)(u_i^{n+1} - u_i^n) = -\Delta t \sum_{j \in K(i)} \alpha_{ij}(\theta_{ij} u_i^n + (1 - \theta_{ij}) u_j^n) \tag{1.37}$$

avec

$$\alpha_{ij} = \eta_x^{ij} \frac{(V_i^x + V_j^x)}{2} + \eta_y^{ij} \frac{(V_i^y + V_j^y)}{2}, \quad \theta_{ij} = \frac{1}{2}(\text{sign}(\alpha_{ij}) + 1) \tag{1.38}$$

PROPOSITION 1.2. *Le schéma défini par (1.37-1.38) préserve la positivité de sa solution si on a l'inégalité suivante pour toute cellule C_i.*

$$Aire(C_i) - \Delta t \max_{j \in K(i)} \| \vec{V}_j \| \int_{\partial C_i} d\sigma \geq 0 \tag{1.39}$$

Preuve :

Il s'agit de démontrer une propriété plus faible du schéma (1.37-1.38) quad $\vec{V}$ n'est plus constant: le schéma n'assure plus que les solutions discrètes sont bornées mais qu'elles restent positives si la solution initiale l'est. (1.37-1.38) s'écrit aussi

$$u_i^{n+1} = u_i^n - \frac{\Delta t}{\text{Aire}(C_i)} \sum_{j \in K(i)} \alpha_{ij}(\theta_{ij} u_i^n + (1 - \theta_{ij}) u_j^n) \tag{1.40}$$

avec

$$\alpha_{ij} = \int_{\partial C_{ij}} \frac{1}{2}(\vec{V}_i + \vec{V}_j) \cdot \vec{\nu} d\sigma \,, \quad \theta_{ij} = \frac{1}{2}(\text{sign}(\alpha_{ij}) + 1) \tag{1.41}$$

Par définition, le schéma défini par (1.40-1.41) préserve la positivité de u si l'insertion suivante est vérifiée pour tout k

$$u_k^o \geq 0 \Longrightarrow u_k^n \geq 0, \forall n \tag{1.42}$$

LEMME 1.3. *Une condition nécessaire et suffisante pour que le schéma (1.40-1.41) vérifie (1.42) est*

$$u_k^n \geq 0 \Longrightarrow u_k^{n+1} \geq 0, \forall k, \quad \forall n \tag{1.43}$$

Il nous suffit donc de vérifier que le schéma vérifie (1.43)

Notons $\vec{V}_{ij} = \frac{1}{2}(\vec{V}_i + \vec{V}_j)$, alors de manière similaire au paragraphe précédent, on définit ($\vec{V}$ est remplacé par $\vec{V}_{ij}$ constant sur chaque ∂C_{ij})

$$K^+(i) = \{j \in K(i); \quad \alpha_{ij} > 0\}$$

$$K^-(i) = \{j \in K(i); \quad \alpha_{ij} < 0\}$$

$$K^o(i) = \{j \in K(i); \quad \alpha_{ij} = 0\}$$

alors

$$\sum_{j\in K(i)} \alpha_{ij}\left(\theta_{ij}u_i^n + (1-\theta_{ij})u_j^n\right) =$$

$$\left(\sum_{j\in K^+(i)} \int_{\partial C_{ij}} \overrightarrow{V}_{ij}\cdot\overrightarrow{\nu}d\sigma\right)u_i^n + \left(\sum_{j\in K^-(i)} \int_{\partial C_{ij}} \overrightarrow{V}_{ij}\cdot\overrightarrow{\nu}d\sigma\right)u_j^n$$

on en déduit que (1.40-1.41) s'écrit sous la forme

$$u_i^{n+1} = \sum_{k\in\{i\}\cup K^-(i)} \beta_k u_k^n \tag{1.44}$$

avec

$$\beta_i = 1 - \frac{\Delta t}{\text{Aire}(C_i)} \sum_{j\in K^+(i)} \int_{\partial C_{ij}} \overrightarrow{V}_{ij}\cdot\overrightarrow{\nu}d\sigma\ ,\ \beta_k = -\frac{\Delta t}{\text{Aire}(C_i)} \int_{\partial C_{ik}} \overrightarrow{V}_{ik}\cdot\overrightarrow{\nu}d\sigma,\ k\in K^-(i) \tag{1.45}$$

LEMME 1.4. *Une condition suffisante pour que le schéma vérifie (1.43) est*

$$\beta_k \geq 0\ ,\quad \forall k\in\{i\}\cup K^-(i) \tag{1.46}$$

Montrons que les coefficients β_k vérifient (1.46)

Pour $k\in K^-(i)$, on a bien par définition de $K^-(i)$ (1.46).Si $j\in K^+(i)$, alors

$$0 \leq \int_{\partial C_{ij}} \overrightarrow{V}_{ij}\cdot\overrightarrow{\nu}d\sigma = \int_{\partial C_{ij}} |\overrightarrow{V}_{ij}\cdot\overrightarrow{\nu}|d\sigma \leq \int_{\partial C_{ij}} \parallel \overrightarrow{V}_{ij}\parallel d\sigma \leq$$

$$\int_{\partial C_{ij}} \max_{k\in K(i)} \parallel \overrightarrow{V}_k\parallel d\sigma = \max_{k\in K(i)} \parallel \overrightarrow{V}_k\parallel \int_{\partial C_{ij}} d\sigma$$

par suite

$$\sum_{j\in K^+(i)} \int_{\partial C_{ij}} \overrightarrow{V}_{ij}\cdot\overrightarrow{\nu}d\sigma \leq \max_{k\in K(i)} \parallel \overrightarrow{V}_k\parallel \left(\sum_{j\in K^+(i)} \int_{\partial C_{ij}} d\sigma\right)$$

mais

$$\sum_{j\in K^+(i)} \int_{\partial C_{ij}} d\sigma = \int_{\bigcup_{j\in K^+(i)}\partial C_{ij}} d\sigma =$$

$$\text{mes}\left(\bigcup_{j\in K^+(i)} \partial C_{ij}\right) \leq \text{mes}\left(\bigcup_{j\in K(i)} \partial C_{ij}\right) = \int_{\partial C_i} d\sigma$$

donc

$$1 - \frac{\Delta t}{\text{Aire}(C_i)} \sum_{j\in K^+(i)} \int_{\partial C_{ij}} \overrightarrow{V}_{ij}\cdot\overrightarrow{\nu}d\sigma \geq 1 - \frac{\Delta t}{\text{Aire}(C_i)} \max_{k\in K(i)} \parallel \overrightarrow{V}_k\parallel \int_{\partial C_i} d\sigma$$

par (1.39), on en déduit que $\beta_i \geq 0$

Les coefficients β_k sont positifs pour tout $k \in \{i\} \cup K^-(i)$, ce qui achève la démonstration du lemme 1.4

Application aux équations d'Euler :

Le pas du temps sera calculé pour chaque cellule C_i comme suit :

$$\Delta t_i = \frac{\text{Aire}(C_i)}{\lambda^i_{\max} \int_{\partial C_i} d\sigma}$$

avec

$$\lambda^i_{\max} = \max(\lambda_i, \max_{j \in K(i)} \lambda_j), \qquad \lambda_i = (u_i^2 + v_i^2)^{\frac{1}{2}} + c_i$$

En ce qui concerne les conditions de stabilité pour notre schéma voir ([27],[28]).

Chapitre 4

A finite volume extension of the Lax-Friedrichs and Nessyahu-Tadmor schemes for conservation laws on unstructured grids

This paper is dedicated to Professor Antony Jameson on the occasion of his 60^{th}-birthday

by

Paul ARMINJON† , Marie-Claude VIALLON* and Aziz MADRANE†

†Dép. de mathématiques et de statistique, Université de Montréal

C.P. 6128, Succ. centre-ville, Montréal, Québec, Canada, H3C 3J7

*Équipe d'analyse numérique, Université de Saint-Étienne,

23 rue Paul Michelon, 42023 Saint-Étienne Cedex 2, France

ABSTRACT – The non-oscillatory central difference scheme of Nessyahu and Tadmor, in which the resolution of Riemann problems at the cell interfaces is by-passed thanks to the use of the staggered Lax-Friedrichs scheme, is extended here to a two-step, two-dimensional non-oscillatory centered scheme in finite volume formulation. The construction of the scheme rests on a finite volume extension of the Lax-Friedrichs scheme, in which the finite volume cells are the barycentric cells constructed around the nodes of an FEM triangulation, for odd time steps, and some quadrilateral cells associated with this triangulation, for even time steps.
Piecewise linear cell interpolants using least-squares gradients combined with a van Leer-type slope limiting allow for an oscillation-free second-order resolution.

Some preliminary numerical experiments suggest that two-dimensional problems can be handled very efficiently by the method presented here.

1. Introduction

In an attempt to construct a simplified version of high resolution non-oscillatory Godunov-type methods for the numerical approximation of hyperbolic conservation laws [17], Nessyahu and Tadmor [13] recently proposed, for one-dimensional problems, an elegant difference scheme based on a combination of the staggered form of the Lax-Friedrichs scheme [20] and the use of van Leer's MUSCL piecewise linear interpolants [11],[12] in a Godunov-type approach, decomposed in two steps for second-order time and space accuracy.

The main feature of their scheme lies in the fact that it does not require the detailed exact or approximate solution of the local Riemann problems ([10],[14],[15],[16]) generated at the cell interfaces, thanks to the use of the staggered form of the Lax-Friedrichs scheme. Since the scheme proposed by Nessyahu and Tadmor was constructed for one space dimension, we shall present in this paper a two-dimensional method, based on the principle of their scheme, in a finite volume formulation, along the lines of some earlier work ([1],[4], [5]).

In [21], we had described an extension of the Lax-Friedrichs and Nessyahu-Tadmor schemes to two-dimensional rectangular grids. In this paper, we present our two-dimensional extension to unstructured triangular grids (see also [3] for other numerical experiments than those presented here).

In other papers, ([6],[18],[19]), we study the convergence of our method for scalar two-dimensional conservation laws, and prove a maximum principle and a result on the L^{∞}-*weak** convergence of the numerical solution to a weak solution of the scalar equation $u_t + \mathrm{div}(u\,\vec{V}) = 0 \quad \text{with} \quad \mathrm{div}\,\vec{V} = 0.$

In section 2, we give a short description of the Nessyahu-Tadmor (NT) scheme; section 3 presents a two-dimensional finite-volume extension of the Lax-Friedrichs scheme using the barycentric cells constructed around the nodes of an arbitrary (unstructured) triangular Finite Element grid and a dual set of quadrilateral cells; we then present in section 4 a two-dimensional finite volume scheme for arbitrary triangular grids which is inspired, in its construction, by our Finite Volume Lax-Friedrichs scheme and the

Nessyahu-Tadmor difference scheme. Some early numerical experiments are then presented in section 5 (Linear advection, Supersonic Euler flow around a NACA 0012 airfoil, Supersonic flow around a double ellipse).

2. Description of the 1-dimensional Nessyahu-Tadmor scheme

To approximate the solution of the scalar conservation law

$$u_t + f(u)_x = 0 \tag{2.1}$$

with initial condition $-\infty < x < \infty$

$$u(x,0) = u_0(x) \tag{2.1'}$$

we first consider Godunov's [10] approximate solution $\bar{u}(x,t^n)$, which is piecewise constant on the cells $C_j = (x_{j-1/2}, x_{j+1/2})$, for $t = t^1, \ldots, t^n, \ldots$ (with $t^0 = 0$):

$$\bar{u}(x,t^n) = \bar{u}_j^n \quad \text{(defined below) for} \quad x_{j-1/2} < x < x_{j+1/2}. \tag{2.2}$$

Starting from the piecewise constant initial approximation

$$\bar{u}^0(x,0) = \bar{u}_j^0 = \frac{1}{\Delta x}\int_{x_{j-1/2}}^{x_{j+1/2}} u_0(x)dx \quad \text{for} \quad x_{j-1/2} < x < x_{j+1/2}, \tag{2.3}$$

Godunov's method evolves this initial function for a time $\Delta t = t^1 - t^0$ small enough to prevent the corresponding Riemann problems generated at the cell interfaces $x_{j+1/2}$ to interact with each other, thus defining an approximate solution

$$v(x,t^1) = R\left(\frac{x - x_{j+1/2}}{\Delta t}; \bar{u}_j^0, \bar{u}_{j+1}^0\right) \quad x_j < x < x_{j+1} \tag{2.4}$$

where $R\left(\frac{x}{t}, u_\ell, u_r\right)$ is the self-similar exact solution of the Riemann problem for (2.1) at $x_0 = 0$, $t \geq t^0 = 0$ with

$$u(x,0) = \begin{cases} u_\ell & x < 0 \\ u_r & x > 0. \end{cases}$$

The new cell values $\bar{u}_j^1$ are then defined by the cell averages of $v(x,t^1)$:

$$\bar{u}_j^1 = \frac{1}{\Delta x}\int_{C_j} v(x,t^1)dx = \frac{1}{\Delta x}\Big\{\int_{x_{j-1/2}}^{x_j} R\left(\frac{x - x_{j-1/2}}{\Delta t}; \bar{u}_{j-1}^0, \bar{u}_j^0\right)dx + \int_{x_j}^{x_{j+1/2}} R\left(\frac{x - x_{j+1/2}}{\Delta t}; \bar{u}_j^0, \bar{u}_{j+1}^0\right)dx\Big\} \tag{2.5}$$

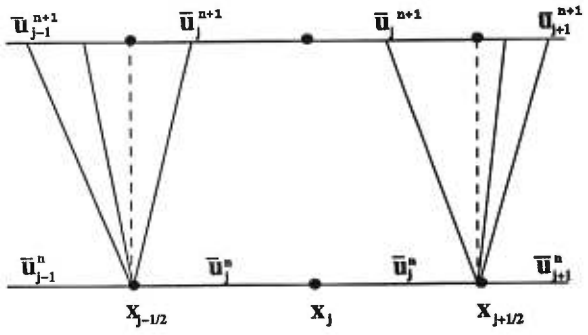

FIGURE 4.27. Non-interacting Riemann problems at the cell endpoints.

The typical time step $t^n \to t^{n+1}$ follows the same pattern, and can be written in conservation form:

$$\bar{u}_j^{n+1} = \bar{u}_j^n - \lambda\Big[f\big(R(o^+; \bar{u}_j^n, \bar{u}_{j+1}^n)\big) - f\big(R(o^+; \bar{u}_{j-1}^n, \bar{u}_j^n)\big)\Big] \quad \Big(\lambda \equiv \frac{\Delta t}{\Delta x}\Big). \tag{2.6}$$

Since our aim is to solve systems of conservation laws, (2.6) shows that Godunov's method requires the detailed (exact or approximate) solution of the Riemann problems posed at the cell interfaces, a time-consuming task which the Nessyahu-Tadmor schemes by-passes thanks to a judicious use of the Lax-Friedrichs scheme [20], written in its staggered form as

$$u_{j+1/2}^{n+1} = \frac{1}{2}(u_j^n + u_{j+1}^n) - \lambda[f(u_{j+1}^n) - f(u_j^n)] \tag{2.7}$$

which can also be interpreted as an application of Godunov's scheme over the staggered grid corresponding to the cells $C_{j+1/2} = (x_j, x_{j+1})$:

$$u_{j+1/2}^{n+1} = \frac{1}{\Delta x}\int_{x_j}^{x_{j+1}} R\left(\frac{x - x_{j+1/2}}{t^{n+1} - t^n}; u_j^n, u_{j+1}^n\right) dx \tag{2.8}$$

starting from cell values $\{u_j^n\}$ defined on the cells $\{(x_{j-1/2}, x_{j+1/2})\}$ of the original grid; the integral in the R.H.S. is computed by integrating (2.1) on $[x_j, x_{j+1}] \times [t^n, t^{n+1}]$ with the help of Green's formula. To complete a computation cycle, and come back to the original gridpoints $\{x_j\}$, we must then perform a second step with the help of the staggered gridpoints:

$$u_j^{n+2} = \frac{1}{2}(u_{j-1/2}^{n+1} + u_{j+1/2}^{n+1}) - \lambda[f(u_{j+1/2}^{n+1}) - f(u_{j-1/2}^{n+1})]. \tag{2.7'}$$

To reduce the numerical dissipation of the scheme and obtain second order accuracy, the Nessyahu-Tadmor scheme then replaces Godunov's piecewise constant cell

values by piecewise linear MUSCL-type interpolants: at the beginning of each time step, we first reconstruct, from the piecewise constant cell average approximation (2.2) obtained at the end of the previous time step, a piecewise linear approximation of the form

$$L_j(x,t^n) = \bar{u}_j^n + (x - x_j)\frac{\delta_j^n}{\Delta x} \quad x_{j-1/2} < x < x_{j+1/2}. \tag{2.9}$$

In this way, conservation is retained

$$\overline{L_j}(t^n) \equiv \frac{1}{\Delta x}\int_{x_{j-1/2}}^{x_{j+1/2}} L_j(x,t^n)dx = \bar{u}_j^n \tag{2.9'}$$

and it can be shown ([13]) that second order accuracy is obtained if the numerical derivative $\delta_j^n/\Delta x$ (to be defined below) satisfies

$$\frac{\delta_j^n}{\Delta x} = \frac{\partial}{\partial x}u(x,t^n)\Big|_{x=x_j} + O(\Delta x). \tag{2.9''}$$

The piecewise linear interpolants (2.9) are then advanced in time by considering the (exact) solution of the non-interacting generalized Riemann problems thus defined at the cell interfaces $x_{j+1/2}$

$$v(x,t^{n+1}) = GR(x,t^{n+1};L_j(x,t^n),L_{j+1}(x,t^n)) \quad x_j < x < x_{j+1} \tag{2.10}$$

from which the new staggered cell average values $\bar{u}_{j+1/2}^{n+1}$ at time t^{n+1} are now defined as

$$\bar{u}_{j+1/2}^{n+1} = \frac{1}{\Delta x}\int_{x_j}^{x_{j+1}} v(x,t^{n+1})dx \tag{2.11}$$

representing the Nessyahu-Tadmor numerical approximation for $x_j < x < x_{j+1}$.

This integral can be computed without actually solving the generalized Riemann problems by first integrating the conservation law (2.1) on the rectangle $\mathcal{R}_{j+1/2}^n \equiv (x_j, x_{j+1}) \times (t^n, t^{n+1})$ to obtain, with Green's theorem (fig. 4.28):

$$\oint_{\partial\mathcal{R}_{j+1/2}^n} (u\,dx - f(u)dt) = 0. \tag{2.12}$$

Applying (2.12) to the function $v(x,t) = GR(x,t;L_j(x,t^n),L_{j+1}(x,t^n))$ then leads to

$$\Delta x \cdot \bar{u}_{j+1/2}^{n+1} = \int_{x_j}^{x_{j+1/2}} L_j(x,t^n)dx + \int_{x_{j+1/2}}^{x_{j+1}} L_{j+1}(x,t^n)dx - \int_{t^n}^{t^{n+1}} f(v(x_{j+1},t))dt + \int_{t^n}^{t^{n+1}} f(v(x_j,t))dt. \tag{2.13}$$

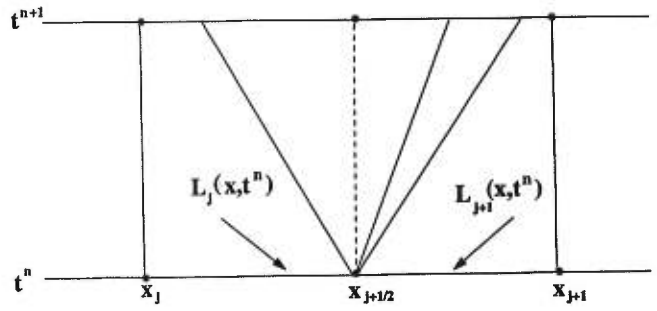

FIGURE 4.28. Line integral on $\partial\mathcal{R}^n_{j+1/2}$.

In the last two integrals, the integrands are smooth functions of t under the CFL condition

$$\lambda \cdot \max_{x_j \le x \le x_{j+1}} \rho\Big(A(v(x,t))\Big) < \frac{1}{2} \tag{2.14}$$

where $\rho(A)$ is the spectral radius of $A(v) \equiv f'(v)$ if (2.1) is a system, and $\rho(A) \equiv |f'(v)|$ if (2.1) is a scalar conservation law. Using (2.9) we can compute the first two integrals exactly, and applying the midpoint rule (with an $O[(\Delta t)^3]$ error) to the flux integrals, we get the numerical approximation

$$\bar{u}^{n+1}_{j+1/2} = \frac{1}{2}(\bar{u}^n_j + \bar{u}^n_{j+1}) + \frac{1}{8}(\delta^n_j - \delta^n_{j+1}) - \lambda\Big[f(v(x_{j+1}, t^{n+1/2})) - f(v(x_j, t^{n+1/2}))\Big] \tag{2.15}$$

where $t^{n+1/2} = t^n + \Delta t/2$,

In [13] the values of $v(x_j, t^{n+1/2})$ needed in (2.15) are approximated as

$$v(x_j, t^{n+1/2}) \cong v(x_j, t^n) + \frac{\Delta t}{2} v_t(x_j, t^n) \cong \bar{u}^n_j - \frac{\Delta t}{2} \cdot \frac{f'_j}{\Delta x} \equiv u^{n+1/2}_j \tag{2.16a}$$

where $\frac{1}{\Delta x} f'_j$ stands for an approximate numerical derivative of the flux $f(v(x,t))$:

$$\frac{1}{\Delta x} f'_j = \frac{\partial}{\partial x} f(v(x,t^n))\Big|_{x=x_j} + O(\Delta x) \tag{2.17}$$

for which several possibilities are studied in [13].

Observe that we could also choose to use (2.9″) in $f(v)_x = f'(v)v_x$ and consider instead of (2.16) the following approximation

$$v(x_j, t^{n+1/2}) \cong \bar{u}^n_j - \frac{\Delta t}{2} f'(\bar{u}^n_j) \frac{\delta^n_j}{\Delta x} \equiv \tilde{u}^{n+1/2}_j. \tag{2.16b}$$

Whatever our choice for the intermediate value, $u_j^{n+1/2}$ or $\tilde{u}_j^{n+1/2}$, the NT scheme can be considered as a predictor (2.16) followed by a corrector (2.15).

To retrieve the original grid $\{x_j\}$ we then perform the alternate time step

$$\bar{u}_j^{n+2} = \frac{1}{2}(\bar{u}_{j+1/2}^{n+1} + \bar{u}_{j-1/2}^{n+1}) + \frac{1}{8}(\delta_{j-1/2}^{n+1} - \delta_{j+1/2}^{n+1}) - \lambda[f(u_{j+1/2}^{n+3/2}) - f(u_{j-1/2}^{n+3/2})]$$

where the definitions of $\delta_{j+1/2}^{n+1}$, $u_{j+1/2}^{n+3/2}$ are similar to (2.9″) and (2.16a)–(2.16b), respectively. One of the approximations considered in [13] for δ_j^n (written as v_j' there) is

$$\begin{aligned} \delta_j^n &= MM\{\alpha\Delta\bar{u}_{j+1/2}^n, \frac{1}{2}(\bar{u}_{j+1}^n - \bar{u}_{j-1}^n), \alpha\Delta\bar{u}_{j-1/2}^n\} \\ &\equiv \text{ min mod } \{\alpha(\bar{u}_{j+1}^n - \bar{u}_j^n), \frac{1}{2}(\bar{u}_{j+1}^n - \bar{u}_{j-1}^n), \alpha(\bar{u}_j^n - \bar{u}_{j-1}^n)\} \end{aligned} \tag{2.18}$$

where $\alpha \in [0, 4]$ is a parameter discussed in [13].

Under appropriate conditions, the NT scheme is then shown to be second-order accurate and TVD (see [13]).

3. 2-dimensional finite volume extension of the Lax-Friedrichs scheme

We consider the solution $u(x, y, t)$ of the two-dimensional scalar conservation equation

$$u_t + f(u)_x + g(u)_y = 0 \tag{3.1}$$

in some region Ω of the $x - y$ plane. In one space dimension, we have seen that both the staggered form of the Lax-Friedrichs scheme and the Nessyahu-Tadmor scheme use two alternate grids $\{x_j\}$ and $\{x_{j+1/2}\}$ at odd and even time steps, respectively. In two dimensions, we proceed in a similar way, starting from an arbitrary FEM triangular grid $\mathcal{T}_h$ such that

$$\Omega = \bigcup_{T \in \mathcal{T}_h} T \text{ and } T \cap T' = \begin{cases} \phi \\ \text{one vertex} \\ \text{one side} \end{cases} \quad \text{for any } T, T' \in \mathcal{T}_h \tag{3.2}$$

The nodes of the FEM triangulation are the vertices a_i of the triangles, and the degrees of freedom are the values of u at the nodes, which can also be considered as cell average values for the cell C_i centered at each individual node a_i (defined below).

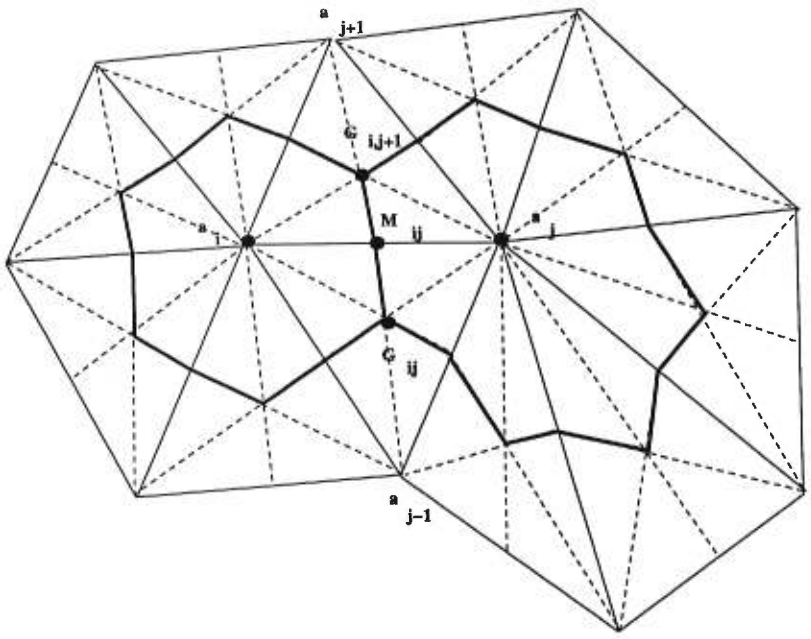

FIGURE 4.29. Barycentric cells around nodes $\mathbf{a_i}$, $\mathbf{a_j}$; quadrilateral cell $\mathbf{a_i G_{ij} a_j G_{i,j+1}}$.

For the first grid associated with our finite volume extension of the Lax-Friedrichs scheme, the nodes are the vertices a_i of $\mathcal{T}_h$ while the finite volume cells are the barycentric cells C_i associated with these nodes, obtained by joining the midpoints M_{ij} of the sides originating in a_i to the centroids G_{ij} of the triangles of $\mathcal{T}_h$ which meet at a_i (fig. 4.29).

For the second grid the nodes are the midpoints M_{ij} of the sides of the original triangulation, while the cells are the quadrilaterals of the form $L_{ij} = a_i G_{ij} a_j G_{i,j+1}$ having M_{ij} as midpoint of one diagonal, obtained by joining two adjacent nodes a_i, a_j to the centroids of the two triangles of $\mathcal{T}_h$ of which $a_i a_j$ is a side.

Let $u_i^n \cong u(a_i, t^n)$ and $u_{ij}^{n+1} \cong u(M_{ij}, t^{n+1})$ denote the nodal (or cell average) values in the first and second grid at time $t = t^n$ and $t = t^{n+1}$, respectively (n even).

For the barycentric cell C_i, let $\vec{\nu}_{ij}^1$ and $\vec{\nu}_{ij}^2$ denote the unit outer normal vectors to $G_{ij}M_{ij}$ and $M_{ij}G_{i,j+1}$ respectively, pointing out of cell C_i (fig. 4.30), and for the quadrilateral cell L_{ij}, let $\vec{n}^{\,1}{}_{ij}, \ldots, \vec{n}_{ij}^4$ be the normal vectors to the cell edges $a_i G_{ij}$, $G_{ij}a_j$, $a_j G_{i,j+1}$ and $G_{i,j+1}a_i$, respectively, pointing out of cell L_{ij} (fig. 4.31).

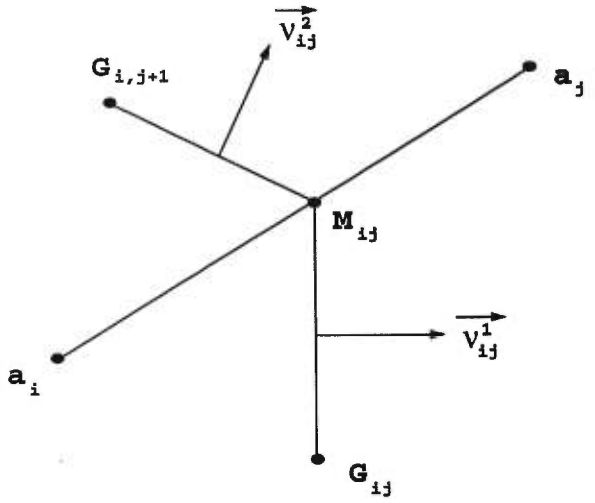

FIGURE 4.30. Barycentric cell boundary element $\Gamma_{ij} = \mathbf{G_{ij}M_{ij}} \cup \mathbf{M_{ij}G_{i,j+1}}$.

We must also define the elementary flux vectors

$$\vec{\eta}_{ij} = \int_{\Gamma_{ij}=G_{ij}M_{ij}G_{i,j+1}} \vec{\nu} d\sigma = |\overrightarrow{G_{ij}M_{ij}}|\vec{\nu}^1_{ij} + |\overrightarrow{M_{ij}G_{i,j+1}}|\vec{\nu}^2_{ij} \tag{3.3a}$$

and

$$\begin{cases} \vec{\theta}_{ij} = |\overrightarrow{a_iG_{ij}}|\vec{n}^1_{ij} + |\overrightarrow{a_iG_{i,j+1}}|\vec{n}^4_{ij} \\ \vec{\theta}_{ji} = |\overrightarrow{a_jG_{ij}}|\vec{n}^2_{ij} + |\overrightarrow{a_jG_{i,j+1}}|\vec{n}^3_{ij}. \end{cases} \tag{3.3b}$$

We write furthermore

$$\vec{\nu}^k_{ij} = \begin{pmatrix} \nu^k_{ijx} \\ \nu^k_{ijy} \end{pmatrix} \text{ for } k = 1,2, \quad \vec{n}^k_{ij} = \begin{pmatrix} n^k_{ijx} \\ n^k_{ijy} \end{pmatrix} \text{ for } k = 1,\ldots,4$$

$$\text{and } \vec{\eta}_{ij} = \begin{pmatrix} \eta_{ijx} \\ \eta_{ijy} \end{pmatrix}, \quad \vec{\theta}_{ij} = \begin{pmatrix} \theta_{ijx} \\ \theta_{ijy} \end{pmatrix}. \tag{3.3c}$$

An advantage of using a finite volume formulation where the degrees of freedom are values of the unknown function at the triangulation vertices lies in the possibility to couple (3.1) with an elliptic equation. This can be very convenient in the case where

$$\begin{cases} f(u) = w_1\, h(u) \\ g(u) = w_2\, h(u) \end{cases}$$

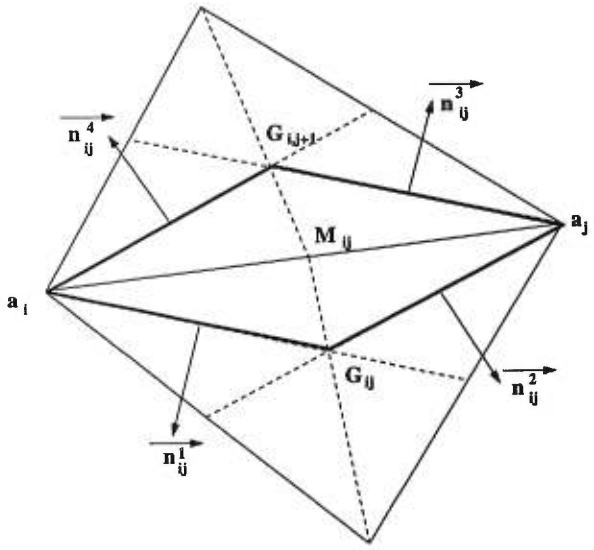

FIGURE 4.31. Quadrilateral cells $\mathbf{L_{ij}}$.

i.e. when (3.1) can be written as $u_t + \operatorname{div}(\vec{W}\, h(u)) = 0$ with $\vec{W} = (w_1, w_2)^T$ and $\vec{W}$ stems from an elliptic problem. This situation arises in the study of polyphase flows in porous media, where fluid mechanical and thermodynamical considerations are combined, leading to coupled hyperbolic and elliptic equations [8].

The first step of the two-dimensional finite volume extension of the Lax-Friedrichs scheme is defined by integrating (3.1) on the 3-dimensional cell $L_{ij} \times [t^n, t^{n+1}]$, assuming that the (barycentric) cell values u_i^n at the vertices a_i of the original triangulation are known:

$$\int_{t^n}^{t^{n+1}} \int_{L_{ij}} (u_t + f(u)_x + g(u)_y) dx dy\, dt = 0. \tag{3.4a}$$

Applying the divergence theorem and observing that $L_{ij} = (L_{ij} \cap C_i) \cup (L_{ij} \cap C_j)$ we get

$$\int_{L_{ij}} u(x,y,t^{n+1}) dA - \int_{L_{ij}\cap C_i} u(x,y,t^n) dA - \int_{L_{ij}\cap C_j} u(x,y,t^n) dA + \int_{t^n}^{t^{n+1}} \int_{\partial L_{ij}} (f(u)n_x + g(u)n_y) d\sigma\, dt = 0. \tag{3.4b}$$

Since $u(x,t)$ is approximated by u_i^n in C_i, u_j^n in C_j, we can choose the approximation u_i^n on $\partial L_{ij} \cap C_i$ and u_j^n on $\partial L_{ij} \cap C_j$, whence the first step of our finite volume

Lax-Friedrichs scheme:

$$A(L_{ij})u_{ij}^{n+1} - A(L_{ij} \cap C_i) \cdot u_i^n - A(L_{ij} \cap C_j) \cdot u_j^n + \Delta t(f(u_i^n)\theta_{ijx} + g(u_i^n)\theta_{ijy}) + \Delta t(f(u_j^n)\theta_{jix} + g(u_j^n)\theta_{jiy}) = 0. \quad (3.5)$$

We note that this approximation corresponds to choosing the approximate time derivative

$$u_t \cong \left(u_{ij}^{n+1} - \frac{A(L_{ij} \cap C_i) \cdot u_i^n + A(L_{ij} \cap C_j) \cdot u_j^n}{A(L_{ij})} \right) / \Delta t. \quad (3.6)$$

For the second step we proceed similarly with the help of the barycentric cells C_i:

$$A(C_i)u_i^{n+2} - \sum_{j \text{ neighbour of } i} A(L_{ij} \cap C_i)u_{ij}^{n+1} + \Delta t \sum_{j \text{ neighbour of } i} (f(u_{ij}^{n+1})\eta_{ijx} + g(u_{ij}^{n+1})\eta_{ijy}) = 0 \quad (3.7)$$

where the value of $u(x, y, t^{n+1})$ on the boundary $\partial C_i = \bigcup_{j \text{ neighbour of } i} \Gamma_{ij}$ is approximated locally, on $\partial C_i \cap L_{ij} = \Gamma_{ij}$, by u_{ij}^{n+1} (i.e. the approximate value of u^{n+1} on the quadrilateral cell L_{ij}. We thus alternately define an approximate solution u_{ij}^{n+1} which is piecewise constant on the quadrilateral cells L_{ij}, at odd time steps ($n = 0, 2, \dots$), and a solution u_i^{n+2} constant on the barycentric cells C_i, at even time steps.

4. A two-dimensional finite volume extension of the Nessyahu-Tadmor scheme

At the beginning of the $(n+1)^{\text{st}}$ time step (n even), we have obtained approximate barycentric cell values u_i^n (a_i : a vertex of $\mathcal{T}_h$). We must now, in order to follow the van Leer MUSCL approach used by Nessyahu and Tadmor, construct a piecewise linear profile on the barycentric cells C_i; this can be achieved as follows.

We first construct a piecewise linear approximant on each triangle T of the original triangulation, continuous on the whole computational domain Ω_h, with the help of the barycentric cell/nodal values u_i^n: if $T \in \mathcal{T}_h$ is a triangle with vertices a_{i_j}, ($j = 1, 2, 3$), we construct $p_T \in P^1$ such that

$$p_T(a_{i_j}) = u_{i_j}^n \ (j = 1, 2, 3)$$

$p_T(x,y)$ is easily obtained from the barycentric coordinates of (x,y) with respect to the vertices of T:

$$p_T(\vec{x}) = \sum_{j=1}^{3} \lambda_j(\vec{x}) u_j^n$$

where the vertices of T have been relabelled $1,2,3$ or a_1, a_2, a_3, and $\vec{x} = (x,y) \in T$.

The gradient of the (barycentric) cellwise *piecewise linear interpolant* $L(x,y,t^n)$ to be defined will now be chosen (as e.g. in [9] p.28), for cell C_i, as the arithmetic average of the gradients of the polynomials p_T for all triangles T such that $a_i \in T$: on C_i we take

$$L = L_i(x,y,t^n) = u_i^n + (x - x_i)P_i^n + (y - y_i)Q_i^n \qquad (x,y) \in C_i \tag{4.1a}$$

where

$$\begin{pmatrix} P_i^n \\ Q_i^n \end{pmatrix} = \underset{a_i \in T}{\text{Average}} \{\text{grad } p_T\}. \tag{4.1b}$$

Contrary to what prevailed in the one-dimensional case, where the average value $\bar{u}_j^n$ of the piecewise linear interpolant $L_j(x,t^n)$ was also its value at the node x_j, we can no longer identify the average value of the piecewise linear interpolant (4.1), on cell C_i, with its nodal value u_i^n at the "center" a_i of C_i, since a_i need not be the centroid of C_i, and $\frac{1}{A(C_i)} \int_{C_i} L_i(x,y,t^n)dA \neq u_i^n$ in general.

The new cell values at t^{n+1} and t^{n+2} will nevertheless again be *defined* by formulas similar to (2.13) and (3.4b), (3.5) (first step), and (3.7) (second step), obtained by integrating (3.1) on $L_{ij} \times [t^n, t^{n+1}]$ for the first step, and on $C_i \times [t^n, t^{n+1}]$ for the second step:

$$A(L_{ij})u_{ij}^{n+1} \equiv \text{numerical approximation of } \int_{L_{ij}} u(x,y,t^{n+1})dA \tag{4.2a}$$

$$A(C_i)u_i^{n+2} \equiv \text{numerical approximation of } \int_{C_i} u(x,y,t^{n+2})dA. \tag{4.2b}$$

For the first step of our scheme we write

$$\int_{t^n}^{t^{n+1}} \int_{L_{ij}} (u_t + f(u)_x + g(u)_y)dAdt = 0 \tag{4.3a}$$

which leads to

$$\int_{L_{ij}} u(x,y,t^{n+1})dA = \int_{L_{ij}\cap C_i} L(x,y,t^n)dA + \int_{L_{ij}\cap C_j} L(x,y,t^n)dA - \int_{t^n}^{t^{n+1}} \int_{\partial L_{ij}} (f(u)n_x + g(u)n_y)d\sigma dt. \quad (4.3b)$$

The numerical approximation of the right-hand side, and (4.2a), will thus lead to u_{ij}^{n+1}, which will be our cell value for the quadrilateral cell L_{ij}.

4.1. Approximation of $\int_{L_{ij}\cap C_i} L(x,y,t^n)dA$.

$L(x,y,t^n)$ is the piecewise linear function defined, on cell C_i, by (4.1). Let $A_iA_{ij}B_{ij}$ $A_{i,j+1}$ be the points of the plane defined by the linear function L_i on C_i which correspond to the four vertices of $L_{ij}\cap C_i = [a_iG_{ij}M_{ij}G_{i,j+1}]$ where [...] denotes the quadrilateral generated by the corresponding vertices (fig. 4.32).

The integral of L on $L_{ij}\cap C_i$ is equal to the total volume of the two prisms with triangular base $a_iG_{ij}M_{ij}A_iA_{ij}B_{ij}$ and $a_iM_{ij}G_{i,j+1}A_iB_{ij}A_{i,j+1}$, constructed on the triangular bases $L_{ij}^r\cap C_i$ and $L_{ij}^\ell\cap C_i$ where L_{ij}^r = triangle $(a_iG_{ij}a_j)$ and L_{ij}^ℓ = triangle $(a_ia_jG_{i,j+1})$; r,ℓ stand for right, left (for an observer at a_i).

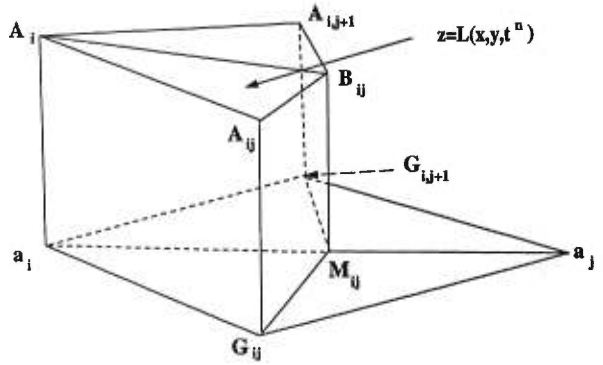

FIGURE 4.32. Prismatic regions for the computation of $\int_{L_{ij}\cap C_i} L(x,y,t^n)dA$.

The volume of the first prism, for instance, is given by

$$\begin{aligned}\text{Vol}\{a_iG_{ij}M_{ij}A_iA_{ij}B_{ij}\} &= \frac{1}{3}\,\text{Area}\,(a_iG_{ij}M_{ij})\cdot[a_iA_i+G_{ij}A_{ij}+M_{ij}B_{ij}]\\ &= \frac{1}{3}\,\text{Area}\,(L_{ij}^r\cap C_i)\{u_i^n+u_i^n+(x_{G_{ij}}-x_i)P_i^n\\ &\qquad +(y_{G_{ij}}-y_i)Q_i^n+u_i^n+(x_{M_{ij}}-x_i)P_i^n\\ &\qquad +(y_{M_{ij}}-y_i)Q_i^n\}\\ &= \text{Area}\,(L_{ij}^r\cap C_i)\{u_i^n+\frac{1}{3}(x_{G_{ij}}+x_{M_{ij}}-2x_i)P_i^n\\ &\qquad +\frac{1}{3}(y_{G_{ij}}+y_{M_{ij}}-2y_i)Q_i^n\}\end{aligned}\tag{4.4a}$$

where

$$\begin{aligned}\text{Area}\,(L_{ij}^r\cap C_i) &\equiv \text{Area triangle}\,(a_iG_{ij}M_{ij})\\ &= \frac{1}{2}\{(x_{G_{ij}}-x_i)(y_{M_{ij}}-y_i)-(x_{M_{ij}}-x_i)(y_{G_{ij}}-y_i)\}.\end{aligned}\tag{4.4b}$$

Similarly, the volume of the second prism is

$$\begin{aligned}\text{Vol}\{a_iM_{ij}G_{i,j+1}\ A_iB_{ij}A_{i,j+1}\} &= \text{Area}(L_{ij}^\ell\cap C_i)\cdot\\ &\{u_i^n+\frac{1}{3}(x_{M_{ij}}+x_{G_{i,j+1}}-2x_i)P_i^n+\frac{1}{3}(y_{M_{ij}}+y_{G_{i,j+1}}-2y_i)\}\end{aligned}\tag{4.4c}$$

Summing (4.4a) and (4.4c), we get

$$\begin{aligned}\int_{L_{ij}\cap C_i}L(x,y,t^n)dA &= \text{Area}(L_{ij}\cap C_i)\{u_i^n+\frac{1}{3}(x_{M_{ij}}-x_i)P_i^n+\frac{1}{3}(y_{M_{ij}}-y_i)Q_i^n\}\\ &+\frac{1}{3}\text{Area}(L_{ij}^r\cap C_i)\{(x_{G_{ij}}-x_i)P_i^n+(y_{G_{ij}}-y_i)Q_i^n\}\\ &+\frac{1}{3}\text{Area}(L_{ij}^\ell\cap C_i)\{(x_{G_{i,j+1}}-x_i)P_i^n+(y_{G_{i,j+1}}-y_i)Q_i^n\}\end{aligned}\tag{4.5a}$$

with

$$\text{Area}(L_{ij}^\ell\cap C_i)\ =\ \frac{1}{2}\{(x_{M_{ij}}-x_i)(y_{G_{i,j+1}}-y_i)-(x_{G_{i,j+1}}-x_i)(y_{M_{ij}}-y_i)\}.\tag{4.4d}$$

4.2. Approximation of $\int_{L_{ij}\cap C_j} L(x,y,t^n)dA$.

Proceeding in the same way we find

$$\begin{aligned}\int_{L_{ij}\cap C_j}L(x,y,t^n)dA &= \text{Area}(L_{ij}\cap C_j)\{u_j^n+\frac{1}{3}(x_{M_{ij}}-x_j)P_j^n+\frac{1}{3}(y_{M_{ij}}-y_j)Q_j^n\}\\ &+\frac{1}{3}\text{Area}(L_{ij}^r\cap C_j)\{(x_{G_{ij}}-x_j)P_j^n+(y_{G_{ij}}-y_j)Q_j^n\}\\ &+\frac{1}{3}\text{Area}(L_{ij}^\ell\cap C_j)\{(x_{G_{i,j+1}}-x_j)P_j^n+(y_{G_{i,j+1}}-y_j)Q_j^n\}\end{aligned}\tag{4.5b}$$

where

$$\text{Area}(L_{ij}^r \cap C_j) = \frac{1}{2}\{(x_{M_{ij}} - x_j)(y_{G_{ij}} - y_j) - (x_{G_{ij}} - x_j)(y_{M_{ij}} - y_j)\}.$$

4.3. Approximation of $\int_{t^n}^{t^{n+1}} \int_{\partial L_{ij}} \{f(u)n_x + g(u)n_y\} d\sigma dt$.

This is achieved with the midpoint rule for integration with respect to time:

$$\int_{t^n}^{t^{n+1}} \int_{\partial L_{ij}} (f(u)n_x + g(u)n_y) d\sigma dt \cong \Delta t \int_{\partial L_{ij}} \Big\{ f(u(x,y,t^{n+1/2}))n_x + g(u(x,y,t^{n+1/2}))n_y \Big\} d\sigma \quad (4.5c)$$

where a first order Taylor expansion is used for $u(x,y,t^{n+1/2})$; using (3.1) we write

$$u(x,y,t^{n+1/2}) \cong u(x,y,t^n) - \frac{\Delta t}{2}\{f'(u(x,y,t^n))u_x(x,y,t^n) + g'(u(x,y,t^n))u_y(x,y,t^n)\} \quad (4.6)$$

On $L_{ij} \cap C_i$ we have chosen $u_x \equiv P_i^n$ and $u_y \equiv Q_i^n$, but we must find an approximate value of $u(x,y,t^n)$ on the line segments a_iG_{ij} and $a_iG_{i,j+1}$ (and similarly on a_jG_{ij} and $a_jG_{i,j+1}$). One possible choice consists in choosing the value of $L(x,y,t^n)$, our linear interpolant, at the midpoints of these segments; we then take, for any (x,y) on a_iG_{ij}:

$$u(x,y,t^n) \cong u_i^n + \frac{1}{2}(x_{G_{ij}} - x_i)P_i^n + \frac{1}{2}(y_{G_{ij}} - y_i)Q_i^n \equiv u_{a_i,G_{ij}}^n \quad (4.7)$$

thus defining our value $u_{a_i,G_{ij}}^n$ for the side a_iG_{ij} of L_{ij}.

In view of (4.6), we can now define an approximate average value of $u(x,y,t^{n+1/2})$ along the side a_iG_{ij} to be used in (4.5c):

$$u_{a_iG_{ij}}^{n+1/2} = u_{a_i,G_{ij}}^n - \frac{\Delta t}{2}\{f'(u_{a_i,G_{ij}}^n)P_i^n + g'(u_{a_i,G_{ij}}^n)Q_i^n\}.$$

Introducing these values in (4.5c), we finally get

$$\begin{aligned}
\frac{1}{\Delta t}\int_{t^n}^{t^{n+1}} \int_{\partial L_{ij}} \{f(u)n_x + g(u)n_y\} d\sigma dt \\
\cong f(u_{a_i,G_{ij}}^{n+1/2})n_{ijx}^1 \cdot |a_iG_{ij}| + f(u_{a_i,G_{i,j+1}}^{n+1/2})n_{ijx}^4 \cdot |a_iG_{i,j+1}| \\
+ f(u_{a_j,G_{ij}}^{n+1/2})n_{ijx}^2 \cdot |a_jG_{ij}| + f(u_{a_j,G_{i,j+1}}^{n+1/2})n_{ijx}^3 \cdot |a_jG_{i,j+1}| \\
+ g(u_{a_i,G_{ij}}^{n+1/2})n_{ijy}^1 \cdot |a_iG_{ij}| + g(u_{a_i,G_{i,j+1}}^{n+1/2})n_{ijy}^4 \cdot |a_iG_{i,j+1}| \\
+ g(u_{a_j,G_{ij}}^{n+1/2})n_{ijy}^2 \cdot |a_jG_{ij}| + g(u_{a_j,G_{i,j+1}}^{n+1/2})n_{ijy}^3 \cdot |a_jG_{i,j+1}|. \quad (4.5e)
\end{aligned}$$

4.4. First step of the finite volume extension of the Nessyahu-Tadmor scheme.

Collecting our approximations (4.5 a,b,e) of the three terms appearing in the R.H.S. of (4.3b) and taking (4.2a) into account, we obtain the following approximation u_{ij}^{n+1} for the first (odd) time step of our scheme:

$$\text{Area}(L_{ij})u_{ij}^{n+1} = \text{R.H.S.(4.5a)} + \text{R.H.S.(4.5b)} - \Delta t \cdot \{\text{R.H.S.(4.5e)}\} \qquad (4.8)$$

where u_{ij}^{n+1} can be considered as a cell value for cell L_{ij} at time t^{n+1}, or as a nodal value at the midpoint M_{ij}, at time t^{n+1}.

In preparation for the second (even) time step, we now construct a piecewise linear approximation of u on the quadrilaterals L_{ij}:

$$u(x,y,t^{n+1}) \cong L^{(o)}(x,y,t^{n+1}) \equiv u_{ij}^{n+1} + (x - x_{M_{ij}})P_{ij}^{n+1} + (y - y_{M_{ij}})Q_{ij}^{n+1} \qquad (4.9)$$

where the slopes P_{ij}^{n+1}, Q_{ij}^{n+1} can be computed as follows.

First we construct a piecewise linear approximate function defined on the triangles $T \in \mathcal{T}_h$ of the original triangulation. On triangle $T = a_i a_j a_k$, we can use for that purpose the newly obtained values u_{ij}^{n+1} at the midpoints of the sides of T. We then compute the average of the slopes of the linear interpolants in the two triangles $T, T' \in \mathcal{T}_h$ sharing $a_i a_j$ as a common side (fig. 4.31), and use these averages in (4.9).

4.5. Second step of the finite volume Nessyahu-Tadmor scheme.

The second step is obtained by integrating (3.1) on the cylindric region $C_i \times [t^{n+1}, t^{n+2}]$, using the same finite volume approach as for the first step, to define a cell average value u_i^{n+2} on cell C_i:

$$\begin{aligned} \text{Area}(C_i)u_i^{n+2} - \sum_{j \text{ neighbour of } i} \int_{L_{ij} \cap C_i} u(x,y,t^{n+1})dxdy \\ = -\Delta t \sum_{j \text{ neighbour of } i} \int_{\Gamma_{ij}} \{f(u(x,y,t^{n+3/2}))\nu_x + g(u(x,y,t^{n+3/2}))\nu_y\}d\sigma \end{aligned} \qquad (4.10)$$

where $u(x,y,t^{n+1})$ is approximated, on $L_{ij} \cap C_i$, by the piecewise linear interpolant (4.9). Its integral on $L_{ij} \cap C_i$ is computed as described in section 4.1.

To obtain an approximate value of $u(x,y,t^{n+3/2})$ we use a Taylor expansion with respect to time combined with (3.1), and we subdivide the cell-boundary element Γ_{ij} into $G_{ij}M_{ij} \cup M_{ij}G_{i,j+1}$. On $G_{ij}M_{ij}$ (resp. $M_{ij}G_{i,j+1}$), $u(x,y,t)$ is then approximated by its value of the midpoint of the line segment $G_{ij}M_{ij}$ (resp. $M_{ij}G_{i,j+1}$).

4.6. Approximation of the slopes.

In order to compute the gradient (P_i^n, Q_i^n) of the piecewise linear interpolant $L(x, y, t^n)$ for the cell C_i, we must first compute the gradient of the first degree polynomials P_T for all triangles $T \in \mathcal{T}_h$ such that $a_i \in T$. Although we could then in principle directly take the average of the gradients of the polynomials P_T, obtained as described at the beginning of section 4, we shall consider here a least-squares technique (cf. [7]). For simplicity, we shall describe it for the case of triangular (finite volume) cells.

Let T be a triangle with centroid G, and let T_j, $j = 1, 2, 3$ be the neighbouring triangles, with centroids $G_j (j = 1, \ldots, 3)$ (fig. 4.33); assume the values of the numerical approximation of the solution u at the four points $\{G, G_j\}_{j=1}^3$ are known at time t^n, equal to u_T^n, $u_{T_j}^n$ $(j = 1, \ldots, 3)$ (these values can be considered as cell values playing for the triangular cells T, T_j the same role as u_i^n, u_{ij}^n for the cells C_i, L_{ij}).

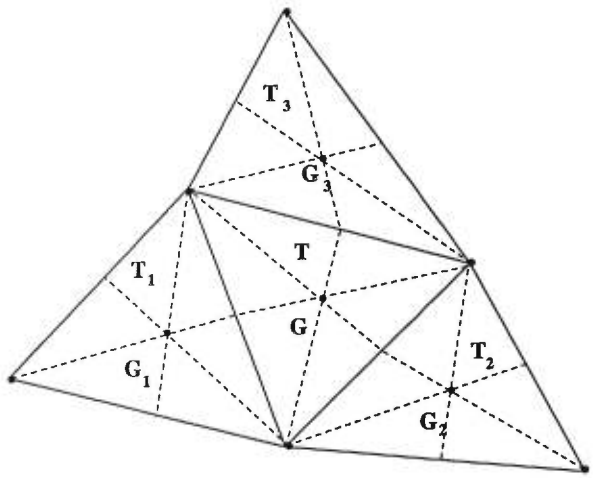

FIGURE 4.33. Computation of the least-squares gradient for a triangular cell **T**.

The least-squares gradient $(\widetilde{grad\ u})_T^n = (\tilde{a}_T^n, \tilde{b}_T^n)$ for triangle T will then be chosen such as to minimize the functional

$$I = \sum_{j=1}^{3} \{u_T^n + \overrightarrow{GG_j} \cdot (grad\ u)_T^n - u_{T_j}^n\}^2 \tag{4.11}$$

where

$$(grad\ u)_T^n = (a_T^n, b_T^n)$$

The minimum is obtained when

$$\frac{\partial I}{\partial a_T^n} = \frac{\partial I}{\partial b_T^n} = 0 \tag{4.12}$$

and is shown in [7] to lead to the following least-squares gradient:

$$\tilde{a}_T^n = \frac{1}{D}\sum_{j=1}^{3}(y_{G_j} - y_G)^2 \sum_{j=1}^{3}(u_{T_j}^n - u_T^n)(x_{G_j} - x_G) - \frac{1}{D}\sum_{j=1}^{3}(x_{G_j} - x_G)(y_{G_j} - y_G)\sum_{j=1}^{3}(u_{T_j}^n - u_T^n)(y_{G_j} - y_G) \tag{4.13a}$$

$$\tilde{b}_T^n = \frac{1}{D}\sum_{j=1}^{3}(x_{G_j} - x_G)^2 \sum_{j=1}^{3}(u_{T_j}^n - u_T^n)(y_{G_j} - y_G) - \frac{1}{D}\sum_{j=1}^{3}(x_{G_j} - x_G)(y_{G_j} - y_G)\sum_{j=1}^{3}(u_{T_j}^n - u_T^n)(x_{G_j} - x_G) \tag{4.13b}$$

where the denominator

$$D = \sum_{j=1}^{3}(x_{G_j} - x_G)^2 \sum_{j=1}^{3}(y_{G_j} - y_G)^2 - \left[\sum_{j=1}^{3}(x_{G_j} - x_G)(y_{G_j} - y_G)\right]^2 \tag{4.13c}$$

is strictly positive for any non-degenerated triangle.

For the barycentric cells C_i or the quadrilateral cells L_{ij}, the procedure is quite similar to the one described above for triangular cells. Alternately, for a barycentric cell C_i with center a_i, we could first compute the least squares gradient grad $u|_{T_j} = (\tilde{a}_{T_j}^n, \tilde{b}_{T_j}^n)$ of each neighbouring triangle T_j (such that $a_i \in T_j$), and then take the cell gradient grad $u|_{C_i}$ = average{grad $u|_{T_j}$}, with a similar procedure for a quadrilateral cell L_{ij}.

Unfortunately, this procedure does not preserve monotonicity of the data in the usual van Leer sense described below, and allows the creation of local extremas between the nodes; this phenomenon may lead to (or amplify already existing) spurious oscillations, with the associated loss of stability and convergence difficulties in the case of steady flows. We have therefore introduced some slope limitation in the computation of the gradients.

4.6.1. Slope limitation. To ensure the stability of the scheme and prevent the generation of oscillations in regions of strong gradients, we must perform a slope correction. Following van Leer's approach ([11], [12]), in which the value at some interface point $x_{i+1/2}$ (in the one dimensional case) must fall within the range of values spanned by

the adjacent grid averages, u_{i-1} and u_{i+1}, we limit the slopes of the linear interpolant L defined by (4.1) (resp. $L^{(o)}$ defined by (4.9)) to ensure that its value at the boundary points $G_{ij}, M_{ij}, G_{i,j+1}$ of ∂C_i (resp. at the vertices $a_i, a_j, G_{ij}, G_{i,j+1}$ of ∂L_{ij}) are bounded by the values at the cell center u_i^n (resp. u_{ij}^{n+1}) and the value u_j^n at the corresponding neighbouring node a_j (resp $u_{i,j-1}^{n+1}$ and $u_{i,j+1}^{n+1}$ at the adjacent quadrilateral cell"midpoints" $M_{i,j-1}$ and $M_{i,j+1}$).

The limitation procedure is implemented on each cell as follows. Let

$$(grad\ u)_i = (P_i, Q_i)^T$$

denote the gradient for cell i, where $P_i \approx u_x$, $Q_i \approx u_y$ at node i. If u satisfies the van Leer requirement we choose

$$P_i^{\lim} = \underset{j \in \mathcal{N}(i)}{\text{minmod}} \{P_j\}$$

$$= \begin{cases} \min_{j \in \mathcal{N}(i)} |P_j| . (\text{common sign of all values } P_j) \\ \qquad\qquad \text{if all the values } P_j \ (j \in \mathcal{N}(i)) \text{ have the same sign} \\ 0 \qquad\qquad \text{otherwise} \end{cases}$$

where $\mathcal{N}(i)$ is the set of nodes j adjacent to node i. If u does not satisfy the van Leer requirement, we set $P_i^{\lim} = 0$. The computation of $Q_i^{\lim}$ is done in the same manner. For quadrilateral cells L_{ij} we proceed in a similar way.

5. Numerical Experiments

The extension to two-dimensional systems of conservation laws is achieved following the procedure described in [1],[2],[5]. In[32], the first author had proposed a finite volume extension of the Nessyahu-Tadmor central difference scheme to 2-dimensional rectangular grids. With his student D.Stanescu, and the second author, he then applied this finite volume scheme to **regular rectangular grids** [21]. Some early numerical experiments (Linear advection, Burgers' equation, Diffraction of a planar shock wave around a 90^o corner [22], Mach 3 wind tunnel with a forward facing step) confirmed the non-oscillatory character as well as the 2^{nd}-order accuracy of the new scheme [21], while computing times were significantly shorter than corresponding times for Godunov's method.

In this paper, we present sample results from some further numerical experiments with our extension of the Nessyahu-Tadmor scheme to **unstructured triangular** FEM grids [6].

The aim here was not to obtain an optimal accuracy to computing time ratio but simply to show the feasibility of the method. Sharper results, including comparison of results obtained with different limiters, will be described in future work [29].

The overall quality of the results and the relatively low level of both the computational complexity and computing times suggest that two-dimensional problems can be handled very efficiently with our method, which should benefit from its multi-dimensional character, as may be seen from the examples presented here.

Example 1 linear advection problem

To test the (predictably) rather unsatisfactory accuracy of our finite volume extension of the Lax-Friedrichs scheme (first order accurate), and compare it to that of our second order accurate finite volume method inspired by the Nessyahu-Tadmor scheme, we solved the linear advection problem

$$u_t + u_x + u_y = 0 \qquad -1 \leq x, y \leq 1 \tag{5.1}$$

$$u_o(x,y) = \begin{cases} 0.5 & \text{if} \quad x^2 + y^2 \leq 0.5; \\ 0 & \text{otherwise.} \end{cases}$$

For this first test case , we felt it might be interesting to show the results obtained with our finite volume extensions of the Lax-Friedrichs and Nessyahu-Tadmor schemes for rectangular grids, with three different choices for the gradients used in the piecewise linear reconstruction at the beginning of each time step, for the second order scheme. We thus tested the following schemes [21].

1) L× F : 2-dimensional staggered finite volume extension of the Lax-Friedrichs scheme (first-order accurate),

2) STG : 2-dimensional Arminjon-Viallon finite volume extension of the Nessyahu-Tadmor scheme with Min-Mod limiter [17],

3) STG-Roe : same as 2, but with Roe's superbee limiter [17],

4) STG-UNO : same as 2, but with UNO- computed slopes (see [21],[13]).

Scheme 1 is first order accurate, while 2,3 and 4 are second order accurate. The solution at time $t = 0.1$ is computed using 50 double time steps (50 integrations on the staggered grid and 50 on the original grid) on a regular 85×85 rectangular grid, with a CFL-number $\nu_x = \nu_y = 0.002$.

The exact solution is

$$u(x, y, t) = u_o(x - t, y - t)$$

and is truly two-dimensional since its wave front is at an angle of 45^o with the x and y axes.

Table 4.1 shows the L^2-norms of the errors, and thus the increasing accuracy obtained, for this example, with the four schemes.

Scheme	$\|\|e\|\|_2$
$L \times F$	$3.055E^{-2}$
STG	$1.313E^{-2}$
STG-Roe	$8.071E^{-3}$
STG-UNO	$6.357E^{-3}$

TABLE 4.1. L^2-norms of the errors

Figure 8 a),b),c) shows the initial function and the results obtained with the schemes STG and L×F, while figure 8 d), e) shows the solution $u(x, y = 0, t = 0.1)$ as obtained with STG-UNO and L×F respectively.

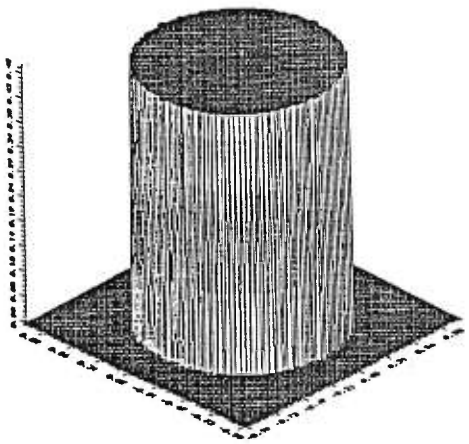

FIGURE 8. **Linear advection problem (a) initial distribution .**

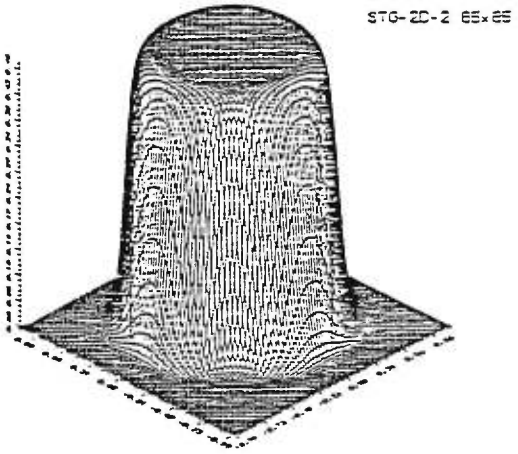

ure 8b.) Convected surface (STG)

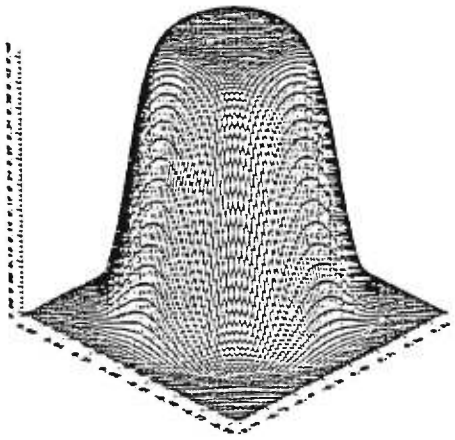

(Figure 8c.) Convected surface (L×F)

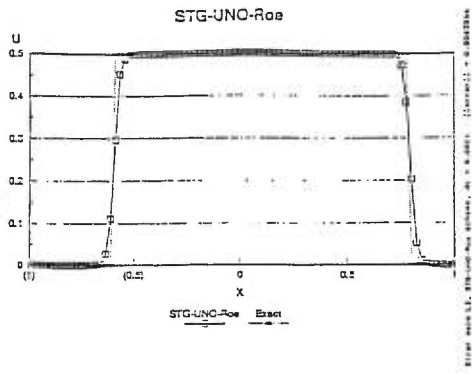

(Figure 8d.) Vertical cut of the convected surface (STG-UNO) $y = 0, t = 0.1$

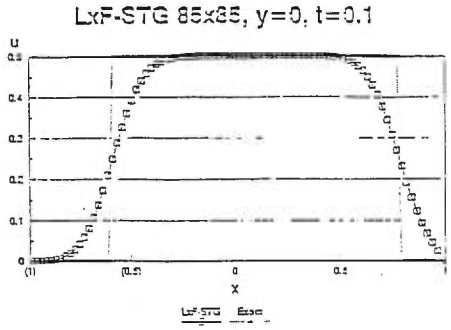

(Figure 8e.) Vertical cut of the convected surface (L×F) $y = 0. t = 0.1$

Example 2 A standard test case Euler flow around a NACA 0012 airfoil

We present results for the NACA 0012 airfoil at Mach number $M_\infty = 2.0$ and incidence $\alpha = 0^o$. The initial mesh had 2274 nodes and 4360 elements (fig. 4.35 and 4.36) . We observe a reasonably good capture of the shock (fig. 4.36) as compared e.g. with [25], where the grid has 4224 nodes. Going to the first improved grid (3557 vertices, fig. 4.38) lets our scheme produce a substantially better shock resolution than that displayed in [25]. As we go on, improving the mesh to 4497 vertices (fig. 4.39) we observe an even better resolution. The final grid (7269 vertices, fig. 4.40) leads to an excellent shock resolution.

The grid adaptation procedure used here has been developed by M.J.Castro Diaz and F.Hecht at INRIA ([30],[31]).

Let us mention, though, that Venkatakrishnan's results are obtained with an implicit scheme using 3 different kinds of limiter; for the best of these, convergence is faster than with our scheme with the basic MinMod limiter; a fact which might be due to the implicit character of the scheme used in [25].

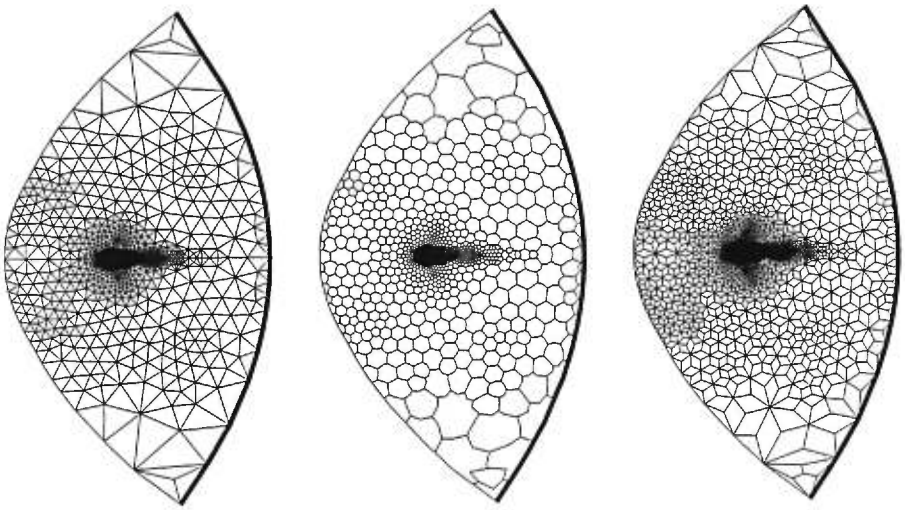

FIGURE 4.35. Euler flow around a NACA 0012 airfoil. Original grid, barycentric cells C_i and quadrilateral cells L_{ij}

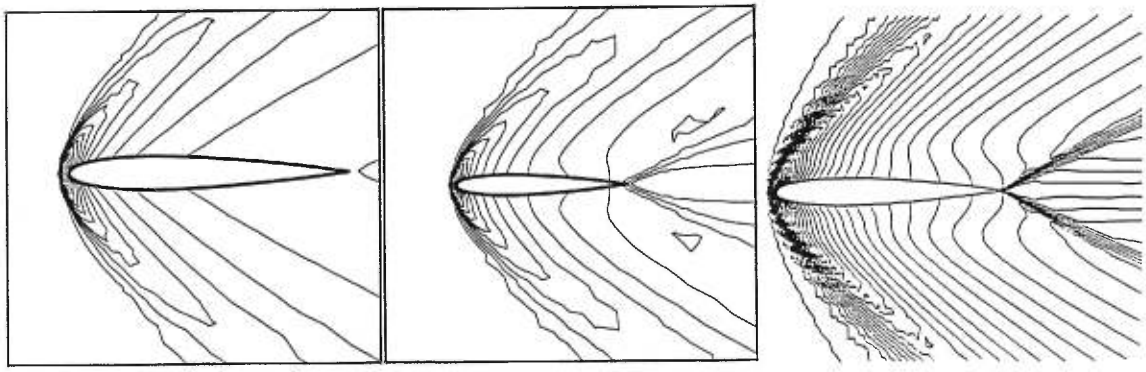

FIGURE 4.36. NACA 0012 airfoil : Pressure contours (left), Mach contours (middle) (Finite Volume, 2274 vertices); Mach contours with Venkatakrishnan's method (right) (4224 vertices; courtesy of Journal of Computational Physics)

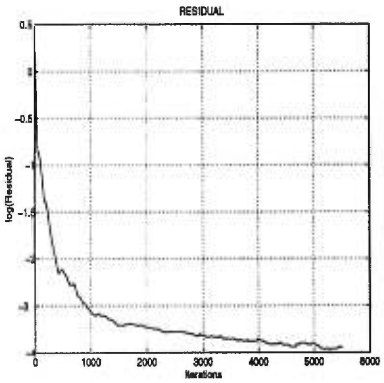

FIGURE 4.37. Residual for the initial mesh (FV)

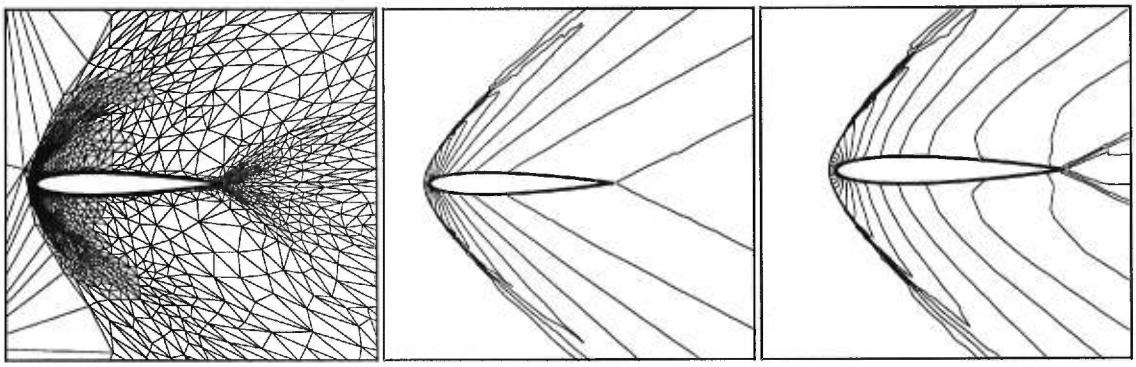

FIGURE 4.38. NACA0012 : First adaptation (3557 vertices) and solution (pressure and Mach contours) (FV)

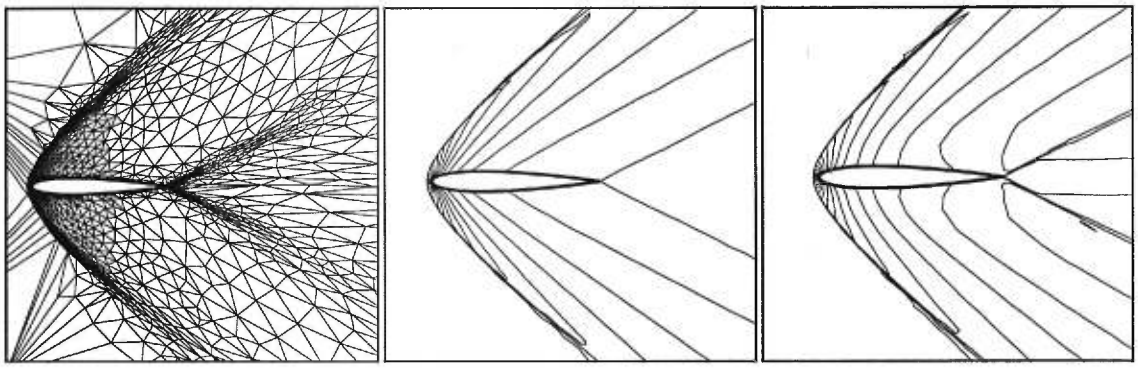

FIGURE 4.39. NACA0012 : 2^{nd} adaptation (4497 vertices) and solution (pressure and Mach contours) (FV)

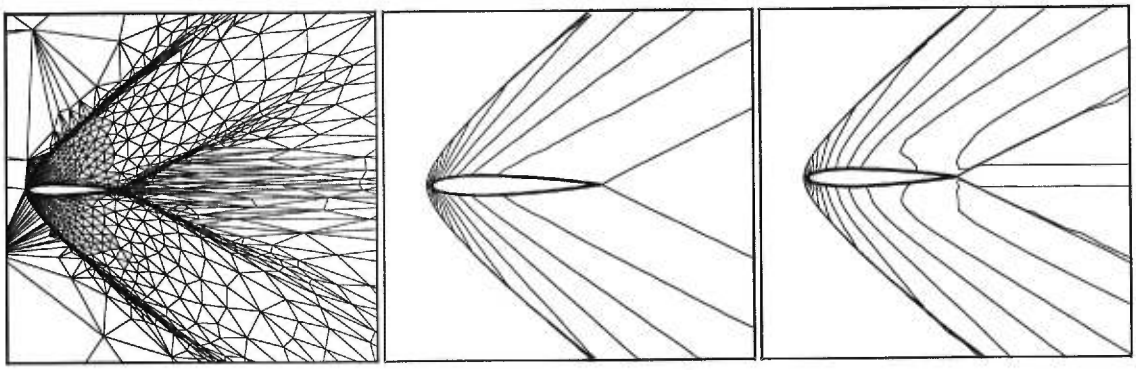

FIGURE 4.40. NACA0012 : Final mesh (7269 vertices) and solution (pressure and Mach contours) (FV)

FV	Pressure	Mach
Initial mesh	$min = 0.1163934$ $max = 0.9815941$	$min = 4.1695271e^{-2}$ $max = 2.112459$
1^{st} mesh	$min = 0.1156657$ $max = 0.9834443$	$min = 1.0001168e^{-2}$ $max = 2.150275$
2^{nd} mesh	$min = 0.1123134$ $max = 0.9810082$	$min = 7.5702323e^{-3}$ $max = 2.179578$
Final mesh	$min = 0.1139615$ $max = 1.000181$	$min = 9.072036e^{-3}$ $max = 2.320326$

TABLE 4.2. The minimal and maximal values of pressure and Mach number (FV)

Example 3 Supersonic flow past a double-ellipse at 20^o of angle of attack and $M_\infty = 2$

For this problem inspired by ([26]), but with Mach number $M_\infty = 2$ instead of the range of hypersonic Mach numbers considered there, and 20^o of angle of attack, the geometry is a double ellipse ; it can be defined by

$$\begin{cases} x \leq 0 & \begin{cases} z \leq 0 & (\frac{x}{0.06})^2 + (\frac{z}{0.015})^2 = 1 \\ z \geq 0 & (\frac{x}{0.035})^2 + (\frac{z}{0.025})^2 = 1 \end{cases} \\ 0 \leq x \leq 0.016 & \begin{cases} z \geq 0 & z = 0.025 \\ z \leq 0 & z = -0.015 \end{cases} \end{cases}$$

For this steady flow problem we compared our finite volume method with a discontinuous finite element method recently proposed by Jaffré et al.([27],[28]) and which seems to be fairly competitive; we used the same three meshes with both methods. For the initial mesh (1558 vertices), both methods give fairly comparable results; notice that the C_p curves can be nearly superposed, which is an indication that both methods are indeed doing some reasonable calculation. The same is true for the pressure and Mach contours of both methods, with perhaps a very small advantage for our finite volume method (FV) which gives slightly sharper shocks.

For the intermediate mesh (2792 vertices), the advantage offered by the Finite Volume method becomes a little more obvious on fig. 4.46 and 4.47, where the breaches of monotonicity are more important with the Discontinuous Finite Element method (DFE) (lower part of the bow shock).Moreover the pressure and Mach contours are more regular with the FV method.

The final mesh shows a clear advantage for the FV method, which gives a nearly perfect shock resolution with very smooth contours, while the DFE method shows a serious breach of monotonicity in the lower part of the bow shock.

As was the case with the initial mesh, the C_p curves can again be nearly exactly superposed, while the Mach line of the FV method is slightly higher, for the left part of the upper curve, than with the DFE method, a fact which is confirmed by tables 4.3 and 4.4.

The major difference between the two methods appears to lie in the convergence history and computing times. Fig. 4.43, 4.46 and 4.52 show a clear advantage for our finite

volume method, for the initial mesh (1558 vertices). Computing times (CPU : 3564 for FV and 48288 for DFE) confirm the advantage of the proposed Finite Volume Method. Let us finally mention that all calculations have been performed on a Silicon Graphics Station of the Centre de Recherches Mathématiques (model Challenge, 100 Mhz , 6 processors).

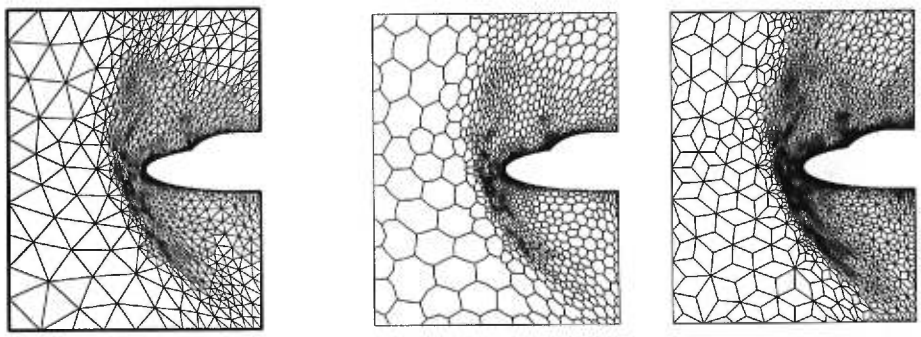

FIGURE 4.41. Euler flow around a double ellipse. Original grid, barycentric cells C_i and quadrilateral cells L_{ij}

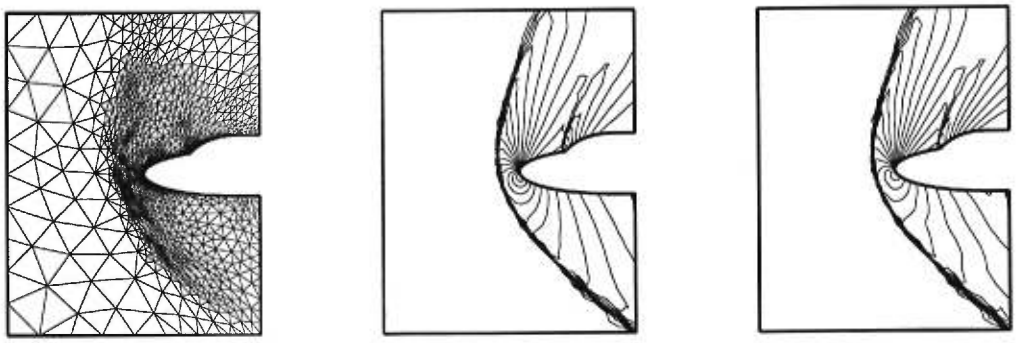

FIGURE 4.42. Double ellipse : Initial mesh (1558 vertices) and solution (pressure and Mach contours) (FV)

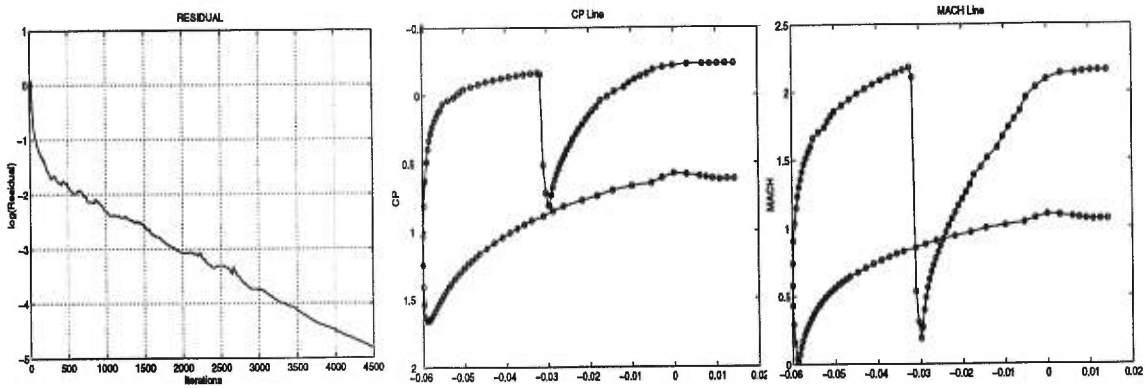

FIGURE 4.43. Residual and C_p and Mach body cuts (initial mesh 1558 vertices) (FV)

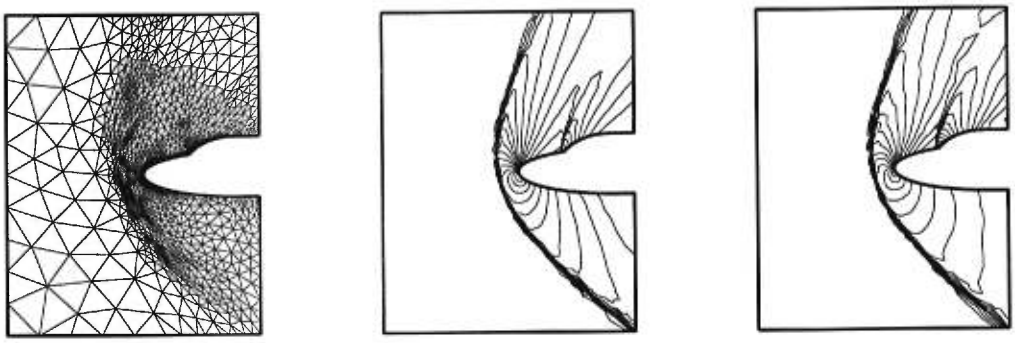

FIGURE 4.44. Double ellipse : Initial mesh (1558 vertices) and solution (pressure and Mach contours) (DFE)

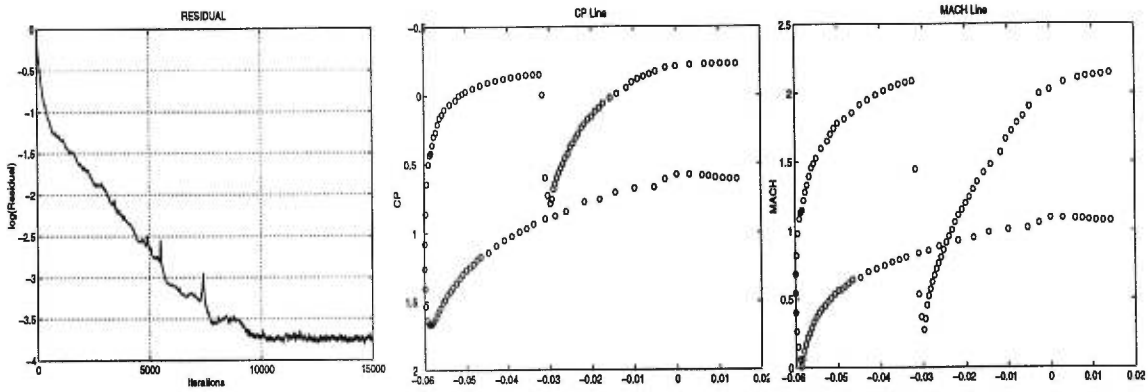

FIGURE 4.45. Residual and C_p and Mach body cuts (initial mesh 1558 vertices) (DFE)

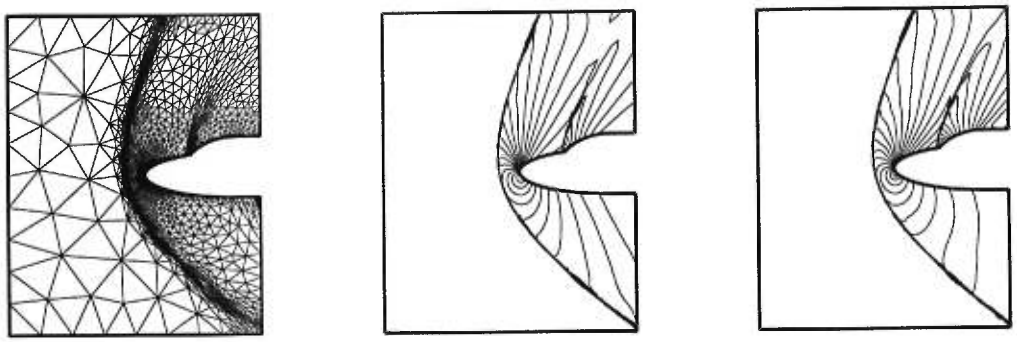

FIGURE 4.46. Double ellipse : First adaptation (2792 vertices) and solution (pressure and Mach contours) (FV)

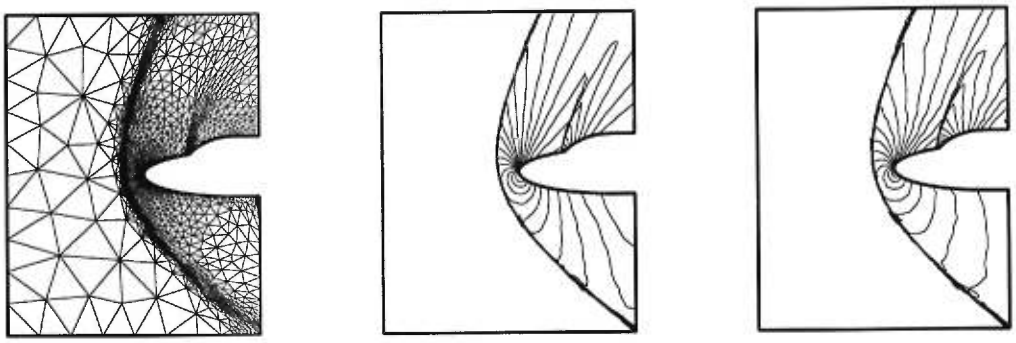

FIGURE 4.47. Double ellipse : First adaptation (2792 vertices) and solution (pressure and Mach contours) (DFE)

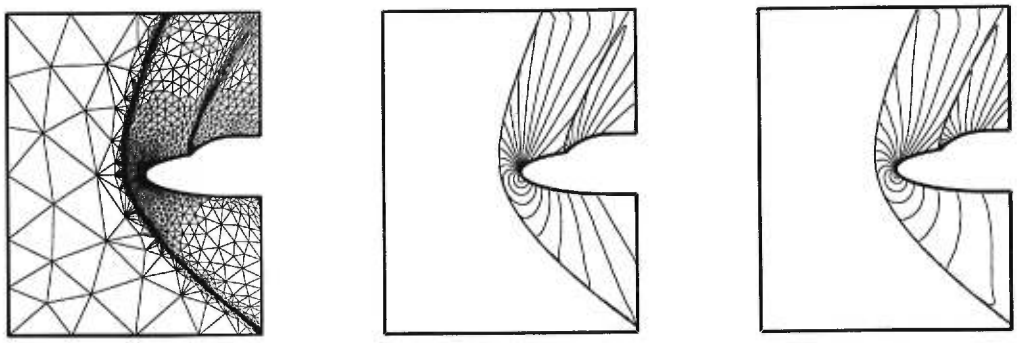

FIGURE 4.48. Double ellipse : Final mesh (5055 vertices) and solution (pressure and Mach contours) (FV)

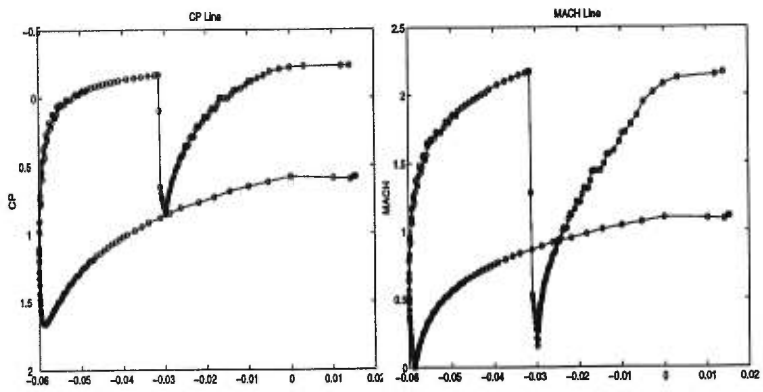

FIGURE 4.49. C_p and Mach body cuts for the final mesh (5055 vertices) (FV)

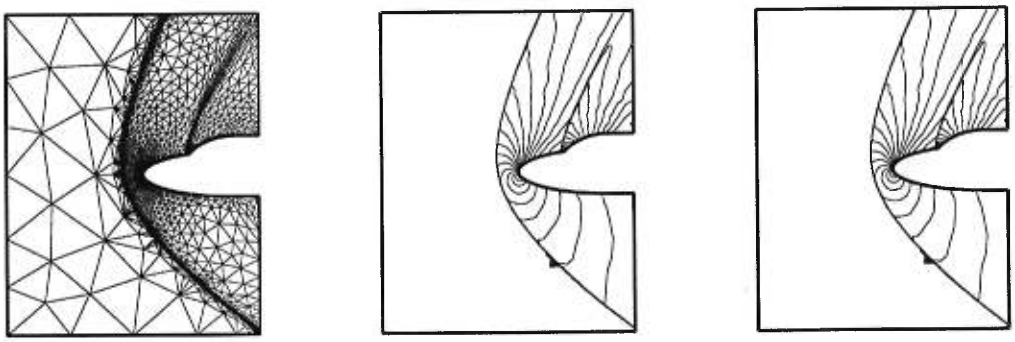

FIGURE 4.50. Double ellipse : Final mesh (5055 vertices) and solution (pressure and Mach contours) (DFE)

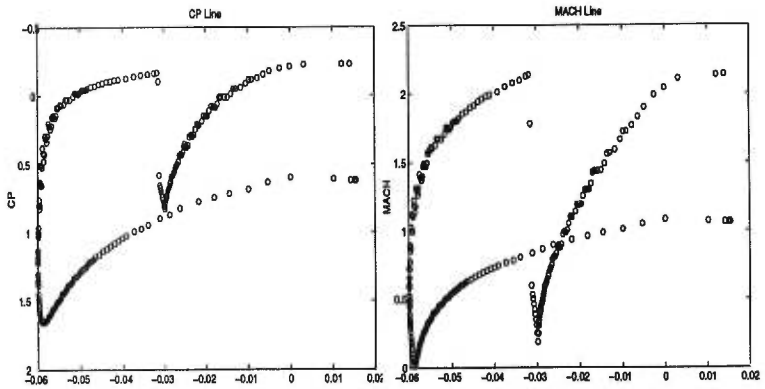

FIGURE 4.51. C_p and Mach body cuts for the final mesh (5055 vertices) (DFE)

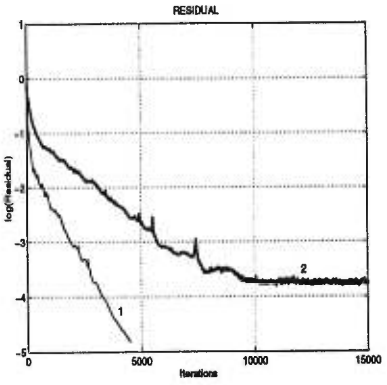

FIGURE 4.52. Residual for initial mesh (1558 vertices) ((1)=FV - (2)=DFE)

FV	Pressure	Mach
Initial mesh	$min = 6.1671760e^{-2}$ $max = 1.009705$	$min = 1.750865e^{-2}$ $max = 2.253697$
2^{nd} mesh	$min = 6.1395669e^{-2}$ $max = 1.006208$	$min = 5.3774943e^{-3}$ $max = 2.266636$
Final mesh	$min = 6.0346086e^{-2}$ $max = 1.009427$	$min = 5.209895e^{-3}$ $max = 2.270716$

TABLE 4.3. The maximal and minimal values of Pressure and Mach number (FV)

DFE	Pressure	Mach
Initial mesh	$min = 6.2501445e^{-2}$ $max = 1.014265$	$min = 8.2084965e^{-3}$ $max = 2.190479$
2^{nd} mesh	$min = 6.2390134e^{-2}$ $max = 1.007068$	$min = 2.0193825e^{-3}$ $max = 2.216612$
Final mesh	$min = 6.3052103e^{-2}$ $max = 1.007425$	$min = 1.3435918e^{-2}$ $max = 2.211899$

TABLE 4.4. The maximal and minimal values of Pressure and Mach number (DFE)

Concluding remarks

By first considering two coupled sets of finite volume cells, we have presented a two-dimensional finite volume extension of the Lax-Friedrichs scheme for scalar hyperbolic conservation laws. This scheme has then been used to construct a two-dimensional finite volume generalization of the one-dimensional Nessyahu-Tadmor scheme, thanks to the introduction of van Leer-type two-dimensional piecewise linear interpolants, which leads to second-order accuracy. Oscillations are suppressed with the help of slope or gradient limiters.

The examples presented here give a reasonable evidence that the FV method proposed by the authors is capable of a very high resolution, with a clear advantage, as compared with DFE, at least at the level of the convergence histories, computing times, smoothness of the pressure and Mach contours, and monotonicity enforcement.

In another paper we consider the particular case of the linear equation $u_t + div(u\vec{V}) = 0$ where $\vec{V} = (V_1(x,y), V_2(x,y))^T$ with $div\ \vec{V} = 0$; we obtain an L^∞ bound for the numerical solution, from which we deduct the existence of a subsequence $\{u_{\mathcal{T}_k, \Delta t_k}\}$ which converges weakly to some function u in $L^\infty(\mathbb{R}^2 \times \mathbb{R}^+)$-weak. Using another set of inequalities, we obtain a total variation-type bound, slightly weaker than a classical bound on the total variation of the numerical solution, called *a* bound on the "weighted total variation", from which we are then able to show that the above weak limit function u is indeed a weak solution of $u_t + div(u\vec{V}) = 0$.

This places the 2-dimensional finite volume generalization of the Nessyahu-Tadmor scheme on a firm theoretical basis, and the authors will now focus their efforts on applications to problems with the Navier-Stokes equations in conservation form for compressible flows and three-dimensional transonic and supersonic flow problems.

Références

[1] F. Angrand, A. Dervieux, L. Loth and G. Vijayasundaram (1983), Simulations of Euler transonic flows by means of explicit finite-element type schemes, INRIA Res. Rep. No. 250, Rocquencourt, 78153 Le Chesnay, France.

[2] F. Angrand and A. Dervieux (1984), Some explicit triangular finite element schemes for the Euler equations, *Int. J. Num. Meth. in Fluids*, Vol. 4, 749–764.

[3] P. Arminjon, M.C. Viallon, A. Madrane (1995), From Lax-Friedrichs to a Multidimensional Finite Volume Extension of the Nessyahu-Tadmor Scheme for Compressible Flows, Proc. Int. Conf. on Numerical Meth. for the Euler and Navier-Stokes Equations. Centre de Rech.Math. Univ de Montréal, P.Arminjon and A.Dervieux, editors, september 1995, to appear in the Am.Math.Soc-CRM series.

[4] P. Arminjon, A. Dervieux, L. Fezoui, H. Steve and B. Stoufflet (1988), Non-oscillatory schemes for multidimensional Euler calculations with unstructured grids, Proc. 2nd Int. Conf. Hyperbolic Problems, Aachen (Germany), March 1988, R. Jeltsch and J. Ballmann, Editors (Notes on Numer. Fluid Mechanics, Vol.24, Vieweg, Braunschweig, Germany).

[5] P. Arminjon and A. Dervieux (1993), Construction of TVD-like Artificial Viscosities on Two-Dimensional Arbitrary FEM Grids, *J. Comp. Phys.*, **106**, No.1, 176–198.

[6] P. Arminjon et M.C. Viallon (1995), Généralisation du schéma de Nessyahu-Tadmor pour une équation hyperbolique à deux dimensions d'espace, Comptes Rendus de l'Acad. des Sciences, Paris, t.320, série I , 85-88.

[7] S. Champier (1992). Convergence de schémas numériques type Volumes Finis pour la résolution d'équations hyperboliques. Thèse, Univ. de St-Etienne.

[8] R.Eymard and T.Gallouët (1993), Convergence d'un schéma de type éléments finis-volumes finis pour un système d'une équation elliptique et d'une équation hyperbolique, M^2AN , Vol.27 , No.7, 843-861.

[9] F. Fezoui (1985). Résolution des équations d'Euler par un schéma de van Leer en élément finis. Rapport INRIA no 358, Rocquencourt, 78153 Le Chesnay, France.

[10] S.K. Godunov (1959). A Difference Method for the Numerical Computation of Discontinuous Solutions of the Equations of Fluid Dynamics, Mat Sbornik., 47 No.3, 271 - 306.

[11] B. van Leer (1974). Towards the Ultimate Conservative Difference Scheme. II. Monotonicity and conservation combined in a second order scheme, *J. Comp. Phys.*, Vol. 14, 361–370.

[12] B. van Leer (1977). IV. A new approach to numerical convection, *J. Comp. Phys.* **23**, 276–299.

[13] H. Nessyahu and E. Tadmor (1990), Non-oscillatory Central Differencing for Hyperbolic Conservation Laws, *J. Comp. Physics* **87**, No. 2, 408–463.

[14] R. Peyret, T.D. Taylor (1983). Computational Methods for Fluid Flow, Springer-Verlag, New-York, Heidelberg, Berlin.

[15] P.L. Roe (1981a). The use of the Riemann problem in finite difference schemes, in Proc. 7th Inter. Conf. Num. Meth. Fluid Dynamics, Stanford/NASA Ames, W.G. Reynolds and R. Mac Cormack, editors, Lecture Notes in Physics, no 141, Springer-Verlag, New York, 354–359.

[16] P.L. Roe (1981b). Approximate Riemann solvers, parameter vectors, and difference schemes, *J. Comp. Phys.***43**, 357–372.

[17] P.K. Sweby (1984). High resolution schemes using flux limiters for hyperbolic conservation laws, *SIAM J. Num. Anal.*, Vol. 21, 995–1011.

[18] M.C. Viallon et P. Arminjon (1994), Convergence du schéma de Nessyahu-Tadmor sur des maillages non structurés pour une équation hyperbolique linéaire bidimensionnelle, Rapport de recherche No. C.N.R.S. U.R.A. 740, Équipe d'Analyse Numérique, Universités de Lyon et Saint-Étienne, septembre 1994.

[19] M.C. Viallon and P. Arminjon, Convergence of a finite volume extension of the Nessyahu-Tadmor scheme on unstructured grids for a two-dimensional linear hyperbolic equation, Rapport de recherche, No. 2239, Centre de Recherches mathématiques, Université de Montréal, january 1995, to appear in SIAM J.Num.Anal.

[20] P.D.Lax (1954), Weak solutions of nonlinear hyperbolic equations and their numerical computation, Comm. Pure and Applied Math. 7, 159-193.

[21] P.Arminjon, D.Stanescu and M.C. Viallon (1995), A two-dimensional finite volume extension of the Lax-Friedrichs and Nessyahu-Tadmor schemes for compressible flows, A Collection of Technical Papers, Proceedings of the 6 th.Int. Symposium on Comp.Fluid Dynamics, Lake Tahoe (Nevada) September 4-8,1995, M. Hafez, editor, Volume 4 , pp. 7-14.

[22] J.J.Quirk (1992), A Contribution to the Great Riemann Solver Debate, NASA-ICASE Rep. No. 92-64, Nov. 1992, and Int.J.Num.Meth.Fluids, pp.555-574 (1994).

[23] J.Peraire, M.Vahdati, K.Morgan and O.C.Zienkiewicz (1987), Adaptative Remeshing for Compressible Flow Computations, J.Comp.Phys.72,449-466.

[24] A.Rizzi - H.Viviand (Eds) (1981) , Numerical methods for the computation of inviscid transonic flow with shock waves. Notes on Numerical Fluid Mechanics, Vol. 3, Vieweg, Braunschweig/Wiesbaden, Germany.

[25] V. Venkatakrishnan (1995), Convergence to Steady State Solutions of the Euler Equations on Unstructured Grids with Limiters, *J. Comp. Phys.*, 118, 120-130 .

[26] INRIA and GAMNI-SMAI (1990), Workshop on hypersonic flows for reentry problems, Problem 6 : Flow over a double ellipse, test case 6.1 : Non-Reactive Flows. Antibes, France, January 22-25, 1990.

[27] G.D.V Gowda and J.Jaffré (1993), A discontinuous finite element method for non linear scalar conservation laws, INRIA Res. Rep. No. 1848, Rocquencourt,78153 Le Chesnay, France.

[28] J.Jaffré and L.Kaddouri (1991), Discontinuous finite elements for the Euler equations. Proc. of the 3^d Int.Conf. on Hyperbolic Problems, June 11-15, 1990, Uppsala, Sweden,

B. Engquist and B.Gustafsson, editors, Studentlitteratur, Chartwell-Bratt, Vol.2, pp. 602-610.

[29] P.Arminjon, M.C.Viallon, L.Kaddouri, and A.Madrane, Discontinuous finite elements and 2-Dimensional Finite Volume Versions of the Lax-Friedrichs and Nessyahu-Tadmor difference schemes for Compressible Flows on Unstructured Grids, to appear in CFD Review, John Wiley, 1997, M.Hafez and K.Oshima, Editors.

[30] M.J.Castro Diaz and F.Hecht, Anisotropic Surface Mesh Generation, INRIA Res. Rep. No. 2672, October 1995, INRIA, Rocquencourt, 78153 Le Chesnay, France.

[31] M.J.Castro Diaz, Mesh Refinement over Triangulated Surfaces, Res. Rep. No 2462.

[32] P.Arminjon (1992). Two-dimensional finite volume extension of the Nessyahu-Tadmor scheme for conservation laws, private communication to A.Jameson, Princeton University, April 1992.

Chapitre 5

Discontinuous finite elements and finite volume versions of the Lax-Friedrichs and Nessyahu-Tadmor schemes for compressible flows on unstructured grids

by

Paul ARMINJON[†] , Marie-Claude VIALLON[*],

Aziz MADRANE[†] and Lahcen KADDOURI[°]

[†]Dép. de mathématiques et de statistique, Université de Montréal

C.P. 6128, Succ. centre-ville, Montréal, Québec, Canada, H3C 3J7

[*]Équipe d'analyse numérique, Université de Saint-Étienne,

23 rue Paul Michelon, 42023 Saint-Étienne Cedex 2, France

[°] Dép. de mathématiques appliquées Université du Littoral

50, Rue F. Buisson , B.P. 699 F-62228 Calais Cedex France

ABSTRACT – We present a new finite volume version ([1],[2],[3]) of the 1-dimensional Lax-Friedrichs and Nessyahu-Tadmor schemes ([5]) for nonlinear hyperbolic equations on unstructured grids, and compare it to a recent discontinuous finite element method ([6],[23]) in the computation of some typical test problems for compressible flows.
The non-oscillatory central difference scheme of Nessyahu and Tadmor, in which the resolution of Riemann problems at the cell interfaces is by-passed thanks to the use of the staggered Lax-Friedrichs scheme, is extended here to a two-step, two-dimensional non-oscillatory centered scheme in finite volume formulation. The construction of the scheme rests on a finite volume extension of the Lax-Friedrichs scheme, in which the finite volume cells are the barycentric cells constructed around the nodes of an FEM triangulation, for even time steps, and some quadrilateral cells associated with this triangulation, for odd time steps. Piecewise linear cell interpolants using least-squares gradients combined with a van Leer-type slope limiting allow for an oscillation-free second-order resolution.
The discontinuous finite element method consists of two steps. We first perform a finite element computation which includes calculation of the fluxes across the edges of the triangular elements using 1-D Riemann solvers with a modification to satisfy the entropy condition. We then proceed to a truly multidimensional slope limitation performed on the physical variables.

Numerical applications to several test problems show the accuracy and stability of the finite volume method.

1. Introduction

We present a new finite volume method for nonlinear hyperbolic systems on unstructured triangular grids inspired by the Lax-Friedrichs and Nessyahu-Tadmor one-dimensional difference schemes [5] , and compare it to a recent discontinuous finite element method introduced by Jaffré, Kaddouri and Gowda ([6],[23]) in the computation of some typical two-dimensional test problems for compressible flows.
Discontinuous finite elements were first introduced independently, for the neutron transport equation and applications to nuclear engineering, by Reed and Hill [7] and Lesaint and Raviart [8], and then adapted to the equations of hydrodynamics and elasticity ([9],[10], [11],[12]) or even to such applications as the motion of a load on an ice layer ([13], in joint work with P.Jamet), reservoir simulation both without slope limiters ([14],[15]) and with limitation ([16],[17],[18]), and many other applications where they proved to be very successful.
Numerical analysis of discontinuous finite element methods can be found e.g. in [8], with improvements in [19] for scalar hyperbolic equations, and in [20].
In the finite element method used in this paper, the solution is approximated by discontinuous piecewise linear polynomials; numerical fluxes are calculated, on the triangle edges, at appropriate integration points through the use of one-dimensional Riemann

solvers. To prevent spurious oscillations, we use a multidimensional version of van Leer's limiter borrowed from ([6],[23]).

Our finite volume method ([1],[2],[3],[4]) is a two-dimensional finite volume scheme inspired by an elegant difference scheme proposed, for one-dimensional problems, by Nessyahu and Tadmor [5], which is itself a high resolution non-oscillatory Godunov-type method for hyperbolic systems of conservation laws constructed on the principle of the staggered Lax-Friedrichs scheme.

It is decomposed in two time steps for second order accuracy in time, performed on alternate, staggered grids, thus allowing a complete by-pass of the (usually expensive) detailed exact or approximate solution of the local Riemann problems generated at the cell interfaces, thanks to the use of staggered form of the Lax-Friedrichs scheme.

In [4], we have presented an extension of the Nessyahu-Tadmor difference scheme to the simpler case of rectangular grids; several applications (linear advection, Burgers' equation, diffraction of a planar shock wave around a 90^o corner for the Euler equations [21] , Mach 3 wind tunnel with forward facing step [22]) showed the feasibility of the method, which led to good results on regular grids without any mesh adaptation.

In ([1],[2],[3]), we had constructed a finite volume scheme for unstructured triangular grids inspired by the Lax-Friedrichs and Nessyahu-Tadmor one-dimensional difference schemes; some numerical experiments (Supersonic flow around a NACA 0012 airfoil, supersonic flow around a double ellipse) showed the high accuracy of the method, but did not provide a systematic comparison with an already well established method.

In this paper we attempt to present such a comparison, and introduce for that purpose in section 3 the discontinuous finite element, second order accurate method recently proposed, and successfully tested, by Jaffré, Kaddouri and Gowda ([6],[23],[25]).

Notice that in this paper, we used Roe's Riemann solver with an entropy correction recently proposed by Dubois and Mehlman, while the solvers used in references ([6],[23],[25]) are the Osher and Osher-Solomon solvers, respectively.

In section 2 we describe the mathematical modelling of the problem; in section 3 we give a detailed presentation of the discontinuous finite element method of Jaffré, Kaddouri and Gowda.

In section 4, we present the first two authors' construction [1], for unstructured triangular grids, of a finite volume version of the staggered Lax-Friedrichs scheme, and then describe their second order accurate non-oscillatory finite volume method [1] inspired by the Nessyahu-Tadmor one-dimensional central difference scheme [5].
In section 5,we present applications to some typical test problems for supersonic flows (supersonic flow past a blunt body;supersonic flow around a double ellipse [35]).
Finally, section 6 is an appendix describing the solution of the projection problems generated by the slope limitation process.

2. Mathematical modelling

2.1. Governing equations.

We consider the two-dimensional Euler equations for compressible flows, written in conservation form as:

$$\frac{\partial}{\partial t}U(x,y;t) + \frac{\partial}{\partial x}F(U(x,y;t)) + \frac{\partial}{\partial y}G(U(x,y;t)) = 0 \text{ for } (x,y;t) \in \Omega \times \mathbf{R}_+ \quad (2.1)$$

where Ω is a closed bounded domain of the plane,

$$U = \begin{pmatrix} \rho \\ \rho u \\ \rho v \\ \rho E \end{pmatrix}, \quad F(U) = \begin{pmatrix} \rho u \\ \rho u^2 + p \\ \rho uv \\ (\rho E + p)u \end{pmatrix}, \quad G(U) = \begin{pmatrix} \rho v \\ \rho uv \\ \rho v^2 + p \\ (\rho E + p)v \end{pmatrix} \quad (2.2)$$

ρ is the density, $\vec{V} = (u, v)$ is the velocity vector, E is the total energy by unit mass, and p is the pressure. We assume that the fluid satisfies the perfect gas law :

$$p = (\gamma - 1)(\rho E - \frac{1}{2}\rho(u^2 + v^2)) \quad (2.3)$$

where γ,the ratio of specific heats, is taken equal to 1.4 for air.

2.2. Boundary conditions :

In the sequel, we consider domains of computation related to external flows around bodies; in fig.5.53 the body is represented by a double-ellipse [40] which limits the

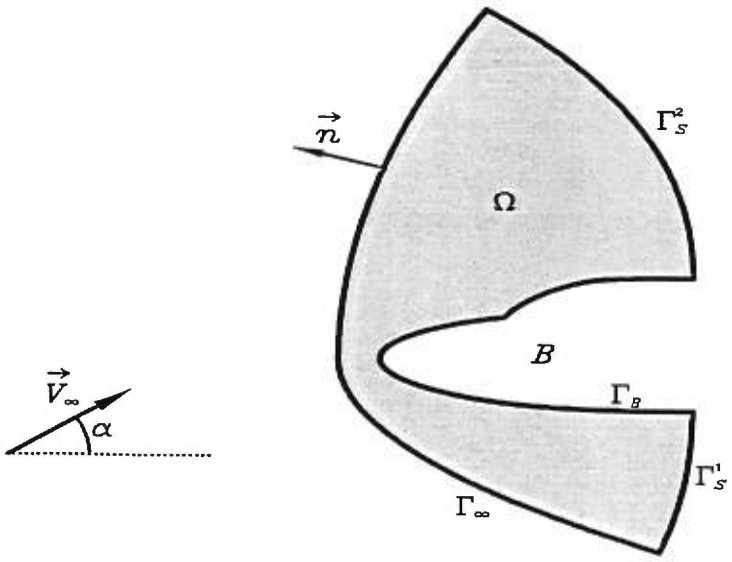

FIGURE 5.53. Boundary of the computational domain

domain of computation by its wall Γ_B . In order to deal with a bounded computational domain, a second (artificial) farfield boundary $\Gamma_\infty \cup \Gamma_S$ is introduced, with $\Gamma_S = \Gamma_S^1 \cup \Gamma_S^2$. The flow is assumed to be uniform at infinity, and we prescribe

$$\rho_\infty = 1, \quad V_\infty = \begin{pmatrix} cos\alpha \\ sin\alpha \end{pmatrix}, \quad p_\infty = \frac{1}{\gamma M_\infty^2} \tag{2.4}$$

where α is the angle of attack and M_∞ denotes the free-stream Mach number.

On the wall Γ_B we use the usual "no normal velocity" condition: $\vec{V}.\vec{n} = 0$, where $\vec{n} \in R^2$ is the outer normal vector to Γ_B.

Finally, for unsteady calculations, an initial flow is prescribed :

$$U(x, y; 0) = U_0(x, y) \quad \forall (x, y) \in \Omega. \tag{2.5}$$

3. A two-dimensional discontinuous finite element method

In this section, we give a detailed description of the discontinuous finite element method proposed by Jaffré,Kaddouri and Gowda ([6], [23],[25]).

We consider here a (P_1)-piecewise linear spatial discretization based on unstructured triangular elements (the number of elements sharing a common node is not

constant); the computational domain Ω is subdivided into triangles by a triangulation $\mathcal{T}_h$:

$$\Omega = \bigcup_{i=1}^{N_e} K_i \ ; \ K_i \in \mathcal{T}_h,$$

where the K_i's are the elements of the triangulation, N_e is the total number of triangles, and h is the largest diameter of all elements.

Let $U_{j,i} = U(A_{j,i}; t)$ denote the value of the dependent variable vector U, at time t and at the j^{th} vertex $A_{j,i}$ of element $K_i \in \mathcal{T}_h$ $(i = 1, \ldots, N_e; j = 1, 2, 3)$.

The degrees of freedom are the components of the vector U at the vertices of all elements of the triangulation (fig. 5.54). Let W denote the approximation space formed by

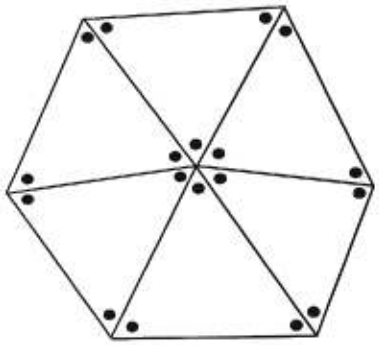

FIGURE 5.54. Degrees of freedom of the triangulation

the piecewise continuous functions which are linear on each triangle $K_i \in \mathcal{T}_h$ (P_1-approximation).

The vector U of conservative variables ρ, ρu, ρv, ρE is approximated by functions in the product space W^4 and the corresponding approximations will again be denoted by ρ, ρu, ρv, ρE, elements of W, for simplicity.

For each element $K_i (i = 1, \ldots, N_e)$ and each node $A_{j,i} \in K_i$ there exists a unique basis or shape function $(\varphi_{j,i})$ with the property

$$\forall\, i = 1, \ldots, N_e \ , \quad \varphi_{j,i}(A_{k,i}) = \begin{cases} 1 & \text{if } j = k \\ 0 & \text{otherwise} \end{cases}$$

The functions $(\varphi_{j,i})_{i=1,\ldots,N_e}^{j=1,\ldots,3}$ form a basis of the approximation space W.

In the present formulation we shall use an explicit Euler time discretization.

We now consider a Galerkin discontinuous finite element approximation, which proceeds from a variational formulation of the Euler equations.

Multiplying (2.1) by a shape function $\varphi_{j,i}$ and integrating by parts the terms with spatial derivatives, we obtain the following system for the piecewise linear vector U^{n+1} of approximate dependent variables to be computed at time t^{n+1}:

$$\left\{ \begin{array}{l} \text{Find } U^{n+1} \in W^4 \\ \\ \displaystyle\int_{K_i} \frac{U^{n+1}-U^n}{\Delta t^n}\varphi_{j,i}\,dS \;=\; \int_{K_i}\left(F(U^n)\frac{\partial \varphi_{j,i}}{\partial x}+G(U^n)\frac{\partial \varphi_{j,i}}{\partial y}\right)dS \\ \qquad\qquad\qquad\qquad - \displaystyle\int_{\partial K_i}\left(\vec{\mathbb{F}}(U^n)\cdot \boldsymbol{n}\right)\varphi_{j,i}\,d\sigma \end{array} \right. \tag{3.1}$$

where $\Delta t^n = t^{n+1} - t^n$ is the time step, $U^n = U(x,y;t^n) \in W^4$, and $\vec{n} = \begin{pmatrix} n_x \\ n_y \end{pmatrix}$ is the unit outer normal (directed towards the exterior of K_i).

In (3.1), $\vec{\mathbb{F}}(U^n)\cdot\vec{n} = F(U^n)\cdot n_x + G(U^n)\cdot n_y \equiv F_n$ is the (outward) numerical flux across an edge $\mathcal{A}$ of ∂K_i; it will be computed with the help of an approximate Riemann solver for the Riemann problem generated, in the direction normal to the edge $\mathcal{A}$, by the limits of the values of the dependent variables on both sides of $\mathcal{A}$ as one tends to $\mathcal{A}$ along $\vec{n}$.

In this paper, we have used Roe's Riemann solver ([28],[24],[34]) with an entropic correction due to Dubois and Mehlman [24].

REMARQUE 5.1. *Replacing the above approximation space by the space of piecewise constant functions (constant on each triangle $K_i \in \mathcal{T}_h$) reduces (3.1) to the equation governing the standard finite volume scheme*

$$\int_{K_i}\frac{U_i^{n+1}-U_i^n}{\Delta t^n}\,dS \;+\; \int_{\partial K_i}\left(\vec{\mathbb{F}}(U^n)\cdot\boldsymbol{n}\right)d\sigma = 0, \quad K_i \in \mathcal{T}_h.$$

3.1. Numerical integration.

To complete the description of the spatial discretization, we must specify the quadrature formulas which will be used to compute the integrals appearing in (3.1). Numerical experiments for scalar equation ([25],[18],[6]) have suggested the following quadrature techniques.

In equation (3.1) the terms containing the spatial derivatives are computed with the help of the values at the centroid M of mesh K_i :

$$\int_{K_i}\left(F(U^n)\frac{\partial\varphi_{j,i}}{\partial x}+G(U^n)\frac{\partial\varphi_{j,i}}{\partial y}\right)dS \simeq \text{Area}(K_i)\left(F(\overline{U}_i^n)\frac{\partial\varphi_{j,i}}{\partial x}(M_i)+G(\overline{U}_i^n)\frac{\partial\varphi_{j,i}}{\partial y}(M_i)\right)$$

where M_i is the centroid of K_i and $\overline{U}_i^n$ is the average value of U^n on K_i :

$$\overline{U}_i^n=\frac{1}{3}\sum_{j=1}^{3}U(A_{j,i})$$

since U^n is linear on K_i.

For the integral associated with the outward flux

$$\int_{\partial K_i}\left(\vec{\mathbb{F}}(U^n)\cdot\boldsymbol{n}\right)\varphi_{j,i}\,d\sigma=\sum_{\mathcal{A}\in\partial K_i}\int_{\mathcal{A}}\left(\vec{\mathbb{F}}(U^n)\cdot\boldsymbol{n}\right)\varphi_{j,i}\,d\sigma$$

we use either the values at the midpoints of the edges $\mathcal{A}$, or the values at both Gauss points of each edge

1st choice :

$$\int_{\mathcal{A}}\left(\vec{\mathbb{F}}(U^n)\cdot\boldsymbol{n}\right)\varphi_{j,i}\,d\sigma \simeq \mathrm{l}(\mathcal{A})\cdot\mathcal{F}^n_{|\mathcal{A}}(U_l,U_r)\cdot\varphi_{j,i}(M)$$

where $\mathrm{l}(\mathcal{A})$ and M denote the length and midpoint of edge $\mathcal{A}$, respectively, and

$\mathcal{F}^n_{|\mathcal{A}}(U_l,U_r)$ is the numerical flux across edge $\mathcal{A}$ which separates the states U_l and U_r, obtained by taking the limits of U along the normal to $\mathcal{A}$ at M; this numerical flux will be computed with Roe's Riemann solver, as described below.

2nd choice :

$$\int_{\mathcal{A}}\left(\vec{\mathbb{F}}(U^n)\cdot\boldsymbol{n}\right)\varphi_{j,i}\,d\sigma \simeq \frac{\mathrm{l}(\mathcal{A})}{2}\left(\mathcal{F}^n_{|\mathcal{A}}(U_l,U_r)(G_1)\varphi_{j,i}(G_1)+\mathcal{F}^n_{|\mathcal{A}}(U_l,U_r)(G_2)\varphi_{j,i}(G_2)\right)$$

where G_1, G_2 are the Gauss points of edge $\mathcal{A}$.

Numerical experiments have shown that the computation at the edge midpoint (1st choice) is sufficient.

For the first integral in (3.1) (time derivative) we use the values at the three vertices:

$$\int_{K_i}\frac{U^{n+1}-U^n}{\Delta t^n}\varphi_{j,i}\,dS \simeq \frac{\text{Area}(K_i)}{3}\frac{U^{n+1}_{K_i,A_j}-U^n_{K_i,A_j}}{\Delta t^n}$$

by the properties of $\varphi_{j,i}$.

3.2. Multidimensional slope limitation.

We will describe a multidimensional extension of a slope limitation procedure which has been successfully used for scalar equations ([17],[6],[23]).

When dealing with the Euler equations, it has been widely recognized that one should limit the physical variables ρ, u, v, p rather than the conservative variables

ρ, ρu, ρv, ρE.

Let $U^n \in W^4$ denote the solution previously computed at time t^n, and $U^\star \in W^4$ the solution predicted at t^{n+1} by solving system (3.1).

We want to modify $U^\star$ and obtain a corrected vector of conservative variables U^{n+1}, by the following procedure.

For each triangle $K_i \in \mathcal{T}_h$, let

- $w_{K,A_i} = w_{|K}(A_i)$: $\quad i = 1, \ldots, 3$ be the value of $w_{|K}$ at node i,
- $\overline{w}_K = \frac{1}{3}\sum_{i=1}^{3} w_{K,A_i}$, the mean value of $w_{|K}$ in element K,
- $T(A)$ be the set of element $K \in \mathcal{T}_h$ such that vertex $A \in K$ (Fig. 5.55).

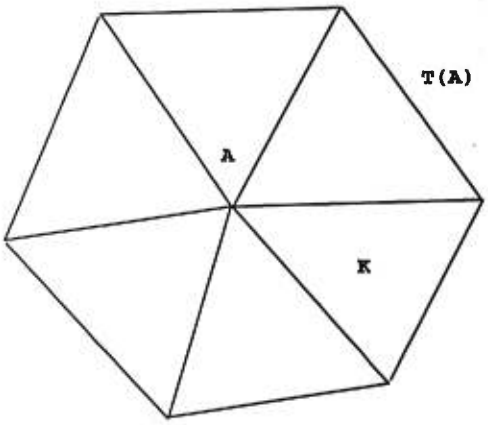

FIGURE 5.55. The set $T(A)$

For each element K, we compute the mean values of the conservative variables, noted $\overline{\rho}^\star_K$, $\overline{(\rho u)}^\star_K$, $\overline{(\rho v)}^\star_K$, $\overline{(\rho E)}^\star_K$,which are simply the arithmetic means of these variables at the three vertices of K.

In order to obtain a conservative scheme, the vectors U^{n+1} and $U^\star$ must have the same mean value on each element.

We then compute the mean values of the physical variables, $\overline{\rho}^\star_K, \overline{u}^\star_K, \overline{v}^\star_K, \overline{p}^\star_K$ (the mean value $\overline{\rho}^\star_K$ of the density has already been calculated).

For pressure we also take the arithmetic mean of p at the vertices of K.

In contrast, the mean value of the velocity components u, v are defined by

$$\overline{u}_K^\star = \frac{\overline{(\rho u)}_K^\star}{\overline{\rho}_K^\star} \ , \ \overline{v}_K^\star = \frac{\overline{(\rho v)}_K^\star}{\overline{\rho}_K^\star} \ . \tag{3.2}$$

For the components of momentum at time t^{n+1}, we will use the following value

$$\overline{(\rho u)}_K^{n+1} = \frac{1}{3}\sum_{i=1}^{3} \rho_{K,A_i}^{n+1} u_{K,A_i}^{n+1} \ , \quad \overline{(\rho v)}_K^{n+1} = \frac{1}{3}\sum_{i=1}^{3} \rho_{K,A_i}^{n+1} v_{K,A_i}^{n+1} \ . \tag{3.3}$$

Observe that these values are different from $\overline{u}_K^\star$, $\overline{v}_K^\star$, as they use the nodal values of density and velocity instead of those of the momentum.

Formulas (3.2)-(3.3) have been chosen to ensure existence and uniqueness of the solution of the minimisation problems to be defined below.

For every node A of the grid we compute the minimum and maximum of the mean values of the physical variables in the elements sharing node A :

$$w_{min}(A) = \min_{K \in T(A)} \overline{w}_K^\star, \quad w_{max}(A) = \max_{K \in T(A)} \overline{w}_K^\star, \qquad \text{for} \qquad w = \rho, u, v, p \tag{3.4}$$

The slopes of the physical variables ρ, u, v, p will be limited, in this order, in the following way.

Let V denote the vector $(\rho, u, v, p)^T$ of physical variables.

In each element K with vertices A_i $(i = 1, \ldots, 3)$, $V_{|K}^{n+1}$ is defined by :

$$\begin{cases} (i) \quad \overline{w}_K^{n+1} = \overline{w}_K^\star, \qquad \text{for} \quad w = \rho, \ p, \ \text{and} \ \overline{(\rho w)}_K^{n+1} = \overline{(\rho w)}_K^\star, \ \text{for} \ w = u, \ v, \\ \\ (ii) \quad \text{For } i = 1, \ldots, 3, \ w = \rho, \ u, \ v, \ p : \\ \\ \qquad (1-\alpha)\overline{w}_K^\star + \alpha w_{min}(A) \le w_{K,A_i}^{n+1} \le (1-\alpha)\overline{w}_K^\star + \alpha w_{max}(A) \ , \ 0 \le \alpha \le 1, \\ \\ (iii) \quad \text{For } w = \rho, \ u, \ v, \ p \text{ the distance in } \mathbf{R}^3 \text{ between } w^{n+1} = (w_{K,A_i}^{n+1})_{i=1,\ldots,3} \\ \\ \qquad \text{and } w^\star = (w_{K,A_i}^\star)_{i=1,\ldots,3} \text{ is minimum .} \end{cases}$$

The computation of $V_{|K}^{n+1}$ from $V_{|K}^\star$ thus amounts to four projection problems in $\mathbf{R}^3$ (one for each physical variable); as (i) defines a plane, and (ii) a cube, we look for the projection, on their intersection, of the corresponding variable $w^\star = (w_{K,A_i}^\star)_{i=1,\ldots,3}$.

Condition (i) allows for mass conservation, (ii) limits the variation of ρ, u, v, p (in that order), and (iii) guarantees uniqueness of the solution.

After computing the vector of physical variables $V^{n+1} = \begin{pmatrix} \rho^{n+1} \\ u^{n+1} \\ v^{n+1} \\ p^{n+1} \end{pmatrix}$ we return to the conservative variables according to

$$U^{n+1} = \begin{pmatrix} \rho^{n+1} \\ \rho^{n+1}u^{n+1} \\ \rho^{n+1}v^{n+1} \\ \dfrac{p^{n+1}}{(\gamma-1)} + \dfrac{1}{2}\rho^{n+1}\left[(u^{n+1})^2 + (v^{n+1})^2\right] \end{pmatrix}.$$

The slope limitation therefore requires the solution of a series of local minimization problems in 3 dimensional space, with the constraints (i) and (ii).

These projection problems can easily be solved by duality, as will be shown in the **appendix.**

In order to ensure the existence of a solution for the projection problems, we have to make sure that the intersection of the corresponding plane and cube is not empty. For density and pressure, it is easily seen that if we let $\rho_{K,A_i}^{n+1} = \overline{\rho}_K^\star$ and $p_{K,A_i}^{n+1} = \overline{p}_K^\star$ for $i = 1, 2, 3$, conditions (i) and (ii) are then satisfied, so that the relevant intersection is not empty.

As regards the velocity components, we can easily check, applying definitions (3.2) and (3.3), that if we let $u_{K,A_i}^{n+1} = \overline{u}_K^\star$ $(i = 1, 2, 3)$, then

$$\begin{aligned} \overline{(\rho u)}_K^{n+1} = \frac{1}{3}\sum_{i=1}^{3} \rho_{K,A_i}^{n+1}\overline{u}_K^\star &= \frac{1}{3}\left(\sum_{i=1}^{3}\rho_{K,A_i}^{n+1}\right)\frac{\overline{(\rho u)}_K^\star}{\overline{\rho}_K^\star} \\ &= \overline{(\rho u)}_K^\star . \end{aligned}$$

with a similar result for the second velocity component.

The parameter α controls the extent of the slope limitation process. For $\alpha = 0$, we get the most stringent limitation: the solution V^{n+1} (and therefore U^{n+1}) is piecewise constant, thus reducing the method to the usual (spatially) first order accurate scheme. In our numerical experiments, we have usually chosen $\alpha = 0.5$, a value which led to optimal results in the scalar case (cf. [25],[23],[6]).

For one-dimensional problems, the limitation procedure reduces to the usual van Leer solpe limitation ([26],[41]).

3.3. The numerical scheme.

The above description of the Jaffré-Kaddouri-Gowda discontinuous finite element method can be summarized within the frame of a two-step scheme.

Assuming for simplicity that we use an explicit Euler time discretization, let $U^n \in W^4$ be the solution obtained at time $t = t^n$. In the first step (predictor), we compute an approximation $U^\star \in W^4$ of the solution at time t^{n+1}. This predictor step consists in a finite element calculation, but features the use of Riemann solvers.

In the second step, which can be viewed as a correction step, we limit the vector $U^\star$ to obtain an approximate solution U^{n+1}.

1 - Predictor step : Finite element calculation

$$\left\{ \begin{array}{l} \text{Compute } U^\star \in W^4 \text{ such that} \\ \\ \displaystyle\int_{K_i} \frac{U^\star - U^n}{\Delta t^n} \varphi_{j,i}\, dS = \int_{K_i} \left(F(U^n) \frac{\partial \varphi_{j,i}}{\partial x} + G(U^n) \frac{\partial \varphi_{j,i}}{\partial y} \right) dS \\ \qquad\qquad\qquad\qquad - \displaystyle\int_{\partial K_i} \left(\vec{\mathbb{F}}(U^n) \cdot \boldsymbol{n} \right) \varphi_{j,i}\, d\sigma \qquad (3.5) \\ \\ \text{for each } K_i \in \mathcal{T}_h \text{ and } \varphi_{j,i} (j = 1, 2, 3) \end{array} \right.$$

2 - Limitation step

This step limits the variation range of components of the vector of physical variables $V^\star = \begin{pmatrix} \rho^\star \\ u^\star \\ v^\star \\ p^\star \end{pmatrix}$ obtained in the predictor step. It leads to V^{n+1} and then U^{n+1}, the final approximation of the vector of conservative variables at time t^{n+1}.

We observe that the two steps are independent from each other, and the limitation process is distinct from the flux calculation, contributing to the originality of the method.

3.4. Riemann solver.

In this subsection we present a short description of Roe's approximate Riemann solver, which will be used here in conjunction with an entropic correction recently proposed by Dubois and Mehlman ([24]) described below.

Let $\mathcal{A}$ be an edge in the grid, and $\vec{n}_{\mathcal{A}}$ a unit vector normal to $\mathcal{A}$; let $F_n(U)$ be the flux in the direction of $\vec{n}_{\mathcal{A}}$, with $U \in W^4$. Let U_l and U_r be the limiting values of U obtained when approaching the edge $\mathcal{A}$ along $\vec{n}_{\mathcal{A}}$ from the upwind and downwind side, respectively, with respect to the direction of $\vec{n}_{\mathcal{A}}$; for the description of Roe's numerical flux, we will provisionally assume that U_l and U_r are two constant states along each side of $\mathcal{A}$ (while we will later use limits of piecewise linear functions, see below).

Let $\widetilde{F}_{\mathcal{A}}(U_l, U_r)$ denote the numerical flux of a specific Riemann solver. It satisfies the consistency relation $\widetilde{F}_{\mathcal{A}}(U, U) = F_n(U)$, for all $U \in W^4$, where

$$F_n(U) = n_1 F(U) + n_2 G(U) = \vec{\mathbb{F}}(U).\vec{n}\,. \tag{3.6}$$

is the physical flux across $\mathcal{A}$, and

$$\vec{n} = \vec{n}_{\mathcal{A}} = \begin{pmatrix} n_1 \\ n_2 \end{pmatrix} = \begin{pmatrix} \cos\theta \\ \sin\theta \end{pmatrix} \in \mathbf{R}^2_* \ \ (\vec{n} \neq \vec{0})$$

If $\vec{V} = \begin{pmatrix} u \\ v \end{pmatrix}$ denotes the velocity, we can write it in the edge-normal to edge local basis formed by $\vec{n}$ and a unit vector $\vec{a}$ along edge $\mathcal{A}$ (fig.5.56) as

$$\vec{V_n} = \begin{pmatrix} u_n = \ u\cos\theta + v\sin\theta \\ v_n = -u\sin\theta + v\cos\theta \end{pmatrix}. \tag{3.7}$$

We can then define an invertible linear transformation T in $\mathbf{R}^4$:

$$T = \begin{bmatrix} 1 & 0 & 0 & 0 \\ 0 & \cos\theta & \sin\theta & 0 \\ 0 & -\sin\theta & \cos\theta & 0 \\ 0 & 0 & 0 & 1 \end{bmatrix} \quad , \quad T^{-1} = \begin{bmatrix} 1 & 0 & 0 & 0 \\ 0 & \cos\theta & -\sin\theta & 0 \\ 0 & \sin\theta & \cos\theta & 0 \\ 0 & 0 & 0 & 1 \end{bmatrix}. \tag{3.8}$$

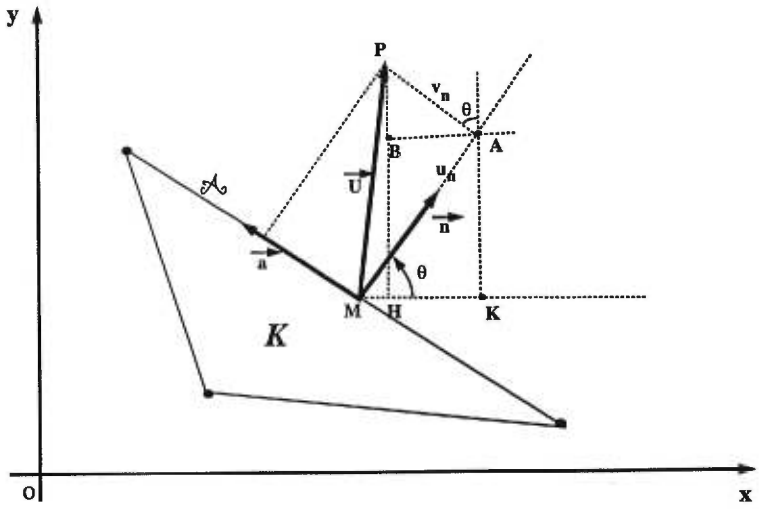

FIGURE 5.56. Local basis for the calculation of the flux

An arbitrary state vector $U = \begin{pmatrix} \rho \\ \rho\vec{V} \\ \rho E \end{pmatrix}$ is then mapped into $\widehat{U}$:

$$U \longrightarrow T \cdot U = \begin{pmatrix} \rho \\ \rho\vec{V}_n \\ \rho E \end{pmatrix} = \widehat{U}\,. \tag{3.9}$$

The flux in the direction $\vec{n}_A$

$$F_n(U) = n_1 F(U) + n_2 G(U)\,.$$

can be written in the edge-normal to edge local basis as

$$F_n(U) = cos\theta \begin{pmatrix} \rho u \\ p + \rho u^2 \\ \rho uv \\ (\rho E + p)u \end{pmatrix} + sin\theta \begin{pmatrix} \rho v \\ \rho uv \\ p + \rho v^2 \\ (\rho E + p)v \end{pmatrix} = \begin{pmatrix} \rho u_n \\ (\rho u)u_n + p\cos\theta \\ (\rho v)u_n + p\sin\theta \\ (\rho H)u_n \end{pmatrix}, \tag{3.10}$$

where $H = E + \frac{p}{\rho}$ is the specific total enthalpy (per unit mass).
It can be easily verified that if $\hat{U} = TU = \left(\rho, \rho\vec{V}_n, \rho E\right)^T$, then

$$F_n(U) = T^{-1} \circ F(\hat{U}) \tag{3.11}$$

where

$$F(\hat{U}) = (\rho u_n, p + \rho u_n^2, \rho u_n v_n, (\rho E + p)u_n)^T \tag{3.12}$$

This relation allows for the computation of $F_n(U)$ with the help of the first (vector) component F of the flux $\vec{\mathbb{F}}$ only, without resorting to G.

This leads to a reduction of the computing time, since the calculation of the matrices T and T^{-1} and the flux component F requires fewer operations than the calculation of the global flux F_n from its original definition.

In the sequel, the flux calculations will therefore be performed for $n_1 = 1$, $n_2 = 0$ (corresponding to $\theta = 0$).

3.5. Numerical flux of Roe's original scheme.

In Roe's scheme for the one-dimensional Euler equations $U_t + F(U)_x = 0$, one computes the exact solution of the linearized Riemann problem defined at the cell interface $x_{i+\frac{1}{2}}$ between cells C_i and C_{i+1} with corresponding constant states U_i, U_{i+1}, by replacing the Jacobian matrix $\frac{\partial F(U)}{\partial U} = A(U)$, computed at $x_{i+\frac{1}{2}}$, by a special constant matrix $\bar{A}_{i+\frac{1}{2}} = \bar{A}(U_i, U_{i+1})$ called Roe' average matrix, with the properties

(i) $F(U_{i+1}) - F(U_i) = \bar{A}_{i+\frac{1}{2}}(U_{i+1} - U_i)$

(ii) For $U_i = U_{i+1} = U$, we have $\bar{A}(U,U) = A(U) \equiv \frac{\partial F(U)}{\partial U}$

(iii) The eigenvalues λ_k of $\bar{A}$ are real and its eigenvectors r_k are linearly independant ($k = 1, \ldots, 3$).

It can be shown that $\bar{A}_{i+\frac{1}{2}} = \bar{A}(U_i, U_{i+1})$ is in fact equal to $A(\bar{U})_{i+\frac{1}{2}} \equiv \frac{\partial F(U)}{\partial U}|_{U=\bar{U}_{i+\frac{1}{2}}}$ (see [27]) where $\bar{U}_{i+\frac{1}{2}} = (\bar{\rho}_{i+\frac{1}{2}}, \bar{u}_{i+\frac{1}{2}}, \bar{H}_{i+\frac{1}{2}})$ is a specific average of the vectors U_i, U_{i+1} called Roe's average, defined by

$$\bar{\rho}_{i+\frac{1}{2}} = \sqrt{\rho_i \rho_{i+1}}, \quad \bar{u}_{i+\frac{1}{2}} = \frac{(u\sqrt{\rho})_i + (u\sqrt{\rho})_{i+1}}{\sqrt{\rho_i} + \sqrt{\rho_{i+1}}}, \quad \bar{H}_{i+\frac{1}{2}} = \frac{(H\sqrt{\rho})_i + (H\sqrt{\rho})_{i+1}}{\sqrt{\rho_i} + \sqrt{\rho_{i+1}}}$$

In the present context of the two-dimensional Euler equations, and owing to the previous remarks at the end of section 3.4, we will consider two adjacents states U_l, U_r separated by a triangle edge $\mathcal{A}$. Roe's average matrix will be given by (see [27] for a description of this matrix)

$$\bar{A}(U_l, U_r) = \frac{\partial F(U)}{\partial U}|_{U=\bar{U}_{lr}} \tag{3.13}$$

where Roe's average vector

$$\bar{U}_{lr} = (\bar{\rho}, \bar{u}, \bar{v}, \bar{H}) \tag{3.14}$$

is defined by

$$\begin{cases} \overline{\rho} = \sqrt{\rho_l \rho_r} \\ \text{and for } \ a = u,\ v \ or\ H \\ \bar{a} = \frac{a_l\sqrt{\rho_l} + a_r\sqrt{\rho_r}}{\sqrt{\rho_l} + \sqrt{\rho_r}} \end{cases} \tag{3.15}$$

The Roe averages of the remaining dependent variables E, p and c are then computed from $\overline{\rho}, \overline{u}, \overline{v}, \overline{H}$:

$$\begin{cases} \bar{E} = \frac{1}{\gamma}\bar{H} + \frac{\gamma-1}{2\gamma}(\bar{u}^2 + \bar{v}^2) \\ \bar{c} = \{(\gamma-1)(\bar{H} - \frac{1}{2}(\bar{u}^2 + \bar{v}^2))\}^{\frac{1}{2}} \\ \bar{p} = \frac{\bar{\rho}\bar{c}^2}{\gamma} \end{cases}$$

Properties (i),(ii) above now read

(*i*) $F(U_l) - F(U_r) = \bar{A}(U_l, U_r)(U_r - U_l)$

(*ii*) $\bar{A}(U, U) = dF(U) \equiv \frac{\partial F(U)}{\partial U}$

We write $\lambda_k(U_l, U_r)(k = 1, \ldots, 4)$ and $r_k(U_l, U_r)$ for the eigenvalues and eigenvectors of $\bar{A}(U_l, U_r)$ (see [27]) and let $\triangle U \equiv U_r - U_l$.

Since the $r_k(U_l, U_r)$ are linearly independent, there exists $(\alpha_k)_{k=1,\ldots,4} \in R^4$ such that

$$\triangle U \equiv U_r - U_l = \sum_{k=1}^{4} \alpha_k r_k(U_l, U_r) \tag{3.16}$$

the numerical flux of Roe's scheme can then be written ([28],[29])

$$\tilde{F}_A(U_l, U_r) = \frac{1}{2}(F(U_l) + F(U_r)) - \frac{1}{2}d(U_l, U_r) \tag{3.17}$$

where $d(U_l, U_r)$ is the viscous term, given by

$$d(U_l, U_r) = |\bar{A}(U_l, U_r)|(U_r - U_l) = \sum_{k=1}^{4} \alpha_k |\lambda_k(U_l, U_r)| r_k(U_r, U_l) \tag{3.18}$$

Unfortunately, Roe's scheme does not satisfy an entropy inegality ([27],[29],[30]) and allows non-physical expansion shocks in the vicinity of sonic points ([21]), violating the Lax-Oleinik entropy condition; it is not an E-scheme ([43],[30],[27]), so that the

numerical solution does not necessarily converge to the (unique) entropy solution of the original nonlinear initial value problem.

To modify Roe's scheme so as to satisfy an entropy inequality, several ideas have been proposed (e.g. [29],[32],[33],[44],[45]), which are based on the representation of sonic rarefaction waves, and are equivalent to introducing a certain amount of artificial viscosity, the exact amount depending on a parameter which requires a case-dependent adjustment.

Dubois and Mehlman ([24]) have recently introduced a parameter-free modification of Roe's scheme based on nonlinear Hermite interpolation of an approximate flux function, leading to an entropic scheme.

3.6. Dubois-Mehlman's entropic correction of Roe's scheme.

This approach is based on a nonlinear modification of the flux function defined by (3.17) , in the neighbourhood of sonic points only.

For a given state U we write $U - U_l$ and $U_r - U_l$ as linear combinations of the eigenvectors.

Denoting by $(w_k)_{k=1,\dots,4}$ and $(\alpha_k)_{k=1,\dots,4}$ the characteristic variables associated[1] with $U - U_l$ and $U_r - U_l$, respectively, we have

$$U - U_l = \sum_{k=1}^{4} w_k \cdot \boldsymbol{r}_k(U_l, U_r) \tag{3.19}$$

$$U_r - U_l = \sum_{k=1}^{4} \alpha_k \cdot \boldsymbol{r}_k(U_l, U_r) \tag{3.20}$$

Following [29], we define the intermediate states

$$\begin{cases} U_0 = U_l \\ \quad \vdots \\ U_k = U_{k-1} + \alpha_k \boldsymbol{r}_k(U_l, U_r) \\ \quad \vdots \\ U_4 = U_r \end{cases} \tag{3.21}$$

Let $\mathbb{S}$ denote the set of sonic indices

$$\mathbb{S} = \{i,\ \lambda_i(U_{i-1}) < 0 < \lambda_i(U_i)\} \tag{3.22}$$

[1] In this quasi one-dimensional context (due to the remarks following (3.12)) we can assume the existence of characteristic variables as in the purely one-dimensional case (cf. [27] Vol II p.155).

We now introduce the Dubois-Mehlman modified flux function, parameterized by the states U_l and U_r

$$F^{\mathrm{dm}}(U_l, U_r; U) = F(U_l) + \sum_{k=1}^{4} g_k(w_k) \cdot \boldsymbol{r}_k(U_l, U_r) \tag{3.23}$$

where the $w_k's$ are the characteristic variables introduced in (3.19), and the $g_k's$ are parameterized by the state $(U_j)_{j=1,\ldots,4}$, and defined as follows:

$$\begin{aligned} &\text{if } k \notin \mathbb{S} \quad \text{then} \quad g_k(w) = \lambda_k(U_l, U_r) \cdot w \quad \forall w \\ &\text{if } k \in \mathbb{S} \quad g_k(w) = \begin{cases} p_k(w) & \text{for } 0 < w < \alpha_k \\ \lambda_k(U_l, U_r) \cdot w & \text{for } w \notin (0, \alpha_k) \end{cases} \end{aligned} \tag{3.24}$$

where $p_k(w)$ is the unique Hermite polynomial of degree 3 determined by the conditions

$$p_k(0) = 0,\ p_k(\alpha_k) = \lambda_k(U_l, U_r) \cdot \alpha_k,\ p_k'(0) = \lambda_k(U_{k-1}),\ p_k'(\alpha_k) = \lambda_k(U_k)$$

We recall that $\lambda_k(U_j)$ denotes the k-th eigenvalue of the jacobian matrix $A(U) \equiv \frac{\partial F}{\partial U}$ calculated at the intermediate state U_j, while $\lambda_k(U_l, U_r)$ is the k-th eigenvalue of the Roe matrix $\hat{A}(U_l, U_r)$. It can be verified that away from sonic points, the modified flux F^{dm} coincides with Roe's linearized flux:

$$F^R(U) = F(U_l) + \hat{A}(U_l, U_r)(U - U_l) \tag{3.25}$$

If the original physical flux $F(U)$ is at least continuously differentiable and if $\hat{A}(U_l, U_r)$ is a continuous function of U_l and U_r, F^{dm} is a continuous function of U_l, U_r and U.

LEMMA 3.1.

The Riemann problem

$$\begin{cases} \dfrac{\partial U}{\partial t} + \dfrac{\partial F^{dm}(U_l, U_r; U)}{\partial x} = 0 \\ U(x;0) = \begin{cases} U_l & x < 0 \\ U_r & x > 0 \end{cases} \end{cases}$$

has a unique entropy solution.

See [24] for the proofs of lemmas 3.1 and 3.2.

LEMMA 3.2. *For $k \in \mathbb{S}$, the Hermite polynomial $p_k(w)$ is defined by*

$$p_k(w) = a_k w^3 + b_k w^2 + c_k w \ ,$$

with

$$\begin{aligned} a_k &= \frac{\lambda_k(U_k) + \lambda_k(U_{k-1}) - 2\lambda_k(U_l, U_r)}{\alpha_k^2} \\ b_k &= \frac{3\lambda_k(U_l, U_r) - 2\lambda_k(U_{k-1}) - \lambda_k(U_k)}{\alpha_k} \\ c_k &= \lambda_k(U_{k-1}) \end{aligned}$$

The modified numerical flux can be written as

$$\tilde{F}_A^{dm}(U_l, U_r) = F(U_l) + \sum_{k \notin \mathbb{S}, \lambda_k(U_l, U_r) < 0} \alpha_k \cdot \lambda_k(U_l, U_r) \cdot \boldsymbol{r}_k + \sum_{k \in \mathbf{S}} g_k(w_k^\star) \cdot \boldsymbol{r}_k \quad (3.26)$$

where

$$w_k^\star = \frac{-\lambda_k(U_{k-1}) \cdot \alpha_k}{3\lambda_k - 2\lambda_k(U_{k-1}) - \lambda_k(U_k) + \sqrt{(3\lambda_k - \lambda_k(U_{k-1}) - \lambda_k(U_k))^2 - \lambda_k(U_{k-1}) \cdot \lambda_k(U_k)}} \quad (3.27)$$

is the argument of the unique extremum of $g_k(w)$ in the interval $0 < w < \alpha_k$, and λ_k in (3.27) denotes $\lambda_k(U_l, U_r)$.

Description of the eigenvectors $r_k(U_l, U_r)$ and characteristic variables α_k

To complete our description of the Dubois-Mehlman entropy correction to Roe's scheme, we must define the eigenvectors $r_k(U_l, U_r)$ and coefficients α_k appearing in (3.19),(3.20), (3.27).

From [28], we have

$$\boldsymbol{r}_1 = \begin{pmatrix} 1 \\ \widehat{u} - \widehat{c} \\ \widehat{v} \\ \widehat{H} - \widehat{u}\widehat{c} \end{pmatrix} , \ \boldsymbol{r}_2 = \begin{pmatrix} 0 \\ 0 \\ \widehat{v} \\ \widehat{v}^2 \end{pmatrix} , \ \boldsymbol{r}_3 = \begin{pmatrix} 1 \\ \widehat{u} \\ \widehat{v} \\ \frac{1}{2}(\widehat{u}^2 + \widehat{v}^2) \end{pmatrix} , \ \boldsymbol{r}_4 = \begin{pmatrix} 1 \\ \widehat{u} + \widehat{c} \\ \widehat{v} \\ \widehat{H} + \widehat{u}\widehat{c} \end{pmatrix}$$

For $w = \rho, \rho u, \rho v$ et ρE, we set $\Delta w = w_r - w_l$. Equation (3.20) defines a linear system in the 4 unknowns $\alpha_1, \ldots, \alpha_4$. For $\widehat{v} \neq 0$, the unique solution is given by

$$\begin{cases} \alpha_1 &= \dfrac{\gamma-1}{2\,\widehat{c}^2}\left\{\Delta(\rho E) - \widehat{v}\Delta(\rho v) - \left(\widehat{u} + \dfrac{\widehat{c}}{\gamma-1}\right)\Delta(\rho u) + \left(\dfrac{\widehat{c}\cdot\widehat{u}}{\gamma-1} + \dfrac{1}{2}(\widehat{u}^2+\widehat{v}^2)\right)\Delta\rho\right\} \\ \alpha_2 &= \dfrac{1}{\widehat{v}}\Delta(\rho v) - \Delta\rho \\ \alpha_3 &= \left(1 + \dfrac{\widehat{u}}{\widehat{c}}\right)\Delta\rho - \dfrac{1}{\widehat{c}}\Delta(\rho u) - 2\,\alpha_1 \\ \alpha_4 &= \alpha_1 + \dfrac{1}{\widehat{c}}\left(\Delta(\rho u) - \widehat{u}\Delta\rho\right) \end{cases}$$

If $\widehat{v} = 0$, α_2 is indeterminate. One can set it equal to 0, in which case there exists a unique $(\alpha_k)_{k=1,\ldots,4} \in \mathbb{R}^4$ satisfying (3.20), given by

$$\begin{cases} \alpha_1 &= \dfrac{\gamma-1}{2\,\widehat{c}^2}\left\{\Delta(\rho E) - \left(\widehat{u} + \dfrac{\widehat{c}}{\gamma-1}\right)\Delta(\rho u) + \left(\dfrac{\widehat{c}\cdot\widehat{u}}{\gamma-1} + \dfrac{\widehat{u}^2}{2}\right)\Delta\rho\right\} \\ \alpha_2 &= 0 \\ \alpha_3 &= \left(1 + \dfrac{\widehat{u}}{\widehat{c}}\right)\Delta\rho - \dfrac{1}{\widehat{c}}\Delta(\rho u) - 2\,\alpha_1 \\ \alpha_4 &= \alpha_1 + \dfrac{1}{\widehat{c}}\left(\Delta(\rho u) - \widehat{u}\Delta\rho\right) \end{cases}$$

The Dubois-Mehlman correction has proved to be useful for explicit schemes, but difficult to implement for implicit schemes, owing to the difficulty of the linearization process.

3.7. Note on the implementation of the time discretization.

In this paper, we limit our applications to the computation of stationary solutions, and will therefore use a local time stepping process described below.
Introducing the diagonal matrix $\Sigma = \operatorname{diag}\left[\dfrac{\text{Area}(K_i)}{\Delta t_i^n}\right]_{K_i \in \mathcal{T}_h}$, we can write (3.5) as follows:

$$\begin{cases} \text{Find } U^\star \in W^4 \quad \text{such that} \\ U^\star - U^n \;=\; -\Sigma^{-1}\,\mathcal{R}(U^n) \end{cases} \tag{3.28}$$

where $\mathcal{R}(U^n)$ is the residual defined from the right-hand side of (3.5)

$$\mathcal{R}(U^n) = \int_{\partial K_i} \left(\vec{\mathbb{F}}(U^n)\cdot n\right)\phi_{j,i}\,d\sigma \;-\; \int_{K_i}\left(F(U^n)\frac{\partial \phi_{j,i}}{\partial x} + G(U^n)\frac{\partial \phi_{j,i}}{\partial y}\right) dS\,. \quad (3.29)$$

The scheme (3.28) is stable under an appropriate $CFL-condition.$

Let μ denote the $CFL-number$ (assumed to be uniform on the whole grid). For each element $K_i \in \mathcal{T}_h$ we note

- ν_i : mean value, in element K_i, of the characteristic speed corresponding to the largest eigenvalue

$$\nu_i = \sqrt{\overline{u}_i^2 + \overline{v}_i^2} + \overline{c}_i\,,$$

- h_i : ratio of the area of K_i by its perimeter

$$h_i = \frac{\text{Area}(K_i)}{\text{L}(K_i)}\,.$$

The local time step is then chosen so that

$$\Delta t_i^n \leq \mu \frac{h_i}{\nu_i}\,. \quad (3.30)$$

In most cases we have used a $CFL-number$ $\mu = 0.5$.

In the numerical experiments presented in this paper, we study the distribution on the body B (fig.1) and the isolines of the Mach number M, the pressure p, or the pressure coefficient C_p, defined by

$$Cp = \frac{p_\infty - p}{\frac{1}{2}\rho_\infty \,\|\boldsymbol{V}_\infty\|^2} \quad (3.31)$$

To study the convergence of the method, we will present graphs of the $\mathbb{L}_2$-norm of the residual $\mathcal{R}(U^n)$ as a function of the number of iterations.

4. Finite volume methods on unstructured triangular grids

4.1. A two-dimensional finite volume method inspired by the Lax-Friedrichs scheme.

We consider the solution $U(x,y,t)$ of the two-dimensional Euler equations (2.1)-(2.2)

$$U_t + F(U)_x + G(U)_y = 0 \quad (4.1)$$

in some region Ω of the $x-y$ plane. In one space dimension [5], both the staggered form of the Lax-Friedrichs scheme and the Nessyahu-Tadmor scheme use two alternate grids $\{x_j\}$ and $\{x_{j+1/2}\}$ at odd and even time steps, respectively. In two dimensions, we proceed in a similar way, starting from an arbitrary FEM triangular grid $\mathcal{T}_h$ such that

$$\Omega = \bigcup_{T\in\mathcal{T}_h} T \text{ and } T\cap T' = \begin{cases} \phi \\ \text{one vertex} \\ \text{one side} \end{cases} \qquad \text{for any } T, T' \in \mathcal{T}_h \tag{4.2}$$

The nodes of the FEM triangulation are the vertices a_i of the triangles, and in this subsection the degrees of freedom are the vector values of U at the nodes, which can also be considered as cell average values for the cell C_i centered at each individual node a_i (defined below).

For the first grid associated with our finite volume extension of the Lax-Friedrichs scheme, the nodes are the vertices a_i of $\mathcal{T}_h$ while the finite volume cells are the barycentric cells C_i associated with these nodes, obtained by joining the midpoints M_{ij} of the sides originating in a_i to the centroids G_{ij} of the triangles of $\mathcal{T}_h$ which meet at a_i (fig.5.57).

For the second grid the nodes are the midpoints M_{ij} of the sides of the original triangulation, while the cells are the quadrilaterals of the form $L_{ij} = a_iG_{ij}a_jG_{i,j+1}$ having M_{ij} as midpoint of one diagonal, obtained by joining two adjacent nodes a_i, a_j to the centroids of the two triangles of $\mathcal{T}_h$ of which a_ia_j is a side.

Let $U_i^n \cong U(a_i, t^n)$ and $U_{ij}^{n+1} \cong U(M_{ij}, t^{n+1})$ denote the nodal (or cell average) vector values in the first and second grid at time $t = t^n$ and $t = t^{n+1}$, respectively (n even).

For the barycentric cell C_i, let $\vec{\nu}_{ij}^1$ and $\vec{\nu}_{ij}^2$ denote the unit outer normal vectors to $G_{ij}M_{ij}$ and $M_{ij}G_{i,j+1}$ respectively, pointing out of cell C_i (fig.5.58) , and for the quadrilateral cell L_{ij}, let $\vec{n}^1{}_{ij}, \ldots, \vec{n}_{ij}^4$ be the normal vectors to the cell edges a_iG_{ij}, $G_{ij}a_j$, $a_jG_{i,j+1}$ and $G_{i,j+1}a_i$, respectively, pointing out of cell L_{ij} (fig.5.59).

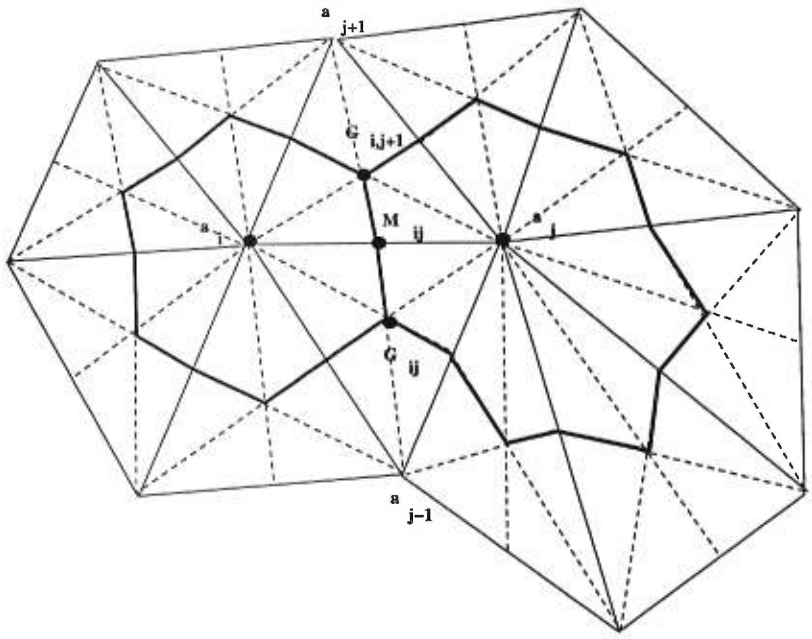

FIGURE 5.57. Barycentric cells around nodes $\mathbf{a_i}$, $\mathbf{a_j}$; quadrilateral cell $\mathbf{a_i G_{ij} a_j G_{i,j+1}}$.

We must also define the elementary flux vectors

$$\vec{\eta}_{ij} = \int_{\Gamma_{ij}=G_{ij}M_{ij}G_{i,j+1}} \vec{\nu} d\sigma = |\overrightarrow{G_{ij}M_{ij}}|\vec{\nu}_{ij}^{\,1} + |\overrightarrow{M_{ij}G_{i,j+1}}|\vec{\nu}_{ij}^{\,2} \tag{4.3}$$

and

$$\begin{cases} \vec{\theta}_{ij} = |\overrightarrow{a_iG_{ij}}|\vec{n}_{ij}^{\,1} + |\overrightarrow{a_iG_{i,j+1}}|\vec{n}_{ij}^{\,4} \\ \vec{\theta}_{ji} = |\overrightarrow{a_jG_{ij}}|\vec{n}_{ij}^{\,2} + |\overrightarrow{a_jG_{i,j+1}}|\vec{n}_{ij}^{\,3}. \end{cases} \tag{4.4}$$

We write furthermore

$$\vec{\nu}_{ij}^{\,k} = \begin{pmatrix} \nu_{ijx}^k \\ \nu_{ijy}^k \end{pmatrix} \text{ for } k = 1,2, \quad \vec{n}_{ij}^{\,k} = \begin{pmatrix} n_{ijx}^k \\ n_{ijy}^k \end{pmatrix} \text{ for } k = 1,\ldots,4$$

$$\text{and } \vec{\eta}_{ij} = \begin{pmatrix} \eta_{ijx} \\ \eta_{ijy} \end{pmatrix}, \quad \vec{\theta}_{ij} = \begin{pmatrix} \theta_{ijx} \\ \theta_{ijy} \end{pmatrix}. \tag{4.5}$$

An advantage of using a finite volume formulation where the degrees of freedom are values of the unknown function at the triangulation vertices lies in the possibility to couple (4.1) with an elliptic equation. This can be very convenient in the case of a

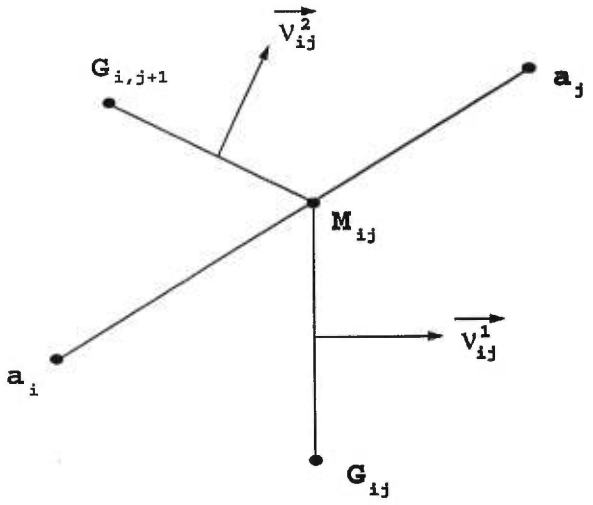

FIGURE 5.58. Barycentric cell boundary element $\Gamma_{ij} = G_{ij}M_{ij} \cup M_{ij}G_{i,j+1}$.

scalar conservation law where

$$\begin{cases} f(u) = w_1\, h(u) \\ g(u) = w_2\, h(u) \end{cases} \tag{4.6}$$

i.e. when (4.1) can be written as $u_t + \operatorname{div}(\vec{W}\, h(u)) = 0$ with $\vec{W} = (w_1, w_2)^T$ and $\vec{W}$ stems from an elliptic problem. This situation arises in the study of polyphase flows in porous media, where fluid mechanical and thermodynamical considerations are combined, leading to coupled hyperbolic and elliptic equations [42].

The first step of the two-dimensional finite volume extension of the Lax-Friedrichs scheme is defined by integrating (4.1) on the 3-dimensional cell $L_{ij} \times [t^n, t^{n+1}]$, assuming that the (barycentric) cell values U_i^n at the vertices a_i of the original triangulation are known:

$$\int_{t^n}^{t^{n+1}} \int_{L_{ij}} (U_t + F(U)_x + G(U)_y) dx dy\, dt = 0. \tag{4.7}$$

Applying the divergence theorem and observing that $L_{ij} = (L_{ij} \cap C_i) \cup (L_{ij} \cap C_j)$ we get

$$\int_{L_{ij}} U(x,y,t^{n+1}) dA - \int_{L_{ij}\cap C_i} U(x,y,t^n) dA - \int_{L_{ij}\cap C_j} U(x,y,t^n) dA + \int_{t^n}^{t^{n+1}} \int_{\partial L_{ij}} (F(U)n_x + G(U)n_y) d\sigma\, dt = 0. \tag{4.8}$$

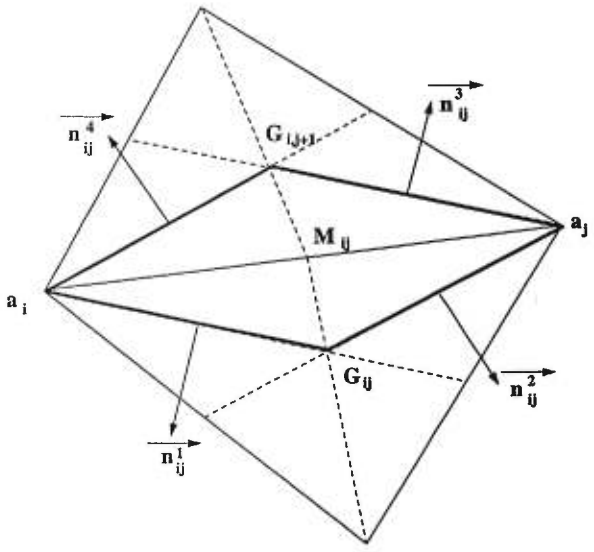

FIGURE 5.59. Quadrilateral cells $\mathbf{L_{ij}}$.

Since $U(x,t)$ is approximated by U_i^n in C_i, U_j^n in C_j, we can choose the approximation U_i^n on $\partial L_{ij} \cap C_i$ and U_j^n on $\partial L_{ij} \cap C_j$, whence the first step of our finite volume Lax-Friedrichs scheme:

$$A(L_{ij})U_{ij}^{n+1} - A(L_{ij} \cap C_i) \cdot U_i^n - A(L_{ij} \cap C_j) \cdot U_j^n + \Delta t(F(U_i^n)\theta_{ijx} + G(U_i^n)\theta_{ijy}) + \Delta t(F(U_j^n)\theta_{jix} + G(U_j^n)\theta_{jiy}) = 0. \quad (4.9)$$

We note that this approximation corresponds to choosing the approximate time derivative

$$U_t \cong \left(U_{ij}^{n+1} - \frac{A(L_{ij} \cap C_i) \cdot U_i^n + A(L_{ij} \cap C_j) \cdot U_j^n}{A(L_{ij})} \right) / \Delta t. \quad (4.10)$$

For the second step we proceed similarly with the help of the barycentric cells C_i:

$$A(C_i)U_i^{n+2} - \sum_{j \text{ neighbour of } i} A(L_{ij} \cap C_i)U_{ij}^{n+1} + \Delta t \sum_{j \text{ neighbour of } i} (F(U_{ij}^{n+1})\eta_{ijx} + G(U_{ij}^{n+1})\eta_{ijy}) = 0 \quad (4.11)$$

where the value of $U(x,y,t^{n+1})$ on the boundary $\partial C_i = \bigcup_{j \text{ neighbour of } i} \Gamma_{ij}$ is approximated locally, on $\partial C_i \cap L_{ij} = \Gamma_{ij}$, by U_{ij}^{n+1} (i.e. the approximate value of U^{n+1} on the quadrilateral cell L_{ij}. We thus alternately define an approximate solution U_{ij}^{n+1} which is piecewise constant on the quadrilateral cells L_{ij}, at odd time steps ($n = 0, 2, \ldots$), and a solution U_i^{n+2} constant on the barycentric cells C_i, at even time steps.

4.2. A two-dimensional finite volume inspired by the Nessyahu-Tadmor scheme.

The construction of a finite volume method inspired by [5] implies the computation of gradients of piecewise linear functions, and the limitation of the gradients. To simplify the presentation, we shall describe our finite volume method in the case of scalar conservation laws in this subsection. The extension to the vector case is obtained from a field by field decomposition (see, e.g. [47] ,[46],[48]).

We consider a scalar nonlinear conservation equation

(4.1′) $$u_t + f(u)_x + g(u)_y = 0$$

At the beginning of the $(n+1)^{\text{st}}$ time step (n even), we have obtained approximate barycentric cell values u_i^n (a_i : a vertex of $\mathcal{T}_h$). We must now, in order to follow the van Leer MUSCL approach used by Nessyahu and Tadmor, construct a piecewise linear profile on the barycentric cells C_i; this can be achieved as follows.

We first construct a piecewise linear approximant on each triangle T of the original triangulation, continuous on the whole computational domain Ω_h, with the help of the barycentric cell/nodal values u_i^n: if $T \in \mathcal{T}_h$ is a triangle with vertices a_{i_j}, $(j = 1, 2, 3)$, we construct $p_T \in P^1$ such that

$$p_T(a_{i_j}) = u_{i_j}^n \ (j = 1, 2, 3)$$

$p_T(x, y)$ is easily obtained from the barycentric coordinates of (x, y) with respect to the vertices of T:

$$p_T(\vec{x}) = \sum_{j=1}^{3} \lambda_j(\vec{x}) u_j^n$$

where the vertices of T have been relabelled $1, 2, 3$ or a_1, a_2, a_3, and $\vec{x} = (x, y) \in T$.

The gradient of the (barycentric) cellwise *piecewise linear interpolant* $L(x, y, t^n)$ to be defined will now be chosen (as e.g. in [39] p.28), for cell C_i, as the arithmetic average of the gradients of the polynomials p_T for all triangles T such that $a_i \in T$: on C_i we take

$$L = L_i(x, y, t^n) = u_i^n + (x - x_i)P_i^n + (y - y_i)Q_i^n \qquad (x, y) \in C_i \tag{4.12}$$

where

$$\begin{pmatrix} P_i^n \\ Q_i^n \end{pmatrix} = \underset{a_i \in T}{\text{Average}} \{\text{grad } p_T\}. \tag{4.13}$$

Contrary to what prevailed in the one-dimensional case, where the average value $\bar{u}_j^n$ of the piecewise linear interpolant $L_j(x,t^n)$ was also its value at the node x_j, we can no longer identify the average value of the piecewise linear interpolant (4.12) , on cell C_i, with its nodal value u_i^n at the "center" a_i of C_i, since a_i need not be the centroid of C_i, and $\frac{1}{A(C_i)}\int_{C_i} L_i(x,y,t^n)dA \neq u_i^n$ in general.

The new cell values at t^{n+1} and t^{n+2} will nevertheless again be *defined* by formulas similar to (4.9) (first step), and (4.11) (second step), obtained by integrating (4.1') on $L_{ij}\times[t^n,t^{n+1}]$ for the first step, and on $C_i\times[t^n,t^{n+1}]$ for the second step:

$$A(L_{ij})u_{ij}^{n+1} \equiv \text{numerical approximation of } \int_{L_{ij}} u(x,y,t^{n+1})dA \tag{4.14}$$

$$A(C_i)u_i^{n+2} \equiv \text{numerical approximation of } \int_{C_i} u(x,y,t^{n+2})dA. \tag{4.15}$$

For the first step of our scheme we write

$$\int_{t^n}^{t^{n+1}}\int_{L_{ij}} (u_t + f(u)_x + g(u)_y)dAdt = 0 \tag{4.16}$$

which leads to

$$\int_{L_{ij}} u(x,y,t^{n+1})dA = \int_{L_{ij}\cap C_i} L(x,y,t^n)dA + \int_{L_{ij}\cap C_j} L(x,y,t^n)dA - \int_{t^n}^{t^{n+1}}\int_{\partial L_{ij}} (f(u)n_x + g(u)n_y)d\sigma dt. \tag{4.17}$$

The numerical approximation of the right-hand side, and (4.14), will thus lead to u_{ij}^{n+1}, which will be our cell value for the quadrilateral cell L_{ij}.

4.3. Approximation of $\int_{L_{ij}\cap C_i} L(x,y,t^n)dA$.

$L(x,y,t^n)$ is the piecewise linear function defined, on cell C_i, by (4.12) . Let $A_iA_{ij}B_{ij}\ A_{i,j+1}$ be the points of the plane defined by the linear function L_i on C_i which correspond to the four vertices of $L_{ij}\cap C_i = [a_iG_{ij}M_{ij}G_{i,j+1}]$ where [...] denotes the quadrilateral generated by the corresponding vertices (fig. 5.60).

The integral of L on $L_{ij}\cap C_i$ is equal to the total volume of the two prisms with triangular base $a_iG_{ij}M_{ij}A_iA_{ij}B_{ij}$ and $a_iM_{ij}G_{i,j+1}A_iB_{ij}A_{i,j+1}$, constructed on the triangular bases $L_{ij}^r\cap C_i$ and $L_{ij}^\ell\cap C_i$ where L_{ij}^r = triangle $(a_iG_{ij}a_j)$ and L_{ij}^ℓ = triangle $(a_ia_jG_{i,j+1})$; r,ℓ stand for right, left (for an observer at a_i).

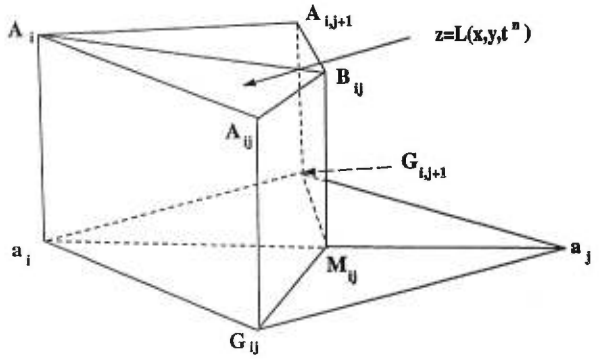

FIGURE 5.60. Prismatic regions for the computation of $\int_{L_{ij}\cap C_i} L(x,y,t^n)dA$.

The volume of the first prism, for instance, is given by

$$\begin{aligned}\text{Vol}\{a_iG_{ij}M_{ij}A_iA_{ij}B_{ij}\} &= \frac{1}{3}\,\text{Area}\,(a_iG_{ij}M_{ij})\cdot[a_iA_i+G_{ij}A_{ij}+M_{ij}B_{ij}]\\ &= \frac{1}{3}\,\text{Area}\,(L_{ij}^r\cap C_i)\{u_i^n+u_i^n+(x_{G_{ij}}-x_i)P_i^n\\ &\qquad +(y_{G_{ij}}-y_i)Q_i^n+u_i^n+(x_{M_{ij}}-x_i)P_i^n\\ &\qquad +(y_{M_{ij}}-y_i)Q_i^n\}\\ &= \text{Area}\,(L_{ij}^r\cap C_i)\{u_i^n+\frac{1}{3}(x_{G_{ij}}+x_{M_{ij}}-2x_i)P_i^n\\ &\qquad +\frac{1}{3}(y_{G_{ij}}+y_{M_{ij}}-2y_i)Q_i^n\}\end{aligned}\tag{4.18}$$

where

$$\begin{aligned}\text{Area}\,(L_{ij}^r\cap C_i) &\equiv \text{Area triangle}\,(a_iG_{ij}M_{ij})\\ &= \frac{1}{2}\{(x_{G_{ij}}-x_i)(y_{M_{ij}}-y_i)-(x_{M_{ij}}-x_i)(y_{G_{ij}}-y_i)\}.\end{aligned}\tag{4.19}$$

Similarly, the volume of the second prism is

$$\begin{aligned}\text{Vol}\{a_iM_{ij}G_{i,j+1}\ A_iB_{ij}A_{i,j+1}\} &= \text{Area}(L_{ij}^\ell\cap C_i)\cdot\\ &\{u_i^n+\frac{1}{3}(x_{M_{ij}}+x_{G_{i,j+1}}-2x_i)P_i^n+\frac{1}{3}(y_{M_{ij}}+y_{G_{i,j+1}}-2y_i)\}\end{aligned}\tag{4.20}$$

Summing (4.18) and (4.20), we get

$$\begin{aligned}\int_{L_{ij}\cap C_i} L(x,y,t^n)dA &= \text{Area}(L_{ij}\cap C_i)\{u_i^n+\frac{1}{3}(x_{M_{ij}}-x_i)P_i^n+\frac{1}{3}(y_{M_{ij}}-y_i)Q_i^n\}\\ &+\frac{1}{3}\text{Area}(L_{ij}^r\cap C_i)\{(x_{G_{ij}}-x_i)P_i^n+(y_{G_{ij}}-y_i)Q_i^n\}\\ &+\frac{1}{3}\text{Area}(L_{ij}^\ell\cap C_i)\{(x_{G_{i,j+1}}-x_i)P_i^n+(y_{G_{i,j+1}}-y_i)Q_i^n\}\end{aligned}\tag{4.21}$$

with

$$\text{Area}(L_{ij}^{\ell} \cap C_i) = \frac{1}{2}\{(x_{M_{ij}} - x_i)(y_{G_{i,j+1}} - y_i) - (x_{G_{i,j+1}} - x_i)(y_{M_{ij}} - y_i)\}. \quad (4.22)$$

4.4. Approximation of $\int_{L_{ij}\cap C_j} L(x,y,t^n)dA$.

Proceeding in the same way we find

$$\begin{aligned}\int_{L_{ij}\cap C_j} L(x,y,t^n)dA = \text{Area}(L_{ij}\cap C_j)\{u_j^n + \frac{1}{3}(x_{M_{ij}} - x_j)P_j^n + \frac{1}{3}(y_{M_{ij}} - y_j)Q_j^n\} \\ + \frac{1}{3}\text{Area}(L_{ij}^r \cap C_j)\{(x_{G_{ij}} - x_j)P_j^n + (y_{G_{ij}} - y_j)Q_j^n\} \quad (4.23) \\ + \frac{1}{3}\text{Area}(L_{ij}^{\ell} \cap C_j)\{(x_{G_{i,j+1}} - x_j)P_j^n + (y_{G_{i,j+1}} - y_j)Q_j^n\}\end{aligned}$$

where

$$\text{Area}(L_{ij}^r \cap C_j) = \frac{1}{2}\{(x_{M_{ij}} - x_j)(y_{G_{ij}} - y_j) - (x_{G_{ij}} - x_j)(y_{M_{ij}} - y_j)\}. \quad (4.24)$$

4.5. Approximation of $\int_{t^n}^{t^{n+1}} \int_{\partial L_{ij}} \{f(u)n_x + g(u)n_y\}d\sigma dt$.

This is achieved with the midpoint rule for integration with respect to time:

$$\begin{aligned}\int_{t^n}^{t^{n+1}} \int_{\partial L_{ij}} (f(u)n_x + g(u)n_y)d\sigma dt \\ \cong \Delta t \int_{\partial L_{ij}} \left\{f(u(x,y,t^{n+1/2}))n_x + g(u(x,y,t^{n+1/2}))n_y\right\}d\sigma \quad (4.25)\end{aligned}$$

where a first order Taylor expansion is used for $u(x,y,t^{n+1/2})$; using (4.1') we write

$$\begin{aligned}u(x,y,t^{n+1/2}) \cong u(x,y,t^n) - \frac{\Delta t}{2}\{f'(u(x,y,t^n))u_x(x,y,t^n) \\ + g'(u(x,y,t^n))u_y(x,y,t^n)\} \quad (4.26)\end{aligned}$$

On $L_{ij}\cap C_i$ we have chosen $u_x \equiv P_i^n$ and $u_y \equiv Q_i^n$, but we must find an approximate value of $u(x,y,t^n)$ on the line segments a_iG_{ij} and $a_iG_{i,j+1}$ (and similarly on a_jG_{ij} and $a_jG_{i,j+1}$). One possible choice consists in choosing the value of $L(x,y,t^n)$, our linear interpolant, at the midpoints of these segments; we then take, for any (x,y) on a_iG_{ij}:

$$u(x,y,t^n) \cong u_i^n + \frac{1}{2}(x_{G_{ij}} - x_i)P_i^n + \frac{1}{2}(y_{G_{ij}} - y_i)Q_i^n \equiv u_{a_i,G_{ij}}^n \quad (4.27)$$

thus defining our value $u_{a_i,G_{ij}}^n$ for the side a_iG_{ij} of L_{ij}.

In view of (4.26), we can now define an approximate average value of $u(x,y,t^{n+1/2})$ along the side a_iG_{ij} to be used in (4.25):

$$u_{a_iG_{ij}}^{n+1/2} = u_{a_i,G_{ij}}^n - \frac{\Delta t}{2}\{f'(u_{a_i,G_{ij}}^n)P_i^n + g'(u_{a_i,G_{ij}}^n)Q_i^n\}. \quad (4.28)$$

Introducing these values in (4.25), we finally get

$$\frac{1}{\Delta t}\int_{t^n}^{t^{n+1}}\int_{\partial L_{ij}}\{f(u)n_x+g(u)n_y\}d\sigma dt \tag{4.29}$$
$$\cong f(u^{n+1/2}_{a_i,G_{ij}})n^1_{ijx}\cdot|a_iG_{ij}|+f(u^{n+1/2}_{a_i,G_{i,j+1}})n^4_{ijx}\cdot|a_iG_{i,j+1}|$$
$$+f(u^{n+1/2}_{a_j,G_{ij}})n^2_{ijx}\cdot|a_jG_{ij}|+f(u^{n+1/2}_{a_j,G_{i,j+1}})n^3_{ijx}\cdot|a_jG_{i,j+1}|$$
$$+g(u^{n+1/2}_{a_i,G_{ij}})n^1_{ijy}\cdot|a_iG_{ij}|+g(u^{n+1/2}_{a_i,G_{i,j+1}})n^4_{ijy}\cdot|a_iG_{i,j+1}|$$
$$+g(u^{n+1/2}_{a_j,G_{ij}})n^2_{ijy}\cdot|a_jG_{ij}|+g(u^{n+1/2}_{a_j,G_{i,j+1}})n^3_{ijy}\cdot|a_jG_{i,j+1}|.$$

4.6. First step of the finite volume extension of the Nessyahu-Tadmor scheme.

Collecting our approximations (4.21),(4.23),(4.29) of the three terms appearing in the R.H.S. of (4.17) and taking (4.14) into account, we obtain the following approximation u^{n+1}_{ij} for the first (odd) time step of our scheme:

$$\text{Area}(L_{ij})u^{n+1}_{ij}=\text{R.H.S.}(4.21)+\text{R.H.S.}(4.23)-\Delta t\cdot\{\text{R.H.S.}(4.29)\} \tag{4.30}$$

where u^{n+1}_{ij} can be considered as a cell value for cell L_{ij} at time t^{n+1}, or as a nodal value at the midpoint M_{ij}, at time t^{n+1}.

In preparation for the second (even) time step, we now construct a piecewise linear approximation of u on the quadrilaterals L_{ij}:

$$u(x,y,t^{n+1})\cong L^{(o)}(x,y,t^{n+1})\equiv u^{n+1}_{ij}+(x-x_{M_{ij}})P^{n+1}_{ij}+(y-y_{M_{ij}})Q^{n+1}_{ij} \tag{4.31}$$

where the slopes P^{n+1}_{ij}, Q^{n+1}_{ij} can be computed as follows.

First we construct a piecewise linear approximate function defined on the triangles $T\in\mathcal{T}_h$ of the original triangulation. On triangle $T=a_ia_ja_k$, we can use for that purpose the newly obtained values u^{n+1}_{ij} at the midpoints of the sides of T. We then compute the average of the slopes of the linear interpolants in the two triangles $T,T'\in\mathcal{T}_h$ sharing a_ia_j as a common side (fig. 5.59), and use these averages in (4.31).

4.7. Second step of the finite volume Nessyahu-Tadmor scheme.

The second step is obtained by integrating (4.1') on the cylindric region $C_i\times[t^{n+1},t^{n+2}]$, using the same finite volume approach as for the first step, to define a cell average value u^{n+2}_i on cell C_i:

$$\text{Area}(C_i)u^{n+2}_i-\sum_{j\text{ neighbour of }i}\int_{L_{ij}\cap C_i}u(x,y,t^{n+1})dxdy$$

$$= -\Delta t \sum_{j \text{ neighbour of } i} \int_{\Gamma_{ij}} \{f(u(x,y,t^{n+3/2}))\nu_x + g(u(x,y,t^{n+3/2}))\nu_y\} d\sigma \quad (4.32)$$

where $u(x,y,t^{n+1})$ is approximated, on $L_{ij} \cap C_i$, by the piecewise linear interpolant (4.31). Its integral on $L_{ij} \cap C_i$ is computed as described in section 4.3.

To obtain an approximate value of $u(x,y,t^{n+3/2})$ we use a Taylor expansion with respect to time combined with (4.1'), and we subdivide the cell-boundary element Γ_{ij} into $G_{ij}M_{ij} \cup M_{ij}G_{i,j+1}$. On $G_{ij}M_{ij}$ (resp. $M_{ij}G_{i,j+1}$), $u(x,y,t)$ is then approximated by its value of the midpoint of the line segment $G_{ij}M_{ij}$ (resp. $M_{ij}G_{i,j+1}$).

4.8. Approximation of the slopes.

In order to compute the gradient (P_i^n, Q_i^n) of the piecewise linear interpolant $L(x,y,t^n)$ for the cell C_i, we must first compute the gradient of the first degree polynomials P_T for all triangles $T \in \mathcal{T}_h$ such that $a_i \in T$. Although we could then in principle directly take the average of the gradients of the polynomials P_T, obtained as described at the beginning of section 4.2, we shall consider here a least-squares technique (cf. [40]). For simplicity, we shall describe it for the case of triangular (finite volume) cells.

Let T be a triangle with centroid G, and let T_j, $j = 1,2,3$ be the neighbouring triangles, with centroids $G_j (j = 1,\ldots,3)$ (fig.5.61); assume the values of the numerical approximation of the solution u at the four points $\{G, G_j\}_{j=1}^3$ are known at time t^n, equal to u_T^n, $u_{T_j}^n$ $(j = 1,\ldots,3)$ (these values can be considered as cell values playing for the triangular cells T, T_j the same role as u_i^n, u_{ij}^n for the cells C_i, L_{ij}).

The least-squares gradient $\widetilde{(grad\ u)}_T^n = (\tilde{a}_T^n, \tilde{b}_T^n)$ for triangle T will then be chosen such as to minimize the functional

$$I = \sum_{j=1}^{3} \{u_T^n + \overrightarrow{GG_j} \cdot (grad\ u)_T^n - u_{T_j}^n\}^2 \quad (4.33)$$

where

$$(grad\ u)_T^n = (a_T^n, b_T^n)$$

The minimum is obtained when

$$\frac{\partial I}{\partial a_T^n} = \frac{\partial I}{\partial b_T^n} = 0 \quad (4.34)$$

and is shown in [40] to lead to the following least-squares gradient:

$$\tilde{a}_T^n = \frac{1}{D} \sum_{j=1}^{3} (y_{G_j} - y_G)^2 \sum_{j=1}^{3} (u_{T_j}^n - u_T^n)(x_{G_j} - x_G)$$

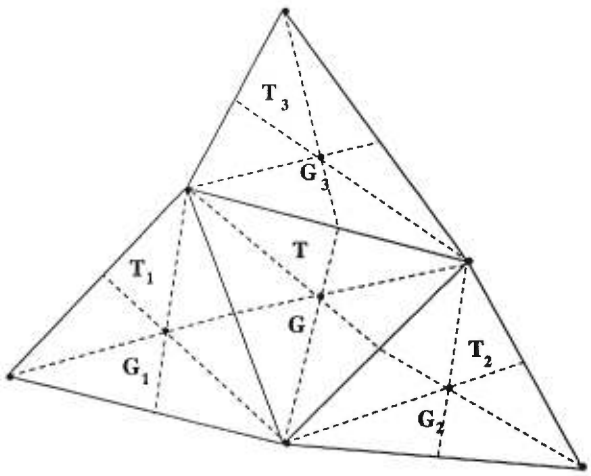

FIGURE 5.61. Computation of the least-squares gradient for a triangular cell T.

$$-\frac{1}{D}\sum_{j=1}^{3}(x_{G_j}-x_G)(y_{G_j}-y_G)\sum_{j=1}^{3}(u^n_{T_j}-u^n_T)(y_{G_j}-y_G) \quad (4.35)$$

$$\tilde{b}^n_T = \frac{1}{D}\sum_{j=1}^{3}(x_{G_j}-x_G)^2\sum_{j=1}^{3}(u^n_{T_j}-u^n_T)(y_{G_j}-y_G)$$
$$-\frac{1}{D}\sum_{j=1}^{3}(x_{G_j}-x_G)(y_{G_j}-y_G)\sum_{j=1}^{3}(u^n_{T_j}-u^n_T)(x_{G_j}-x_G) \quad (4.36)$$

where the denominator

$$D=\sum_{j=1}^{3}(x_{G_j}-x_G)^2\sum_{j=1}^{3}(y_{G_j}-y_G)^2-\left[\sum_{j=1}^{3}(x_{G_j}-x_G)(y_{G_j}-y_G)\right]^2 \quad (4.37)$$

is strictly positive for any non-degenerated triangle.

For the barycentric cells C_i or the quadrilateral cells L_{ij}, the procedure is quite similar to the one described above for triangular cells. Alternately, for a barycentric cell C_i with center a_i, we could first compute the least squares gradient grad $u|_{T_j} = (\tilde{a}^n_{T_j}, \tilde{b}^n_{T_j})$ of each neighbouring triangle T_j (such that $a_i \in T_j$), and then take the cell gradient grad $u|_{C_i}$ = average{grad $u|_{T_j}$}, with a similar procedure for a quadrilateral cell L_{ij}.

Unfortunately, this procedure does not preserve monotonicity of the data in the usual van Leer sense described below, and allows the creation of local extremas between the nodes; this phenomenon may lead to (or amplify already existing) spurious oscillations, with the associated loss of stability and convergence difficulties in the case of

steady flows. We have therefore introduced some slope limitation in the computation of the gradients.

4.8.1. Slope limitation.

To ensure the stability of the scheme and prevent the generation of oscillations in regions of strong gradients, we must perform a slope correction. Following van Leer's approach ([26], [25]), in which the value at some interface point $x_{i+1/2}$ (in the one dimensional case) must fall within the range of values spanned by the adjacent grid averages, u_{i-1} and u_{i+1}, we limit the slopes of the linear interpolant L defined by (4.12) (resp. $L^{(o)}$ defined by (4.31) to ensure that its value at the boundary points $G_{ij}, M_{ij}, G_{i,j+1}$ of ∂C_i (resp. at the vertices $a_i, a_j, G_{ij}, G_{i,j+1}$ of ∂L_{ij}) are bounded by the values at the cell center u_i^n (resp. u_{ij}^{n+1}) and the value u_j^n at the corresponding neighbouring node a_j (resp $u_{i,j-1}^{n+1}$ and $u_{i,j+1}^{n+1}$ at the adjacent quadrilateral cell"midpoints" $M_{i,j-1}$ and $M_{i,j+1}$). The limitation procedure is implemented on each cell as follows. Let

$$(grad\ u)_i = (P_i, Q_i)^T$$

denote the gradient for cell i, where $P_i \approx u_x$, $Q_i \approx u_y$ at node i. If u satisfies the van Leer requirement we choose

$$P_i^{\lim} = \min_{j \in \mathcal{N}(i)} \mathrm{mod}\ \{P_j\}$$

$$= \begin{cases} \min_{j \in \mathcal{N}(i)} |P_j| .(\text{common sign of all values } P_j) \\ \qquad\qquad \text{if all the values } P_j \ (j \in \mathcal{N}(i)) \text{ have the same sign} \\ 0 \qquad\qquad \text{otherwise} \end{cases}$$

where $\mathcal{N}(i)$ is the set of nodes j adjacent to node i. If u does not satisfy the van Leer requirement, we set $P_i^{\lim} = 0$. The computation of $Q_i^{\lim}$ is done in the same manner. For quadrilateral cells L_{ij} we proceed in a similar way.

5. Numerical Experiments

In order to assess the relative advantages of both methods , we applied them to several typical test problems; we present results for

- Euler flow around a Double-ellipse at supersonic regime.

- Supersonic flow past a blunt body at 0^o of angle of attack and $M_\infty = 2$

Both methods, which are second-order accurate and non-oscillatory thanks to the use of limiters, have been applied on the same grids, to compute the steady flows by stationarization, with the help of grid adaptation to improve the resolution. For the grid adaptation, we have used a procedure developed by M.J.Castro Diaz and F.Hecht at INRIA (France) ([37],[38]).For the finite volume method, the extension of section 4.2 to two-dimensional systems of conservation laws is achieved by the procedure described in ([46],[47],[48]).

On the whole, the finite volume version of the Nessyahu-Tadmor scheme has proved to be less time-consuming and significantly more accurate, for given grids. . The discontinuous finite element method required more computing time to reach convergence. Nevertheless, both methods seem to provide a reliable alternative to other well established schemes, and lend themselves to an extension to three-dimensional problems for unstructured grids.

Example 1 Supersonic flow past a double-ellipse at 20^o of angle of attack and $M_\infty = 2$

For this problem inspired by ([35]), but with Mach number $M_\infty = 2$ instead of the range of hypersonic Mach numbers considered there, and 20^o of angle of attack, the geometry is a double ellipse ([35]), defined by

$$\begin{cases} x \leq 0 & \begin{cases} z \leq 0 & \left(\frac{x}{0.06}\right)^2 + \left(\frac{z}{0.015}\right)^2 = 1 \\ z \geq 0 & \left(\frac{x}{0.035}\right)^2 + \left(\frac{z}{0.025}\right)^2 = 1 \end{cases} \\ 0 \leq x \leq 0.016 & \begin{cases} z \geq 0 & z = 0.025 \\ z \leq 0 & z = -0.015 \end{cases} \end{cases}$$

For this steady flow problem we used the same three grids with both methods.We present the results obtained with the initial and final grid only.

For the initial mesh (1558 vertices), both methods give fairly comparable results; notice that the C_p curves can be nearly superposed, which is an indication that both methods are indeed doing some reasonable calculation. The same is true for the pressure contours of both methods, with perhaps a very small advantage for our finite volume method (FV) which gives slightly sharper shocks.

The final grid (5055 vertices) shows a clear advantage for the FV method, which gives a nearly perfect shock resolution with very smooth contours, while the DFE method shows a serious breach of monotonicity in the lower part of the bow shock.
As was the case with the initial grid, the C_p curves can again be nearly exactly superposed.
The major difference between the two methods appears to lie in the convergence history and computing times. Fig. 5.64 shows a clear advantage for our finite volume method, for the initial grid (1558 vertices). Computing times for the initial grid (CPU : 3564 for FV and 48288 for DFE) confirm the advantage of the proposed Finite Volume Method.

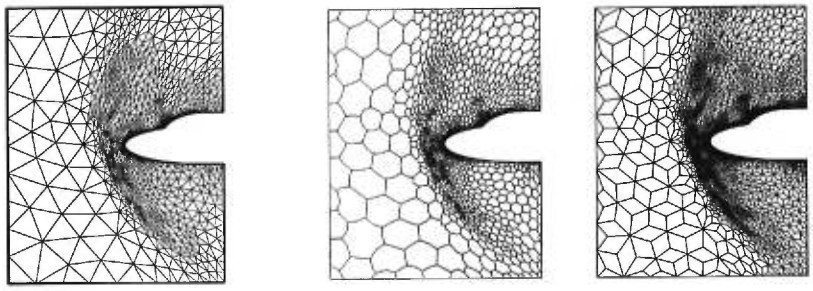

FIGURE 5.62. Euler flow around a double ellipse. Original grid, barycentric cells C_i and quadrilateral cells L_{ij}

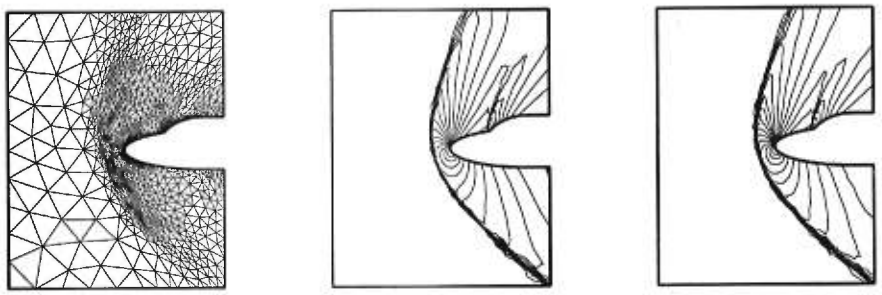

FIGURE 5.63. Double ellipse : Initial grid (1558 vertices) and solution (pressure contours) (FV, middle) and (DFE, right)

Example 2 Supersonic flow past a blunt body at 0^o of angle of attack. see ([4]).

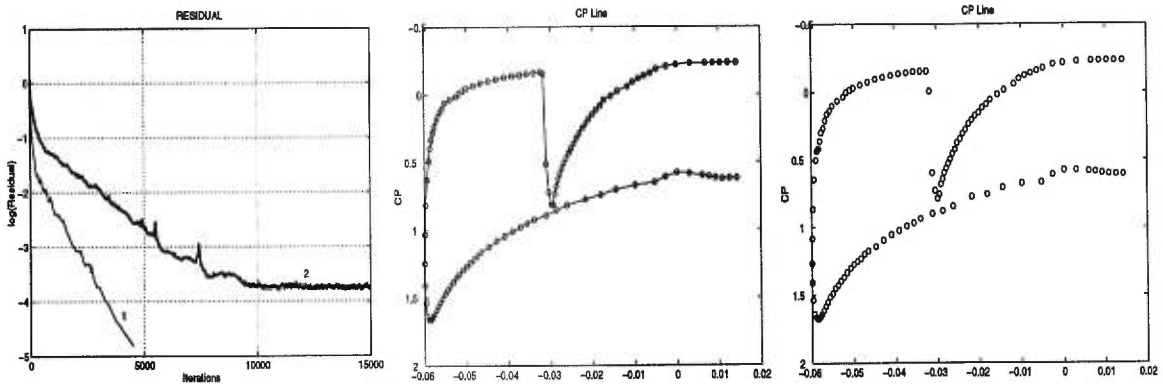

FIGURE 5.64. Residual for initial grid (1558 vertices)(1=FV,2=DFE) and C_p body cuts (FV, middle) and (DFE, right) (Double ellipse)

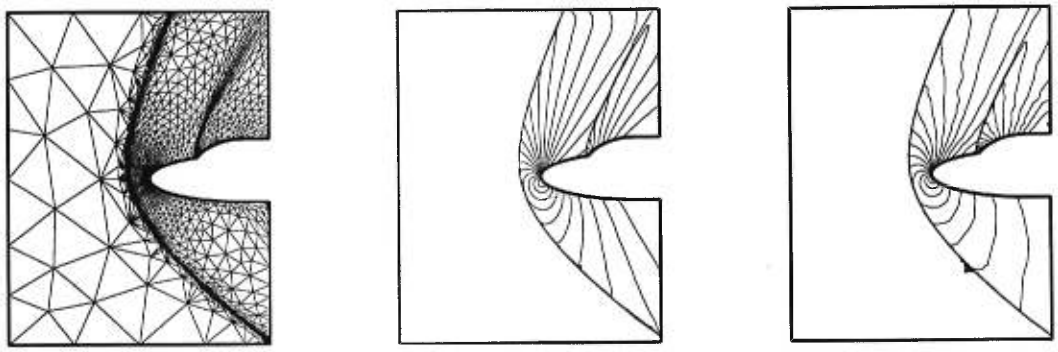

FIGURE 5.65. Double ellipse : Final grid (5055 vertices) and solution (pressure contours) (FV, middle) and (DFE, right)

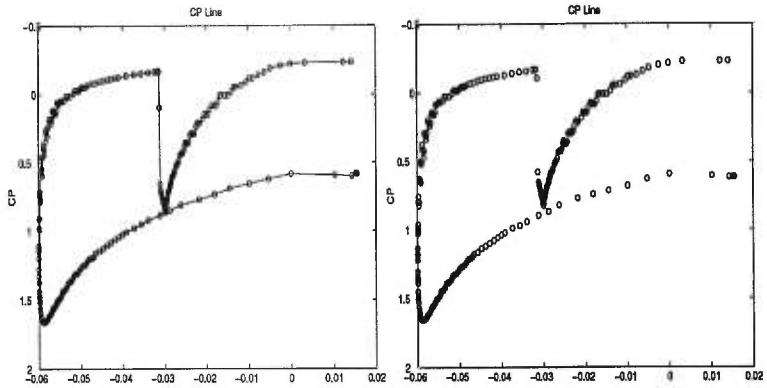

FIGURE 5.66. C_p body cuts for the final grid (5055 vertices) (FV, left) and (DFE) (Double ellipse)

This is a standard test problem which has been considered by many authors. The problem definition is borrowed from [4].The Mach number is $M_\infty = 2.0$ with an incidence $\alpha = 0^o$. The initial and final grid had 2737 and 7039 nodes, respectively. Fig.5.68 and 5.69 show the corresponding pressure contours. Our results, obtained with grid adaptation ([37],[38]), sustain comparison with other results for which grid adaptation has also been used.

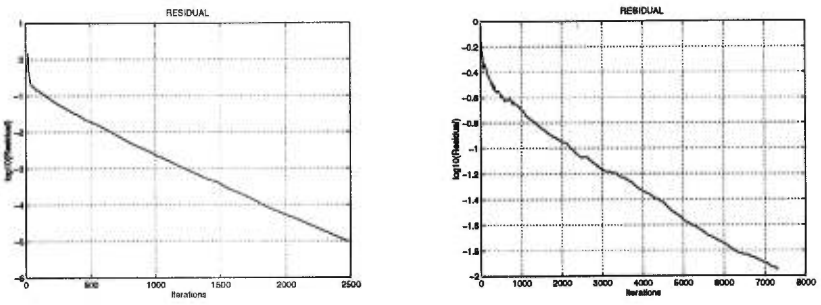

FIGURE 5.67. Convergence histories for Finite Volume scheme (left) and Discontinuous finite element method (right) (Blunt body)

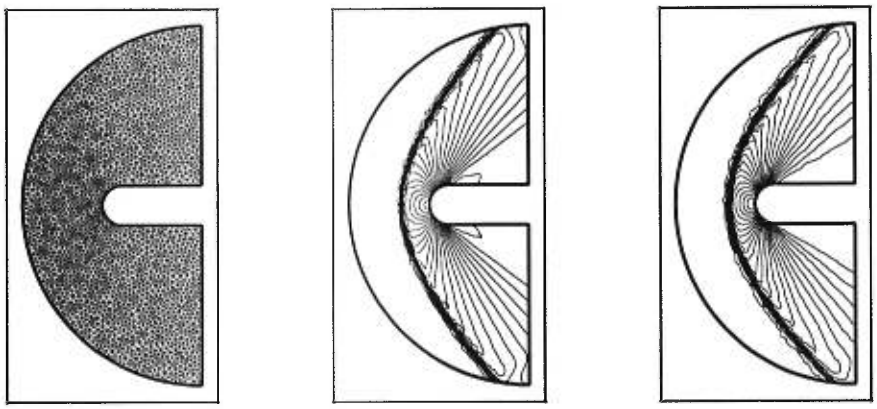

FIGURE 5.68. Initial grid and solution (pressure contours) FV (middle) and DFE (right)

Fig. 5.67 , which presents the residuals for both methods, shows a strong advantage in favour of our finite volume method, considering the results on fig.5.68 and 5.69, a fact which is confirmed by table 5.5: both the CPU-times and the speed of convergence are substantially better.

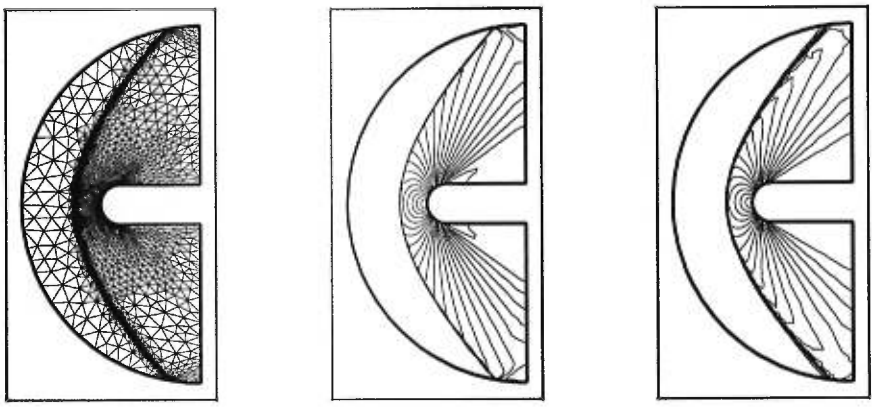

FIGURE 5.69. Final grid and solution (pressure contours) FV (middle) and DFE (right)

Method	CPU	nodes	elements	Solution
F.V	2701	2737	5244	without adaptation
D.F.E.M	11700	2737	5244	without adaptation
F.V	16905	7039	13801	with adaptation
D.F.E.M	46886	7039	13801	with adaptation

TABLE 5.5. Characteristics of F.V and D.F.E.M (Initial and Final Grids, Blunt Body)

This test case displays the robustness and the accuracy of the finite volume method, given the fact that the discontinuous finite element method is already an excellent and well established method.

Concluding remarks

The examples presented here suggest that the finite volume method proposed by the authors is capable of a very high resolution, with a clear advantage, as compared with the discontinuous finite element method studied here, at least at the level of the convergence histories, computing times, smoothness of the pressure contours, and monotonicity enforcement.

We are presently adapting the finite volume method to a mixed finite volume/Galerkin finite element method for the Navier-Stokes equations ([49]) where the convective part of the Navier-Stokes equations are treated with the finite volume method presented here while the diffusive term will be handled by a finite element method.

In another paper ([50],[51]) we consider the particular case of the linear equation $u_t + div(u\vec{V}) = 0$ where $\vec{V} = (V_1(x,y), V_2(x,y))^T$ with $div\,\vec{V} = 0$; we obtain an L^∞ bound for the numerical solution, from which we deduct the existence of a subsequence $\{u_{\mathcal{T}_k,\Delta t_k}\}$ which converges weakly to some function u in $L^\infty(\mathbb{R}^2 \times \mathbb{R}^+)$-weak. Using another set of inequalities, we obtain a total variation-type bound, slightly weaker than a classical bound on the total variation of the numerical solution, called a bound on the "weighted total variation", from which we are then able to show that the above weak limit function u is indeed a weak solution of $u_t + div(u\vec{V}) = 0$.

Références

[1] P. ARMINJON ET M.C. VIALLON , Généralisation du schéma de Nessyahu-Tadmor pour une équation hyperbolique à deux dimensions d'espace, Comptes Rendus de l'Acad. des Sciences, Paris, t.320, série I , 85-88, January 1995.

[2] P. ARMINJON, M.C. VIALLON, A. MADRANE , From Lax-Friedrichs to a Multidimensional Finite Volume Extension of the Nessyahu-Tadmor Scheme for Compressible Flows, Proc. Int. Conf. on Numerical Meth. for the Euler and Navier-Stokes Equations. Centre de Rech.Math. Univ de Montréal, P.Arminjon and A.Dervieux, editors, september 1995, to appear in the Am.Math.Soc-CRM series.

[3] P. ARMINJON, M.C. VIALLON AND A. MADRANE (1997), A Finite Volume Extension of the Lax-Friedrichs and Nessyahu-Tadmor Schemes for Conservation Laws on Unstructured Grids, Int.J. Comp.Fluid Dynamics, in press.

[4] P.ARMINJON, D.STANESCU AND M.C. VIALLON , A two-dimensional finite volume extension of the Lax-Friedrichs and Nessyahu-Tadmor schemes for compressible flows, Proc. of the 6 th.Int.Symp. on Comp. Fluid Dynamics, Lake Tahoe (Nevada), September 4-8,1995, M. Hafez and K.Oshima, editors,vol.4.

[5] H. NESSYAHU AND E. TADMOR , Non-oscillatory Central Differencing for Hyperbolic Conservation Laws, J. Comp. Physics 87, No. 2, 408–463, 1990.

[6] G.D.V GOWDA AND J.JAFFRÉ , A discontinuous finite element method for non linear scalar conservation laws, INRIA Res. Rep. No. 1848, Rocquencourt,78153 Le Chesnay, France, 1993.

[7] W. REED AND T. HILL, Triangular mesh methods for the neutron transport equation, Tech.Rep. LA-UR-73-479, Los Alamos Scientific Laboratory, 1973.

[8] P. LESAINT AND P. RAVIART, On a finite element method for solving the neutron transport equations, in Mathematical Aspects of Finite Elements in Partial Differential Equations, Academic Press, New York, 1974.

[9] P.JAMET AND R.BONNEROT, Numerical solution of the Eulerian equations of compressible flow by a finite element method which follows the free boundary and the interfaces, J. Comput. Phys., 18, 21-45, 1975.

[10] J.T.ODEN , Mathematical Aspect of Finite Element Approximations in Theoretical Mechanics, in Nemat-Nasser, Ed., Mechanics Today, Vol II, Pergamon Press, Oxford, pp. 159-250, 1975.

[11] T.J.R. HUGHES ET AL., A new finite element formulation for computational fluid dynamics 1,2,3,4, Computer Methods in Applied Mechanics and Engineering, 54 (1986), pp. 223-234 and 341-355 and 58,(1986), pp.305-336.

[12] P.ARMINJON AND A.ROUSSEAU, Discontinuous finite elements and Godunov-type methods for the Eulerian equations of gas dynamics. Comput.Meths.Appl.Mech.Engrg., 49, pp.17-36, 1985.

[13] P.ARMINJON, Finite element analysis of moving loads on a floating ice sheet, in Topics in Numerical Analysis III, Proc.Royal Irish Acad. Conf. on Num. Anal., 1976, J.J.H.Miller, editor, Academic Press, 1977.

[14] G. CHAVENT AND G. SALZANO, A finite element method for the 1-D water flooding problem with gravity, J. Comp. Phys., 45, pp. 1-21, 1982.

[15] G. CHAVENT, G. COHEN, AND J. JAFFRÉ, Discontinuous upwinding and mixed finite elements for two-phase flow in reservoir simulation. Comp. Meth. Appl. Mech. Eng., 47 , pp. 93-118, 1984.

[16] G. CHAVENT, B. COCKBURN, G. COHEN, AND J. JAFFRÉ, A discontinuous finite element method for nonlinear hyperbolic equations, in Innovative Numerical Methods in Engineering, R.P.Schaw, J.Periaux, A.Chaudouet, J.Wu, C.Marino and C.A. Bredia, Eds, Berlin, 1986.

[17] G. CHAVENT AND J. JAFFRÉ, Mathematical Models and Finite Elements for Reservoir Simulation, North Holland, Amsterdam, 1986.

[18] G. CHAVENT, J. JAFFRÉ, R. EYMARD, D. GUÉRILLOT AND L. WEILL, Discontinuous and mixed finite elements for two-phase incompressible flow, SPE Reservoir Engineering, 5 , pp. 567-575, 1990.

[19] C. JOHNSON AND J.PITKARANTA, An analysis of the discontinuous Galerkin method for a scalar hyperbolic equation, Math. Comp., 46 , pp. 1-26, 1986.

[20] G. RICHTER, An optimal order error estimate for the discontinuous Galerkin method, Math. Comp., 50 , pp. 75-88, 1988.

[21] J.J.QUIRK, A Contribution to the Great Riemann Solver Debate, NASA-ICASE Rep. No. 92-64, Nov. 1992, and Int.J.Num.Meth.Fluids,Vol.18, pp.555-574, 1994.

[22] P.WOODWARD AND P.COLELLA, The Numerical Simulation of Two-Dimensional Fluid Flow with Strong Shocks, J.Comp.Phys.54,p.115-173, 1984.

[23] J. JAFFRÉ AND L. KADDOURI, Discontinuous finite elements for the Euler equations, Proc. Third Int. Conf. Hyperbolic Problems, Uppsala 1990, B.Engquist and B.Gustafsson, Eds. Studentlitteratur (Lund,Sweden)- Chartwell-Bratt (Bromley, England), Vol.III, pp.602-610.

[24] F. DUBOIS AND G. MEHLMAN, A non-parameterized Entropy Correction for Roe's Approximate Riemann Solver, rapport CMAP-Ecole Polytechnique, n^o 248, 1991; see also Proc. 10th AIAA CFD Conf., Honolulu, June 1991, and AIAA Journal.

[25] G.D.V. GOWDA, Discontinuous finite elements for nonlinear scalar conservation laws, Thèse de Doctorat, Université Paris IX-Dauphine, 1988.

[26] B.V. LEER, Towards the ultimate conservative difference scheme: IV. A new approach to numerical convection,J.Comput.Physics,23,276–299,1977.

[27] C. HIRSCH, Numerical Computation of Internal and External Flows, Vol.2 : Computational Methods for Inviscid and Viscous Flows, Wiley Series in Numerical Methods in Engineering, J. Wiley & Sons, 1990.

[28] P.L. ROE , Approximate Riemann solvers, parameter vectors, and difference schemes, J. Comp. Phys. 43, 357–372, 1981.

[29] A. HARTEN,P.D. LAX AND B. V. LEER, On Upstream Differencing and Godunov Type Schemes for Hyperbolic Conservation Laws, SIAM Review, 25(1), 35–61, 1983.

[30] E.GODLEWSKI AND P.A.RAVIART , Hyperbolic Systems of Conservation Laws. Soc.Math. Appl.Ind., Ellipses, Paris, 1990.

[31] S. OSHER AND F. SOLOMON, Upwind difference schemes for hyperbolic systems of conservation laws, Math. Comp, 38, 339–374, 1982.

[32] A. HARTEN AND J.M. HYMAN, Self-Adjusting Grid Methods for One-Dimensional Hyperbolic Conservation Laws, J. Comput. Physics, 50, 235–269, 1983.

[33] HARTEN A., High resolution schemes for hyperbolic conservation laws, J. Comp Phys., 49, pp. 357-393, 1983.

[34] D.W.LEVY, K.G.POWELL AND B.VAN LEER, An implementation of a grid independent upwind scheme for the Euler equations, AIAA paper, 89-1931, 1989.

[35] INRIA and GAMNI-SMAI , Workshop on hypersonic flows for reentry problems, Problem 6 : Flow over a double ellipse, test case 6.1 : Non-Reactive Flows. Antibes, France, January 22-25, 1990.

[36] J.PERAIRE, M.VAHDATI, K.MORGAN AND O.C.ZIENKIEWICZ , Adaptative Remeshing for Compressible Flow Computations, J.Comp.Phys.72,449-466,1987.

[37] M.J.CASTRO DIAZ AND F.HECHT, Anisotropic Surface Mesh Generation, INRIA Res. Rep. No. 2672, October 1995, INRIA, Rocquencourt, 78153 Le Chesnay, France.

[38] M.J.CASTRO DIAZ, Mesh Refinement over Triangulated Surfaces, INRIA Res. Rep. No. 2462, June 1994, INRIA, Rocquencourt, 78153 Le Chesnay, France.

[39] F. FEZOUI , Résolution des équations d'Euler par un schéma de van Leer en élément finis. Res.Rep. INRIA No. 358, Rocquencourt, 78153 Le Chesnay, France, 1985.

[40] S. CHAMPIER , Convergence de schémas numériques type Volumes Finis pour la résolution d'équations hyperboliques. Thèse, Univ. de St-Etienne, 1992.

[41] B. VAN LEER , Towards the Ultimate Conservative Difference Scheme.II. Monotonicity and conservation combined in a second order scheme,J. Comp. Phys., Vol.14, 361–370, 1974.

[42] R.EYMARD AND T.GALLOUËT, Convergence d'un schéma de type éléments finis-volumes finis pour un système d'une équation elliptique et d'une équation hyperbolique, M^2AN , Vol.27 , No.7, 843-861, 1993.

[43] S. OSHER, Riemann solvers, the entropy condition and difference approximations, SIAM J.Num.Analysis, 21, 217-235, 1984

[44] P.L.ROE, Some contributions to the modelling of discontinuous flows, in Lectures in Applied Mathematics, vol.22, pp.163-193, (B.Engquist, S.Osher and R.C.J.Somerville, Editors), SIAM, Philadelphia, 1985.

[45] P.L.ROE AND J.PIKE, Efficient construction and utilisation of approximate Riemann solutions, in Computing Meth. in Appl.Sciences and Engineering, VI (R.Glowinski and J.L.Lions, Editors) North-Holland (1984), pp. 499-518.

[46] F.ANGRAND, A. DERVIEUX, L. LOTH AND G. VIJAYASUNDARAM , Simulations of Euler transonic flows by means of explicit finite-element type schemes, INRIA Res. Rep. No. 250, Rocquencourt, 78153 Le Chesnay, France, 1983.

[47] F. ANGRAND AND A. DERVIEUX , Some explicit triangular finite element schemes for the Euler equations, Int. J. Num. Meth. in Fluids, Vol. 4, 749–764, 1984.

[48] P. ARMINJON AND A. DERVIEUX , Construction of TVD-like Artificial Viscosities on Two-Dimensional Arbitrary FEM Grids, J. Comp. Phys., 106, No.1, 176–198, 1993.

[49] F.BEUX, S.LANTERI, A.DERVIEUX AND B.LARROUTUROU, Upwind stabilization of Navier-Stokes solvers, INRIA Res.Rep.No. 1885, Rocquencourt, 78153 Le Chesnay, France, 1993.

[50] M.C. VIALLON ET P. ARMINJON , Convergence du schéma de Nessyahu-Tadmor sur des maillages non structurés pour une équation hyperbolique linéaire bidimensionnelle, Rapport de recherche No. C.N.R.S. U.R.A. 740, Équipe d'Analyse Numérique, Universités de Lyon et Saint-Étienne, septembre 1994.

[51] M.C. VIALLON AND P. ARMINJON, Convergence of a finite volume extension of the Nessyahu-Tadmor scheme on unstructured grids for a two-dimensional linear hyperbolic equation, Rapport de recherche, No. 2239, Centre de Recherches mathématiques, Université de Montréal, january 1995, to appear in SIAM J.Num.Anal.

6. APPENDIX

Solution of the projection problem for the slope limitation

The slope limitation process consists in solving a series of local minimization problems of dimension $nv(K) = 3$, with two constraints.

In this appendix we will show how these minimization problems can be solved; we follow the description given in [6] for the scalar case.

For $w = \rho,\ u,\ v,\ p$: we denote by

- P_K, the plane with equation

$$\sum_{i=1}^{3} X_i = 3\overline{w}_K^\star = w_{K,A_1} + w_{K,A_2} + w_{K,A_3}$$

- Q_K, the cube

$$\prod_{i=1}^{3} [wmin(A_i), wmax(A_i)] \quad \text{with} \quad \begin{cases} wmin(A_i) &= (1-\alpha)\overline{w}_K^\star + \alpha w_{min}(A_i) \\ wmax(A_i) &= (1-\alpha)\overline{w}_K^\star + \alpha w_{max}(A_i) \end{cases}$$

where $w_{min}(A_i), w_{max}(A_i)$ are defined by (3.4).

For $0 \leq \alpha \leq 1$, $\overline{w}_K^\star$ satisfies the inequalities

$$wmin(A_i) \leq \overline{w}_K^\star \leq wmax(A_i)\ ,\ i = 1, \ldots, 3 \tag{6.1}$$

- $J(X) = \frac{1}{2}\|X - w_K^\star\|^2$ where $w_K^\star = (w_{K,A_i})_{i=1,\ldots,3}$
- $V = \begin{pmatrix} 1 \\ 1 \\ 1 \end{pmatrix}$ is a vector normal to P_K

With these notations, the computation of w_K^{n+1} amounts to the following minimization problem:

$$\begin{cases} \text{Find } w_K^{n+1} \in P_K \cap Q_K \quad \text{such that} \\ \\ J(w_K^{n+1}) = \min\limits_{X \in P_K \cap Q_K} J(X) \end{cases} \tag{6.2}$$

This is a convex minimization problem which has a unique solution since $P_K \cap Q_K \neq \emptyset$ (the point $X = (X_i)_{i=1,\dots,3}$ with $X_i = \bar{w}_K^\star, i = 1, \dots, 3$, belongs to $P_K \cap Q_K$ by (6.1)) .

In order to solve the minimization problem (6.2), we dualize the constraint $X \in P_K$.

We introduce the Lagrangian L defined in $\mathbf{R}^3 \times \mathbf{R}$ by

$$L(X, \mu) = J(X) + \mu \left\{ \left(\sum_{i=1}^{3} X_i \right) - 3\overline{w}_K^\star \right\} \tag{6.3}$$

Problem (6.2) is then equivalent to the following associated saddle point problem:

$$\begin{cases} \text{Find the saddle point } (w_K^{n+1}, \lambda) \in Q_K \times \mathbf{R} \text{ such that} \\ \\ L(w_K^{n+1}, \lambda) = \min\limits_{X \in P_K} \max\limits_{\mu \in \mathbb{R}} L(X, \mu) = \max\limits_{\mu \in \mathbf{R}} \min\limits_{X \in P_K} L(X, \mu) \end{cases} \tag{6.4}$$

To solve problem (6.4), we first solve, for any given $\mu \in \mathbf{R}$, the minimization problem

$$\begin{cases} \text{Find } \widehat{X}(\mu) \in Q_K \quad \text{such that} \\ \\ L(\widehat{X}(\mu), \mu) = \min\limits_{X \in Q_K} L(X, \mu) \end{cases} \tag{6.5}$$

We observe that $w_K^\star = (w_{K,A_i})_{i=1,\dots,3} \in P_K$, so that $< V, w_K^\star >= 3\overline{w}_K^\star$.

The Lagrangian can therefore be written as

$$L(X, \mu) = \frac{1}{2} \{ \| X - w_K^\star \|^2 + 2\mu < V, X - w_K^\star > \}$$

or

$$L(X, \mu) = \frac{1}{2} \| X - (w_K^\star - \mu V) \|^2 - \frac{\mu^2}{2} \| V \|^2 \tag{6.6}$$

The minimization problem (6.5) is thus equivalent to minimizing the distance between $w_K^\star - \mu V$ and the cube Q_K; the solution $\widehat{X}(\mu)$ is therefore given by the projection of $w_K^\star - \mu V$ on Q_K : $\widehat{X}(\mu) = \text{Proj}_{(Q_K)} (w_K^\star - \mu V)$.

$\widehat{X}(\mu)$ can be obtained by truncation of the components of $w_K^\star - \mu V$:

$$\begin{cases} \text{if } \; w_{K,A_i}^\star - \mu \in [wmin(A_i), wmax(A_i)] & \text{then } \; \left(\widehat{X}(\mu) \right)_i = w_{K,A_i}^\star - \mu \\ \\ \text{if } \; w_{K,A_i}^\star - \mu > wmax(A_i) & \text{then } \; \left(\widehat{X}(\mu) \right)_i = wmax(A_i) \\ \\ \text{if } \; w_{K,A_i}^\star - \mu < wmin(A_i) & \text{then } \; \left(\widehat{X}(\mu) \right)_i = wmin(A_i) \end{cases} \tag{6.7}$$

To complete the solution of problem (6.4), we must now find the real number λ which maximizes the real function

$$\mu \longmapsto F(\mu) = L\left(\widehat{X}(\mu), \mu\right)$$

The desired limited vector $w_K^{n+1} = (w_{K,A_i}^{n+1})_{i=1,\dots,3}$ will then be given by

$$w_K^{n+1} = \widehat{X}(\lambda) \quad \text{where} \quad \lambda \quad \text{yields} \quad \max_{\mu \in \mathbf{R}} F(\mu)$$

To find the maximum of F, let us write its first and second derivatives:

$$F'(\mu) = < V, \widehat{X}(\mu) - w_K^\star > = \sum_{i=1}^{3} \left(\widehat{X_i}(\mu) - w_{K,A_i}^\star\right)$$

$$F''(\mu) = \sum_{i=1}^{3} \widehat{X_i}'(\mu)$$

where $\widehat{X}(\mu)$ is given by (6.7), so that

$$\begin{cases} \text{if} \quad w_{K,A_i}^\star - \mu \in [wmin(A_i), wmax(A_i)] \,, \quad \text{then} \quad \widehat{X}'(\mu) = -1 \\ \text{otherwise,} \quad \widehat{X}'(\mu) = 0 \,. \end{cases}$$

We therefore get

$$F''(\mu) = -\text{ card } \left\{ i \in \{0, 1, \dots, 3\} / w_{K,A_i}^\star - \mu \in [wmin(A_i), wmax(A_i)] \right\} \leq 0 \,.$$

F is thus a continuous and differentiable, piecewise quadratic concave function.

F'' has $2 \times 3 = 6$ points of discontinuity which arise when $\widehat{X}(\mu)$ crosses a face of the cube Q_K.

The function F is therefore unambiguously defined and readily available, so that one can easily find the value λ for which is attains its maximum.

Fig.5.70 shows how the duality method works in the case of the slope limitation of a variable w in the one-dimensional case ($nv(K) = 2$).

Conclusion

The limitation process, for the slopes of the physical variables, reduces to the maximization, for each element K of the grid, of a piecewise quadratic function of one real variable, which is differentiable and easy to calculate; as the limitation is only active in the neighborhood of strong gradients or fronts of the vector of physical variables, it turns out to be a simple, relatively inexpensive part of the Jaffré-Kaddouri-Gowda discontinuous finite element method.

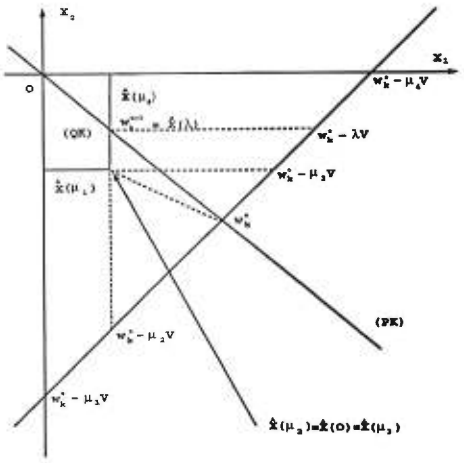

FIGURE 5.70. Determination of w_K^{n+1} by the duality method in the one-dimensional case ($nv(K) = 2$)

Chapitre 6

A staggered Lax-Friedrichs-type mixed finite volume/finite element method for the simulation of viscous compressible flows on unstructured triangular grids

by

Paul ARMINJON† and Aziz MADRANE†

†Dép. de mathématiques et de statistique, Université de Montréal

C.P. 6128, Succ. centre-ville, Montréal, Québec, Canada, H3C 3J7

ABSTRACT

To solve flow problems associated with the Navier-Stokes equations, we construct a mixed finite volume/finite element method for the spatial approximation of the convective and diffusive parts of the flux, respectively. The finite volume component of the method is adapted from the authors' construction ([1],[2],[3],[4]), for hyperbolic conservation laws and rectangular or unstructured triangular grids, of 2-dimensional finite volume extensions of the Lax-Friedrichs and Nessyahu-Tadmor central difference schemes, in which the resolution of Riemann problems at cell interfaces is by-passed thanks to the use of the Lax-Friedrichs scheme on two specific staggered grids. MUSCL-type piecewise linear cell interpolants, slope limiters and a 2-step predictor corrector time discretization lead to an oscillation-free quasi second order resolution.

For the viscous terms we use a centred finite element approximation inspired by Rostand-Stoufflet ([15],[16]); for applications to problems in aerodynamics using this approach, see ([17],[19]).

In this paper, we consider flows with relatively low Reynolds numbers, so that we do not have to resort to the limiters introduced in our finite volume method. However, to improve the quality of the resolution, we use a grid adaptation algorithm recently proposed by Castro Diaz and Hecht ([28],[29]).

Numerical experiments on classical test problems (supersonic viscous flow over a flat plate, supersonic viscous flow around a NACA 0012 airfoil, supersonic viscous flows around an ellipse, and a HERMES-type double ellipse), including comparison with other methods, lead to fairly competitive results with favourable computing times, very sharp capture of shocks and boundary layers, and accurate simulation of the boundary layer detachment.

1. Introduction. Mathematical modelling

1.1. Introduction.

In recent papers ([1],[2],[4]), we have presented, for the scalar conservation equation

$$u_t + f(u)_x + g(u)_y = 0$$

and for hyperbolic systems of conservation laws

$$U_t + f(U)_x + g(U)_y = 0$$

a two-step, two dimensional finite volume method inspired by the principle of using the Lax-Friedrichs scheme on two staggered grids at alternate time steps in order to by-pass the detailed computation of the solution of the Riemann problems generated by the method at the cell interfaces. In one space dimension, this approach, which had been already considered by van Leer, on the occasion of his work for the papers [22] and [23], but not implemented in actual computations, had been applied by several authors [12],[13] and, in a particulary efficient and elegant way, by Nessyahu and Tadmor [18], who constructed a non-oscillatory central differencing scheme resting on

this principle and on van Leer's [23],[24] MUSCL piecewise linear cellwise interpolation with appropriate limiters, to obtain oscillation free, quasi-second order resolution away from shocks and strong gradients.

In [3], we have presented finite volume extensions of the Lax-Friedrichs and Nessyahu-Tadmor (NT) (one-dimensional) difference schemes to two-dimensional rectangular grids, with several very convincing numerical applications, while in ([2], [1],[4]), [6], [5], as well as at the 5^{th} International Conference on Hyperbolic Problems (The University at Stony Brook, N.Y., June 13-17, 1994), we had presented a high resolution finite volume method of Lax-Friedrichs type, generalizing the NT 1-dimensional scheme to unstructured two-dimensional triangular grids. Comparisons with other methods [2] including a systematic comparison [5],[6] with the now well established discontinuous finite element method proposed by Jaffré et al. [20],[21] showed the high level of competitivity of our new method.

Let us mention here that our finite volume method for triangular grids was first presented at the Stony Brook Conference on Hyperbolic Problems , but did not appear in the Proceedings for technical reasons.

In this paper, we show how our method can be extended and built into an efficient solver for the Navier-Stokes equations. For that purpose, we have chosen the approach of a mixed Galerkin-type finite volume/finite element method on unstructured triangular grids inspired by Rostand and Stoufflet ([15],[16], see also [17],[19]), in which the convective and viscous parts of the Navier-Stokes equations are treated with different techniques: starting from a general Galerkin formulation, we compute the convective terms with the help of our finite volume method ([1],[2],[3]) while the viscous terms are handled with a centred finite element procedure proposed by Rostand and Stoufflet [15] (see also [17]).

The purpose of this paper is to describe our mixed method and apply it to several typical test problems associated with non-turbulent compressible flows past aerodynamic bodies. In the numerical experiments presented in this paper we only consider steady flows, approximated by the usual time-marching approach with an explicit Euler time discretization.

The presentation of the paper is as follows:

1.2. Mathematical modelling.

In the sequel, we consider domains of computation related to external flows around bodies; in fig.6.71, the body is represented as a double ellipse which limits the domain of computation by its wall Γ_B.

Let $\Omega \subset \mathbb{R}^2$ be the flow domain of interest and Γ be its boundary, we write $\Gamma = \Gamma_B \cup \Gamma_\infty \cup \Gamma_E$, where Γ_B denotes that part of the body boundary which is relevant for the computational domain (fig.6.71).

Γ_∞ is the (upwind) farfield boundary, and $\Gamma_E = \Gamma_E^1 \cup \Gamma_E^2$ is the (downwind) exit part of the boundary (labelled Γ_S on fig.6.71).

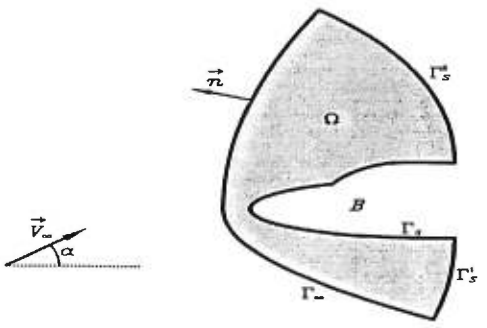

FIGURE 6.71. Boundary of the computational domain

The equations describing two-dimensional compressible viscous flows are the Navier-Stokes equations, written here in their dimensionless form [14], given by

$$\frac{\partial U}{\partial t} + \vec{\nabla} \cdot \vec{\mathcal{F}}(U) = \frac{1}{R_e} \vec{\nabla} \cdot \vec{\mathcal{R}}(U) \tag{1.1}$$

where

$$U = (\rho, \rho u, \rho v, E)^T, \ \vec{\nabla} = \left(\frac{\partial}{\partial x}, \frac{\partial}{\partial y}\right)^T, \ \vec{\mathcal{F}}(U) = \begin{pmatrix} F(U) \\ G(U) \end{pmatrix}, \ \vec{\mathcal{R}}(U) = \begin{pmatrix} R(U) \\ S(U) \end{pmatrix}. \tag{1.2}$$

The convective fluxes are given by

$$F(U) = \begin{pmatrix} \rho u \\ \rho u^2 + p \\ \rho uv \\ u(E+p) \end{pmatrix} \quad , \quad G(U) = \begin{pmatrix} \rho v \\ \rho uv \\ \rho v^2 + p \\ v(E+p) \end{pmatrix} \tag{1.3}$$

and the diffusive fluxes are defined by

$$R(U) = \begin{pmatrix} 0 \\ \tau_{xx} \\ \tau_{xy} \\ u\tau_{xx} + v\tau_{xy} + \frac{\gamma k}{Pr}\frac{\partial \epsilon}{\partial x} \end{pmatrix} \quad , \quad S(U) = \begin{pmatrix} 0 \\ \tau_{xy} \\ \tau_{yy} \\ u\tau_{xy} + v\tau_{yy} + \frac{\gamma k}{Pr}\frac{\partial \epsilon}{\partial y} \end{pmatrix} \tag{1.4}$$

where ρ is the density, $\vec{V} = (u, v)$ is the velocity vector , $E = \rho e = \rho\epsilon + \frac{1}{2}\rho(u^2 + v^2)$ is the total energy per unit volume; p is the pressure of the fluid, with the equation of state written, for a perfect gas, as :

$$p = (\gamma - 1)\rho\epsilon = (\gamma - 1)\rho(e - \frac{1}{2}\|\vec{V}\|^2) \tag{1.5}$$

γ is the ratio of specific heats ($\gamma = 1.4$ for air) ; ϵ denotes the specific internal energy related to the temperature by :

$$\epsilon = C_v T = e - \frac{1}{2}(\|\vec{V}\|^2) \tag{1.6}$$

In the expression for the diffusive fluxes, τ_{xx} , τ_{xy} and τ_{yy} are the components of Cauchy's viscous shear stress tensor, given by :

$$\tau_{xx} = \frac{2}{3}\left(2\frac{\partial u}{\partial x} - \frac{\partial v}{\partial y}\right) \quad , \quad \tau_{yy} = \frac{2}{3}\left(2\frac{\partial v}{\partial y} - \frac{\partial u}{\partial x}\right) \quad , \quad \tau_{xy} = \left(\frac{\partial u}{\partial y} + \frac{\partial v}{\partial x}\right) \tag{1.7}$$

Finally $R_e = \frac{\rho_o V_o L_o}{\mu}$ and $Pr = \frac{\mu_o C_p}{k_o}$ are the Reynolds and Prandtl (dimensionless) numbers, respectively, where the subscript o stands for some appropriate reference quantities.

1.3. Boundary conditions.

The flow is assumed to be uniform at the farfield boundary Γ_∞ and we impose

$$\rho_\infty = 1, \quad \overrightarrow{V}_\infty = \begin{pmatrix} cos\alpha \\ sin\alpha \end{pmatrix}, \quad p_\infty = \frac{1}{\gamma M_\infty^2} \tag{1.8}$$

which implies

$$T_\infty = \frac{1}{\gamma(\gamma-1)M_\infty^2} \tag{1.9}$$

where α is the angle of attack and M_∞ denotes the free-stream Mach number.On the wall boundary Γ_B, we assume the no-slip condition together with an inhomogeneous Dirichlet condition on the temperature (isothermal wall):

$$\overrightarrow{V}_{|\Gamma_B} = \begin{pmatrix} u \\ v \end{pmatrix} = \overrightarrow{0} \quad , \quad T_{|\Gamma_B} = T_B = \left(1 + \frac{\gamma-1}{2} M_\infty^2\right) T_\infty \tag{1.10}$$

while the density is free of any condition (determined by the continuity equation); these conditions are enforced with the help of a strong formulation : for a vertex $a_i \in \Gamma_B$, ρ_i is computed by equalling to zero the mass flux through the cell boundary element $\partial C_i \cap \Gamma_B$, and we then impose $\overrightarrow{V}_i = \overrightarrow{0}$ and $T_i = T_B$.

The total energy per unit of volume and the pressure on the wall are then given by :

$$e = C_v T_B \qquad , \quad p = (\gamma-1)e\rho \tag{1.11}$$

2. Discretization with respect to space and time

2.1. Definitions.

Assuming that the computational domain Ω_h is polygonal and bounded in $\mathbb{R}^2$, we start from an arbitrary FEM triangular grid $\mathcal{T}_h$ with the property that the intersection of two triangles is either empty or consists of one common vertex or side.

As mentioned in the introduction, the discretization of the convective terms is performed with the help of our two-step finite volume method of Lax-Friedrichs type (see

[1],[2],[6] for a detailed description) inspired by the one-dimensional difference scheme of Nessyahu and Tadmor [18].

The method is a two-step scheme defined with the help of two alternate, staggered grids; for the first grid, the nodes are the vertices $a_i \quad 1 \leq i \leq nv$ of the triangles $K \in \mathcal{T}_h$, and the finite volume cells are the barycentric cells C_i obtained by joining the midpoints m_{ij} of the sides originating at node a_i to the centroids G_{ij} of the triangles of $\mathcal{T}_h$ which meet at a_i (fig.6.72). For the second grid the nodes are the midpoints m_{ij} of the sides, while the cells are the quadrilaterals $L_{ij} = a_i G_{ij} a_j G_{i,j+1}$ ("diamond cells") obtained by joining two nodes a_i , a_j to the centroids of the two triangles of $\mathcal{T}_h$ of which $a_i a_j$ is a side. Let $U_i^n \cong U(a_i, t^n)$ and $U_{ij}^{n+1} \cong U(m_{ij}, t^{n+1})$ denote the nodal (or cell

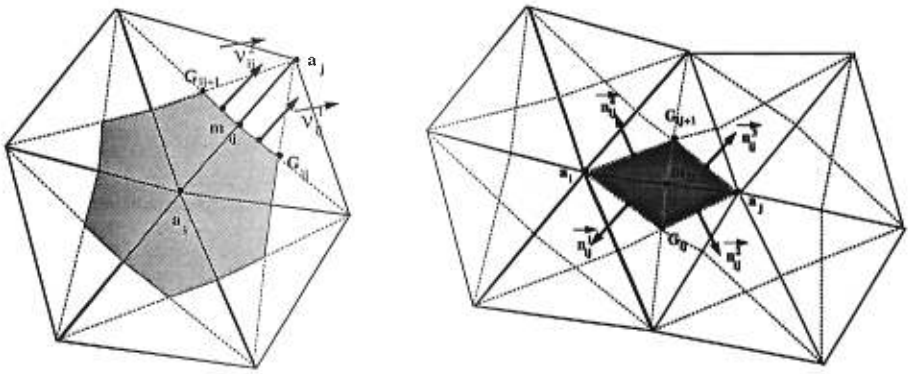

FIGURE 6.72. Barycentric cell C_i around node a_i and quadrilateral cell $a_i G_{ij} a_j G_{i,j+1}$.

average) values in the first and second grid at time $t = t^n$ and $t = t^{n+1}$, respectively (n even).

For the barycentric cell C_i, let $\vec{\nu}_{ij}^1$ and $\vec{\nu}_{ij}^2$ denote the unit outer normal vectors to $G_{ij}M_{ij}$ and $M_{ij}G_{i,j+1}$ respectively, pointing out of cell C_i (fig. 6.73), and for the quadrilateral cell L_{ij}, let $\vec{n}^1{}_{ij}, \ldots, \vec{n}_{ij}^4$ be the normal vectors to the cell edges $a_i G_{ij}$, $G_{ij} a_j$, $a_j G_{i,j+1}$ and $G_{i,j+1} a_i$, respectively, pointing out of cell L_{ij} (fig. 6.73).

For the formulation of our finite volume generalization of the Lax-Friedrichs 1-dimensional difference scheme, we must also define the elementary flux vectors, first for the barycentric cell C_i :

$$\vec{\eta}_{ij} = \int_{\Gamma_{ij} = G_{ij}M_{ij} \cup M_{ij}G_{i,j+1}} \vec{\nu} d\sigma \quad = \quad |\overrightarrow{G_{ij}M_{ij}}| \vec{\nu}_{ij}^1 + |\overrightarrow{M_{ij}G_{i,j+1}}| \vec{\nu}_{ij}^2 \qquad (2.1)$$

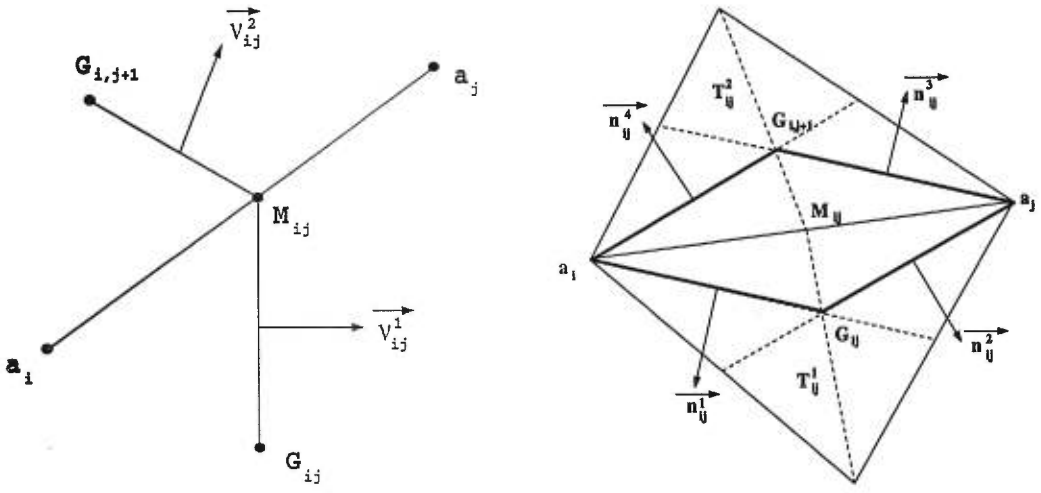

FIGURE 6.73. Barycentric cell boundary element $\Gamma_{ij} = G_{ij}M_{ij} \cup M_{ij}G_{i,j+1}$ and quadrilateral cell L_{ij} with normals to the boundary

and similarly for the quadrilateral cell L_{ij}

$$\begin{cases} \vec{\theta}_{ij} = |\overrightarrow{a_iG_{ij}}|\vec{n}^1_{ij} + |\overrightarrow{a_iG_{i,j+1}}|\vec{n}^4_{ij} \\ \vec{\theta}_{ji} = |\overrightarrow{a_jG_{ij}}|\vec{n}^2_{ij} + |\overrightarrow{a_jG_{i,j+1}}|\vec{n}^3_{ij}. \end{cases} \tag{2.2}$$

We write furthermore

$$\vec{\nu}^k_{ij} = \begin{pmatrix} \nu^k_{ijx} \\ \nu^k_{ijy} \end{pmatrix} \text{ for } k = 1, 2, \quad \vec{n}^k_{ij} = \begin{pmatrix} n^k_{ijx} \\ n^k_{ijy} \end{pmatrix} \text{ for } k = 1, \cdots, 4 \tag{2.3}$$

and

$$\vec{\eta}_{ij} = \begin{pmatrix} \eta_{ijx} \\ \eta_{ijy} \end{pmatrix}, \quad \overrightarrow{\theta}_{ij} = \begin{pmatrix} \theta_{ijx} \\ \theta_{ijy} \end{pmatrix} \tag{2.4}$$

The union of all these barycentric cells constitutes a partition of the domain Ω_h and the same holds for quadrilateral cells:

$$\Omega_h = \bigcup_{i=1}^{nv} C_i, \quad \Omega_h = \bigcup_{k=1}^{ne} L_k$$

where nv and ne are the number of vertices and number of edges, respectively, of the original finite element triangulation $\mathcal{T}_h$.

2.2. Approximation spaces.

Let ψ_i denote the characteristic function of cell C_i and, for every edge l_k $(1 \leq k \leq ne)$, let χ_k be the characteristic function of the diamond cell L_k. In order to set

the appropriate frame for the discrete problem which will be solved to approximate the solution of the original problem, we introduce the following discrete spaces ([15],[16]).

$$\mathcal{V}_h = \{v_h | v_h \in C^o(\Omega), v_h|_T \in P_1, \forall T \in \mathcal{T}_h\}$$

$$\mathcal{W}_h = \{v_h | v_h \in L^2(\Omega), v_h|_{C_i} = v_i = const;\ \ i = 1, \cdots, nv\}$$

$$\mathcal{Z}_h = \{v_h | v_h \text{ is continuous at the edge midpoints};\ \ v_h|_T \in P_1, \forall T \in \mathcal{T}_h\}$$

$$\mathcal{U}_h = \{v_h | v_h \in L^2(\Omega), v_h|_{L_k} = v_k = const;\ \ k = 1, \cdots, ne\}$$

Any function $f \in \mathcal{V}_h$ is uniquely determined by its values $f(a_i)$ at the vertices, and if we note $(N_i)_{i=1}^{nv}$ the basis set of $\mathcal{V}_h$ we have :

$$f(\overrightarrow{X}) = \sum_{i=1}^{nv} f(a_i) N_i(\overrightarrow{X}) \qquad \overrightarrow{X} \in \Omega_h$$

There exists a natural bijection S between the spaces $\mathcal{V}_h$ and $\mathcal{W}_h$ defined by :

$$\forall f \in \mathcal{V}_h \quad , \quad S(f(\overrightarrow{X})) = \sum_{i=1}^{nv} f(a_i) \psi_i(\overrightarrow{X})$$

and S can be viewed as a projection operator from $\mathcal{V}_h$ on $\mathcal{W}_h$.

Similarly, any function $g \in \mathcal{Z}_h$ is uniquely determined by its values $g(m_{ij})$ where m_{ij} is the midpoint of edge $a_i a_j$ (or by the values $g(m_k)$, $1 \leq k \leq ne$, if we consider, instead, a numbering of the edge midpoints), and if $(M_k)_{k=1}^{ne}$ is the basis set of $\mathcal{Z}_h$, we have

$$g(\overrightarrow{X}) = \sum_{k=1}^{ne} g(m_k) M_k(\overrightarrow{X}) \qquad \overrightarrow{X} \in \Omega_h$$

There exists a natural bijection between spaces $\mathcal{Z}_h$ and $\mathcal{U}_h$ defined by :

$$\forall g \in \mathcal{Z}_h \quad , \quad B(g(\overrightarrow{X})) = \sum_{k=1}^{ne} g(m_k) \chi_k(\overrightarrow{X})$$

2.3. A mixed finite volume/finite element method for the Navier-Stokes equations.

Mixed finite volume/finite element methods are constructed on the principle of a typical Galerkin formulation, but where the convective terms are treated with a finite volume method, while the viscous terms are handled with a finite element approach. This allows for a reduction of the order of the viscous terms from two to one thanks to an integration by parts.

In the mixed method considered here, the finite volume method is borrowed from earlier work ([1]-[6]) on first and second-order accurate methods based on the use of two dual

grids at alternate time steps, and extending to a 2-dimensional finite volume method the non-oscillatory one-dimensional central difference scheme of Nessyahu and Tadmor [18].

Since our finite volume method is a two-step algorithm using two dual grids, the combined mixed finite volume/finite element method also involves two steps.

Starting from the discrete spaces introduced above, we first write a general variational formulation of (1.1):

Find $U_h \in (\mathcal{V}_h)^4$ (or $(\mathcal{Z}_h)^4$ at alternate steps) such that

$$\int_{\Omega_h} \frac{\partial U_h}{\partial t}\varphi_h dxdy + \int_{\Omega_h} \overrightarrow{\nabla} \cdot \overrightarrow{\mathcal{F}}(U_h)\varphi_h dxdy = \frac{1}{R_e}\int_{\Omega_h} \overrightarrow{\nabla} \cdot \overrightarrow{\mathcal{R}}(U_h)\varphi_h dxdy \qquad \text{for all } \varphi_h \in \mathcal{V}_h (or \mathcal{Z}_h) \tag{2.5}$$

Then a **mixed** finite volume/finite element approximation ([15]) is **defined** by using different techniques to compute the left and right-hand side integrals in (2.5).

We now define the two steps of our mixed method; we use the above discrete spaces, shape functions and dual grids at alternate time steps.

First step

In this step, starting from known barycentric cell values $U_i^n = U(cellC_i; t^n)$ $(1 \leq i \leq nv)$, we compute new values for the diamond cells $U_{ij}^{n+1} = U(cellL_{ij}; t^{n+1})$, $(1 \leq i, j \leq nv)$. Starting from $U_h \in (\mathcal{Z}_h)^4$ in (2.5), choosing for $\varphi_h \in \mathcal{Z}_h$ the shape function $M_{ij} \in \mathcal{Z}_h$ associated with the midpoint m_{ij} of edge $a_i a_j = l_{ij}$, and applying the operator B to the left-hand side, leads to the definition of the first step:

$$\int_{Supp\chi_i = L_{ij}} \frac{\partial U_h}{\partial t} dxdy + \int_{Supp\chi_i = L_{ij}} \overrightarrow{\nabla} \cdot \overrightarrow{\mathcal{F}}(U_h) dxdy = \frac{1}{R_e}\int_{SuppM_{ij}} M_{ij} \overrightarrow{\nabla} \cdot \overrightarrow{\mathcal{R}}(U_h) dxdy \tag{2.6}$$

where $SuppM_{ij} = T_{ij}^1 \cup T_{ij}^2$ (see figs.6.73,6.74).

Second step

Starting from known diamond cell values U_{ij}^{n+1}, we compute barycentric cell values $U_i^{n+2} (1 \leq i \leq nv)$; starting from $U_h \in (\mathcal{V}_h)^4$ in (2.5), choosing for φ_h the shape function $N_i \in \mathcal{V}_h$ associated with node a_i, and applying the operator S to the left-hand

side, we obtain

$$\int_{Supp\psi_i=C_i}[\frac{\partial U_h}{\partial t}+\overrightarrow{\nabla}\cdot\overrightarrow{\mathcal{F}}(U_h)]dxdy=\frac{1}{R_e}\int_{SuppN_i}N_i\overrightarrow{\nabla}\cdot\overrightarrow{\mathcal{R}}(U_h)dxdy \qquad (2.7)$$

where $SuppN_i=\bigcup_{T,a_i\in T}T$ (see fig.6.74).

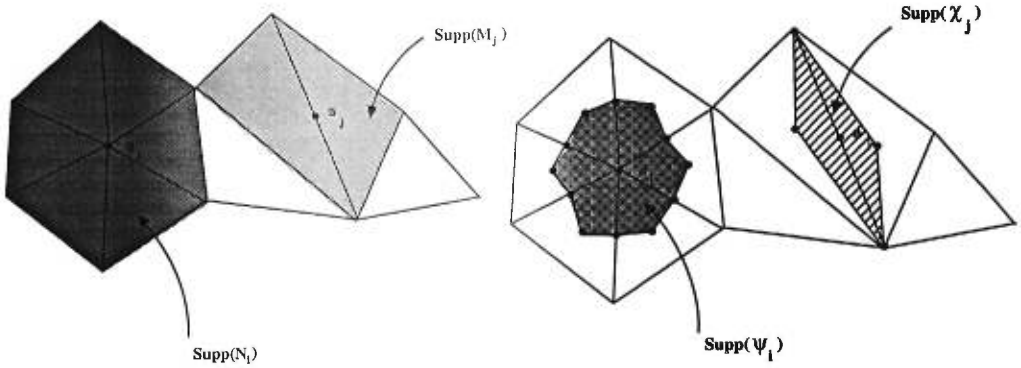

FIGURE 6.74. Support of N_i, M_j, ψ_i and χ_j

Applying Green's formula to the convective terms of (2.6),(2.7), and integration by parts to the diffusive terms, we obtain

First step :

$$\int_{L_{ij}}\frac{\partial U_h}{\partial t}dxdy+\int_{\partial L_{ij}}\overrightarrow{\mathcal{F}}(U_h)\cdot\overrightarrow{n_{ij}}d\sigma=-\frac{1}{R_e}\sum_{T\in[T_{ij}^1,T_{ij}^2]}\int_T\overrightarrow{\mathcal{R}}(U_h)\cdot\overrightarrow{\nabla}M_{ij}^T dxdy + \frac{1}{R_e}\int_{\partial\{SuppM_{ij}\}}M_{ij}\overrightarrow{\mathcal{R}}(U_h)\cdot\overrightarrow{n}d\sigma \qquad (2.8)$$

where $\overrightarrow{\nabla}M_{ij}^T$ denotes the (constant) gradient of M_{ij} on triangle T.

Second step :

$$\int_{C_i}\frac{\partial U_h}{\partial t}dxdy+\int_{\partial C_i}\overrightarrow{\mathcal{F}}(U_h)\cdot\overrightarrow{\nu_i}d\sigma=-\frac{1}{R_e}\sum_{T,a_i\in T}\int_T\overrightarrow{\mathcal{R}}(U_h)\cdot\overrightarrow{\nabla}N_i^T dxdy + \frac{1}{R_e}\int_{\Gamma_h\cap\partial\{SuppN_i\}}N_i\overrightarrow{\mathcal{R}}(U_h)\cdot\overrightarrow{n}d\sigma \qquad (2.9)$$

where $\overrightarrow{\nabla}N_i^T$ denotes the (constant) gradient of N_i on triangle T.

The boundary integrals in the right-hand sides of (2.8)-(2.9) vanish by the properties of shape functions and the homogeneous Dirichlet condition $\overrightarrow{V}_{|\Gamma_B}=0$, or they can be neglected on Γ_∞ since viscous effects can be neglected away from the body; observing

that

$$\partial L_{ij} \equiv \partial L_k = \bigcup_{l \in K(k)} \{\partial L_k \cap \partial L_l\} \cup \{\partial L_k \cap \Gamma_B\} \cup \{\partial L_k \cap \Gamma_\infty\}$$

where we have relabelled cell L_{ij} as L_k and $K(k) = \{1,2,3,4\}$ is a set of indices for the 4 cells adjacent to L_{ij}, and that

$$\partial C_i = \bigcup_{j \in K(i)} \{\partial C_i \cap \partial C_j\} \cup \{\partial C_i \cap \Gamma_B\} \cup \{\partial C_i \cap \Gamma_\infty\}$$

we thus get

First time step :

$$\begin{aligned}
&\int_{L_{ij}} \frac{\partial U_h}{\partial t} dxdy + \sum_{l=1}^{4} \int_{\partial L_{ij} \cap \partial L_l} \overrightarrow{\mathcal{F}}(U_h) \cdot \overrightarrow{n_{ij}} d\sigma \\
&+ \int_{\partial L_{ij} \cap \Gamma_B} \overrightarrow{\mathcal{F}}(U_h) \cdot \overrightarrow{n_{ij}} d\sigma \\
&+ \int_{\partial L_{ij} \cap \Gamma_\infty} \overrightarrow{\mathcal{F}}(U_h) \cdot \overrightarrow{n_{ij}} d\sigma \\
&= -\frac{1}{R_e} \sum_{T \in [T_{ij}^1, T_{ij}^2]} \int_T \overrightarrow{\mathcal{R}}(U_h) \cdot \overrightarrow{\nabla} M_{ij}^T dxdy
\end{aligned} \tag{2.10}$$

Second time step :

$$\begin{aligned}
&\int_{C_i} \frac{\partial U_h}{\partial t} dxdy + \sum_{j \in K(i)} \int_{\partial C_{ij}} \overrightarrow{\mathcal{F}}(U_h) \cdot \overrightarrow{\nu_{ij}} d\sigma \\
&+ \int_{\partial C_i \cap \Gamma_B} \overrightarrow{\mathcal{F}}(U_h) \cdot \overrightarrow{\nu_i} d\sigma \\
&+ \int_{\partial C_i \cap \Gamma_\infty} \overrightarrow{\mathcal{F}}(U_h) \cdot \overrightarrow{\nu_i} d\sigma \\
&= -\frac{1}{R_e} \sum_{T, a_i \in T} \int_T \overrightarrow{\mathcal{R}}(U_h) \cdot \overrightarrow{\nabla} N_i^T dxdy
\end{aligned} \tag{2.11}$$

where $K(i) = \{j : 1 \leq j \leq nv \quad a_j \text{ is a neighbour of } a_i\}$, and $\partial C_{ij} = \partial C_i \cap \partial C_j \equiv \Gamma_{ij} = [G_{ij}, m_{ij}] \cup [m_{ij}, G_{i,j+1}]$

For the normal vectors $\overrightarrow{\nu_{ij}}$ to ∂C_{ij} and $\overrightarrow{n}_{ij}$ to ∂L_{ij} see fig.6.73.

The computation of the convective term integrals in (2.10-2.11) is performed according to the procedure used for our finite volume method ([2],[3], [6]); see section 2.4.

For the viscous fluxes in (2.10-2.11), we observe that the components of the stress tensor and of $\overrightarrow{\nabla} N_i^T$, $\overrightarrow{\nabla} M_{ij}^T$ are constant in each triangle.

The average velocity vector on a triangle T is computed as

$$\overrightarrow{V}_T = \frac{1}{3} \sum_{k=1, a_k \in T}^{3} \overrightarrow{V}_k$$

and the viscous fluxes are approximated as follows: for the first step,

$$\sum_{T \in [T_{ij}^1, T_{ij}^2]} \int_T \overrightarrow{\mathcal{R}}(U_h) \cdot \overrightarrow{\nabla} M_{ij}^T dxdy \equiv \sum_{k=1}^{2} Area(T_{ij}^k) \left[R(T_{ij}^k) \frac{\partial M_{ij}^{T_{ij}^k}}{\partial x} + S(T_{ij}^k) \frac{\partial M_{ij}^{T_{ij}^k}}{\partial y} \right] \tag{2.12}$$

and for the second step

$$\sum_{T, a_i \in T} \int_T \overrightarrow{\mathcal{R}}(U_h) \cdot \overrightarrow{\nabla} N_i^T dxdy \equiv \sum_{T, a_i \in T} Area(T) (R(T) \frac{\partial N_i^T}{\partial x} + S(T) \frac{\partial N_i^T}{\partial y}) \tag{2.13}$$

where the values of $R(T)$ and $S(T)$ are constant on the triangle T, computed from the average velocity vector $\overrightarrow{V}_T$.

For each triangle $T \in \mathcal{T}_h$, if k_1, k_2 and k_3 are the nodes of T, we have

$$\begin{cases} u(T) = \frac{1}{3} \sum_{k_i \in T} u_{k_i}, \qquad v(T) = \frac{1}{3} \sum_{k_i \in T} v_{k_i} \\ \tau_{xx}(T) = \frac{2}{3} \sum_{k_i \in T} \left(2u_{k_i} \frac{\partial N_{k_i}}{\partial x} - v_{k_i} \frac{\partial N_{k_i}}{\partial y} \right) \\ \tau_{xy}(T) = \sum_{k_i \in T} \left(u_{k_i} \frac{\partial N_{k_i}}{\partial y} + v_{k_i} \frac{\partial N_{k_i}}{\partial x} \right) \\ \tau_{yy}(T) = \frac{2}{3} \sum_{k_i \in T} \left(2v_{k_i} \frac{\partial N_{k_i}}{\partial y} - u_{k_i} \frac{\partial N_{k_i}}{\partial x} \right) \end{cases} \tag{2.14}$$

$$R(T) = \begin{pmatrix} 0 \\ \tau_{xx}(T) \\ \tau_{xy}(T) \\ u(T)\tau_{xx}(T) + v(T)\tau_{xy}(T) + \frac{\gamma k}{Pr} \sum_{k_i \in T} \epsilon_{k_i} \frac{\partial N_{k_i}}{\partial x} \end{pmatrix} \tag{2.15}$$

$$S(T) = \begin{pmatrix} 0 \\ \tau_{xy}(T) \\ \tau_{yy}(T) \\ u(T)\tau_{xy}(T) + v(T)\tau_{yy}(T) + \frac{\gamma k}{Pr} \sum_{k_i \in T} \epsilon_{k_i} \frac{\partial N_{k_i}}{\partial y} \end{pmatrix} \tag{2.16}$$

2.4. Time discretization .

First step

In order to obtain the first step of our time discretization, we integrate equation (2.10) on the 3-dimensional cell $L_{ij} \times [t^n, t^{n+1}]$, assuming we have obtained from the barycentric cell average values U_i^n piecewise linear reconstructions, according to the MUSCL technique [23],[24], given by

$$U_h(x,y,t^n)_{|C_i} = \mathcal{L}_i(x,y,t^n) = U_i^n + (x-x_i)P_i^n + (y-y_i)Q_i^n \qquad (x,y) \in C_i \tag{2.17}$$

For the integration with respect to time, in order to ensure "nearly" second-order accuracy (up to the treatment of the viscous terms), we adopt a " quasi-midpoint formula" time discretization, where the convective flux is computed at the intermediate time $t^{n+\frac{1}{2}}$ (thus requiring the computation of predicted value $U_h(x,y,t^{n+\frac{1}{2}})$ along ∂L_{ij}), while the viscous term in the R.H.S. of (2.10) is treated, in the integration with respect to time, in a fully explicit Euler approach.

This leads to

$$\begin{aligned}
&\int_{t^n}^{t^{n+1}} \int_{L_{ij}} \frac{\partial U_h}{\partial t} dxdydt + \int_{t^n}^{t^{n+1}} \sum_{l=1}^{4} \int_{\partial L_{ij} \cap \partial L_l} \overrightarrow{\mathcal{F}}(U_h) \cdot \overrightarrow{n_{ij}} d\sigma dt \qquad (2.18)\\
&+ \int_{t^n}^{t^{n+1}} \int_{\partial L_{ij} \cap \Gamma_B} \overrightarrow{\mathcal{F}}(U_h) \cdot \overrightarrow{n_{ij}} d\sigma dt\\
&+ \int_{t^n}^{t^{n+1}} \int_{\partial L_{ij} \cap \Gamma_\infty} \overrightarrow{\mathcal{F}}(U_h) \cdot \overrightarrow{n_{ij}} d\sigma dt\\
&= -\frac{1}{R_e} \int_{t^n}^{t^{n+1}} \sum_{T \in [T_{ij}^1, T_{ij}^2]} \int_T \overrightarrow{\mathcal{R}}(U_h) \cdot \overrightarrow{\nabla} M_{ij}^T dxdy
\end{aligned}$$

and thus, applying the divergence theorem to the first integral and (for integration with respect to time) the midpoint quadrature formula to the second integral, and the left rectangular formula to the third and fourth integrals, we obtain

$$\begin{aligned}
&\int_{L_{ij}} U_h(x,y,t^{n+1}) dxdy - \int_{L_{ij}} U_h(x,y,t^n) dxdy + \Delta t \sum_{l=1}^{4} \int_{\partial L_{ij} \cap \partial L_l} \overrightarrow{\mathcal{F}}(U_h^{n+\frac{1}{2}}) \cdot \overrightarrow{n_{ij}} d\sigma \qquad (2.19)\\
&+ \Delta t \int_{\partial L_{ij} \cap \Gamma_B} \overrightarrow{\mathcal{F}}(U_h^n) \cdot \overrightarrow{n_{ij}} d\sigma\\
&+ \Delta t \int_{\partial L_{ij} \cap \Gamma_\infty} \overrightarrow{\mathcal{F}}(U_h^n) \cdot \overrightarrow{n_{ij}} d\sigma
\end{aligned}$$

$$= -\frac{\Delta t}{Re} \sum_{T \in [T_{ij}^1, T_{ij}^2]} \int_T \overrightarrow{\mathcal{R}}(U_h^n) \cdot \overrightarrow{\nabla} M_{ij}^T dxdy$$

At this stage, we will define the predicted values required for the convective flux boundary integral of the left hand side.

Predictor (First step) :

On each side of the diamond cell L_{ij}, using the Euler equations (neglecting the viscous terms) we define a predicted vector

$$U_{a_i G_{ij}}^{n+1/2} = U_{a_i, G_{ij}}^n - \frac{\Delta t}{2} \{ F'(U_{a_i, G_{ij}}^n) P_i^n + G'(U_{a_i, G_{ij}}^n) Q_i^n \} \tag{2.20}$$

where, using (2.17), the value of U_h^n along the side $a_i G_{ij}$ of diamond cell L_{ij} is taken equal to

$$U_h(x, y, t^n) \cong U_i^n + \frac{1}{2}(x_{G_{ij}} - x_i) P_i^n + \frac{1}{2}(y_{G_{ij}} - y_i) Q_i^n \equiv U_{a_i, G_{ij}}^n \tag{2.21}$$

The corrector can now be written, from (2.19)-(2.20), as

Corrector (First step)

$$\begin{aligned} & Area(L_{ij}) U_{ij}^{n+1} - \left\{ \int_{L_{ij} \cap C_i} U_h(x, y, t^n) dxdy + \int_{L_{ij} \cap C_j} U_h(x, y, t^n) dxdy \right\} \\ & + \Delta t \sum_{l=1}^{4} \int_{\partial L_{ij} \cap \partial L_l} \overrightarrow{\mathcal{F}}(U_h^{n+\frac{1}{2}}) \cdot \overrightarrow{n_{ij}} d\sigma + \\ & + \Delta t \int_{\partial L_{ij} \cap \Gamma_B} \overrightarrow{\mathcal{F}}(U_h^n) \cdot \overrightarrow{n_{ij}} d\sigma \\ & + \Delta t \int_{\partial L_{ij} \cap \Gamma_\infty} \overrightarrow{\mathcal{F}}(U_h^n) \cdot \overrightarrow{n_{ij}} d\sigma \\ & = -\frac{\Delta t}{Re} \sum_{T \in [T_{ij}^1, T_{ij}^2]} \int_T \overrightarrow{\mathcal{R}}(U_h^n) \cdot \overrightarrow{\nabla} M_{ij}^T dxdy \end{aligned} \tag{2.22}$$

where the right hand side is computed according to (2.12)-(2.16). The integrals in the left-hand-side of (2.22) are computed as follows:

$$\begin{aligned} & \left\{ \int_{L_{ij} \cap C_i} U_h(x, y, t^n) dxdy + \int_{L_{ij} \cap C_j} U_h(x, y, t^n) dxdy \right\} \equiv \\ & \int_{L_{ij}} U_h(x, y, t^n) dxdy = \int_{L_{ij} \cap C_i} \mathcal{L}(x, y, t^n) dxdy + \int_{L_{ij} \cap C_j} \mathcal{L}(x, y, t^n) dxdy \end{aligned} \tag{2.23}$$

where

$$\int_{L_{ij}\cap C_i}\mathcal{L}(x,y,t^n)dxdy = \text{Area}(L_{ij}\cap C_i)\{U_i^n + \frac{1}{3}(x_{m_{ij}}-x_i)P_i^n + \frac{1}{3}(y_{m_{ij}}-y_i)Q_i^n\} \tag{2.24}$$

$$+\frac{1}{3}\text{Area}(L_{ij}^r\cap C_i)\{(x_{G_{ij}}-x_i)P_i^n + (y_{G_{ij}}-y_i)Q_i^n\}$$
$$+\frac{1}{3}\text{Area}(L_{ij}^\ell\cap C_i)\{(x_{G_{i,j+1}}-x_i)P_i^n + (y_{G_{i,j+1}}-y_i)Q_i^n\}$$

with L_{ij}^r = triangle $a_iG_{ij}a_j$ and $\text{Area}(L_{ij}^r\cap C_i) =$
$\frac{1}{2}\{(x_{G_{ij}}-x_i)(y_{m_{ij}}-y_i) - (y_{G_{ij}}-y_i)(x_{m_{ij}}-x_i)\}$ and L_{ij}^l = triangle $a_iG_{ij+1}a_j$,
and $\text{Area}(L_{ij}^l\cap C_i) = \frac{1}{2}\{(x_{m_{ij}}-x_i)(y_{G_{i,j+1}}-y_i) - (x_{G_{ij+1}}-x_i)(y_{m_{ij}}-y_i)\}$

$$\int_{L_{ij}\cap C_j}\mathcal{L}(x,y,t^n)dxdy = \text{Area}(L_{ij}\cap C_j)\{U_j^n + \frac{1}{3}(x_{m_{ij}}-x_j)P_j^n + \frac{1}{3}(y_{m_{ij}}-y_j)Q_j^n\} \tag{2.25}$$

$$+\frac{1}{3}\text{Area}(L_{ij}^r\cap C_j)\{(x_{G_{ij}}-x_j)P_j^n + (y_{G_{ij}}-y_j)Q_j^n\}$$
$$+\frac{1}{3}\text{Area}(L_{ij}^\ell\cap C_j)\{(x_{G_{i,j+1}}-x_j)P_j^n + (y_{G_{i,j+1}}-y_j)Q_j^n\}$$

where $\text{Area}(L_{ij}^r\cap C_j) = \frac{1}{2}\{(x_{m_{ij}}-x_j)(y_{G_{ij}}-y_j) - (x_{G_{ij}}-x_j)(y_{m_{ij}}-y_i)\}$,
and finally

$$\Delta t\int_{\partial L_{ij}\cap\partial L_l}\vec{\mathcal{F}}(U_h^{n+\frac{1}{2}})\cdot\vec{n_{ij}}d\sigma$$
$$\cong \Delta t\int_{\partial L_{ij}\cap\partial L_l}\Big\{F(U_h(x,y,t^{n+1/2}))n_x + G(U_h(x,y,t^{n+1/2}))n_y\Big\}d\sigma \tag{2.26}$$

where the intermediate time value $U_h(x,y,t^{n+\frac{1}{2}})$ is defined by the predictor (2.20).
We thus get for the convective flux

$$\sum_{l=1}^{4}\int_{\partial L_{ij}\cap\partial L_l}\vec{\mathcal{F}}(U_h^{n+\frac{1}{2}})\cdot\vec{n_{ij}}d\sigma \tag{2.27}$$
$$\cong F(U_{a_i,G_{ij}}^{n+1/2})n_{ijx}^1\cdot|a_iG_{ij}| + F(U_{a_i,G_{i,j+1}}^{n+1/2})n_{ijx}^4\cdot|a_iG_{i,j+1}|$$
$$+F(U_{a_j,G_{ij}}^{n+1/2})n_{ijx}^2\cdot|a_jG_{ij}| + F(U_{a_j,G_{i,j+1}}^{n+1/2})n_{ijx}^3\cdot|a_jG_{i,j+1}|$$
$$+G(U_{a_i,G_{ij}}^{n+1/2})n_{ijy}^1\cdot|a_iG_{ij}| + G(U_{a_i,G_{i,j+1}}^{n+1/2})n_{ijy}^4\cdot|a_iG_{i,j+1}|$$
$$+G(U_{a_j,G_{ij}}^{n+1/2})n_{ijy}^2\cdot|a_jG_{ij}| + G(U_{a_j,G_{i,j+1}}^{n+1/2})n_{ijy}^3\cdot|a_jG_{i,j+1}|.$$

For the computation of the boundary flux integrals in (2.19), see section 2.6 on the treatment of the boundary condition.

Collecting the results obtained in (2.23-2.27) and (2.12-2.16) completes the description of the first step.

Second step

To obtain the second step of the time discretization, we integrate (2.11) on the 3-dimensional cell $C_i \times [t^{n+1}, t^{n+2}]$, assuming we have obtained, from the diamond cell average values U_{ij}^{n+1} computed in the first time step, piecewise linear reconstructions, given by

$$U_h(x,y,t^{n+1})_{|L_{ij}} = \mathcal{L}_{ij}(x,y,t^{n+1}) = U_{ij}^{n+1} + (x - x_{ij})P_{ij}^{n+1} + (y - y_{ij})Q_{ij}^{n+1}. \quad (2.28)$$

Proceeding as for the first step, we obtain

Predictor (second step)

$$U_{G_{ij}m_{ij}}^{n+\frac{3}{2}} = U_{G_{ij}m_{ij}}^{n+1} - \frac{\Delta t}{2}\{F'(U_{G_{ij}m_{ij}}^{n+1})P_{ij}^{n+1} + G'(U_{G_{ij}m_{ij}}^{n+1})Q_{ij}^{n+1}\}. \quad (2.29)$$

where

$$U_h(x,y,t^{n+1}) \cong U_{ij}^{n+1} + \frac{1}{2}(x_{G_{ij}} - x_{m_{ij}})P_{ij}^{n+1} + \frac{1}{2}(y_{G_{ij}} - y_{m_{ij}})Q_{ij}^{n+1} \equiv U_{G_{ij}m_{ij}}^{n+1} \quad (2.30)$$

is an approximation of $U(x,y,t^{n+1})$ on the barycentric cell boundary element $G_{ij}m_{ij}$

Corrector (second step)

$$\begin{aligned} &\text{Area}(C_i)U_i^{n+2} - \sum_{j\in K(i)} \int_{C_i \cap L_{ij}} U(x,y,t^{n+1})dxdy \quad (2.31)\\ &+ \Delta t \sum_{j\in K(i)} \int_{\partial C_i \cap \partial C_j = \Gamma_{ij}} \overrightarrow{\mathcal{F}}(U(x,y,t^{n+3/2}) \cdot \overrightarrow{\nu_{ij}} d\sigma \\ &+ \Delta t \int_{\partial C_i \cap \Gamma_B} \overrightarrow{\mathcal{F}}(U_h^{n+1}) \cdot \overrightarrow{\nu_i} d\sigma \\ &+ \Delta t \int_{\partial C_i \cap \Gamma_\infty} \overrightarrow{\mathcal{F}}(U_h^{n+1}) \cdot \overrightarrow{\nu_i} d\sigma = \\ &- \frac{\Delta t}{R_e} \sum_{T, a_i \in T} \int_T \overrightarrow{\mathcal{R}}(U_h^{n+1}) \cdot \overrightarrow{\nabla} N_i^T dxdy \end{aligned}$$

2.5. Approximation of the slopes.

In order to compute the gradient (P_i^n, Q_i^n) of the piecewise linear interpolant $L(x,y,t^n)$ for the cell C_i, we must first compute the gradient of the first degree polynomials P_T for all triangles $T \in \mathcal{T}_h$ such that $a_i \in T$. Although we could then in principle directly take the average of the gradients of the polynomials P_T, obtained as described

at the beginning of section 4 in [2], we shall consider here a least-squares technique (cf.[2],[25],[26]). For simplicity, we shall describe it for the case of triangular (finite volume) cells. Note that the interpolation is performed on the physical variables.

Let T be a triangle with centroid G, and let T_j, $j = 1,2,3$ be the neighbouring triangles, with centroids $G_j (j = 1,\ldots,3)$ (fig. 6.75); assume the values of the numerical approximation of the solution U at the four points $\{G, G_j\}_{j=1}^{3}$ are known at time t^n, equal to U_T^n, $U_{T_j}^n$ $(j = 1,\ldots,3)$ (these values can be considered as cell values playing for the triangular cells T, T_j the same role as U_i^n, U_{ij}^n for the cells C_i, L_{ij}).

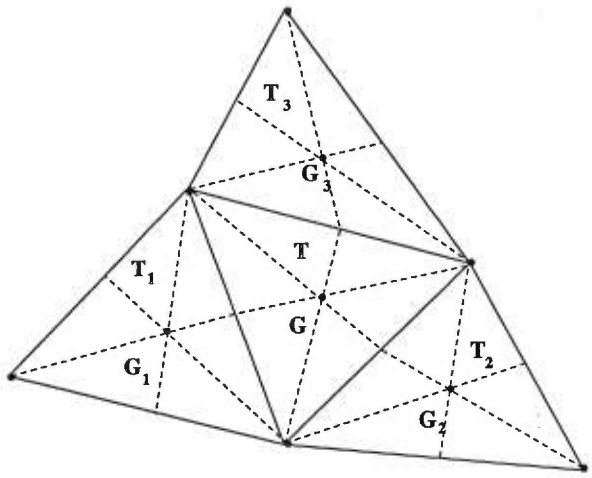

FIGURE 6.75. Computation of the least-squares gradient for a triangular cell **T**.

The least-squares gradient $(\widetilde{grad\ U})_T^n = (\tilde{a}_T^n, \tilde{b}_T^n)$ for triangle T will then be chosen such as to minimize the functional

$$I = \sum_{j=1}^{3} \{U_T^n + \overrightarrow{GG_j} \cdot (grad\ U)_T^n - U_{T_j}^n\}^2 \tag{2.32}$$

where

$$(grad\ U)_T^n = (a_T^n, b_T^n)$$

The minimum is obtained when

$$\frac{\partial I}{\partial a_T^n} = \frac{\partial I}{\partial b_T^n} = 0 \tag{2.33}$$

and is shown in [25] to lead to the following least-squares gradient:

$$\tilde{a}_T^n = \frac{1}{D}\sum_{j=1}^{3}(y_{G_j}-y_G)^2\sum_{j=1}^{3}(U_{T_j}^n-U_T^n)(x_{G_j}-x_G) - \frac{1}{D}\sum_{j=1}^{3}(x_{G_j}-x_G)(y_{G_j}-y_G)\sum_{j=1}^{3}(U_{T_j}^n-U_T^n)(x_{G_j}-x_G) \quad (2.34)$$

where the denominator

$$D = \sum_{j=1}^{3}(x_{G_j}-x_G)^2\sum_{j=1}^{3}(y_{G_j}-y_G)^2 - \left[\sum_{j=1}^{3}(x_{G_j}-x_G)(y_{G_j}-y_G)\right]^2 \quad (2.35)$$

is strictly positive for any non-degenerated triangle.

For the barycentric cells C_i or the quadrilateral cells L_{ij}, the procedure is quite similar to the one described above for triangular cells. Alternately, for a barycentric cell C_i with center a_i, we could first compute the least squares gradient grad $U|_{T_j} = (\tilde{a}_{T_j}^n, \tilde{b}_{T_j}^n)$ of each neighbouring triangle T_j (such that $a_i \in T_j$), and then take the cell gradient grad $U|_{C_i}$ = average{grad $U|_{T_j}$}, with a similar procedure for a quadrilateral cell L_{ij}. When considering flows for which the viscous terms are dominant (small values of the Reynolds number) the limitation procedure is generally not necessary.

2.6. Treatment of the boundary conditions.

The third term and the fourth term of (2.10) and (2.11) contain the physical boundary conditions. These are represented by the vector U_h which involves quantities that depend on the interior value of U_h and quantities that are determined by the physical boundary conditions.

Wall boundary Γ_B: the no-slip condition is taken into account using a strong formulation so that we do not need to compute the corresponding boundary integral in the third term of (2.10) and (2.11). We make a direct use of the expressions given by (1.10) and (1.11).

Inflow and outflow boundaries Γ_∞, Γ_E: at these boundaries, a precise set of compatible exterior data which depend on the flow regime and the velocity direction, is to be specified. For this purpose a plus-minus flux splitting is applied between exterior data and interior values. More precisely, the boundary integral (third term of (2.10) and (2.11)) is evaluated using a non-reflective version of the flux-splitting of Steger and

Warming [27]:

$$\int_{\partial C_i \cap \Gamma_\infty} \overrightarrow{\mathcal{F}(\mathcal{U})}_h \cdot \vec{n}_i d\sigma = \mathcal{A}^+(U_i, \vec{\nu}_{i\infty}) \cdot U_i + \mathcal{A}^-(U_i, \vec{\nu}_{i\infty}) \cdot U_\infty \qquad (2.36)$$

where $\mathcal{A}$ is the flux Jacobian matrix $\frac{\partial \vec{\mathcal{F}}(U)}{\partial U} \cdot \vec{\nu} = \frac{\partial F}{\partial U}\nu_x + \frac{\partial G}{\partial U}\nu_y$, and $\mathcal{A}^+, \mathcal{A}^-$ are the positive and negative parts of $\mathcal{A}$, respectively.

3. Numerical experiments

3.1. Supersonic Navier-Stokes flow past a flat plate.

In order to assess the basic qualities of our method, we treated several typical test cases of viscous flows, of which we will present two in this paper. We observe that the viscous flows calculated here are confined to laminar (low Reynolds number) flow problems, as is also the case in one of the reference papers we have used for comparison's sake [30]. We first consider the classical test problem of the flow over a flat plate (fig.6.76) with a Reynolds number $R_e = 1000$, and Mach number M_∞ at the farfield equal to 3. The

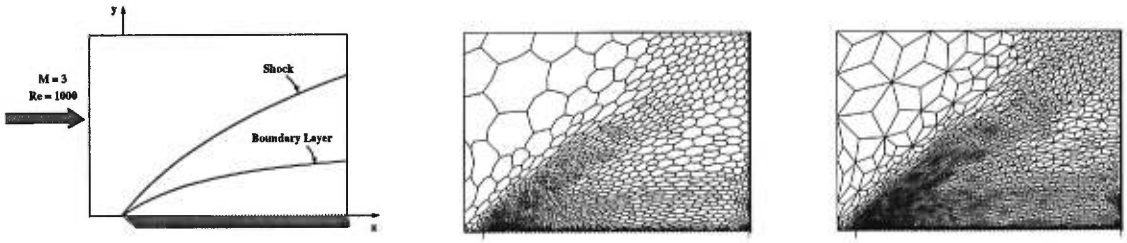

FIGURE 6.76. Supersonic flow over a flat plate, barycentric cells C_i and quadrilateral cells L_{ij} with the initial grid

initial grid (1637 vertices) (fig.6.77) is adapted twice with the help of a grid adaptator developed by Castro Diaz and Hecht at INRIA [28]-[29], resulting in a 1726-vertex final grid (fig.6.78).

The results obtained with the initial grid (fig.6.77) are already valuable, as can be seen from a comparison with those obtained in [19],[30],[31], where the same conditions have been used.

In fact our initial results (1637 vertices) can sustain comparison with the final results in [30] (6750 vertices); but the method used in [30] is based on mesh refinement only, while ours also resorts to mesh adaptation.

With the adapted final grid (1726 vertices), we observe (fig.6.78) a very clean capture of the shock and the boundary layer.

The final grid also leads to a substantial improvement in the resolution of the pressure coefficient $C_p = \frac{p-p_\infty}{1/2\rho_\infty ||\vec{V}_\infty||^2}$ (fig. 6.79).

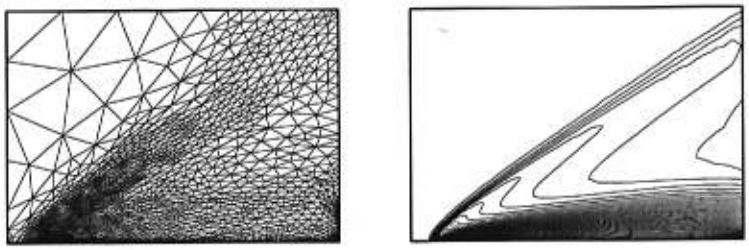

FIGURE 6.77. Initial mesh for the plate problem (1637 vertices) and solution (Mach contours)

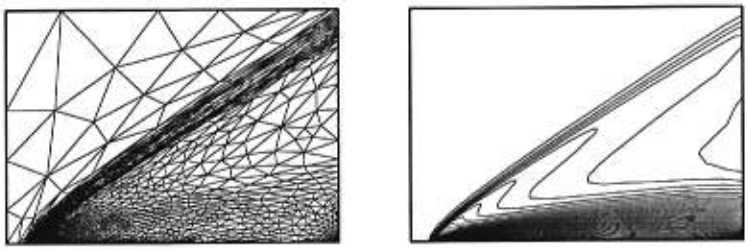

FIGURE 6.78. Enriched mesh for the plate problem (1726 vertices) and solution (Mach contours)

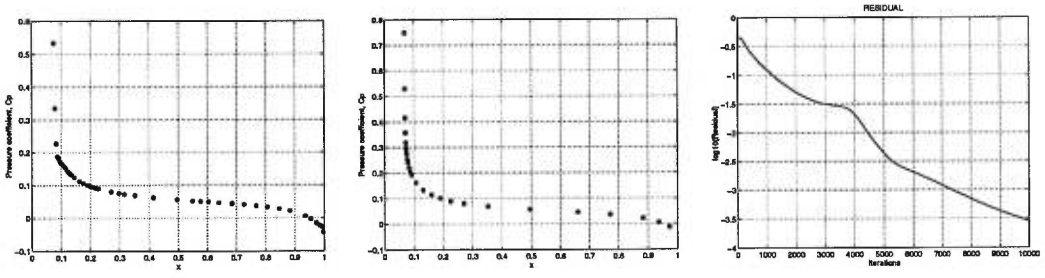

FIGURE 6.79. Flat plate problem. Pressure coefficient C_p with initial mesh and enriched mesh and residual for initial mesh

3.2. Supersonic flow around a NACA0012 airfoil.

We consider a more complex flow around a NACA0012 airfoil, with a farfield Mach number of 2, angle of attack 10 degrees and a Reynolds number of 1000.This case was also studied in [19].

A very thin detached shock is present. The starting mesh (2274 vertices,fig.6.81) is adapted 3 times . The final mesh contains 7114 nodes (fig.6.82). We present the corresponding Mach contours (figs.6.81,6.82) ; the initial contours, rather irregular, are transformed into very smooth curves by the grid adaptation process. The extra refinement has also led to a thin capture of the shock. Here again, the results obtained for this test case can be favourably compared with those of reference [19]. In particular, we have obtained a sensibly sharper shock capture and smoother Mach isolines, and a very clean resolution of the boundary layer, with the corresponding detachment at the trailing edge.

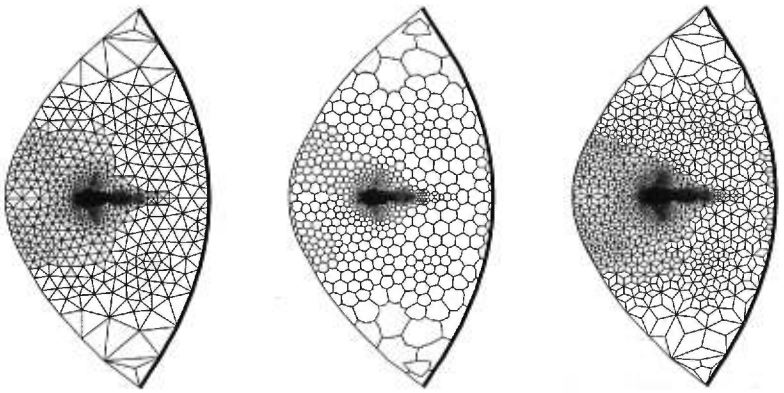

FIGURE 6.80. Euler flow around a NACA 0012 airfoil. Original grid, barycentric cells C_i and quadrilateral cells L_{ij}

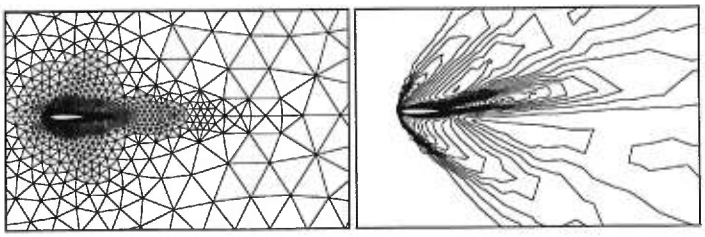

FIGURE 6.81. NACA0012 : Initial mesh (2274 vertices) and Mach contours

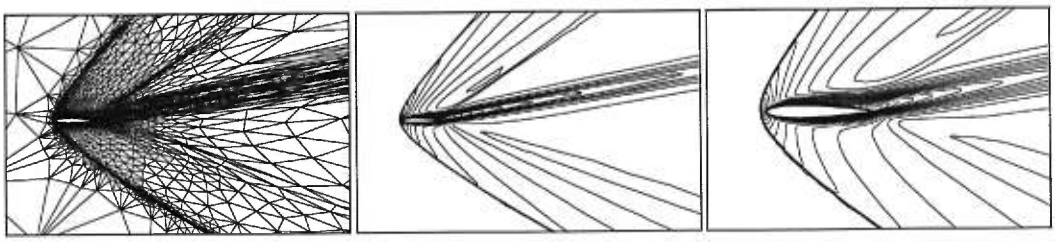

FIGURE 6.82. NACA0012 : Final mesh (7114 vertices) Mach contours with enlarged details.

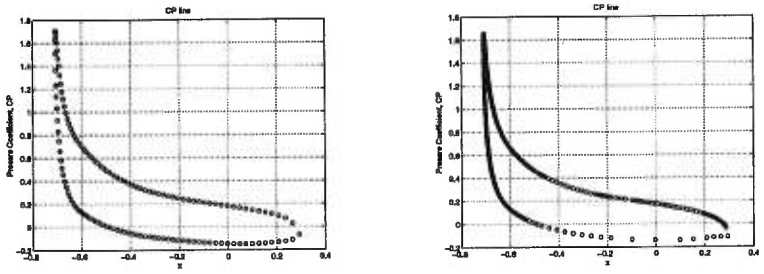

FIGURE 6.83. NACA 0012. Pressure coefficient C_p with initial mesh and enriched mesh

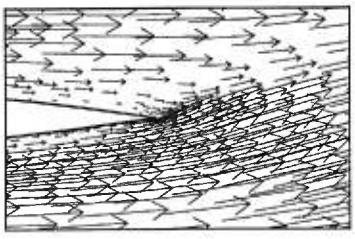

FIGURE 6.84. NACA0012 : Velocity field, trailing edge

3.3. Supersonic Flow around an Ellipse.

We consider here the numerical simulation of the 2-dimensionl steady flow past an ellipse (see fig.6.85) with farfield Mach number $M_\infty = 2$, angle of attack of 0^o degrees and Reynolds number $R_e = 1000$. Both the shock and the boundary layer are very accurately represented. The Mach contours, already fairly regular with the initial grid, become very smooth with the final grid. For comparison's sake see e.g.[32].

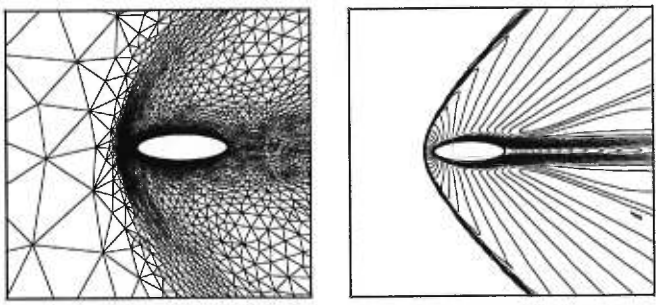

FIGURE 6.85. Initial grid (3611 vertices) and Mach contours

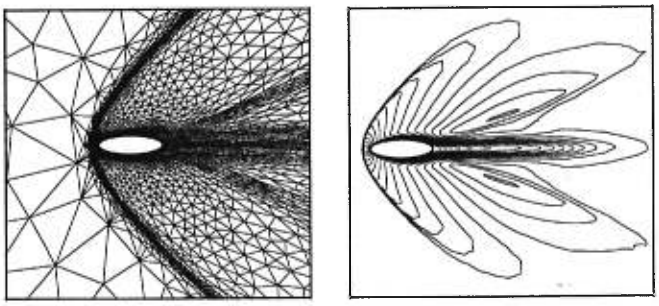

FIGURE 6.86. First adaptation (4682 vertices) and Mach contours

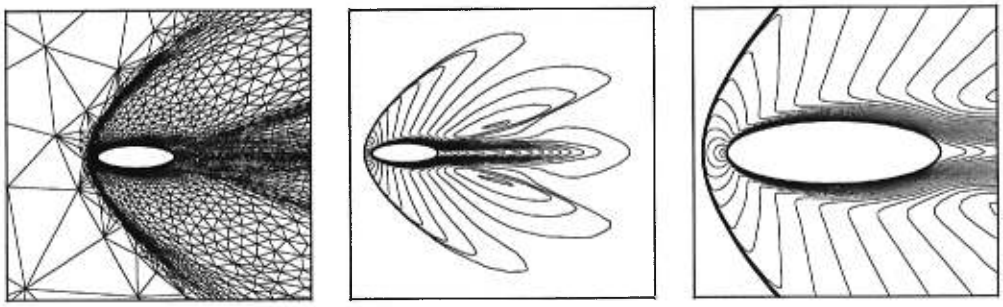

FIGURE 6.87. Second adaptation (5934 vertices) and Mach contours and Zoom of Mach contours for the final adaptation

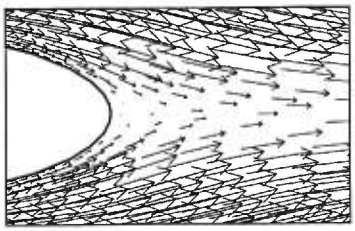

FIGURE 6.88. Ellipse : Velocity field, trailing edge

3.4. Supersonic flow past a double-ellipse.

For this problem inspired by ([33]), but with Mach number $M_\infty = 2$ instead of the range of hypersonic Mach numbers considered there, and 20^o of angle of attack, the geometry is a double ellipse ; it can be defined by

$$\begin{cases} x \leq 0 & \begin{cases} z \leq 0 & \left(\frac{x}{0.06}\right)^2 + \left(\frac{z}{0.015}\right)^2 = 1 \\ z \geq 0 & \left(\frac{x}{0.035}\right)^2 + \left(\frac{z}{0.025}\right)^2 = 1 \end{cases} \\ 0 \leq x \leq 0.016 & \begin{cases} z \geq 0 & z = 0.025 \\ z \leq 0 & z = -0.015 \end{cases} \end{cases}$$

Although the results obtained with the initial grid (1558 vertices, fig.6.90) already

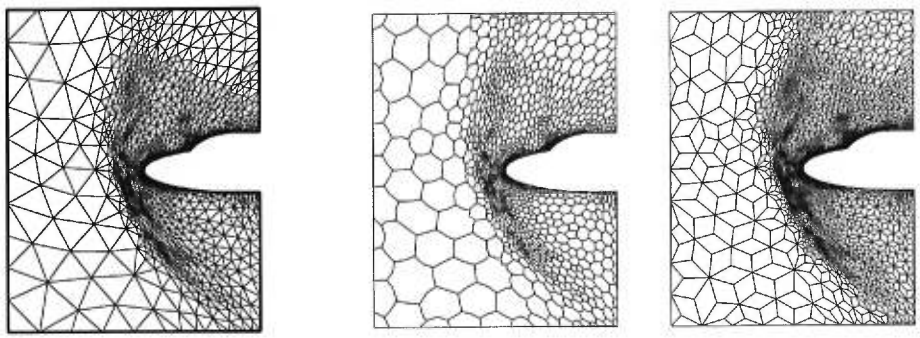

FIGURE 6.89. Euler flow around a double ellipse. Original grid, barycentric cells C_i and quadrilateral cells L_{ij}

give a reasonably good simulation of the bow shock and the boundary layer, the Mach contours are not very smooth, and thus rather unsatisfactory. With the final grid (6399 vertices, fig.6.91), the capture of the shock is very sharp, with a good resolution of the boundary layer, and smooth Mach contours.

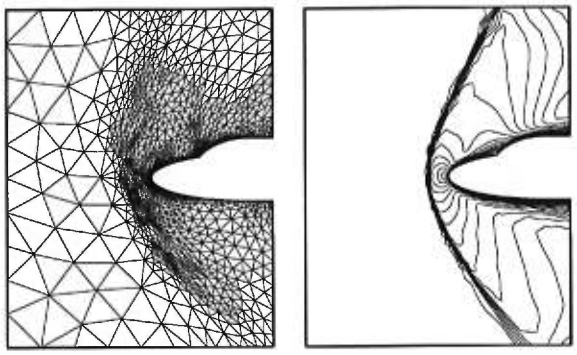

FIGURE 6.90. Euler flow around a double ellipse. Initial grid (1558 vertices) and Mach contours

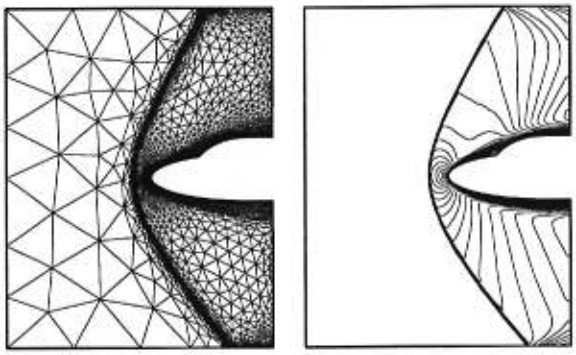

FIGURE 6.91. Euler flow around a double ellipse. Final grid (6399 vertices) and Mach contours

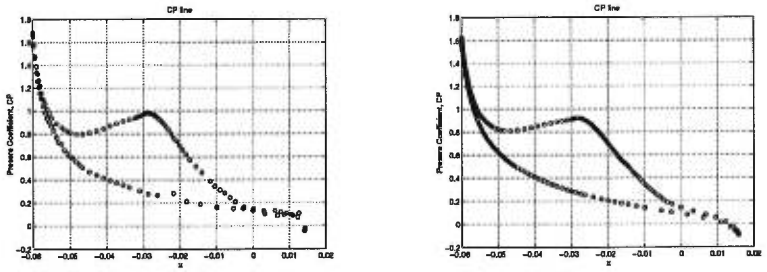

FIGURE 6.92. Double-ellipse (Hermes). Pressure coefficient C_p with initial mesh and enriched mesh

4. Concluding remarks

Starting from the principle of mixed Finite Volume/Finite Element methods, we have constructed a new method for the two-dimensional compressible Navier-Stokes equations, whose main component lies in our recent staggered grid central finite volume method inspired from the one-dimensional Lax-Friedrichs and Nessyahu-Tadmor difference schemes.

The convective terms are treated according to our Finite Volume method, while the viscous terms are computed with a typical Finite Element procedure. Piecewise linear MUSCL cell interpolants using least-squares gradients allow for an oscillation-free quasi-second order resolution, thanks to a two-step time discretization and a predictor-corrector approach.

From a theoretical viewpoint, L^∞-weak convergence of the solution provided by our Finite Volume method has been proved first for a linear hyperbolic equation [10], using L^∞-and weighted total variation estimates, and more recently, for a nonlinear scalar hyperbolic equation [11], with the help of Young measures.

In this paper, we have concentrated on the presentation of the method, and its validation through a comparative study of four classical numerical test problems, where our new method has shown excellent capabilities both for an accurate and oscillation-free, sharp capture of shocks and boundary layer, and for the high quality of the boundary layer resolution with an accurate simulation of the boundary layer detachment.

Références

[1] P. ARMINJON ET M.C. VIALLON , Généralisation du schéma de Nessyahu-Tadmor pour une équation hyperbolique à deux dimensions d'espace, Comptes Rendus de l'Acad. des Sciences, Paris, t.320, série I , 85-88, January 1995.

[2] P. ARMINJON, M.C. VIALLON AND A. MADRANE (1997), A Finite Volume Extension of the Lax-Friedrichs and Nessyahu-Tadmor Schemes for Conservation Laws on Unstructured Grids, Int.J. Comp.Fluid Dynamics, Vol.9, 1-22

[3] P.ARMINJON, D.STANESCU AND M.C. VIALLON , A two-dimensional finite volume extension of the Lax-Friedrichs and Nessyahu-Tadmor schemes for compressible flows, Proc. of the 6 th.Int.Symp. on Comp. Fluid Dynamics, Lake Tahoe (Nevada), September 4-8, 1995, M. Hafez and K.Oshima, editors, vol.4, p.7-14.

[4] P. ARMINJON, M.C. VIALLON AND A. MADRANE (1995), From Lax-Friedrichs to a multi-dimensional finite volume extension of the Nessyahu-Tadmor scheme for compressible flows, Proc. Int. Conf. on Numerical Methods for the Euler and Navier-Stokes Equations, Centre de Recherches Mathématiques, Montréal, September 14-16, 1995, P. Arminjon and A. Dervieux, editors. To be published in the American Math. Soc. - Centre de Recherches Mathématiques Series.

[5] P. ARMINJON, A. MADRANE AND M.C. VIALLON (1997), Comparison of a finite volume version of the Lax-Friedrichs and Nessyahu-Tadmor schemes and discontinuous finite element methods for compressible flows on unstructured grids , Proceedings of a Symposium Honouring S.K.Godunov, May 1-2, 1997, The University of Michigan, Ann Arbor (Mi.),to appear as special volume in J.Comp.Physics, B.van Leer, editor, 134(1) : 199, 1997.

[6] P. ARMINJON, M.C. VIALLON, A. MADRANE AND H. KADDOURI (1997). Discontinuous finite elements and a 2-dimensional finite volume generalization of the Lax-Friedrichs and Nessyahu-Tadmor schemes for compressible flows on unstructured grids, to appear in Comp. Fluid Dynamics Review, M. Hafez and K. Oshima, editors.

[7] P. ARMINJON, A. MADRANE (1998), A mixed finite volume/finite element method for 2-dimensional compressible Navier-Stokes equations on unstructured grids, 7^{th} Int.Conf. on Hyperbolic Problems, Zürich, February 9-13, 1998, Book of abstracts + Proceedings (to appear), M.Fey and R.Jeltsch, editors.

[8] P. ARMINJON, A. MADRANE (1998), A staggered Lax-Friedrichs type finite volume/finite element method for the two-dimensional Navier-Stokes equations, Proc. 6th. Conf. of the Computational Fluid Dynamics Society of Canada, Québec, june 7-9, 1998, E.Fournier and M.Fortin, editors, pp. VIII 103-108.

[9] P. ARMINJON, A. MADRANE (1998), A mixed finite volume/finite element method for viscous compressible flows on staggered unstructured grids, in Progress in Numerical Solutions of Partial Differential Equations, A Conference to honour P.Roe on the occasion of his 60th. birthday, Arcachon, France, July 11-13, 1998.

[10] P. ARMINJON, M.C. VIALLON (1995), Convergence of a finite volume extension of the Nessyahu-Tadmor scheme on unstructured grids for a two-dimensional linear hyperbolic equation, Rapport de recherche, No. 2239, Centre de Recherches Mathématiques, Université de Montréal, January 1995, accepted for publication, SIAM J.Num.Analysis.

[11] P. ARMINJON, M.C. VIALLON (1998), Convergence of a 2-step staggered grid Lax-Friedrichs type Finite volume method for nonlinear hyperbolic equations on unstructured triangular grids, Res. Report, Université de St Etienne, july 1998, to appear in Numerische Mathematik.

[12] R. SANDERS AND A.WEISER (1992) A high order staggered mesh approach for nonlinear hyperbolic system of conservation laws, JCP 1010, pp. 314-329.

[13] H.T.HUYNH (1995), A piecewise-parabolic dual-mesh method for the Euler equations, AIAA-95-1739CP, The 12^{th} AIAA CFD Conf., 1995.

[14] R.PEYRET, T.D.TAYLOR (1983). Computational Methods for Fluid Flow, Springer-Verlag, New-York, Heidelberg, Berlin.

[15] P. ROSTAND AND B. STOUFFLET (1988), Finite Volume Galerkin Methods for Viscous Gas Dynamics, INRIA Res. Rep. No. 863, Rocquencourt, 78153 Le Chesnay, France.

[16] PH. ROSTAND, Sur une méthode de volumes finis en maillage non structuré pour le calcul d'écoulements visqueux compressibles, Thèse de Doctorat, Université Paris VI, 1989

[17] L.FEZOUI, S. LANTERI, B. LARROUTUROU AND C. OLIVIER (1989), Résolution Numérique des Équations de Navier-Stokes pour un Fluide Compressible en Maillage triangulaire, INRIA Rep. Rep. No. 1033, Rocquencourt, 78153 Le Chesnay, France.

[18] H. NESSYAHU AND E. TADMOR , Non-oscillatory Central Differencing for Hyperbolic Conservation Laws, J. Comp. Physics 87, No. 2, 408–463, 1990.

[19] B. PALMERIO, L.FEZOUI, C. OLIVIER AND A. DERVIEUX (1990), On TVD criteria for mesh adaption for Euler and Navier-Stokes calculations. INRIA Res. Rep. No. 1175, Rocquencourt, 78153 Le Chesnay, France.

[20] G.D.V. GOWDA AND J. JAFFRÉ (1993), A discontinuous finite element method for nonlinear scalar conservation laws, INRIA Res. Rep. No. 1848, Rocquencourt, 78153 Le Chesnay, France.

[21] J. JAFFRÉ AND L. KADDOURI (1991), Discontinuous finite elements for the Euler equations. Proc. 3^d. Int. Conf. on Hyperbolic Problems, June 11-15, 1990, Uppsala (Sweden), B. Engquist and B. Gustafsson, editors, Studentlitteratur, Chartwell-Bratt, Vol. 2, 602–610.

[22] B. VAN LEER (1972), Towards the Ultimate Conservative Difference Scheme. I. The Quest of Monotonicity, in proc. Third Int. Conf. on Numerical Meth. in Fluid Mech., Lecture Notes in Physics 18, H.Cabannes and R.Temam, editors, Springer Verlag (1973), 163-168.

[23] B. VAN LEER (1974), Towards the Ultimate Conservative Difference Scheme. II. Monotonicity and conservation combined in a second order scheme, *J. Comp. Phys.*, Vol. 14, 361–370.

[24] B. VAN LEER (1977), IV. A new approach to numerical convection, J. Comp. Phys., Vol. 23, 276–299.

[25] S. CHAMPIER (1992), Convergence de schémas numériques type Volumes Finis pour la résolution d'équations hyperboliques. Thèse, Univ. de St-Étienne.

[26] G.A.ASHFORD (1996), An unstructured grid generation and adaptive solution technique for high-Reynolds-number compressible flows. Thesis (Aerospace Engineering and Scientific Computing) University of Michigan, Ann Arbor, Michigan.

[27] J. STEGER, R.F. WARMING (1981), Flux vector splitting for the inviscid gas dynamic with applications to finite-difference methods, J. of Comp. Phys., 40,(2), p.263-293, (1981).

[28] M.J.CASTRO DIAZ AND F.HECHT, Anisotropic Surface Mesh Generation, INRIA Res. Rep. No. 2672, October 1995, INRIA, Rocquencourt, 78153 Le Chesnay, France.

[29] M.J.CASTRO DIAZ, Mesh Refinement over Triangulated Surfaces, INRIA Res. Rep. No. 2462, June 1994, INRIA, Rocquencourt, 78153 Le Chesnay, France.

[30] B.V.K. SATYA SAI, O.C.ZIENKIEWICZ, M.T.MANZARI, P.R.M. LYRA AND K.MORGAN (1998), General purpose versus special algorithms for high-speed flows with shocks. Int. J. Num.Meth. in Fluids, Vol.27, 57-80.

[31] T.J.R. HUGHES (1992), Finite Element Method for Fluids, in AGARD Special Course on Unstructured Methods for Advection Dominated Flows, AGARD Rep. 787, AGARD, Neuilly sur Seine, France.

[32] M.D.TIDRIRI (1994), Domain Decomposition for Compressible Navier-Stokes Equations with Different Discretization and Formulations, J.of Comp. Phys., 119,271-282.

[33] INRIA AND GAMNI-SMAI (1990), Workshop on hypersonic flows for reentry problems, Problem 6 : Flow over a double ellipse, test case 6.1 : Non-Reactive Flows. Antibes, France, January 22-25, 1990.

Conclusion

Dans ce travail nous avons présenté une méthode de volumes finis pour les systèmes hyperboliques de lois de conservation, faisant appel à deux maillages emboîtés, utilisés alternativement aux pas de temps pairs et impairs, de manière à éviter, grâce à une généralisation à 2 dimensions spatiales du schéma décalé de Lax-Friedrichs, la résolution exacte ou approximative des problèmes de Riemann générés normalement, pour toute méthode de type volumes finis, aux interfaces des cellules.

Dans un premier temps, nous avons présenté la généralisation, par Arminjon et Viallon, du schéma aux différences uni-dimensionnel de Lax-Friedrichs, à ce système à double maillage en formulation en volumes finis. Cette méthode a conduit à un schéma aux volumes finis d'ordre 1, non oscillatoire, mais trop dissipatif.

Pour passer à une méthode d'ordre de précision 2, on a choisi, en s'inspirant d'un article de Nessyahu et Tadmor décrivant une méthode aux différence finies en une dimension spatiale d'ordre 2 grâce à l'emploi d'interpolation de la solution, sur chaque cellule, par une fonction linéaire par morceaux telle que proposée par van Leer (méthode "MUSCL"), de procéder, dans chacune des cellules des deux types correspondant aux deux maillages emboîtés, à une interpolation linéaire également de type MUSCL. Ici encore le caractère non oscillatoire (préservation de la monotonie) a été assuré par l'utilisation de limiteurs de pente de type minmod, à partir d'estimation des gradients par une méthode de type moindres carrés.

La passage d'une formulation en différences finies en une dimension à une formulation en volumes finis en deux dimensions a soulevé de nombreuses difficultés, et nous avons dû renoncer aux limiteurs utilisés par Nessyahu et Tadmor, et introduire un générateur de maillage couplé à un dispositif d'adaptation du maillage, pour parvenir à une résolution quasi d'ordre deux et tout à fait non oscillatoire.

Pour vérifier la qualité de cette méthode, nous avons choisi de la comparer systématiquement, au cours d'une série de calculs tests typiques en aérodynamique, à une méthode d'éléments finis discontinus récemment proposée par Jaffré et al. (INRIA, France), qui repose sur le solveur de Riemann de Roe avec la correction entropique de Dubois-Mehlmann.

Les résulats ont montré la qualité de notre méthode, qui a conduit à des ondes de choc mieux captées, une préservation de monotonie beaucoup plus stricte, des convergences plus rapides vers l'état stationnaire à calculer, et des temps de calcul nettement inférieurs.

Dans la dernière partie de notre travail nous avons construit une extension de cette méthode de volumes finis à une méthode mixte volumes finis/éléments finis pour les équations de Navier-Stokes, en s'inspirant d'une construction de ce type par Rostand et Stoufflet (Avions Marcel Dassault), dans laquelle la partie convective des equations de Navier-Stokes est traitée à l'aide de notre méthode de volumes finis adaptée à cette situation, et la partie diffusive (visqueuse) est évaluée à l'aide d'une méthode d'éléments finis (élément P1-Lagrange).

On a utilisé un système d'adaptation du maillage pour parvenir à une bonne capture des ondes de choc et du décollement de la couche limite.

Les résultats, comparés à ceux notamment de Dervieux et co-auteurs, ont montré la très bonne compétitivité de notre méthode.

Nous avons récemment commencé à géneraliser la méthode Arminjon-Viallon à des équations et systèmes hyperboliques de conservation en 3 dimensions spatiales (équations de convection, équations d'Euler) d'abord pour des maillages cartésiens et plus récemment pour des maillages tétraédriques.

Si les qualités de la méthode en 2 dimensions se transmettent bien au cas tridimensionnel nous espérons obtenir des résultats au moins comparables à ceux existant actuellement.

ANNEXE 1
Expression des jacobiens et des matrices de passage

5. Expression des jacobiens

Les matrices $A(U)$ et $B(U)$ sont respectivement les jacobiens des flux $F(U)$ et $G(U)$

$$\begin{cases} A(U) = F'(U) \\ B(U) = G'(U) \end{cases}$$

Rappelons que le système des équations d'Euler s'écrit

$$U_t + A \cdot U_x + B \cdot U_y = 0 \tag{5.1}$$

Les matrices A et B sont données par

$$A = \begin{bmatrix} 0 & 1 & 0 & 0 \\ \frac{\gamma-3}{2}u^2 + \frac{\gamma-1}{2}v^2 & (3-\gamma)u & (1-\gamma)v & \gamma-1 \\ -uv & v & u & 0 \\ u\left(-\gamma E + (\gamma-1)(u^2+v^2)\right) & \gamma E - \frac{\gamma-1}{2}(3u^2+v^2) & (1-\gamma)uv & \gamma u \end{bmatrix},$$

$$B = \begin{bmatrix} 0 & 0 & 1 & 0 \\ -uv & v & u & 0 \\ \frac{\gamma-1}{2}u^2 + \frac{\gamma-3}{2}v^2 & (1-\gamma)u & (3-\gamma)v & \gamma-1 \\ v\left(-\gamma E + (\gamma-1)(u^2+v^2)\right) & (1-\gamma)uv & \gamma E - \frac{\gamma-1}{2}(u^2+3v^2) & \gamma v \end{bmatrix}$$

6. Expression des matrices de passage

Soit A_n la matrice caractéristique du système des équations d'Euler

$$A_n = n_1 A + n_2 B \ , \quad \vec{n} = \begin{pmatrix} n_1 \\ n_2 \end{pmatrix} \in \mathbf{R}^2$$

D'après la proposition (1.1) du chapitre (1), A_n est diagonalisable et il existe une matrice inversible P_n et une matrice diagonale Λ_n contenant les valeurs propres de A_n, telles que $A_n = P_n \Lambda_n P_n^{-1}$.

Le calcul direct des valeurs propres de A_n et des matrices P_n et P_n^{-1} est fastidieux. Il est plus simple de considérer les équations écrites dans les variables physiques (vecteur R)

$$R_t + \widetilde{A} \cdot R_x + \widetilde{B} \cdot R_y = 0 \tag{6.1}$$

$$R = \begin{pmatrix} \rho \\ u \\ v \\ p \end{pmatrix} \ , \quad \widetilde{A} = \begin{bmatrix} u & \rho & 0 & 0 \\ 0 & u & 0 & \frac{1}{\rho} \\ 0 & 0 & u & 0 \\ 0 & \gamma p & 0 & u \end{bmatrix} \ , \quad \widetilde{B} = \begin{bmatrix} v & 0 & \rho & 0 \\ 0 & v & 0 & 0 \\ 0 & 0 & v & \frac{1}{\rho} \\ 0 & 0 & \gamma p & v \end{bmatrix}$$

Les équations (5.1) et (6.1) sont équivalentes et il existe une matrice inversible M telle que $\widetilde{A} = M^{-1} \cdot A \cdot M$, et $\widetilde{B} = M^{-1} \cdot B \cdot M$

$$M = \begin{bmatrix} 1 & 0 & 0 & 0 \\ u & \rho & 0 & 0 \\ v & 0 & \rho & 0 \\ \frac{u^2+v^2}{2} & \rho u & \rho v & \frac{1}{\gamma - 1} \end{bmatrix} \ ,$$

$$M^{-1} = \begin{bmatrix} 1 & 0 & 0 & 0 \\ -\frac{u}{\rho} & \frac{1}{\rho} & 0 & 0 \\ -\frac{v}{\rho} & 0 & \frac{1}{\rho} & 0 \\ (\gamma-1)\frac{u^2+v^2}{2} & (1-\gamma)u & (1-\gamma)v & \gamma-1 \end{bmatrix}$$

La matrice $\widetilde{A}_n = n_1\widetilde{A} + n_2\widetilde{B}$ est reliée à A_n par $A_n = M \cdot \widetilde{A}_n \cdot M^{-1}$. Par conséquent les valeurs propres de A_n et $\widetilde{A}_n$ sont identiques. Les valeurs propres de $\widetilde{A}_n$ sont

$\lambda_1(\vec{n}; U) = n_1 u + n_2 v - c\sqrt{n_1^2 + n_2^2}$

$\lambda_2(\vec{n}; U) = \lambda_3(\vec{n}; U) = n_1 u + n_2 v$

$\lambda_4(\vec{n}; U) = n_1 u + n_2 v + c\sqrt{n_1^2 + n_2^2}$

Les transformations $\widetilde{P}_n$, $\widetilde{P}_n^{-1}$ qui diagonalisent $\widetilde{A}_n$ sont

$$\widetilde{P}_n = \begin{bmatrix} 1 & 0 & 1 & 1 \\ -\frac{c}{\rho}\widetilde{n}_1 & -\frac{v}{\rho}\widetilde{n}_2 & 0 & \frac{c}{\rho}\widetilde{n}_1 \\ -\frac{c}{\rho}\widetilde{n}_2 & \frac{v}{\rho}\widetilde{n}_1 & 0 & \frac{c}{\rho}\widetilde{n}_2 \\ c^2 & 0 & 0 & c^2 \end{bmatrix} \quad , \quad \widetilde{P}_n^{-1} = \begin{bmatrix} 0 & -\frac{\rho}{2c}\widetilde{n}_1 & -\frac{\rho}{2c}\widetilde{n}_2 & \frac{1}{2c^2} \\ 0 & -\frac{\rho}{v}\widetilde{n}_2 & \frac{\rho}{v}\widetilde{n}_1 & 0 \\ 1 & 0 & 0 & -\frac{1}{c^2} \\ 0 & \frac{\rho}{2c}\widetilde{n}_1 & \frac{\rho}{2c}\widetilde{n}_2 & \frac{1}{2c^2} \end{bmatrix}$$

avec $\widetilde{n}_1 = \dfrac{n_1}{\sqrt{n_1^2+n_2^2}}$, $\widetilde{n}_2 = \dfrac{n_2}{\sqrt{n_1^2+n_2^2}}$.

Les matrices $M \cdot \widetilde{P}_n$ et $\widetilde{P}_n^{-1} \cdot M^{-1}$ diagonalisent A_n, donc P_n et P_n^{-1} sont données par

$$P_n = \begin{bmatrix} 1 & 0 & 1 & 1 \\ u - c\widetilde{n}_1 & -v\widetilde{n}_2 & u & u + c\widetilde{n}_1 \\ v - c\widetilde{n}_2 & v\widetilde{n}_1 & v & v + c\widetilde{n}_2 \\ H - c(u\widetilde{n}_1 + v\widetilde{n}_2) & v(v\widetilde{n}_1 - u\widetilde{n}_2) & \frac{u^2+v^2}{2} & H + c(u\widetilde{n}_1 + v\widetilde{n}_2) \end{bmatrix} ,$$

$$P_n^{-1} = \begin{bmatrix} \frac{1}{2}\left(b_1 + \frac{1}{c}(u\tilde{n}_1 + v\tilde{n}_2)\right) & \frac{1}{2}\left(-b_2 u - \frac{1}{c}\tilde{n}_1\right) & \frac{1}{2}\left(-b_2 v - \frac{1}{c}\tilde{n}_2\right) & \frac{1}{2}b_2 \\ \frac{1}{v}\left(-v\tilde{n}_1 + u\tilde{n}_2\right) & -\frac{1}{v}\tilde{n}_2 & \frac{1}{v}\tilde{n}_1 & 0 \\ 1 - b_1 & b_2 u & b_2 v & -b_2 \\ \frac{1}{2}\left(b_1 - \frac{1}{c}(u\tilde{n}_1 + v\tilde{n}_2)\right) & \frac{1}{2}\left(-b_2 u + \frac{1}{c}\tilde{n}_1\right) & \frac{1}{2}\left(-b_2 v + \frac{1}{c}\tilde{n}_2\right) & \frac{1}{2}b_2 \end{bmatrix}$$

avec $b_2 = \dfrac{\gamma - 1}{c^2}$, $b_1 = b_2 \cdot \dfrac{u^2 + v^2}{2}$.

Références

[1] CHORIN A.J.AND MARSDEN J.E., A Mathematical Introduction to Fluid Mechanics, Springer-Verlag (1979)

[2] SMOLLER J.A., Shocks waves and reaction diffusion equations, Springer Verlag, (1983)

[3] KEYFITZ B.L. AND KRANZER H.C., A system of non strictly hyperbolic conservation laws arising in elasticity theory, Arch. Rat .Mech. Anal.,72,(1980),pp. 219-241.

[4] LEROUX A.Y., Approximation de quelques problèmes hyperboliques non-linéaires, Thèse d'Etat, Rennes (1979)

[5] LEROUX A.Y. ET AL , Modélisation océanique avec topographie, Rapport CNEXO, Université de Rennes

[6] VILA J.P, Sur la théorie et l'approximation numérique de problèmes hyperboliques non linéaire, application aux équations de Saint Venant et à la modélisation des avalanches denses, Thèse, Paris 6 (1986)

[7] GALLOUET T. AND PFERZEL A., On some new upstream weighting schemes for oil recovery simulation, (à paraître).

[8] WAGNER D., The Riemann problem in two space dimensions for a single conservation law, SIAM J. Math. Anal., 14, (1983), pp.534-559.

[9] P.ARMINJON, L.SMITH, Upwind finite volume schemes with anti-diffusion for the numerical study of electric discharges in gas-filled cavities, Rapport de recherche, Dépt. de Math. et stat., No. 90-10, éffectué pour l'Institut de Recherche d'Hydro-Québec (IREQ), (avril 1990), 39 pages; Computer Methods in Applied Mechanics and Engineering 100, No. 2 (1992), 149-168.

[10] LUSKIN M., On the existence of global smooth solutions for a model equation for a fluid flow in a pipe, J. Math. Anal. Appl., 84, (1981), pp.614-630.

[11] RASCLE M., Perturbations par viscosité de certains systèmes hyperboliques non linéaires, Thèse d'Etat Lyon 1 , (1983).

[12] DIPERNA R.J. , Convergence of approximate solutions to conservation laws, Arch. Rational Mech. Anal. , 82, (1983), pp. 285-314

[13] TARTAR L., Compensated compactness and applications to partial differential equations, in : Nonlinear Analysis and Mechanics, Herriot-Watt Symposium, vol. 4 , R.J. Knops editor Pitman (1979), pp. 136-212.

[14] GLIMM J., Solutions in large for non linear hyperbolic systems of equations, Comm. pure Appl. Math.,15 (1965), pp.697-715.

[15] HARTEN A., High resolution schemes for hyperbolic conservation laws, J. Comp Phys., 49, (1983), pp. 357-393.

[16] CHAKRAVARTHY R., ENGQUIST B. HARTEN A. AND OSHER S., Uniformly high accurate essentially non-oscillatory schemes III, Ecoles CEA-EDF-INRIA, (1988).

[17] HARTEN A., LAX P. AND VAN LEER B., On upstream differencing and Godunov-type schemes for hyperbolic conservation laws, SIAM Review, 25, (1983), pp. 279-322.

[18] VILA J.P. , Simplified Godunov schemes for 2×2 systems of conservation laws, SIAM J. Numer. Anal., 23,6, (1986), pp. 1173-1192.

[19] DUBOIS F AND LE FLOCH P., Boundary conditions for nonlinear hyperbolic systems of conservation laws, J. Diff. Eq. 71,1, (1988), pp 93-122.

[20] LE FLOCH P. AND RAVIART P.A., An asymptotic expansion for the solution of the generalized Riemann problem I, Annales de l'I.H.P.,5,2 (1988), pp. 179-207.

[21] LEROUX A.Y., Numerical stability of some equations of gas dynamics, Math. Comp., 37, (1980), pp. 307-320.

[22] ROE P.L., Upwind differencing schemes for hyperbolic laws with sources terms, Proc. Nonlinear Hyperbolic Problems, Eds. C Carasso, P.A Raviart, et D. Serre, Springer, Lectures Notes in Mathematics 1270, (1986)

[23] VAN LEER B., On the relation between the upwind-differencing schemes of Godunov,Engquist-Osher and Roe, SIAM. SCI. Stat. Comput.,5,1,(1984), pp.1-20.

[24] LE FLOCH P., Contributions à l'étude théorique et à l'approximation numérique des systèmes hyperboliques non linéaires. Application aux équations de la dynamique des gaz, Thèse, Ecole Polytechnique Paris (1988).

[25] S. CHAMPIER (1992), Convergence de schémas numériques type Volumes Finis pour la résolution d'équations hyperboliques. Thèse, Univ. de St-Étienne.

[26] G.A.ASHFORD (1996), An unstructured grid generation and adaptive solution technique for high-Reynolds-number compressible flows. Thesis (Aerospace Engineering and Scientific Computing) University of Michigan, Ann Arbor, Michigan.

[27] P. ARMINJON, M.C. VIALLON (1995), Convergence of a finite volume extension of the Nessyahu-Tadmor scheme on unstructured grids for a two-dimensional linear hyperbolic equation, Rapport de recherche, No. 2239, Centre de Recherches Mathématiques, Université de Montréal, January 1995, accepted for publication, SIAM J.Num.Analysis.

[28] P. ARMINJON, M.C. VIALLON (1998), Convergence of a 2-step staggered grid Lax-Friedrichs type Finite volume method for nonlinear hyperbolic equations on unstructured triangular grids, Res. Report, Université de St Etienne, july 1998, to appear in Numerische Mathematik.

[29] G. CHAVENT AND B. COCKBURN, Consistence et stabilité des schémas LRG, rapport INRIA, n^o 710, 1987

[30] G. CHAVENT AND B. COCKBURN AND G. COHEN AND J. JAFFRÉ, Une méthode d'éléments finis pour la simulation dans un réservoir de déplacements bidimensionnels d'huile par de l'eau, rapport INRIA, n^o 353, 1985

[31] S. N. KRUZHKOV, First order quasilinear equation with several independant variables, Math. Sbornik USSR, n^o 10, 217–243, 1970

[32] G. CHAVENT AND J. JAFFRÉ AND R. EYMARD AND D. GUÉRILLOT AND L. WEILL, Discontinuous and mixed finite elements for two-phase incompressible flow, SPE paper, 16018, 1987

[33] P. COLLELA, Multidimensional upwind methods for hyperbolic conservation laws, J. Comput. Physics, 87, 171–200, 1990

[34] A. Y. LEROUX, Approximation de quelques problèmes hyperboliques non linéaires, Thèse d'état, Université de Rennes, 1979

[35] F. DUBOIS, Quelques problèmes liés au calcul d'écoulements de fluides parfaits dans les tuyères, Thèse de Doctorat, Université Paris VI, 1988

[36] F. DUBOIS, Boundary conditions and the Osher scheme for the Euler equations of gas dynamics, rapport CMAP-Ecole Polytechnique, n^o 170, 1987

[37] F. DUBOIS AND G. MEHLMAN, A non-parameterized Entropy Correction for Roe's Approximate Riemann Solver, rapport CMAP-Ecole Polytechnique, n^o 248, 1991

[38] F. FEZOUI, Résolution des équations d'Euler par un schéma de Van Leer en éléments finis, rapport INRIA, n^o 358, 1985

[39] VAN LEER, B., Towards the Ultimate Conservative Differencing Scheme V.A Second Order Sequel to Godunov's Method, Journal of Computational Physics, v.32, 1979

[40] L. FEZOUI AND B. STOUFFLET, A class of implicit upwind schemes for Euler simulations with unstructured meshes, J. Comput. Physics, 84(1), 174–206, 1989

[41] B. STOUFFLET, Résolution numérique des équations d'Euler des fluides parfaits compressibles par des schémas implicites en éléments finis, Thèse de Docteur-Ingénieur, Université Paris VI, 1984

[42] STEGER J. - WARMING R.F., Flux vector splitting for the invicid gas dynamic with applications to finite difference methods, J.Comput. Physics, Vol. 40 N^o pp 263-293 (1981)

[43] VAN LEER B., Computational methods for ideal compressible flow, Cours Von Karmann Institute, lectures serie 1983-04 computational fluid dynamic (1983)

[44] A. HARTEN, High Resolution Schemes for Hyperbolc Conservation Laws, J. Comput. Physics, 49, 357–393, 1983

[45] A. HARTEN AND J.M. HYMAN, Self-Adjusting Grid Methods for One-Dimensional Hyperbolic Conservation Laws, J. Comput. Physics, 50, 235–269, 1983

[46] T.J.R. HUGHES AND ET AL., A new finite element formulation for computational fluid dynamics 1, 2, 3, 4, Comp. Meth. Apll. Mech. Eng., 54, 223–234 et 341–355 et 58, (1986), pp. 305–336 , 1986

[47] C. JOHNSON AND A. SZEPESSY, Shock-capturing streamline diffusion finite elements for nonlinear conservation laws, Recent Developments in Computational Physics, AMD, 95, 101–108, 1988

[48] P.D. LAX AND A. HARTEN AND B. V. LEER, On Upstream Differencing and Godunov Type Schemes for Hyperbolic Conservation Laws, SIAM Revue, 25(1), 35–61, 1983

[49] P.D. LAX, Weak solutions of nonlinear hyperbolic equation and their numerical computation, Communication. on Pure and Applied Mathematics, 7, 159–193, 1954

[50] P.D. LAX, Shock waves and entropy, in Contributions to nonlinear functional analysis of shock waves,Proc. Symposium at the Univ. of Wisconsin 11, 603–634, E.H. Zarantonello, ed., Academic press, 1971

[51] B.V. LEER, Towards the ultimate conservative scheme: IV. A new approach to numerical convection, J. Comput. Physics, 23, 276–299, 1977

[52] D.W. LEVY, K.G. POWELL AND B.V. LEER, An Implementation of a Grid-Independant Upwind Scheme for the Euler Equations, AIAA paper, 89-1931, 1989

[53] S. OSHER AND F. SOLOMON, Upwind difference schemes for hyperbolic systems of conservation laws, Math. Comp, 38, 158, 339–374, 1982

[54] J. PERAIRE, L. FORMAGGIA, J. PEIRO, K. MORGAN AND O.C. ZIENKIEWICZ, Finite element Euler computation in 3D, AIAA paper, 87-0032, 1987

[55] J. PERAIRE, M. VAHDATI, K. MORGAN AND O.C. ZIENKIEWICZ, Adaptive remeshing for compressible flow computations, J. Comput. Physics, 72, 449–466, 1987

[56] P.L ROE, Approximate Riemann Solvers, Parameter Vectors, and Difference Schemes J. Comput. Physics, 43, 357–372, 1981

[57] P.ARMINJON AND A.DERVIEUX, Construction of TVD-like Artificial Viscosities on Two-Dimensional Arbitrary FEM Grids, J of Comp Phy 106, 176-198 (1993)

[58] B.R.BALIGA ET S.V.PATANKAR, A control volume finite-element method for two-dimensional fluid flow and heat transfer, Numer.Heat Transfer, 6, pp. 245-262, (1983)

[59] B.R.LATIMER AND A.POLLARD, Comparaison of pressure-velocity coupling solution algorithms, Numer. Heat .Transfer, 8, pp. 635-652, (1985)

[60] S.V.PATANKAR, Numerical heat transfer and fluid flow . Series in Computational Methods in Mechanics and Thermal Sciences, (1980).

[61] G.D.RAITHBY, P.F.GALPIN AND J.P. VAN DOORMAAL, Prediction of heat transfer and fluid flow in complex geometries using general orthogonal coordinates, Numer. Heat Transfer, 9,pp.125-142,(1986)

[62] W.RODI, S.MAJUMDAR ET B.SCHÖNUNG : Finite volume methods for two-dimensional incompressible flow with complex boundaries, Comp.Meth.Appl.Mech.Eng., 75,pp.369-392, (1989)

[63] P.A.RAVIART AND J.M.THOMAS, A Mixed finite element method for $2-nd$ order elliptic problems, Lecture Notes in Mathematics, 606, Springer-Verlag, New-York, pp.292-315, (1977).

[64] I.BABUSKA, Error bounds for finite element methods, Numer. Math., 16, pp. 322-333, (1971).

[65] F. BREZZI, On the existence, uniqueness and approximation of saddle-point problem arising from lagrangian multipliers, RAIRO, Anal. Numer.,2, pp. 129-151, (1974)

[66] P.G. CIARLET, The Finite Element Method for Elliptic Problems, North-Holland, (1978).

[67] V.GIRAULT AND P.A.RAVIART, Finite Element for Navier-Stokes Equations, Theory and Algorithms, Springer S.C.M., 5, Springer-Verlag, (1986).

[68] F.BREZZI AND M.FORTIN, Mixed and Hybrid Finte Element Methods, Springer-Verlag, (1990)

[69] E.HOPF, The partial differential equation $u_t + uu_x = \mu u_{xx}$, Comm. Pure Appl. Math 3 (1950) 201-230. P.D. LAX, Hyperbolic systems Conservation Laws and the mathematical theory of shock waves, SIAM regional conference in applied mathematics, V.11, (1973)

[70] S. GODUNOV, A. ZABRODIN, M.IVANOV, A. KRAÏKO AND G.PROKOPOV, Résolution numérique des problèmes multidimensionnels de la dynamique des gaz, MIR, Moscou, (1979)

[71] INRIA AND GAMNI-SMAI, Workshop on Hypersonic Flows for Reentry Problems, Antibes, France, Janvier, 1990

[72] J. JAFFRÉ AND L. KADDOURI, Discontinuous finite elements for the Euler equations, Article présenté à la $3^{\text{ème}}$ Conférence Internationale sur les Problèmes Hyperboliques,Uppsala, Suède, Juin 1990